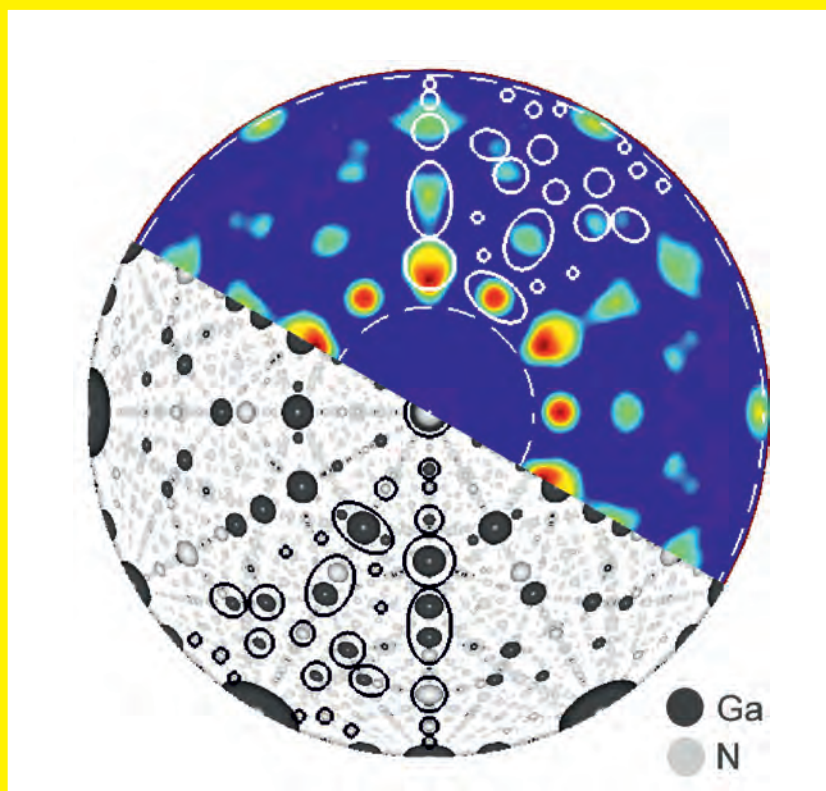


SYNCHROTRON RADIATION IN NATURAL SCIENCE

Bulletin of the Polish Synchrotron Radiation Society
Volume 11, Number 1-2, May 2012



Includes: News, regular papers, information on PTPS,
Programme and Abstracts of the 11th International
Symposium and School on Synchrotron Radiation
in Natural Science (ISSRNS-11),
(Cracow, Poland, 20-25 May, 2012)



Organised by:

Polish Synchrotron Radiation Society and Institute of Nuclear Physics PAN, Cracow,
under the honorary patronage of Mayor of the Royal City of Cracow Jacek Majchrowski,
General Director of the Institute of Nuclear Physics, PAN Marek Jeżabek,
and Rector of the Jagiellonian University in Kraków Karol Musioł

Sponsored by: Ministry of Science and Higher Education, Hamamatsu
Bruker, Panalitycal, Netzsch, Spectro-Lab

SYNCHROTRON RADIATION IN NATURAL SCIENCE

Bulletin of the Polish Synchrotron Radiation Society

Address: al. Lotników 32/46, 02-668 Warsaw, Poland,
phone/fax 228436034, e-mail: paszk@ifpan.edu.pl

Editorial Board

Wojciech Paszkowicz, Editor
Institute of Physics
Polish Academy of Sciences
al. Lotników 32/46
02-668 Warsaw
e-mail: paszk@ifpan.edu.pl

Zbigniew Kaszukur, Secretary
Institute of Physical Chemistry
Polish Academy of Sciences
Kasprzaka 44/52
01-224 Warsaw, Poland
e-mail: zkaszkur@ichf.edu.pl

Bogdan J. Kowalski
Institute of Physics
Polish Academy of Sciences
al. Lotników 32/46
02-668 Warsaw, Poland
e-mail: kowab@ifpan.edu.pl

Paweł Piszora
Faculty of Chemistry
A. Mickiewicz University
ul. Grunwaldzka 6
60-780 Poznań
e-mail: pawel@amu.edu.pl

Radosław Przeniosło
Institute of Experimental Physics
Warsaw University
ul. Hoża 69
00-681 Warszawa
e-mail:
radek.przenioslo@fuw.edu.pl

Wojciech Szuszkiewicz
Institute of Physics
Polish Academy of Sciences
al. Lotników 32/46
02-668 Warsaw, Poland
e-mail: szusz@ifpan.edu.pl

Advisory Board

Krystyna Jabłońska
Institute of Physics
Polish Academy of Sciences
al. Lotników 32/46
02-668 Warsaw
e-mail: jablo@ifpan.edu.pl

Czesław Kapusta
Department of Solid State Physics
AGH University of Science and
Technology
al. Mickiewicza 30
30-059 Kraków,
e-mail: kapusta@agh.edu.pl

Maciej Kozak
Faculty of Physics
A. Mickiewicz University
ul. Umultowska 85
61-614 Poznań
e-mail: mkozak@amu.edu.pl

Wojciech Kwiatek
Institute of Nuclear Physics
Polish Academy of Sciences
ul. Radzikowskiego 152
31-342 Kraków
e-mail:
wojciech.kwiatek@ifj.edu.pl

Marek Stankiewicz
Institute of Physics
Jagellonian University
ul. Reymonta 4
30-059 Kraków
e-mail: m.j.stankiewicz@uj.edu.pl

Jacek Szade
Institute of Physics
Silesian University
ul. Uniwersytecka 4
40-007 Katowice
e-mail: szade@us.edu.pl

Note for contributors: Contributions in English (preferred) or in Polish should be sent to the Editor. The topics include: synchrotron and alternative radiation sources such as free electron lasers, beamline instrumentation, experimental and theoretical results connected with application of various methods and approaches (x-ray scattering, x-ray diffraction, x-ray absorption, fluorescence and photoelectron spectroscopies, magnetic dichroism, etc.) in connection with application of synchrotron radiation in physics, chemistry, crystallography, materials science and life sciences.

Layout by Arkadiusz Zarzycki. Cover design by W. Paszkowicz. **Figure on the cover page: Illustration from the abstract "Wavelet analysis of X-ray absorption anisotropy: Accuracy and limitations of atomic structure imaging" by D.T. Dul et al. (this issue).**

SYNCHROTRON RADIATION IN NATURAL SCIENCE is published and distributed by the Polish Synchrotron Radiation Society (PSRS). Detailed information on PSRS is given on cover page 3.

SOLARIS — NATIONAL SYNCHROTRON RADIATION CENTRE, THE POLISH RESEARCH INFRASTRUCTURE ROADMAP FACILITY

STATUS IN SPRING 2012

Wojciech Paszkowicz¹ and Marek Stankiewicz²

¹*Institute of Physics, Polish Academy of Sciences, ul. Lotników 32, 02-668 Warszawa, Poland*

²*National Synchrotron Radiation Centre SOLARIS, Jagiellonian University,
ul. Gronostajowa 7/P.1.6, 30-387 Kraków, Poland*

Interaction of the electromagnetic radiation with matter is fundamental to the universe. From the big bang up to the current times such interactions have been activating the processes and phenomena at the atomic level up to the scale of the whole Universe. The radiation influences short and long term processes on our globe at the micro and macro scales affecting such areas as the plant growth, earth atmosphere, climate changes, weather, *etc.*

In the Universe the Stars are natural sources of EM radiation. In our planetary system the Sun supplies the Earth with a very broad spectrum of electromagnetic radiation spreading from the infrared, through the visible region to X-rays. Significant part of the radiation interacts with and is absorbed by the atmosphere, the transmitted part interacts with the Earth ecosystem providing the necessary energy, catalyzing reactions and stimulating biological processes.

The knowledge and control of the radiation interaction with matter is therefore extremely important and allowing for understanding the ongoing

reactions and processes and opening the possibilities of their control.

Until 1970 there was no man made source of such properties and intensities enabling for research of EM radiation stimulated processes in such a broad spectrum of energies. This situation has changed in 1970 when the first synchrotron radiation source was built.

The advent of synchrotron radiation sources and their constant development and improvement has revolutionized the research in many areas of fundamental as well as applied science. Since then the potential of such facilities has been widely recognized and led to the development and construction of very high intensity light sources (synchrotrons and free electron lasers) emitting the radiation of unprecedented properties:

- broad spectral range and tunability (opportunity of selection of a single energy),
- high collimation, with opportunity for focusing down to the size of the order of 10 nm,

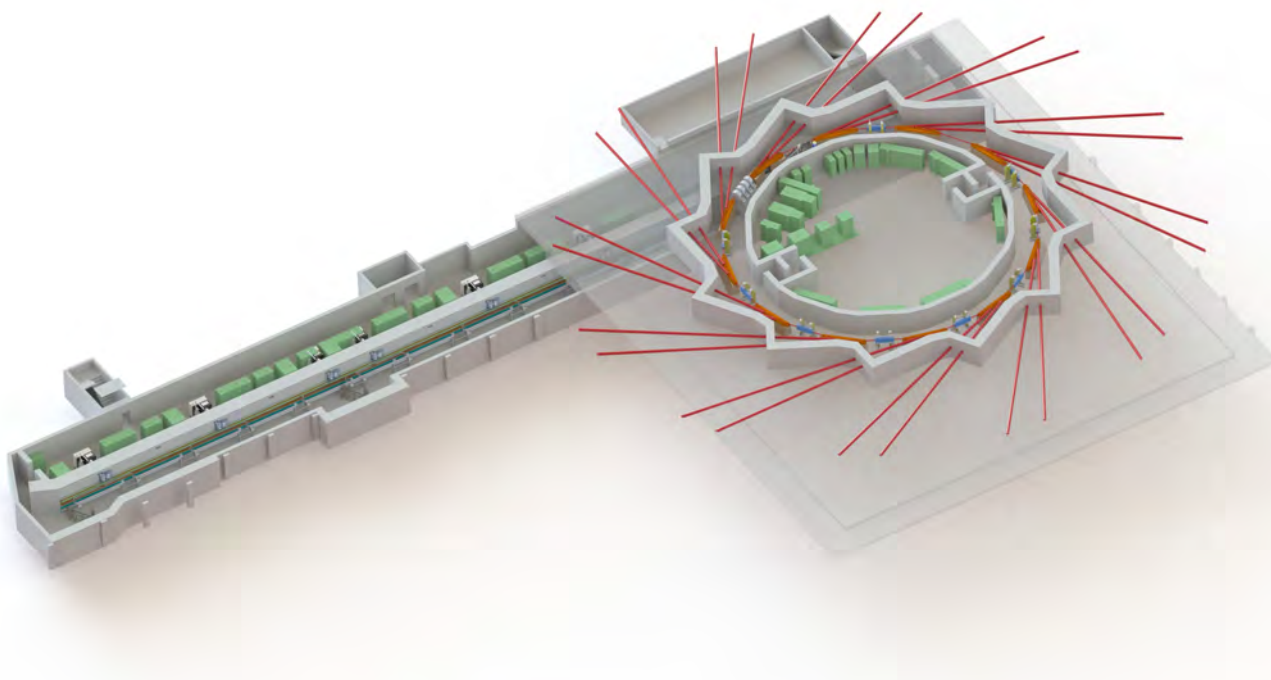


Figure 1: SOLARIS facility layout.

- high coherence,
- extremely high intensity,
- specific time structure (pulses down to femtosecond scale and up to gigawatt power).

Synchrotrons, despite being big devices (their circumference ranges from several tens to several thousand of meters), emit a very compact photon beam, which can be described as a light scalpel that can operate on the surface or inside the investigated objects. It is not only the photon beam size but also the precision of the applied photon energy that means the light scalpel has unique applications. This kind of site specific surgery opens up a vast range of research that is available only with synchrotron radiation. The systems investigated range from single atoms and molecules, through biological complex molecules (proteins, DNA) to bulk materials and crystals.

Over the last three decades, synchrotron light has supported cutting-edge research in physics, chemistry, biology and material sciences, and has opened up many new areas of research in fields such as medicine, geological and environmental studies, structural genomics and archaeology. The synchrotron radiation centers are truly multidisciplinary and multi-user facilities.

Many tens of such sources have been built in all developed countries having population of 40 million or more, but also in less populated Canada, Australia, Switzerland, Taiwan, Sweden, Denmark and Singapore or just developing Brazil and Thailand. Each of the existing sources is surrounded by tens of beamlines where specific tasks are performed by the users. It is difficult to imagine a technologically advanced country without at least one intense light source; the number of sources in each of most developed countries, USA and Japan, is of the order of twenty.

The unique properties of the radiation and the huge research and development potential offered by synchrotron light sources have been explored by the community of Polish scientists from the very beginning and their scientific output is perceptible, especially in the time following the access to European Community. The synchrotron radiation users in Poland have formalized the existence of their community by creation of Polish Synchrotron Radiation Society (PSRS) in 1990. In 1998 the efforts to construct a synchrotron radiation source in Poland emerged. The goal was achieved in 2010 when the project “National Centre of Electromagnetic Radiation for Research Applications” (stage I) was granted. The project is run by Jagiellonian University and the facility will be located within the new University campus area, the new location for the Science Faculties and the site of the Jagiellonian Centre of Innovation - the Life Science Park.

Construction of the building accommodating the Polish Synchrotron “SOLARIS” started in

December 2011, the project completion is scheduled for September 2014. The SOLARIS building (for an artistic view see Fig. 1) will be ready in autumn 2013 and then the installation of the machine will start. The project is run in a very close collaboration with MAX-lab in Lund. SOLARIS synchrotron ring (96 m circumference) is a twin to the new 1.5 GeV facility of MAX IV project. Using the same design allowed for a fundamental reduction of the development and construction costs. Moreover, the modern, technologically advanced, novel Swedish design leads to improved parameters of the ring. The storage ring is composed of 12 magnet blocks forming a 12 double bend achromatic structures. Differences between the two projects will include the injector and the beamlines. SOLARIS, and its twin Swedish counterpart, are the first facilities in the new generation of compact, high current, high brilliance 1.5 GeV synchrotrons.

The synchrotron will be capable of delivering radiation in a broad spectral range. Its characteristics:

- particle energy 1.5 GeV (injection 0.6 – 0.7 GeV),
- current 500 mA,
- radiation energy at bending magnets — optimal at 0.1 – 5 keV (nominal critical energy 2 keV),
- radiation energy at wigglers — optimal at 2 – 20 keV, radiation available at still higher energies (~ 30 or more) (nominal critical energy 6 keV),
- radiation energy at undulators — individually tuned in a broad range beamlines

are considerably better than those for older 1.5 GeV machines.

Both, the bending magnets and insertion devices installed in the straight sections will be used for generation of radiation. Installation of up to 20 beamlines and still more experimental end stations will be possible. There is an opportunity to build 10 beamlines at bending magnets and 10 beamlines at wigglers (undulators). Each beamline may have more than one endstation, so there is a perspective that the number of endstations will be of the order of 40. The formal and financial status of the beamlines is under consideration. The budget of the project includes one experimental line. However, the initiatives for the next beamlines have emerged. The applications for funding of EXAFS beamline (led by University of Silesia), U-ARPES beamline (led by Jagiellonian University), have been submitted and further two applications for: diffraction beamline with 3 endstations (led by A. Mickiewicz University), and for in the infrared range studies beamline (led by University of Rzeszów,) are being completed. The community is asked to provide new beamline projects.

There are various scientific, economic, educational and social benefits which SOLARIS will bring to the community:

- as all intense light sources, it will become a center of modern materials science, solid state physics and chemistry and will be helpful in other domains (medicine, mineralogy, archaeometry, biology, forensic studies, ...),
- SOLARIS will attract foreign groups to conduct or participate in experiments here, promoting thus the experiment-base scientific exchange and collaboration on the basis of its unique beamlines,
- SOLARIS is going to be the first research infrastructure of such substantial size and potential constructed of the region. It will thus reduce the asymmetry still observed between the older and newer parts of EU, and hopefully will initiate further actions of this kind in the region (an important example is the project for building a free electron laser, POLFEL, in Świerk near Warsaw),
- it will play an important role in education at the graduate and post graduate level,
- as for the first time advanced material and device studies will become possible, Polish enterprises having access to SOLARIS will have an opportunity to become internationally competitive,
- reduction of the outflow of highly qualified manpower.

It is noteworthy, that on 20th March 2010, the SOLARIS Project has been awarded by the European Medal for the Functional and Application

Program and Technological Concept of SOLARIS (Fig. 2). The award was given in concert by three institutions: Integration office of European Union, Business Centre Club and the Socio-Economic European Committee.

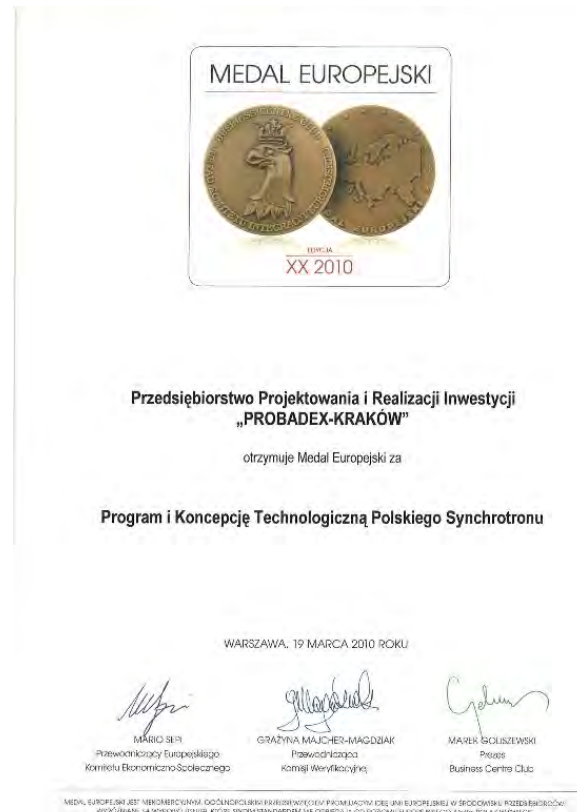


Figure 2: The European Medal for the Functional and Application Program and technological Concept of SOLARIS awarded in 2010 after acceptance of the project by the Ministry.

(For more details see pages 1 – 4 of this issue.)

Content

| | | | |
|---|---|--|----|
| W. Paszkowicz and M.J. Stankiewicz | SOLARIS — National Synchrotron Radiation Centre, the Polish research infrastructure roadmap facility. Status in spring 2012 | | I |
| | Content | | IV |
| C.J. Bocchetta, P. Goryl, K. Królas, M. Młynarczyk, M.J. Stankiewicz, P. Tracz, L. Walczak, A. Wawrzyniak, M. Eriksson, J. Ahlback, A. Andersson, P. Fernandes Tavares, M. Johansson, D. Kumbaro, S.C. Leeman, L. Malmgren, J. Modeer, S. Thorin, D. Einfeld, and E. Al-dmour | Project status of the Polish Synchrotron Radiation Facility SOLARIS | | 1 |
| M. Kozak, W. Rypniewski, and M. Jaskólski | Koncepcja budowy linii pomiarowej MX/SAXS/XRD w NCPS SOLARIS | | 5 |
| C. Habfast and G. Admans | ESRF Upgrade Programme Reaches Halfway Mark | | 10 |
| A. Kisiel | Dwadzieścia lat PTPS z perspektywy Prezesów. Wystąpienie na sesji KSUPS-9 w dniu 26 września 2011 r. | | 14 |
| | The 9 th National Meeting of Synchrotron Radiation Users (Warsaw 2011) | | 17 |

ISSRNS-11 — 11th International School and Symposium on Synchrotron Radiation in Natural Science

| | |
|--|----|
| Welcome to the 11 th ISSRNS | 18 |
| ISSRNS-11 — Information | 19 |
| Conference Schedule | 21 |

ISSRNS-11 — Invited lecturers and oral presentations

| | | | |
|---|---|---------------------|----|
| C.M. Schneider, M. Patt, V. Feyer, C. Wiemann, I.P. Krug, F. Nickel, D. Gottlob, and S. Cramm | Photoelectron spectromicroscopy — opportunities and challenges | L 01 <i>Ext.</i> | 24 |
| W. Rypniewski, P.H. Małecki, and C.V. Vorgias | Working hard and in the cold: Chitinase from <i>M. marina</i> | L 02 | 27 |
| P. Dumas | What role does synchrotron infrared micro-spectroscopy play in biomedical applications? | L 03 | 28 |
| M. Korbas, T.C. MacDonald, N.J. Sylvain, I.J. Pickering, G.N. George, and P.H. Krone | Shedding synchrotron light on mercury toxicity | L 04 <i>Ext.</i> | 29 |
| J. Chwiej, J. Kutorasinska, K. Janeczko, K. Gzielo-Jurek, L. Uram, K. Appel, R. Simon, and Z. Setkowicz | The progress of elemental anomalies of hippocampal formation in pilocarpine model of temporal lobe epilepsy — X-ray fluorescence microscopy study | O 01 | 31 |
| J. Czapla W.M. Kwiatek, J. Lekki, J. Dulińska, R. Steininger, and J. Göttlicher | The chemical species of sulphur in prostate cancer cells studied by XANES | O 02 | 32 |
| B. Ziaja-Motyka | European X-ray free electron laser: Status and applications | L 05 | 33 |

| | | | |
|---|---|---------------------|----|
| M. Gilski | Atomic resolution macromolecular crystallography with synchrotron radiation | L 06 | 34 |
| Z. Pietralik and M. Kozak | Complexation of nucleic acids by cationic gemini surfactant | O 03 | 35 |
| J. Kutorasinska, Z. Setkowicz, K. Janeczko, C. Sandt, P. Dumas, and J. Chwiej | Investigation of differences in frequency of creatine inclusions within hippocampal formation between the acute and latent periods of pilocarpine model of TLE-SRFTIR microspectroscopy study | O 04 | 36 |
| M. Stankiewicz | SOLARIS — new light for Polish research | L 07 | 37 |
| P. Olko and M. Jeżabek | National Centre for Hadron Radiotherapy — Bronowice Cyclotron Centre | L 08 <i>Ext.</i> | 38 |
| G. Wrochna, J.B. Pełka, R. Nietubyć, R. Sobierajski, and J. Sekutowicz | POLFEL – Polish Free Electron Laser from THz to XUV | L 09 | 40 |
| H. Tomizawa | The features and design overview of state-of-the-art XFEL | L 10 | 41 |
| A. Galler, W. Gawelda, K. Haldrup, K. Kjaer, T. van Driel, A.M. March, G. Doumy, E. Kanter, D. Ray, R. Dunford, J. Uhlig, S. Canton, G. Smolentsev, D. Fritz, M. Cammarata, H. Lemke, U. Bergmann, R. Alonso Mori, N. Sás, A. Bordage, G. Vankó, E. Gallo, P. Glatzel, K. Gaffney, V. Sundström, M.M. Nielsen, L. Young, S. Southworth, and C. Bressler | Observing molecular reactions via simultaneous ultrafast X-ray spectroscopy and scattering | L 11 <i>Ext.</i> | 42 |
| G. Dietler | Interplay between topology and statistical properties of DNA: A polymer physics approach | L 12 | 44 |
| M. Gateshki, H. te Nijenhuis, D. Beckers, A. Kharchenko, and M. Fransen | High-energy X-ray scattering studies of nanomaterials using a laboratory system | O 05 | 45 |
| T. Togashi, E.J. Takahashi, K. Midorikawa, M. Aoyama, K. Yamakawa, T. Sato, A. Iwasaki, S. Owada, K. Yamanouchi, T. Hara, S. Matsubara, T. Ohshima, Y. Otake, H. Tanaka, T. Tanaka, H. Tomizawa, T. Watanabe, M. Yabashi, and T. Ishikawa | Seeding of extreme ultraviolet free electron laser with high-order harmonic | L 13 | 46 |
| V. Petříček and M. Dušek | Solving and refining difficult structures by the program package JANA2006 | L 14 | 47 |
| C.J. Bocchetta | Techniques and technologies for ultra bright synchrotron light sources | O 06 | 48 |
| P. Rudolf | Graphene growth on Cu(111): Microscopic angle-resolved photoemission and scanning tunneling microscopy investigations | L 15 | 49 |
| V.M. Kaganer | X-ray diffraction peak profiles from relaxed epitaxial films | L 16 | 50 |
| A. Bartnik, P. Wachulak, H. Fiedorowicz, R. Jarocki, J. Kostecki, and M. Szczurek. | Luminescence of gases induced with EUV pulses from a laser plasma source | O 07 <i>Ext.</i> | 51 |

| | | | |
|---|---|---------------------|----|
| P.W. Wachulak, A. Baranowska-Korczyc, D. Pánek, P. Brůža, A. Bartnik, J. Kostecki, L. Węgrzyński, R. Jarocki, M. Szczurek, D. Elbaum, and H. Fiedorowicz | Imaging in nanoscale using laser-plasma sources of extreme ultraviolet (EUV) | O 08 | 53 |
| A. Marcelli, K. Zhang, Z. Wu, V. Della Corte, A. Rotundi, G. Della Ventura, M. Ferrari, F.J.M. Rietmeijer, and E. Pace | X-ray CT scan of stratospheric micron-sized dust particles: An attempt to a non-destructive morphological reconstruction | L 17 | 54 |
| H. Oyanagi | Nanocrystals and small clusters investigated by synchrotron radiation and microfluidics | L 18 | 55 |
| F. Masiello, S.H. Connell, and J. Härtwig | Measurement of residual strains with quantitative X-ray topography | O 09 | 56 |
| C. Pettenkofer and A. Hofmann | Energy converting interfaces studied by synchrotron radiation | L 19 | 57 |
| M. Taniguchi | Electronic and spin structures of solids by means of synchrotron radiation photoemission | L 20 <i>Ext.</i> | 58 |
| K. Lawniczak-Jablonska, A. Wolska, M.T. Klepka, and V. Sessi | XMCD studies of the magnetic properties of nanoclusters in GaAs matrix | O 10 | 60 |
| C.S. Fadley | Probing the electronic and magnetic properties of bulk materials and buried layers and interfaces with standing-wave and hard-x-ray photoemission | L 21 <i>Ext.</i> | 61 |
| M. Sikora | Electronic structure of A_2FeReO_6 double perovskites probed with Re 2p RXES | O 11 | 63 |
| A. Rogalev and F. Wilhelm | X-ray Magnetic Circular Dichroism under high magnetic field | O 12 | 64 |
| P. Zajdel, A. Kisiel, A. Szytuła, P. Starowicz, J. Goraus, J. Konior, A. Banaś, A. Balerna, G. Cinque, A. Grilli | Valence of constituents of selected rare earth silicides — XANES and LAPW numerical study | O 13 <i>Ext.</i> | 65 |
| A. Fernández-Pacheco, A. Szkudlarek, L.E. Serrano-Ramón, T. Tyliczszak, Cz. Kapusta, M.R. Ibarra, and J.M. De Teresa | Studies of cobalt nanoconstrictions by scanning transmission X-ray microscopy and micromagnetic simulations | O 14 | 67 |
| Cz. Kapusta, M. Sikora, J. Przewoźnik, J. Żukrowski, J. Fedotova, and J. Kasiuk | Study of magnetoresistive nanogranular films with X-ray spectroscopies | L 22 | 68 |
| E. Guzewicz, B.A. Orlowski, A. Reszka, L. Wachnicki, S. Gieraltowska, M. Godlewski, I.A. Kowalik, B.J. Kowalski, and R.L. Johnson | Resonant photoemission of 4f electrons on clean semiconductor surfaces | L 23 <i>Ext.</i> | 69 |
| J. Kubacki, D. Kajewski, J. Szade, A. Köhl, Ch. Lenser, R. Dittmann, K. Szot, and K. Schulte | Resonant photoemission studies of Fe doped $SrTiO_3$ thin films | O 15 | 71 |
| P. Goryl, C.J. Bocchetta, M.J. Stankiewicz, A.I. Wawrzyniak, K. Wawrzyniak, M. Zajęc, Ł. Żytniak, and D. Spruce | The Solaris concepts for the beamlines control systems | O 16 | 72 |

| | | | |
|--|--|---------------------|----|
| M. Kozak, M. Taube, M. Murawska, V. Lindström, and A. Grubb | Structural studies of covalently stabilised oligomers of human cystatin C | O 17 | 73 |
| H. Drozdowski, A. Romaniuk, and, Z. Błaszczak | Structure and intermolecular interactions in selected binary solutions studied by X-ray methods | O 18 | 74 |
| K. Won-in, T. Sako, W. Pattanasiriwisana, S. Tancharakorn, and P. Dararutana | Characterization of ancient burnt rice excavated in Thailand archaeological sites | O 19 | 75 |
| J. Kowalska, W.M. Kwiatek, M. Gajda, K. Appel, and P. Dumas | Effect of AVE 0991 – angiotensin-(1-7) receptor agonist treatment on elemental and biomolecules distribution in atherosclerotic plaques of apoE-knockout mice | O 20 <i>Ext.</i> | 76 |
| A. Kubala-Kukuś, D. Banaś, M. Pajek, J. Szlachetko, J.-Cl. Dousse, J. Hoszowska, Y. Kayser, S. Nowak, P. Jagodziński, J. Susini, and M. Salomé | Synchrotron radiation based micro X-ray fluorescence analysis of the calibration samples used in surface sensitive TXRF and GEXRF techniques | O 21 <i>Ext.</i> | 78 |

ISSRNS–11 — Poster presentations

| | | | |
|---|---|---------------------|----|
| K. Balin, J. Szade, and Z. Celinski | Reversible valency transitions of europium in MBE grown Eu-Mn thin films | P 01 | 80 |
| D. Banaś, J. Braziewicz, A. Kubala-Kukuś, U. Majewska, M. Pajek, J. Wudarczyk-Moćko, K. Czech, M. Garnuszek, P. Słomkiewicz, and B. Szczepanik | Study of absorption properties of chemically modified halloysite samples with X-ray fluorescence and X-ray powder diffraction methods | P 02 | 81 |
| K. Banas, A.M. Banas, M. Gajda, W.M. Kwiatek, B. Pawlicki, and M.B.H. Breese | Analysis of synchrotron radiation induced X-ray emission spectra with R environment | P 03 | 82 |
| A. Baranowska-Korczyn, K. Fronc, J.B. Pełka, K. Sobczak, P. Dłużewski, and D. Elbaum | Structural studies of magnetic Fe doped ZnO nanofibers | P 04 | 83 |
| M.R. Bartosik, C.J. Bocchetta, P. Goryl, M.J. Stankiewicz, P. Tracz, L. Walczak, A.I. Wawrzyniak, K. Wawrzyniak, J. Wiechecki, M. Zajęc, and L. Żytniak | SOLARIS — National Synchrotron Radiation Centre, project progress, May 2012 | P 05 <i>Ext.</i> | 84 |
| J. Bielecki, E. Lipiec, and W.M. Kwiatek | First-principle approach to interpretation of changes in IR spectra of cellular DNA | P 06 | 86 |
| K. Biernacka, M. Sikora, Cz. Kapusta, A. Brudnik, K. Zakrzewska, and M. Radecka | X-ray absorption and emission spectroscopy of titanium dioxide with modified anionic sublattice | P 07 | 87 |
| M. Brancewicz, A. Andrejczuk, E. Żukowski, L. Dobrzyński, Y. Sakurai, and M. Itou | Compton profile of Mg single crystal: High resolution experiment and theory | P 08 | 88 |
| K.M. Dębrowski, D.T. Dul, M. Tolkiehn, D.V. Novikov, and P. Korecki | Detection of X-ray absorption anisotropy using fluorescence radiation for atomic resolved imaging | P 09 | 89 |
| I.N. Demchenko, R. Minikayev, T. Tyliczszak, M. Chernyshova, K.M. Yu, J.D. Denlinger, D. Speaks, and W. Walukiewicz | Electronic structure of irradiated CdO thin films | P 10 | 90 |

| | | | |
|---|---|------|-----|
| A. Dowierciał, A. Jarmuła, W.R. Rypniewski, T. Frączyk, P. Wilk, and W. Rode | Searching for the differences between <i>trichinella spiralis</i> and mouse thymidylate synthases: A quest for species-specific drugs | P 11 | 91 |
| H. Drozdowski, T. Hałas, and Z. Błaszczak | A molecular structure study of 1,3,5-trichlorobenzene | P 12 | 92 |
| H. Drozdowski, A. Romaniuk, and Z. Błaszczak | The determination of molecular structure of chloroanisoles by X-ray diffraction | P 13 | 93 |
| J. Dudala, M. Szczerbowska-Boruchowska, M. Lankosz, and M. Białas | Distribution of biomolecules in the adrenal gland tumors — FTIR results compared with histological view of samples | P 14 | 94 |
| D.T. Dul and P. Korecki | Wavelet analysis of X-ray absorption anisotropy: Accuracy and limitations of atomic structure imaging | P 15 | 95 |
| E. Dynowska, J.Z. Domagała, P. Romanowski, E. Janik, P. Wojnar, and W. Caliebe | Structural characterization of the core-shell ZnTe/ZnMgTe nanowires | P 16 | 96 |
| E. Dynowska, W. Paszkowicz, P. Aleshkevych, L. Gładczuk, W. Szuszkiewicz, S. Müller, C. Ronning, and W. Caliebe | Observation of extremely slow ordering effects in Co-implanted ZnO | P 17 | 97 |
| K. Dziedzic-Kocurek and J. Stanek | XANES evaluation of iron local structures in monomer and dimersed forms of porphyrins | P 18 | 98 |
| O.N. Ermakova, R. Minikayev, H. Dabkowska, C. Lathe, J. de Groot, and W. Paszkowicz | Elastic properties of praseodymium orthovanadate | P 19 | 99 |
| P. Jagodziński, M. Pajek, D. Banaś, A. Kubala-Kukuś, J. Szlachetko, J.-Cl. Dousse, J. Hoszowska, Y. Kayser, and S. Nowak | Simulations of X-ray transmission in polycapillaries for synchrotron radiation applications | P 20 | 100 |
| A. Jarmuła, A. Dowierciał, P. Wilk, W.R. Rypniewski, B. Kierdaszuk, and W. Rode | Crystal structures of mouse thymidylate synthase in binary complex with a strong inhibitor, N(4)-OH-dCMP, and ternary complex with N(4)-OH-dCMP and the cofactor product, dihydrofolate | P 21 | 101 |
| M. Johansson, R. Nietubyć, and A. Wawrzyniak | Linac and storage ring magnets for SOLARIS synchrotron | P 22 | 102 |
| Z. Kaszukur | XRD study of uniformity and interdiffusion in PdCo and PdAg nanoalloys | P 23 | 103 |
| W. Kida and M. Kozak | Influence of gemini surfactants with different chain length on the structure of DPPC bilayers | P 24 | 104 |

| | | | |
|--|--|------|-----|
| D. Klinger, R. Sobierajski, J. Pelka, E. Lusakowska, D. Żymierska, W. Wierzchowski, K. Wieteska, T. Balcer, J. Chalupský, V. Hájková, T. Burian, A.J. Gleeson, L. Juha, K. Tiedtke, S. Toleikis, L. Vyšín, H. Wabnitz, and J. Gaudin | Damage of two-component materials such as GaAs, ZnO, SiO ₂ created after irradiation by ultra-short VUV laser pulses | P 25 | 105 |
| W. Knoff, M.A. Pietrzyk, A. Reszka, B.A. Orłowski, T. Story, and R.L. Johnson | Photoemission study of amorphous and crystalline GeTe and (Ge,Mn)Te semiconductors | P 26 | 106 |
| B. Korczyk, A. Bartnik, J. Kostecki, and H. Fiedorowicz | Changes in chemical and physical structure of polymers under EUV radiation | P 27 | 107 |
| I.A. Kowalik, M.I. Lukaszewicz, E. Guziewicz, M. Godlewski, F.J. Luque, M.A. Nino, A. Zakharov, and D. Arvanitis | Electronic structure and magnetism of (Zn,Co)O films: A soft x-ray spectroscopy study | P 28 | 108 |
| B.J. Kowalski, R. Nietubyć, and J. Sadowski | Resonant and angle-resolved photoemission spectroscopy of Ga _{1-x} Mn _x Sb | P 29 | 109 |
| A. Kubala-Kukuś, M. Ludwikowska-Kędzia, D. Banaś, J. Braziewicz, U. Majewska, M Pajek, and J. Wudarczyk-Moćko | Application of the X-ray fluorescence analysis and X-ray diffraction in geochemical studies of till samples | P 30 | 110 |
| K. Lawniczak-Jablonska, M.T. Klepka, A. Wolska, and M.A. Borysiewicz | The X-ray absorption studies of the Ti-Si-C films stoichiometry in function of the technological parameters | P 31 | 111 |
| E. Lipiec, G. Birarda, J. Lekki, L. Vaccari, A. Wiecheć, and W.M. Kwiatek | First approach of the FTIR microspectroscopy for studying the effect of ionising radiation in single cells | P 32 | 112 |
| A.F. Mabied, S. Nozawa, M. Hoshino, A. Tomita, T. Sato, and S. Adachi | Singular value decomposition analysis of time-resolved powder diffraction data | P 33 | 113 |
| M. Małachowski and M. Kozak | Crystallisation of polymer phases and its influence on structure and mechanical properties of multilayered polymer systems | P 34 | 114 |
| P. Mazalski, Z. Kurant, A. Maziewski, M.O. Liedke, J. Fassbender, L.T. Baczewski, A. Wawro, A. Rogalev, and F. Wilhelm | XAS/XMCD studies of Pt/Co/Pt nanostructures with out-of-plane magnetization induced by Ga ⁺ ions low fluence irradiation | P 35 | 115 |
| J. Mesjasz-Przybyłowicz, A. Barnabas, I. Yousef, P. Dumas, F. Jamme, Ch. Sandt, F. Guillon, P. Sechogela, and W. Przybyłowicz | Differences and similarities in roots of the nickel hyperaccumulating and non-accumulating genotypes of <i>Senecio coronatus</i> from South Africa | P 36 | 116 |

| | | | |
|--|---|---------------------|-----|
| J. Mesjasz-Przybylowicz, E. Montargès-Pelletier, A. Barnabas, G. Echevarria, V. Briois, P. Sechogela, S. Groeber, and W. Przybylowicz | Distribution and speciation of nickel in hyperaccumulating plants from South Africa | P 37 | 117 |
| R. Minikayev, E. Dynowska, T. Story, A. Szczerbakow, A.M.T. Bell, D. Trots, and W. Szuszkiewicz | X-ray studies of thermal properties of $Pb_{1-x}Cd_xTe$ solid solution in a broad temperature range | P 38 | 118 |
| R. Minikayev, W. Paszkowicz, P. Piszora, M. Knapp, C. Bähz, and S. Podsiadło | Thermal expansion of gallium nitride | P 39 | 119 |
| M. Murawska, A. Grubb, and M. Kozak | Small angle X-ray scattering (SAXS) studies of monomeric human cystatin C in solution | P 40 | 120 |
| M. Murawska, K. Smolarek, A. Skrzypczak, and M. Kozak | Rod-like morphology of silver nanoparticles produced in cationic gemini surfactants systems | P 41 | 121 |
| M. Murawska, M. Wiatr, P. Nowakowski, K. Szutkowski, A. Skrzypczak, and M. Kozak | The structure and morphology of gold nanoparticles produced in cationic gemini surfactants systems | P 42 | 122 |
| A. Nasr, U. Werthenbach, H.W. Schenk, and A.H. Walenta | Multi-channel ionization chamber development for synchrotron beam fluctuation monitoring and time resolve measurement | P 43 | 123 |
| B.A. Orlowski, A. Szczerbakow, P. Dziawa, K. Gas, A. Reszka, S. Thiess, and W. Drube | Photoemission binding energy local change caused by crystalline local structure | P 44 <i>Ext.</i> | 124 |
| C. Paluszkiwicz, W.M. Kwiatek, and E. Stodolak | Characterization of polymer nanocomposites by mikro SR-FTIR spectroscopy | P 45 <i>Ext.</i> | 126 |
| W. Paszkowicz, O.N. Ermakova, W. Wierzchowski, K. Wieteska, M. Berkowski, M. Głowacki, H. Dąbkowska, J. Domagała, J. Bąk-Misiuk, and C. Paulmann | Topographic and high-resolution diffraction study of defect structure of RVO_4 single crystals | P 46 <i>Ext.</i> | 128 |
| W. Paszkowicz, R. Minikayev, P. Piszora, M. Knapp, D. Trots, and R. Bacewicz | Thermal expansion of $CuInSe_2$ | P 47 <i>Ext.</i> | 130 |
| W. Paszkowicz, P. Piszora, R. Minikayev, M. Brunelli, and A. Fitch | Thermal expansion of polycrystalline cBN in the low-temperature range | P 48 | 132 |

| | | | |
|---|---|------|-----|
| J.B. Pełka, O. Chołuj-Dziewiecka, J. Lorkiewicz, R. Nietubyć, J. Sekutowicz, R. Sobierajski, J. Szewiński, T. Wasiewicz, and G. Wrochna | Terahertz FEL source at the Polish National Center POLFEL. A conceptual design | P 49 | 133 |
| Z. Pietralik, M. Kręcisz, and M. Kozak | Spectroscopic and structural studies of interactions between gemini surfactants and phosphatidylcholine derivatives | P 50 | 134 |
| Z. Pietralik, R. Krzysztoń, and M. Kozak | Structural analysis of selected gemini surfactant (1-imidazolilo-3-decylooxymethyl) pentane chloride lipoplexes | P 51 | 135 |
| Z. Pietralik, I. Mucha-Kruczyńska, and M. Kozak | FTIR analysis of protein secondary structure in solid and solution states | P 52 | 136 |
| P. Piszora and J. Darul | Hydrogen reduction of LiMn_2O_4 : Identification of products with synchrotron X-ray powder diffraction | P 53 | 137 |
| A. Romaniuk, H. Drozdowski, and Z. Błaszczak | X-ray diffraction study of some liquid binary solutions | P 54 | 138 |
| P. Romanowski, J. Bąk-Misiuk, K. Sobczak, P. Dziawa, E. Dynowska, A. Szczepańska, and A. Misiuk | Mn_4Si_7 nanoinclusions in Mn-implanted Si | P 55 | 139 |
| K. Schneider, M. Sikora, J. Stępień, K. Biernacka, Cz. Kapusta, D. Zajac, K. Michalow-Mauke, Th. Graule, A. Vital, K. Zakrzewska, and M. Rekas | XAS study of Mo doped TiO_2 nanoparticle materials | P 56 | 140 |
| W. Sławiński, R. Przeniosło, I. Sosnowska, and V. Petricek | Helical screw-type magnetic structure of the multiferroics $\text{CaMn}_7\text{O}_{12}$ | P 57 | 141 |
| R. Sobierajski, J.B. Pełka, R. Nietubyć, G. Wrochna, and J. Sekutowicz | XFEL — European X-ray Free Electron Laser | P 58 | 142 |
| R. Sobierajski, D. Klinger, P. Dłużewski, M. Klepka, J. Gaudin, C. Özkan, J. Chalupský, S. Bajt, T. Burian, L. Vyšín, N. Coppola, S.D. Farahani, H.N. Chapman, G. Galasso, V. Hájková, M. Harmand, L. Juha, M. Jurek, R. Loch, S. Mölle, M. Nagasono, H. Sinn, K. Saskl, J. Schulz, P. Sovak, S. Toleikis, K. Tiedtke, T. Tschentscher, and J. Krzywinski | Damage of multilayer optics under irradiation with multiple femtosecond XUV pulses | P 59 | 143 |

| | | | |
|--|--|---------------------|-----|
| W. Szczerba, J. Kaiser, H. Riesemeier, U. Reinholz, M. Radtke, L. Yu, M. Ballauff, and A.F. Thünemann | On the local structure of catalytic Au/Pd nanoparticles stabilized on spherical polyelectrolyte brushes | P 60 | 144 |
| W. Szczerba, H. Riesemeier, U. Reinholz, M. Radtke, and A.F. Thünemann | Combined small angle X-ray scattering and X-ray absorption spectroscopy studies of electrochrome metallopolyelectrolytes | P 61 | 145 |
| W. Szczerba, H. Riesemeier, U. Reinholz, M. Radtke, A.F. Thünemann, A. Kaupner, and C. Giordano | Local structure of iron carbide nanoparticles | P 62 | 146 |
| M. Szczerbowska-Boruchowska, M. Lankosz, M. Czyzycki, A. Wandzilak, P. Wrobel, E. Radwanska, and D. Adamek | Synchrotron radiation based studies of the elemental composition and chemical forms of Fe and Zn in brain gliomas | P 63 | 147 |
| M. Szczerbowska-Boruchowska, P. Wrobel, A. Sorowka, E. Radwanska, and D. Adamek | Evaluation of the variability in elemental composition of dopamineergic neurons in senile brains using synchrotron radiation based X-ray fluorescence | P 63a | 148 |
| J. Szlachetko, M. Nachtegaal, J.-Cl. Dousse, J. Hozzowska, E. Kleymenov, M. Janousch, J. Sa, O.V. Safonova, and J.A. van Bokhoven | Direct XES to XAS relation for off-resonant excitations at L3 absorption edge: Towards high-resolution XAS at single-shot | P 64 | 149 |
| Cz. Ślusarczyk | Structure development during isothermal crystallization of high-density polyethylene: Synchrotron small-angle X-ray study | P 65 | 150 |
| W. Tokarz, M. Kowalik, R. Zalecki, and A. Kołodziejczyk | Electronic band structure of $\text{La}_{0.67}\text{Pb}_{0.33}\text{Mn}_{0.92}\text{Fe}_{0.08}\text{O}_3$ | P 66 | 151 |
| L. Walczak, J. Alhback, M. Berglund, E. Al-dmour, J. Pasquaud, P. Fernandes Tavares, M. Eriksson, D. Einfeld, C.J. Bocchetta, and M.J. Stankiewicz | Vacuum system of the Polish light source — SOLARIS | P 67 | 152 |
| D. Wardecki, R. Przeniosło, A. Fitch, M. Bukowski, and R. Hempelmann | Size dependence of microstrain fluctuations in nanocrystalline chromium | P 68 | 153 |
| A. Wiecheć, E. Lipiec, J. Lekki, M. Widel, and W.M. Kwiatek | SR-FTIR spectroscopy in study of the double strand breaks in single cells irradiated by proton microbeam | P 69 | 154 |
| K. Wieteska, W. Wierzchowski, A. Malinowska, M. Lefeld-Sosnowska, M. Swirkowicz, T. Lukasiewicz, and C. Paulmann | Synchrotron diffraction topography of SBN ($\text{Sr}_x\text{Ba}_{1-x}\text{Nb}_2\text{O}_6$) and CBN ($\text{Ca}_x\text{Ba}_{1-x}\text{Nb}_2\text{O}_6$) crystals | P 70 <i>Ext.</i> | 155 |

| | | | |
|---|---|---------------------|-----|
| W. Wierzchowski, K. Wieteska, D. Klinger, R. Sobierajski, J. Pelka, D. Zymierska, T. Balcer, and C. Paulmann | The investigations of the damages induced by flash pulses in silicon crystals by means of white beam synchrotron section topography | P 71 <i>Ext.</i> | 157 |
| A. Wolska, K. Lawniczak-Jablonska, M.T. Klepka, and V. Sessi | XMCD studies of the GaSb:MnSb layers on the GaSb and GaAs substrates | P 72 | 159 |
| D.A. Zajac, A. Bikowski, M. Vinnichenko, and K. Ellmer | Near-order structure of transparent conducting oxides: X-ray absorption study of Al-doped ZnO and ZnMgO films | P 73 | 160 |
| D.A. Zając, W.M. Woch, J. Stępień, Cz. Kapusta, A. Kołodziejczyk, H. Sudra, and G. Gritzner | XANES and EXAFS study of $(\text{Tl}_{0.5}\text{Pb}_{0.5})\text{Sr}_2(\text{Ca}_{1-x}\text{Gd}_x)\text{Cu}_2\text{O}_z$ superconductors | P 74 | 161 |
| P. Zajdel, I. Jendrzewska, J. Goraus, T. Goryczka, and T. Mydlarz | Local electronic structure and physical properties of $\text{Zn}_{1-x}\text{Ni}_x\text{Cr}_2\text{Se}_4$ | P 75 | 162 |
| | Synchrotron Light News | | 163 |
| | ISSRNS climbs to the top: Three proceedings papers on the <i>Radiation Physics and Chemistry</i> Top25 list | | 177 |
| A. Katrusiak | Frolic GOATS workshops on high pressure diffraction | | 178 |
| A. Kuczumow | Jubileuszowe X Krajowe Sympozjum Użytkowników Promieniowania Synchrotronowego | | 179 |
| | Future conferences and workshops | | 180 |
| | Conference proceedings of meetings organised by Polish Synchrotron Radiation Society (1992 – 2012) | | 182 |
| | Authors Index | | 183 |
| | Subject Index | | 186 |

ISSRNS–11 — Abstracts missing in the printed version

| | | | |
|---|---|---------------------|-----|
| E. Guzewicz, M.I. Łukasiewicz, K. Kopalko, L. Wachnicki, M. Godlewski | Co 3d states in ferromagnetic and paramagnetic (Zn, Co)O films – resonant photoemission studies | P 76 <i>Ext.</i> | 188 |
|---|---|---------------------|-----|

PROJECT STATUS OF THE POLISH SYNCHROTRON RADIATION FACILITY SOLARIS¹⁾

C.J. Bocchetta^{1*}, P. Goryl¹, K. Królas¹, M. Młynarczyk¹, M.J. Stankiewicz¹, P. Tracz¹,
L. Walczak¹, A. Wawrzyniak¹, M. Eriksson², J. Ahlback², A. Andersson²,
P. Fernandes Tavares², M. Johansson², D. Kumbaro², S.C. Leeman², L. Malmgren²,
J. Modeer², S. Thorin², D. Einfeld³, and E. Al-dmour³

¹*National Synchrotron Radiation Centre Solaris at the Jagiellonian University, Kraków, Poland*

²*MAX-lab, Lund, Sweden*

³*CELLS-ALBA Synchrotron, Cerdanyola del Valles, Spain*

Abstract The Polish synchrotron radiation facility Solaris is being built at the Jagiellonian University in Krakow. The project is based on an identical copy of the 1.5 GeV storage ring being concurrently built for the MAX IV project in Lund, Sweden. A general description of the facility is given together with a status of activities. Unique features associated with Solaris are outlined, such as infrastructure, the injector and operational characteristics.

*e-mail: carlo.bocchetta@uj.edu.pl

1. INTRODUCTION

The first ideas for a national synchrotron radiation facility in Poland were put forward in 1998 and several proposals made in subsequent years. In 2008 the government pledged funds of 143 MPLN with formal allocation after approval of a feasibility study from the Jagiellonian University for the construction of a light source with such a budget. In 2009 this study, based on the innovative ideas and technology of MAX-lab (ref. MAX III, [2]), was submitted and the National Synchrotron Radiation Centre Solaris was approved for construction in February 2010 using EU structural funds. The facility will be built on land allocated by the Jagiellonian university on the new campus in Krakow. In December 2010 an agreement was signed between the Jagiellonian University and Lund University Sweden, for the mutual cooperation and sharing of ideas and designs related to the construction of the two facilities. Solaris will be an identical copy of the 1.5 GeV ring of the MAX IV project and will use identical parts of the linac injector and transfer line [2, 3]. Major differences between the two machines are the infrastructures, the lower energy linac and the beamlines.

2. FACILITY

Building

The synchrotron radiation facility will be built at the campus III site of the Jagiellonian University in the city of Krakow. The land with an area of ~ 22000 m² will site the machine, experimental hall, auxiliary service buildings, laboratories, offices and auditorium. The contract for the design and construction was awarded in the March 2011 to the consortium of companies: ALPINE Con-

struction Polska Spółka z o.o. and Przedsiębiorstwo Budowlano-Produkcyjne ŁĘGPRZEM Spółka z o.o. The building permit was granted in December 2011 and the construction is in progress. The building is composed of a linac tunnel and an adjacent modulator and service gallery placed below the storage ring level. The length of the tunnel ~ 100 m, within the constraints of land availability, foresees an upgrade to the linac to increase its energy for top-up injection. All services, power, HVAC and cooling will be built with this upgrade in mind. The experimental hall for beamlines houses the storage ring tunnel. The experimental hall has a surface area of 3000 m² and provision is made for its future extension on one side by 600 m². Access to the storage ring tunnel will be through chicanes on the inner side and the roof shielding will be removable for machine installation and maintenance. All equipment for the storage ring will be housed on the inner side of the ring tunnel. A crane, rated at 8 tonnes, spanning the experimental hall, will be used for machine and beamline installation and maintenance.

Injector

The linac injector for Solaris will initially be operated at 550 MeV with options for a full energy upgrade. The linac is composed of an RF gun and six normal conducting 3 GHz accelerating sections, of length 5.2 m, grouped into three units containing two accelerating sections [2]. Each unit will be powered through SLED cavities fed by a solid-state modulator driving a klystron. The linac sections are being manufactured by Research Instruments GmbH (D) and will have a guaranteed performance of 20 MV/m. The RF power from the SLED cavities feeding each unit will be split equally to the two linac sections. The first unit, however, will be configured to deliver RF power to the gun too.

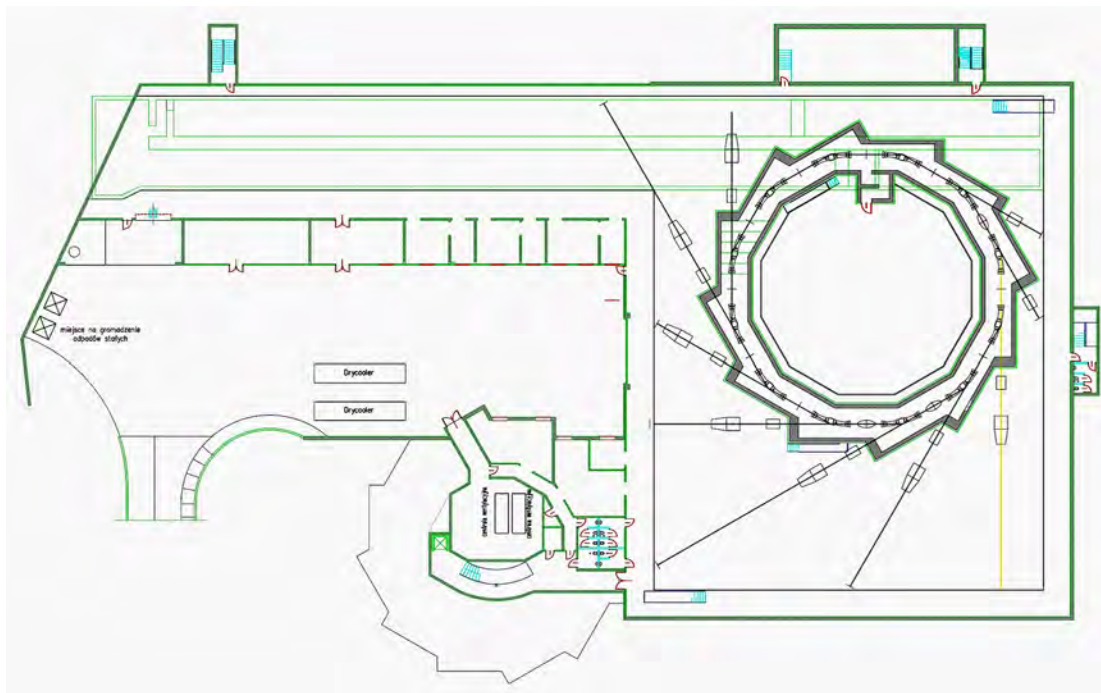


Figure 1: Concept layout of the facility. The experimental hall can be extended by 10 m on the right hand side at a later date. Above the linac tunnel ample covered space is available for pre-assembly and general laboratories.

In this case the first linac section will be given more RF power. The solid-state modulators, ordered and being manufactured by ScandiNova Systems AB (S), will power 35 MW klystrons at 10 Hz. The electron gun will be an upgraded version of that presently used at MAXlab. It will have a BaO cathode and a 180° bending magnet will be used for energy filtering.

Transfer line

The beam is transferred to the storage ring via a 27° vertical ramp. The linac will initially be placed close to the storage to reduce the length of transfer line and the gun relocated when the full energy upgrade will be performed. The vertical ramp is optically mirror symmetric and composed of two pulsed 10° magnets, two dipole magnets deflecting 17° and six quadrupoles. The pulsed dipole magnet in the linac tunnel in combination with a kicker magnet will in the future be used to share the linac beam between topping up and possible FEL experiments. The pulsed septum magnet at the end of the transfer line is a vertical Lamberston type, deflecting the beam into the horizontal plane. All magnets and power supplies are identical to MAX IV systems.

Injection process

Injection into the storage ring will be performed with a pulsed sextupole magnet [4, 5]. The scheme has many advantages over a conventional four-kicker injection bump especially for top-up operation. In the case of Solaris with straight section lengths of 3.5 m, a fourkicker scheme would require it to span two achromat sections that contain strong

sextupoles and large dispersion that would affect the stored beam. Furthermore the conventional scheme would reduce the available space for insertion devices. The use of a pulsed sextupole magnet will simplify the scheme and circumvent the aforementioned disadvantages. The injection dynamics at a lower energy compared to the MAX IV case is considered in reference [4]. Care must be taken in the design of the pulsed sextupole magnet and associated power supply given the 320 ns revolution time of the storage ring, since a two turn injection scheme is less efficient compared to a single turn scheme. The possibility of using a single dipole kicker is also being evaluated to help facilitate the commissioning of the pulsed sextupole scheme [6]. Once accumulated the beam will be ramped to its final energy of 1.54 GeV. The behaviour and response of the magnets during ramping is expected to be similar to that of MAX III.

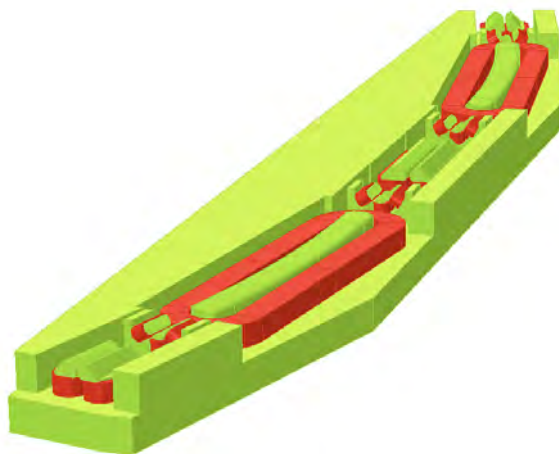


Figure 2: Magnet half block with coils in red [7].

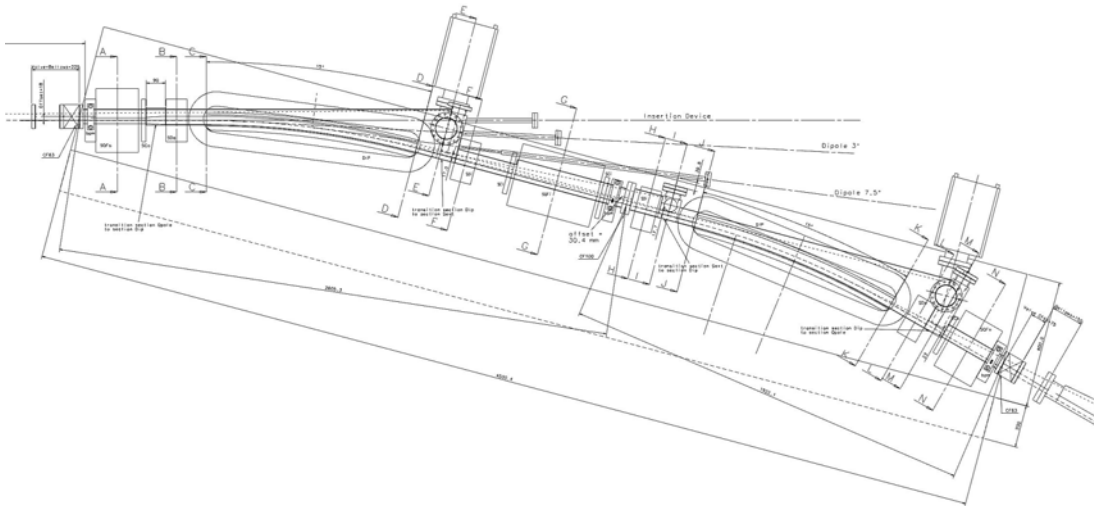


Figure 3: Preliminary vacuum chamber in stainless steel with antechambers [9].

Storage Ring Technology

The storage ring will be technologically identical to the MAX IV 1.5 GeV ring and is composed of 12 magnet blocks forming a 12 double bend achromatic structure. Bending magnet synchrotron radiation will be extracted for users from the first dipole in the achromat. The iron blocks machined to high precision will contain all magnetic elements allowing for a very compact design. The iron for the magnets has been purchased and is being thermally treated prior to machining. Magnet design [7] is in the final stages of completion and is being performed in parallel with the design activities of the vacuum chamber.

An evaluation has been performed of the technology to be used for the vacuum system. Both a wholly NEG coated chamber, similar to that adopted for the MAX IV 3.0 GeV ring [8], and a conventional system with antechamber and absorbers were examined. A conventional stainless-steel system was chosen on the basis of manufacturer availability, costs, technology requirements and project time-schedule. The vacuum system is being designed and the construction drawings prepared by the group from CELLS-ALBA Synchrotron in Cedanyola del Valles (E) in collaboration with MAXlab and Solaris. The system and magnet configuration foresees extraction of bending magnet radiation at either 3 or 7.5 degrees from the first bending magnet of the achromat.

The storage ring RF system is composed of two 100 MHz cavities similar to those used in MAX II and III. The cavities are normal conducting and of the capacity loaded type that have relatively high frequency higher order modes compared to pill-box type cavities. The cavities will be equipped with higher order mode coupling loops that will extract the residual high frequency modes. Cavities and couplers have been ordered and are being manufactured by Research Instruments GmbH. The ring also foresees operation with two passive Landau

cavities at 300 MHz as designed by MAX-lab similar to the main cavities [10]. Either solid state or tetrode amplifiers will power the main cavities. Two such amplifiers will be combined to provide 60 kW of power per cavity via a circulator. The RF units will be controlled with a digital LLRF system.

Optics and Dynamics

The integrated magnets permit an ultra-compact double bend achromatic structure with low emittance and zero dispersion in the straight sections. The compact magnet design has three quadrupoles that focus in the horizontal plane while the vertical focusing is done by the gradient in the dipoles. Pole strips on the bending magnets will allow tuning of the vertical focusing. The focusing sextupoles have also been integrated into the focusing quadrupoles. Recently the lattice has been optimised for the ramped operation in Solaris where Touschek lifetime is important since the facility will not operate in top-up mode but in decay mode. The optimisation has focused on increasing the momentum acceptance by ensuring the lattice momentum acceptance match the RF acceptance of 4%. Together with the use of Landau cavities the Touschek lifetime at 500 mA is expected to reach 13 hours [6]. In each magnet block there will be three BPMs and three horizontal/vertical corrector coils mounted on the sextupole magnets. Two of the BPMs will be positioned at the ends of the achromatic block and one in the centre.

Table 1: 1.5 GeV Storage Ring Parameters

| | |
|--|-----------------------|
| Current | 500 mA |
| Circumference | 96 m |
| Horizontal emittance (bare lattice) | 6 nm rad |
| Coupling | 1% |
| Tunes Q_x, Q_y | 11.22, 3.14 |
| Natural chromaticities ξ_x, ξ_y | -22.9, -17.1 |
| Momentum compaction | 3.04×10^{-3} |
| Momentum acceptance | 4% |

Beamlines

For the first phase of the project one beamline is planned to be financed from the project budget. The beamline will use bending magnet radiation and will have a X-PEEM/XAS/XMCD end-station. This activity is in cooperation with PSI. Funding proposals have been submitted for additional beamlines from undulators.

3. SCHEDULE AND MILESTONES

The project deadline for first light is the third quarter of 2014. The building construction has started and the beneficial occupancy of the building is programmed for the end of August 2013. Component schedules and purchasing milestones are linked to the MAX IV project schedule and are compatible with Solaris installation.

4. CONCLUSIONS

The Solaris project is a prime example of the benefits of sharing of state-of-the-art knowledge and resources for the rapid establishment of a national research infrastructure. Scientific collaboration is certainly not new in the field of accelerators but the direct utilisation of a design and its complete replication is unique. The collaboration maximises the utilisation of human and financial capital leading to more effective and efficient use of public funds. The collaboration permits quick training of new people with an initial focus on mobility and networking and an optimal use of mentorship and expert knowledge. Procurement efforts are rendered more effective by not duplicating tasks and allow industry to program its response to large-scale research infrastructure requirements. The advantages also extend to building

design and construction since critical knowledge is shared. Furthermore there is benefit of the Solaris-MAX IV collaboration on other European laboratories from collaborations that are unique to either Solaris or MAX IV which extend the network and knowledge base.

Acknowledgments: The work was supported by the European Regional Development Fund within the frame of the Innovative Economy Operational Program:POIG.02.01.00-12-213/09.

References

- [1] MAX III reference.
- [2] MAX IV Detailed Design Report, <http://www.maxlab.lu.se/maxlab/max4/index.html>.
- [3] M. Eriksson *et al.*, “The MAX IV Synchrotron Light Source,” THPC058, this conference.
- [4] A.I. Wawrzyniak *et al.*, “Injector layout and beam injection into Solaris”, THPC123, this conference.
- [5] S.C. Leemann, Particle Accelerator Conference, New York, USA, THP214 (2011).
- [6] S.C. Leeman, “Recent improvements to the lattices for the MAX IV storage rings,” THPC056, this conference.
- [7] M. Johansson, “Design of the MAX IV/Solaris 1.5 GeV storage ring magnets”, WEPO016, this conference.
- [8] J. Ahlback, “Vacuum system design for the MAX IV 3 GeV ring”, TUPS016, this conference.
- [9] E. D’Amour, ALBA, private communication.
- [10] Å. Andersson, “The 100 MHz RF system for the MAX IV storage rings”, MOPC051, this conference.

¹)Updated version of the paper presented at Proceedings of IPAC2011, San Sebastián, Spain.

KONCEPCJA BUDOWY LINII POMIAROWEJ MX/SAXS/XRD W NCPS SOLARIS

M. Kozak^{1*}, W. Rypniewski², and M. Jaskólski^{2,3}

¹*Wydział Fizyki, Uniwersytet im. Adama Mickiewicza, ul. Umultowska 85, 61-614 Poznań, Polska*

²*Instytut Chemii Bioorganicznej Polskiej Akademii Nauk, ul. Noskowskiego 12/14, 61-704 Poznań, Polska*

³*Wydział Chemii, Uniwersytet im. Adama Mickiewicza, ul. Grunwaldzka 6, 60-780 Poznań, Polska*

Keywords: synchrotron radiation, synchrotron, SOLARIS, beam line, protein crystallography, small-angle X-ray scattering, SAXS, structural biology, materials science, powder diffraction, tuneable synchrotron radiation

*e-mail: mkozak@amu.edu.pl

W grudniu 2011 zainicjowana została budowa pierwszego polskiego synchrotronu — Narodowego Centrum Promieniowania Synchrotronowego SOLARIS w Krakowie. Parametry energetyczne synchrotronu SOLARIS (1.5 GeV) pozwalają na zaprojektowanie linii pomiarowej wykorzystującej promieniowanie synchrotronowe z zakresu twardego promieniowania rentgenowskiego, która będzie mogła być wykorzystywana na potrzeby biokrytalografii oraz badań materiałowych. Planowana linia pomiarowa posiadać będzie trzy końcowe stacje pomiarowe — biokrytalograficzną (MX), małokątowego rozpraszania promieniowania rentgenowskiego (SAXS) i dyfrakcji promieniowania synchrotronowego na materiałach polikrystalicznych (XRD).

In December 2011 the construction of the first Polish synchrotron — The National Synchrotron Radiation Centre SOLARIS — was initiated in Kraków. The energy parameters of SOLARIS (1.5 GeV) allow planning of a beam line utilising the synchrotron radiation (hard X-rays range), that can be used in biocrystallography and material science. The planned beam line has three end-stations — for biocrystallography (MX), small-angle X-ray scattering (SAXS) and diffraction of synchrotron radiation on polycrystalline materials (XRD).

Rozwój niektórych dziedzin nauki stymulowany jest dostępem do źródeł promieniowania elektromagnetycznego. Należą do nich przede wszystkim te dziedziny badań, które wykorzystują zjawisko dyfrakcji czy rozpraszania promieniowania rentgenowskiego, między innymi jest to krytalografia. Jeżeli prześledzimy jej rozwój od początku ubiegłego wieku z łatwością zauważymy jak ściśle są te powiązania. Praktycznie na każdym etapie odkrycia naukowe stymulowane były rozwojem nowych źródeł promieniowania rentgenowskiego, a szczególnie spektakularne odkrycia ostatnich lat ściśle wiążą się z dostępem do promieniowania synchrotronowego [1, 2].

Od początku XX wieku Nagrodę Nobla za badania związane z krytalografią przyznano 33 razy <http://www.iucr.org/people/nobel-prize>). Szczególnie dynamiczny rozkwit biokrytalografii zapoczątkowały w latach 60-tych wiekopomne prace Watsona i Cricka [3, 4] oraz Perutza i Kendrew [5, 6]. Od tego czasu Nagrodę Nobla za badania krytalograficzne struktury biomolekuł przyznano szesnaście razy, ostatnio w 2009 roku za zbadanie struktury rybosomu — ogromnego kom-

pleksu łańcuchów RNA oraz białek, na którym w każdej żywej komórce na Ziemi zachodzi biosynteza białek [7]-[9]. Dzięki biokrytalografii uzyskiwane są modele strukturalne białek o rozdzielczości atomowej, które służą między innymi do projektowania leków. Najbardziej spektakularnym tego przykładem są leki stosowane w leczeniu AIDS, które powstały dzięki poznaniu struktury białek wirusa HIV [10]-[12]. Zaprojektowana w oparciu o wyniki badań krytalograficznych i stosowana obecnie zmodyfikowana insulina jest łatwiej przyswajalna i ma przedłużony czas działania [13]. Co więcej badania krytalograficzne pozwalają także na poznanie struktury nie tylko pojedynczych białek wirusa, ale nawet całych wirusów [14]. Trudno więc przecenić znaczenie tego typu badań w opracowywaniu nowych leków, szczepionek czy nowych terapii.

Od połowy lat 80-tych ubiegłego wieku biokrytalografia stymulowana jest dostępem do źródeł promieniowania synchrotronowego. Dobrym odzwierciedleniem tego trendu jest nie tylko wzrastająca liczba struktur białkowych deponowanych w bazie Protein Data Bank <http://www.pdb.org>) ale przede wszystkim relacja liczby struktur

rozwiązywanych z wykorzystaniem promieniowania synchrotronowego do całkowitej liczby zdeponowanych struktur. Porównując tylko ostatnie 15-lecie warto zauważyć, że w 1996 roku zdeponowano w PDB 1148 struktur białkowych rozwiązanych w oparciu o dane dyfrakcyjne z czego 275 stanowiły struktury zbadane z pomocą promieniowania synchrotronowego (co stanowi 24% ogólnej liczby struktur rentgenowskich). Z kolei w roku 2011 na 8359 zdeponowanych struktur makromolekuł uzyskanych z użyciem promieniowania rentgenowskiego przypada aż 7076 struktur rozwiązanych w oparciu o dane synchrotronowe (czyli około 85%).

Z upowszechnieniem się dostępu do źródeł synchrotronowych związany jest też intensywny rozwój metod badania struktury biomolekuł w roztworach w oparciu o małokątowe rozpraszanie promieniowania synchrotronowego. Technika ta stanowi komplementarne wobec krystalografii narzędzie badawcze pozwalające na badanie struktur makromolekuł w ich naturalnym środowisku i jest niezwykle atrakcyjną do badań tych układów, dla których nie można uzyskać kryształów (białka o strukturze dynamicznej, złożone kompleksy multimetryczne, czy niektóre peptydy) [15].

Biokrystalografia w Polsce

Polscy naukowcy od początku brali aktywny udział w badaniach biokrystalograficznych. Należy tu wymienić przede wszystkim prof. Tadeusza Baranowskiego, który w 1939 roku jako pierwszy Polak przeprowadził krystalizację białek [16]-[18]. W latach powojennych polska szkoła krystalografii rozwijała się nadal, ale w wyniku pogłębiających się trudności z prowadzeniem nowoczesnych badań w Polsce, jak również z innych względów, większość polskich biokrystalografów wyemigrowała na Zachód.

Dopiero w okresie ostatnich kilkunastu lat ta sytuacja zaczęła się zmieniać. Powstało w kraju kilka nowoczesnych ośrodków i krystalografia makromolekuł w Polsce znów rozwija się dynamicznie. Ten rozwój nie byłby możliwy bez dostępu do promieniowania synchrotronowego. Dotychczas dość swobodnie można było korzystać z linii synchrotronowych za granicą. Jednak w najbliższym czasie w dużym stopniu ograniczone mają zostać programy międzynarodowe finansujące dostęp do tych ośrodków dla badaczy europejskich. Aby podtrzymać poziom i zapewnić dalszy rozwój badań biostrukturalnych w Polsce zaistniała pilna potrzeba zapewnienia polskim biokrystalografom warunków do pracy w kraju w oparciu o narodowe centrum synchrotronowe wyposażone we własne linie synchrotronowe. Już na etapie prac nad projektem koncepcyjnym polskiego synchrotronu pojawił się pomysł budowy w nim linii pomiarowej przeznaczonej do badań biokrystalograficznych. W grudniu 2011 rozpoczęła się budowa długo wyczekiwane go pierwszego polskiego synchrotronu — Narodowego Centrum Promieniowania Synchrotronowego SO-

LARIS w Krakowie. Znając uwarunkowania konstrukcyjne, możliwości badawcze tego urządzenia oraz uwarunkowania finansowe na obecnym etapie możliwe jest zaproponowanie linii pomiarowej opartej o promieniowanie synchrotronowe z zakresu twardego promieniowania rentgenowskiego, która będzie mogła być wykorzystywana na potrzeby biologii strukturalnej i badań materiałowych. W środowisku poznańskich naukowców z Uniwersytetu im. Adama Mickiewicza oraz Instytutu Chemii Bioorganicznej PAN powstał projekt takiej linii.

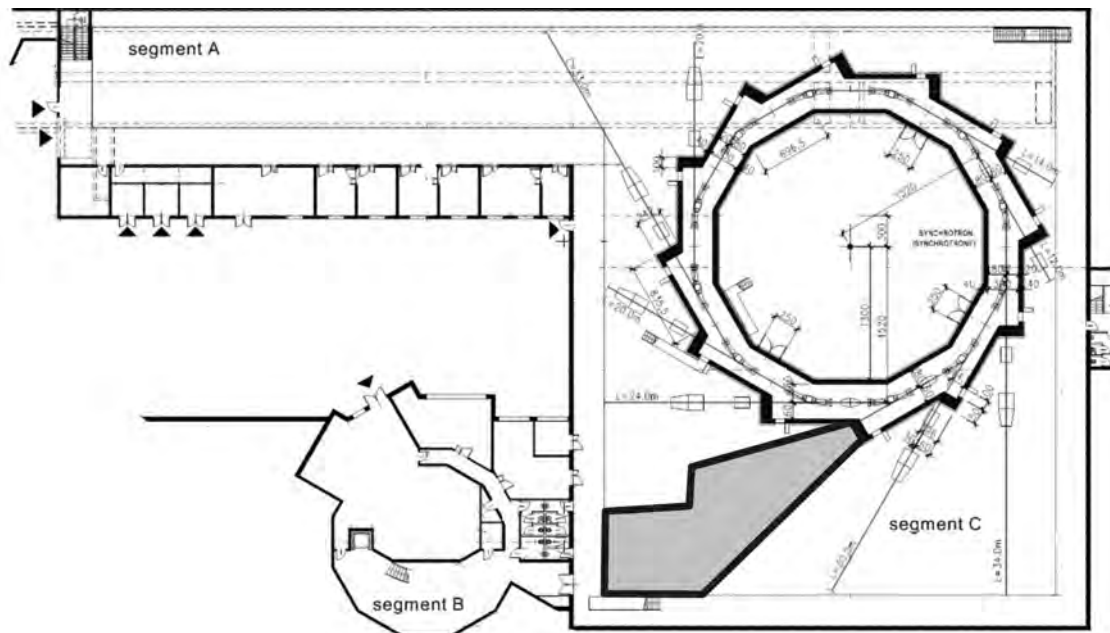
Koncepcja linii

Biorąc pod uwagę parametry synchrotronu (obwód 96 m, energia 1.5 GeV), wielkość hali eksperymentalnej (50 m × 60 m) oraz możliwość lokalizacji na jego obwodzie 9 – 10 stacji pomiarowych należy w pierwszym rzędzie rozważyć budowę linii, która zapewniałaby dostęp do infrastruktury pomiarowej dla możliwie najszerszej grupy badaczy. Nie bez znaczenia obok badań krystalograficznych są także badania strukturalne układów niekryształicznych takich jak polimery i nanokompozyty polimerowe, szkła, błony biologiczne, nośniki leków czy szczepionek. Tego typu obiekty badane są również z wykorzystaniem promieniowania synchrotronowego i techniki rozpraszania małokątowego. Osobnym i niezwykle istotnym aspektem dla postępu technologicznego w kraju są także badania strukturalne nowych materiałów (nanokompozytów, polimerów, półprzewodników itp.), które również będą mogły rozwijać się przy udziale nowej linii pomiarowej. Warto nadmienić, że tego typu linie (złożone z kilku końcowych stacji pomiarowych) w synchrotronach za granicą, ze względu na swą specyfikę, są najbardziej produktywne w przeliczeniu na liczbę i wagę publikacji naukowych. Wyniki tych badań są publikowane w najlepszych czasopismach naukowych i mają zawsze najsilniejszy oddźwięk w środowisku naukowym.

Dlatego przedstawiona poniżej koncepcja obejmuje stworzenie obok końcowej stacji pomiarowej przeznaczonej do badań biokrystalograficznych budowę dwóch stacji końcowych do pomiarów małokątowego rozpraszania promieniowania rentgenowskiego (SAXS) i dyfrakcji na układach polikryształicznych. Potencjalna lokalizacja stacji, wstępnie uzgodniona z dyrekcją synchrotronu SOLARIS zaprezentowana została na rysunku 1.

Z uwagi na wymagania optyki rentgenowskiej oraz powierzchnię niezbędną do konstrukcji poszczególnych stacji pomiarowych konieczna jest lokalizacja stacji w możliwie najdłuższym (36 m) i przestronnym miejscu hali pomiarowej (segment C). Projekt przewiduje umieszczenie stacji w narożniku hali pomiarowej bezpośrednio sąsiadującym z segmentem B.

Przeprowadzone wcześniej konsultacje z zespołami zajmującymi się konstrukcją aparatury pomiarowej w ośrodkach synchrotronowych (między



Rysunek 1: Lokalizacja stacji MX/SAXS/XRD (jako szary wielobok) na planie synchrotronu SOLARIS. Plan sytuacyjny synchrotronu SOLARIS został udostępniony dzięki uprzejmości dyrekcji NCPS.

innymi w MAX-lab Lund czy DESY Hamburg) oraz z firmami zajmującymi się budową komponentów lub całych synchrotronowych linii pomiarowych pozwoliły stworzyć spójną koncepcję oraz realistycznie oszacować wymagane środki finansowe. Projekt tej linii przewiduje wyposażenie jej w urządzenia pomiarowe najnowszej generacji, co zapewni jej konkurencyjność wobec innych ośrodków na świecie.

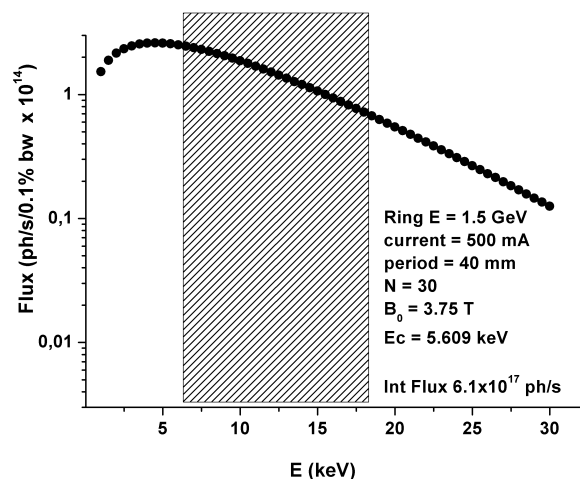
Wiggler nadprzewodzący i optyka rentgenowska

Energia krytyczna na magnesach uginających dla synchrotronu SOLARIS wynosi 1.96 keV. Promieniowanie rentgenowskie w pożądanym zakresie energetycznym (6 – 18 keV) uzyskiwane będzie więc za pomocą wigglera nadprzewodzącego w polu $B_0 = 3.5 - 4$ T (energia krytyczna 5.5 – 6 keV), który zapewni nie tylko odpowiedni zakres energetyczny ale też wysoką intensywność promieniowania. Przykładowy teoretyczny zakres widmowy dla tego typu wigglera zaprezentowany został na rysunku 2.

Elementy optyki stacji będą dostosowane do wymagań krystalografii białek. W szczególności konieczne są lustra kolimujące pozwalające na osiągnięcie wymaganej dla pomiarów z wykorzystaniem rozpraszania anomalnego wysokiej rozdzielczości energetycznej.

Koncepcja linii pomiarowej złożonej z kilku końcowych stacji pomiarowych jest najbardziej efektywnym wykorzystaniem miejsca oraz wiązki promieniowania rentgenowskiego emitowanej z jednego wigglera. W ostatnich latach podobna konstrukcja została zbudowana i z powodzeniem uruchomiona w ośrodku synchrotronowym MAX-lab w

Lund (Szwecja) [19]. Linia I911 zawiera aż pięć stacji końcowych (jedną pracującą w szerszym zakresie energii i dostosowaną do techniki dostrojonej dyfrakcji anomalnej (Multiwavelength Anomalous Diffraction - MAD) [20], oraz cztery pracujące przy stałej długości fali). Linia ta zainstalowana została na pierścieniu akumulacyjnym MAX-II o obwodzie (90 m) i parametrach zbliżonych do planowanych dla pierścienia akumulacyjnego w synchrotronie SOLARIS



Rysunek 2: Teoretyczny profil energetyczny promieniowania synchrotronowego generowanego z użyciem wigglera nadprzewodzącego 3.75 T. Na wykresie zaznaczony został zakres energetyczny możliwy do wykorzystania przez planowaną linię.

Stacje końcowe

Pierwsza stacja końcowa przeznaczona do badań dyfrakcyjnych monokryształów biomakromolekuł - białek i kwasów nukleinowych (MX)

pracować powinna w pełnym zakresie energetycznym (6 – 18 keV). Oprócz standardowego goniostatu do badań monokryształów wyposażona powinna być także w system umożliwiający pełną automatyzację pomiarów dyfrakcyjnych oraz w przyszłości docelowo umożliwiać prowadzenie pomiarów zdalnych. Tego typu rozwiązania są już rutynowo stosowane w najlepszych liniach biokrytalograficznych [21]-[24]. Z uwagi na podatność próbek biologicznych na destrukcję indukowaną promieniowaniem rentgenowskim pomiary będą prowadzone w warunkach kriogenicznych. Z kolei dzięki wykorzystaniu pełnego zakresu energetycznego stacji możliwe będzie rejestrowanie danych dyfrakcyjnych w eksperymentach opartych na technice MAD [20]. Aby w pełni wykorzystać możliwości stacji na potrzeby techniki MAD jej energetyczna zdolność rozdzielcza powinna wynosić $\Delta E/E = 10^{-4}$.

Druga stacja końcowa (pomiarowa) powinna także pracować w tym zakresie energetycznym co stacja MX (6 – 18 keV, $\Delta E/E = 10^{-4}$) i być wyposażona w wysokiej klasy optykę umożliwiającą pomiary układów biologicznych w roztworach (bioSAXS). Rejestracja danych oparta będzie o najlepszy dostępny na światowym rynku detektor półprzewodnikowy (np. typu PILATUS 1M) oraz system pomiarowy umożliwiający pomiary w szerokim zakresie temperatur, przynajmniej od 80 K do 573 K. Z uwagi na potencjalne szerokie wykorzystanie tej stacji pomiarowej także przez fizyków materii miękkiej oraz badaczy polimerów system wyposażony powinien być w układ umożliwiający wytłaczanie próbek polimerowych w trakcie pomiarów oraz zintegrowany kalorymetr skaningowy do rejestracji efektów energetycznych towarzyszącym przejściom fazowym generowanym w funkcji temperatury.

Z kolei trzecia stacja pomiarowa operować będzie przy stałej energii (15 keV) i wyposażona zostanie w dyfraktometr proszkowy wraz z wysokiej klasy detektorem liniowym lub powierzchniowym. Cały system pozwalał będzie na pomiary dyfrakcyjne w szerokim zakresie temperatur (60 – 1500 K) oraz pomiary ciśnieniowe.

Podsumowanie

Linie o podobnym charakterze do planowanej funkcjonują w prawie wszystkich synchrotronach na świecie. Warto ponownie podkreślić, że w większości przypadków tego typu linie pomiarowe należą do najbardziej produktywnych naukowo linii badawczych. Wielkość środowiska potencjalnych użytkowników stacji MX w Polsce oszacować można na 12 grup biokrytalograficznych oraz przynajmniej 5 kolejnych grup badawczych sporadycznie korzystających z technik biokrytalograficznych, co daje szacunkową liczbę 50 – 60 potencjalnych użytkowników stacji MX. Szacunki zapotrzebowania na czas pomiarowy bazujące tylko na wyko-

rzystaniu linii przez te grupy, nie licząc potencjalnych użytkowników z zagranicy (w szczególności z Europy środkowej), to ponad 100 dni pomiarowych. Co więcej w związku z rozwojem biologii strukturalnej w Polsce i powstawaniem w kraju nowych grup biokrytalograficznych należy szacować, że liczebność tej grupy użytkowników ma tendencje wzrostowe. Jeśli chodzi o pozostałe końcowe stacje pomiarowe (SAXS, XRD) to z uwagi na szerszy (multidyscyplinarny) profil badań liczba użytkowników jest znacznie większa.

W powyższych szacunkach uwzględnić należy również efekt generowania zapotrzebowania poprzez dostępność technologii (*technology-driven research*) oraz prowadzone przez personel linii badania własne (*in-house*) w efekcie można powiedzieć, że możliwości planowanej linii pomiarowej będą w pełni wykorzystywane.

Acknowledgments: The work was supported by the European Regional Development Fund within the frame of the Innovative Economy Operational Program: POIG.02.01.00-12-213/09.

References

- [1] Z. Dauter, M. Jaskolski, A. Wlodawer, "Impact of synchrotron radiation on macromolecular crystallography: A personal view," *J. Synchrotron Rad.* **17** (2010) 433 – 444.
- [2] Z. Dauter, A. Wlodawer, M. Jaskolski, "Promieniowanie rentgenowskie ze źródeł synchrotronowych jako katalizator rozwoju krystalografii białek", *Synchrotron Radiation in Natural Science* **9** (2010) 4 – 16.
- [3] J.D. Watson, F.H.C. Crick, "Molecular structure of nucleic acids — a structure for deoxyribose nucleic acid," *Nature* **171** (1953) 737 – 738.
- [4] J.D. Watson, F.H.C. Crick, "Genetical implications of the structure of deoxyribonucleic acid," *Nature* **171** (1953) 964 – 967.
- [5] J.C. Kendrew, R.E. Dickerson, B.E. Strandberg, R.G. Hart, D.R. Davies, D.C. Phillips, V.C. Shore, "Structure of myoglobin — 3-dimensional Fourier synthesis at 2 Å resolution," *Nature* **185** (1960) 422 – 427.
- [6] M.F. Perutz, M.G. Rossmann, A.F. Cullis, H. Muirhead, G. Will, A.C.T. North, "Structure of haemoglobin — 3-dimensional Fourier synthesis at 5.5 Å resolution, obtained by X-ray analysis," *Nature* **185** (1960) 416 – 422.
- [7] N. Ban, P. Nissen, J. Hansen, P.B. Moore, T.A. Steitz, "The complete atomic structure of the large ribosomal subunit at 2.4 angstrom resolution," *Science* **289** (2000) 905 – 920.
- [8] J. Harms, F. Schluenzen, R. Zarivach, A. Bashan, S. Gat, I. Agmon, H. Bartels, F. Franceschi, A. Yonath, "High resolution structure of the large ribosomal subunit from a mesophilic Eubacterium," *Cell* **107** (2001) 679 – 688.
- [9] B.T. Wimberly, D.E. Brodersen, W.M. Clemons, R.J. Morgan-Warren, A.P. Carter, C. Vonrhein, T.

- Hartsch, V. Ramakrishnan, “Structure of the 30S ribosomal subunit,” *Nature* **407** (2000) 327 – 339.
- [10] A. Wlodawer, M. Miller, M. Jaskolski, B.K. Sathyanarayana, E. Baldwin, I.T. Weber, L.M. Selk, L. Clawson, J. Schneider, S.B.H. Kent, “Conserved folding in retroviral proteases — crystal-structure of a synthetic HIV-1 protease,” *Science* **245** (1989) 616 – 621.
- [11] M. Jaskolski, “From atomic resolution to molecular giants: An overview of crystallographic studies of biological macromolecules with synchrotron radiation,” *Acta Phys. Polon. A* **117** (2009) 257 – 263; *Synchrotron Radiation in Natural Science* **9** (2009) 17 – 23.
- [12] Z. Dauter, M. Jaskolski, “Zastosowanie promieniowania synchrotronowego w krystalografii białek,” in: *Promieniowanie synchrotronowe w spektroskopii i badaniach strukturalnych. Wybrane zagadnienia*, B.J. Kowalski, W. Paszkowicz, E.A. Gorlich, eds., pp. 305 – 328 (PTPS Kraków, 2011).
- [13] J.L. Whittingham, I. Jonassen, S. Havelund, S.M. Roberts, E.J. Dodson, C.S. Verma, A.J. Wilkinson, G.G. Dodson, “Crystallographic and solution studies of N-lithocholyl insulin: A new generation of prolonged-acting human insulins,” *Biochemistry* **43** (2004) 5987 – 5995.
- [14] S.A. Wynne, R.A. Crowther, A.G.W. Leslie, “The crystal structure of the human hepatitis B virus capsid,” *Mol. Cell* **3** (1999) 771 – 780.
- [15] C.D. Putnam, M. Hammel, G.L. Hura, J.A. Tainer, “X-ray solution scattering (SAXS) combined with crystallography and computation: Defining accurate macromolecular structures, conformations and assemblies in solution,” *Quarterly Rev. Biophys.* **40** (2007) 191 – 285.
- [16] T. Baranowski, “Die Isolierung von kristallisierten Proteinen aus Kaninchenmuskel,” *Z. Physiol. Chem.* **260** (1939) 43 – 55.
- [17] L. Chrobak, T. Baranowski, “Über verschiedene Kristalle des A-Myogens aus Kaninchenmuskelatur. Comptes Rendus,” (Doklady) *l’Academie des Science de l’USSR* **XXVIII** (1940) 724 – 725.
- [18] T. Baranowski, “Crystalline glycerophosphate dehydrogenase from rabbit muscle,” *J. Biol. Chem.* **180** (1949) 535 – 541.
- [19] C.B. Mammen, T. Ursby, M. Thunnissen, and J. Als-Nielsen, “Bent diamond crystals and multilayer based optics at the new 5-Station Protein Crystallography Beamline ‘Cassiopeia’ at MAX-lab, *AIP Conference Proceedings* **705** (2004) 808 – 811.
- [20] W.A. Hendrickson, “Determination of macromolecular structures from anomalous diffraction of synchrotron radiation,” *Science* **254** (1991) 51 – 58.
- [21] G. Snell, C. Cork, R. Nordmeyer, E. Cornell, G. Meigs, D. Yegian, J. Jaklevic, J. Jin, R.C. Stevens, T. Earnest, “Automated sample mounting and alignment system for biological crystallography at a synchrotron source,” *Structure* **12** (2004) 537 – 545.
- [22] S.M. Soltis, A.E. Cohen, A. Deacon, T. Eriksson, A. Gonzalez, S. McPhillips, H. Chui, P. Dunten, M. Hollenbeck, I. Mathews, M. Miller, P. Moorhead, R.P. Phizackerley, C. Smith, J. Song, H. van dem Bedem, P. Ellis, P. Kuhn, T. McPhillips, N. Sauter, K. Sharp, I. Tsyba, G. Wolf, “New paradigm for macromolecular crystallography experiments at SSRL: Automated crystal screening and remote data collection,” *Acta Cryst. D* **64** (2008) 1210 – 1221.
- [23] X.D. Wang, M. Gleaves, D. Meredith, R. Allan, C. Nave, “E-science technologies in synchrotron radiation beamline — Remote access and automation (A case study for high throughput protein crystallography),” *Macromol. Res.* **14** (2006) 140 – 145.
- [24] M. Gilski, “Automation and remote synchrotron data collection,” *Acta Phys. Polon. A* **114** (2008) 331 – 338.

ESRF UPGRADE PROGRAMME REACHES HALFWAY MARK

Claus Habfast and Gary Admans

ESRF Communication Group, Grenoble, France

In 2012, the ESRF reached the peak activity of the first phase of its Upgrade Programme. This included a 5-month shutdown until May 2012, the first time ever in 18 years that the user operation was shut down for such an extended period of time.

The first new beamlines are now available for user operation, and many more will become operational until the end of Phase I of the upgrade in 2015. Remarkably, the performance of the ESRF for its users did not drop significantly despite a period of heavy works. The X-ray source performs better than ever, with record values for the mean time between failure and availability. Although the number of hours of user operations is slightly lower than in the past years, due to the construction-related shutdown periods, the interest in the ESRF remains high, and the number of proposals did not decrease, on the contrary!

Upgrade Beamlines

Eight Upgrade Beamline Projects are a core deliverable of the Upgrade Programme. These are now all under development, and most of them are al-

ready under construction. Together, the eight Upgrade Beamline Projects actually comprise 11 different new beamlines with 15 independently operable end stations (Figure 1).

In the following, short descriptions are given of these eight projects, including the opening dates of the end stations for users and whom to contact for any enquiry:

ID01 Diffraction imaging for nano-analysis

Long beamline for nano-X-ray diffraction across a wide energy range (2.2 – 50 keV), offering coherent imaging of individual nanostructures as well as basic surface diffraction and small-angle scattering. Combines X-ray diffraction with atomic-force microscopy to allow investigations of the structure-function relationship at the nanoscale. Targets the study of properties of device-like structures in unprecedented detail.

Open late 2014, scientist in charge: Tobias Schulli, schulli@esrf.fr.

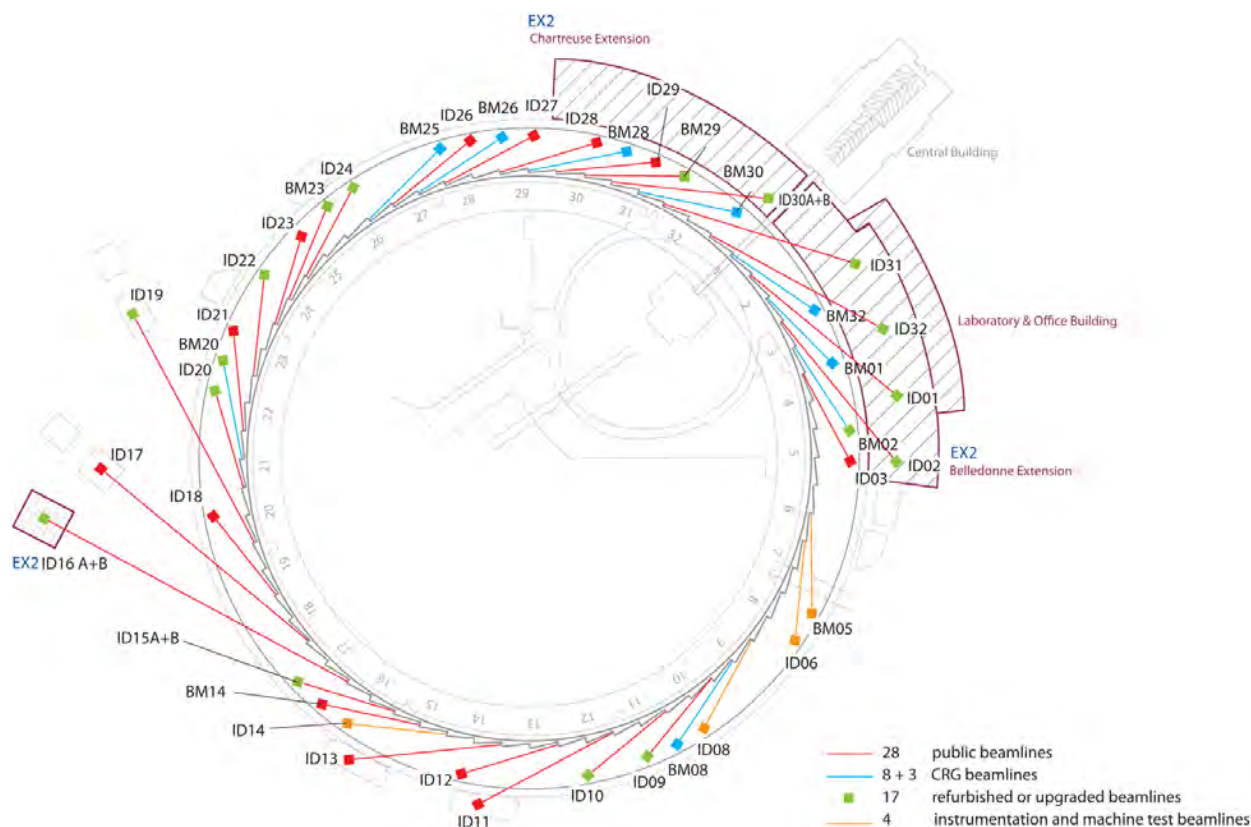


Figure 1: ESRF experimental hall.

ID31 High-energy beamline for buried interface structures and materials processing (previously ID15)

Long beamline covering energies 30 – 150 keV for the study of working devices *in situ*, with new optics allowing the beam size to be reduced to 200 nm at the push of a button. The smaller spot size will allow users to study less perfect, more realistic, interfaces to understand the interplay between microscopic material properties and macroscopic device performance — in particular concerning advanced materials for fuel cells, organic solar cells, rechargeable batteries and catalytic materials.

Open early 2015, scientist in charge: Veijo Honkimäki, honkimak@esrf.fr.

ID16 Nano-imaging and nano-analysis (previously ID22)

Long, high-brilliance beamline providing nanofocused beams for two end stations. Operated in a cryogenic environment, the nano-imaging end station will focus hard X-rays at specific energies to a spot size as small as 15 nm and combine fluorescence analysis and nanotomography. The nano-analysis end station will provide a monochromatic beam tunable in a large energy range, offering a multianalysis nanoprobe for spectroscopic studies. ID16 will focus on biomedical research, for instance allowing subcellular processes to be studied, as well as environmental sciences, energy and nanotechnology.

Open February 2014, scientist in charge: Peter Cloetens, cloetens@esrf.fr.

ID20 Inelastic hard X-ray scattering for electronic spectroscopy (previously ID16)

Two end stations offering a spectroscopic tool with all the advantages of a hard X-ray probe — bulk information, high-penetrating power and elemental and spin sensitivity — designed to enhance the ESRF's inelastic scattering programme. The upgrade will decrease the size of the beam from around 100 microns to 10 microns, allowing experiments in extreme conditions, for example at very high pressure. The energy range will also increase from 6 – 10 KeV to 5 – 20 KeV, enabling resonant experiments at a large number of absorption edges with increased compatibility with more complex sample environments. Finally, more luminous spectrometers will broaden the scientific impact of inelastic X-ray scattering.

Open March 2013, scientist in charge: Giulio Monaco, gmonaco@esrf.fr.

ID32 Soft X-rays for magnetic and electronic spectroscopy (previously ID08)

State-of-the art facility for soft X-ray absorption spectroscopy and very high-energy resolution resonant inelastic X-ray scattering, with

sophisticated sample environments and tunable X-ray beam sizes ranging from microns to hundreds of microns. The beamline will provide new facilities for users to study the electronic and magnetic properties of materials, offering magnetic dichroism techniques and soft resonant inelastic X-ray scattering to meet the demands of an expanding user community.

Open August 2014, scientist in charge: Nick Brookes, brookes@esrf.fr.

ID02 / ID09 Time-resolved experiments (previously ID02 / ID09B)

Two independent beamlines. The long beamline ID02 will extend SAXS to ultra-small (microradian) angles with sub-millisecond time resolution, pushing the technique's applicability to systems ranging from colloidal plasmas to highly self-assembled biomimetic systems. ID09 is dedicated to time-resolved diffraction and scattering, with picosecond laser pulses initiating structural changes in the sample that can then be probed with ultrashort X-ray pulses.

Open: ID02 April 2014, scientist in charge: Theyencheri Narayanan, narayan@esrf.fr

ID09 operational, scientist in charge: Michael Wulff, wulff@esrf.fr.

ID30/BM29 Massively automated sample selection integrated facility for macromolecular crystallography

A unique resource based on second-generation automation for macromolecular crystallography experiments, designed to help structural biologists tackle ever more ambitious projects, such as complex membranes. The hub of the project is a sample-evaluation and sorting facility (MASSIF), from which the most suitable crystals for data collection will be distributed to the best suited of seven end stations (MASSIF-1/-2/-3, ID23-1/-2, ID29 or ID30B). Such screening is vital to cope with the problem of inter- and intra-sample variations in modern macromolecular crystallography experiments.

Open: BM29A June 2012; ID30A May 2013; ID30B May 2014, scientist in charge: Christoph Mueller-Dieckmann, christoph.mueller_dieckmann@esrf.fr.

ID24/BM23 Time resolved and extreme conditions X-ray absorption spectroscopy (previously ID24/BM29)

High-brilliance energy dispersive X-ray absorption spectroscopy (EDXAS) allows users to study the local and electronic structure of matter in real time and *in situ*; the behaviour of matter under extreme pressures and temperatures, such as those in the Earth's core, or the structure-function relationship in industrially-relevant catalysts. Two independent end stations (EDXAS_S “small spot” and EDXAS_L “large spot”) on ID24 combined with the general

purpose EXAFS station on BM23 will permit X-ray absorption spectroscopy in sample volumes 20 times smaller and with time resolution a 1000 times better than before.

Open: BM23 since November 2011; EDXAS_S May 2012; EDXAS_L Sep 2012, scientist in charge: Sakura Pascarelli, sakura@esrf.fr.

Beamline Refurbishments

During the Upgrade, every ESRF beamline will undergo at least some form of refurbishment, and those with only light improvements will be candidates for Phase II of the upgrade beginning in 2015. The national "CRG" beamlines, which include the Italian GILDA beamline, do not receive ESRF funding, but they stand to benefit from improvements to the X-ray source, sample environments and larger experimental halls.

Major refurbishments to the beamlines ID19 and ID10 are now nearing completion, and they will boost ESRF's imaging, soft-matter and interface science as of the summer of 2012:

Today, palaeontology represents more than 35% of the ID19 microtomography proposals. After more than ten years of operation, ID19 is currently undergoing an in-depth refurbishment with palaeontology as the science driver, but benefiting also other research areas such as materials science, engineering, environmental sciences and biology. ID19 will provide a high-flux pink beam allowing multi-scale imaging at sub-micron resolution of objects measuring up to 40 cm across.

The refurbishment will be complete by spring 2013. The neighbouring ID17 beamline will be equipped with a new sample stage for large fossil scanning plus a refurbished monochromator for higher-energy operation and eventually a new detector. Contacts: Paul Tafforeau, paul.tafforeau@esrf.fr (ID19) and Alberto Bravin, bravin@esrf.fr (ID17).

In parallel, the ID10 beamline complex — previously known as the Troika I, II and III beamlines — will restart in June 2012 after an in-depth refurbishment under the new name "soft interfaces and coherent scattering" (SICS). ID10A/C and ID10B have been transformed into one beamline with two end stations working in time-sharing mode. One station (SICS-CS) will be devoted to X-ray photon correlation spectroscopy and coherent X-ray diffraction imaging, while the other (SICS-LSIS) will offer liquid surfaces and interfaces scattering based on X-ray reflectivity and grazing incidence scattering. Each station will benefit from independent optics and instrumentation optimised for each of the techniques, and will be served by two different silicon monochromators. Contacts: Oleg Kononov, kononov@esrf.fr (SICS-LSIS) and Yuriy Chushkin, yuriy.chushkin@esrf.fr (SICS-CS).

Instrumentation and Data Handling

Developing state-of-the-art instrumentation is another pillar of the Upgrade Programme. Driven by the projects for new beamlines, the need for new technologies was identified in the fields of X-ray mirror engineering, diamond technologies, nanofocussing optics, pixel detectors, on-line data analysis and high-rate data collection.

Handling the massive flux of data coming in particular from the latest generation of 2D detectors is a challenge which requires a coordinated approach between different groups at the ESRF. Today, the petabyte has become the standard unit for data-intensive facilities like the LHC at CERN (15 petabytes/year) or the ESRF (several petabytes/year).

Work has started to optimise the integration of the data flow from the detectors into the ESRF IT infrastructure in order to minimise bottlenecks between data collection and the actual data analysis. Already in 2011, a new data centre was inaugurated, equipped with state-of-the-art file servers capable of storing almost 1 petabyte of data, a tape-based archiving facility of several petabytes, computing clusters with a peak performance of 15 teraflops and an extensive 10 Gbit/s Ethernet infrastructure. This can easily be extended thanks to pre-installed power, cooling and networking resources, allowing a flexible response to changing demands of the users for storage, data analysis capacity and data backup, for many years to come. Plan of the ESRF experimental hall (Figure 1) showing the location of the beamlines at the end of phase I of the ESRF Upgrade Programme. Refurbished and Upgraded beamlines are marked in green; new buildings are outlined in red (Image credit: ESRF/M. Collignon)

View of construction works for the Belledonne experimental hall extension area, March 2012 (Figure 2). About 8500 m² of new experimental halls, laboratory and office space is being created. The buildings are scheduled for completion by June 2013. (Image credit: ESRF/C. Argoud).

Inauguration of Upgrade Beamline ID24.

Ribbons were cut during the inauguration ceremony on 11 November 2011 to mark the opening of two new beamline branches (Figure 3). Left: High-pressure / extreme conditions branch. From left to right: Francesco Sette, ESRF Director General, Sakura Pascarelli, Scientist in charge of ID24, Harald Reichert, ESRF Research Director. Right: Chemistry branch. From left to right: Michel van der Rest, vice-chairman ESRF Council, Geneviève Fioraso, Députée de l'Isère et Adjointe au Maire chargée de l'Economie, l'Emploi, l'Université, la Recherche, Rafael Abela, Chairman ESRF SAC. (Image credit: ESRF/C. Argoud).



Figure 2: construction works for the Belledonne experimental hall.



Figure 3: Inauguration of Upgrade Beamline ID24.

Dwadzieścia lat PTPS z perspektywy Prezesów. Wystąpienie na sesji KSUPS-9 w dniu 26 września 2011 r.

Twenty years of PTPS from the perspective of the Presidents. Speech at the KSUPS-9 session on 26 September 2011. The author reminds the two decades of the activity of Polish Synchrotron Radiation Society seen from the perspective of the first presidents. International collaboration, organization of conferences and initiative of building radiation sources in Poland are briefly presented.

Szanowni Państwo,

Obchodzona przez nas dzisiaj dwudziesta rocznica utworzenia Polskiego Towarzystwa Promieniowania Synchrotronowego jest wdzięczną okazją do przypomnienia i podsumowania niektórych wydarzeń sprzed 20 lat. Entuzjazm, z którym podejmowaliśmy decyzję o utworzeniu Towarzystwa i dążeniu do jego rozwoju, trwa do dnia dzisiejszego. Napawa to uzasadnionym optymizmem na przyszłe lata.

W ostatnim zeszycie Biuletynu PTPS w imprezach rocznicowych, skupiłem się na kilku szczegółach rozwoju naszego Towarzystwa. Dzisiaj chciałbym wskazać komu szczególnie zawdzięczamy obecnie dobrą kondycję Towarzystwa.

Jest godne uwagi to, że powstanie PTPS zainicjowane w trzy miesiące po zarejestrowaniu Europejskiego Towarzystwa Promieniowania Synchrotronowego, ma już swoją dwudziestoletnią historię, gdy działalność organizacyjna Europejskiego Towarzystwa Promieniowania Synchrotronowego zanikła po około sześciu latach, a Włoskie Towarzystwo utworzone w 1992 roku, jako swoisty związek zawodowy użytkowników promieniowania synchrotronowego również zaginęło w niepamięci.

Z perspektywy minionych lat widać, że obecne istnienie PTPS zawdzięczamy ogromnemu i trwałemu entuzjazmowi wielu członków założycieli Towarzystwa i ich następców. Tym wszystkim animatorom Towarzystwa należy się nasza wdzięczność.

W pierwszym rzędzie chciałbym wspomnieć o trzech nieżyjących już założycielach Towarzystwa prof. Julianie Auleytnerze, Jacku Grochowskim i Jerzym Gronkowskim. Prof. J. Auleytner, najstarszy z nas wszystkich, człowiek bardzo serdeczny, przyjacielski i bezpośredni, były dyrektor Instytutu Fizyki PAN, z własnego wyboru vice prezes Towarzystwa kolejnych kadencji Zarządu, dzielił się z nami ogromną kompetencją naukową i wielkim doświadczeniem w zarządzaniu nauką. Był moderatorem i uczestnikiem większości działań Towarzystwa. Koledzy Jacek Grochowski z Uniwersytetu Jagiellońskiego i Jerzy Gronkowski z Uniwe-

rsytetu Warszawskiego zarażali nas swoim entuzjazmem oraz nowymi pomysłami rozwoju i popularyzacji działalności Towarzystwa. Wśród nas żyjących szczególną aktywnością odznaczali się w działalności Towarzystwa niezmiennie od dwudziestu lat nasz skarbnik Wojciech Kwiatek oraz kolejni prezesi Towarzystwa Bronisław Orłowski i Krystyna Ławniczak-Jabłońska. Również koledzy założyciele Towarzystwa profesorowie Maria Lefeld-Sosnowska, Izabela Sosnowska, Ewa Sobczak, Andrzej Burian i Jerzy Pielaszek nie żalowali czasu na współpracę, działali we władzach PTPS oraz służyli nam zawsze pomocą i celną radą. Jednakże bez codziennej, czasem mało efektywnej, działalności koleżanek i kolegów młodszej generacji z Krakowa Marty Zinnal-Starnawskiej, Barbary Pukowskiej, Andrzeja Rodzika, Ewy Such i Krystyny Stankiewicz oraz z Warszawy Elżbiety Dynowskiej, Haliny Granat, Bogdana Kowalskiego, Wojciecha Paszkowicza i Danuty Żymierskiej, dzisiejszy sukces Towarzystwa nie byłby możliwy. Przypominam nazwiska zasłużonej „starej gwardii” bo niektórzy z wymienionych rozluźnili z nami kontakty i są nieobecni na tej sali.

Istnienie PTPS w dobrym zdrowiu jest wynikiem realizacji istotnych założeń statutowych. W ramach realizacji ułatwiania dostępu polskim użytkownikom do promieniowania synchrotronowego, w wyniku wieloletnich starań PTPS a następnie Instytutu Fizyki PAN w Warszawie, została zawarta umowa o współpracy z ESRF w Grenoble na zasadach Współpracującej Grupy Badawczej. Niestety umowa ta wygasła w tym roku. Ubocznym, ale bardzo ważnym rezultatem żmudnych negocjacji PTPS z KBN i Państwową Agencją Atomistyki o dostęp polskich użytkowników do źródeł promieniowania synchrotronowego, było przebudowywanie świadomości w polskim środowisku nauk przyrodniczych w kwestii podziału środków finansowych na badania w różnych dziedzinach fizyki, w tym w szczególności w kwestii uczestniczenia w Polsce badaczy w kosztownych badaniach z użyciem promieniowania synchrotronowego. Trzeba bowiem pamiętać, że w latach siedemdziesiątych ubiegłego

stulecia bardzo istotnym i ówczesnie aktualnym problemem była potrzeba zmodyfikowania przekonania, dość powszechnego w światowym, a także polskim środowisku naukowym, że spośród uprawianych dziedzin fizyki tylko niektóre wymagają wysokich nakładów finansowych. Do tych wyróżnionych dziedzin należały wtedy kriogenika oraz badania z zakresu fizyki jądrowej i fizyki wysokich energii. Stosowanie w fizyce jądrowej i w fizyce wysokich energii bardzo kosztownych akceleratorów cząstek oraz skomplikowanej i drogiej aparatury pomiarowej, wynikało z potrzeby pogłębienia rezultatów badań z pierwszej połowy XX wieku, fundamentalnych dla poznania własności jądra atomowego. Ważnym i powszechnie akceptowanym wyjątkiem było stosowanie reaktorów neutronowych w badaniach z fizyki i fizyko-chemii ciała stałego. Przekonanie decydentów, że inne badania w dziedzinie fizyki, chemii, biologii i medycyny mogą potrzebować również bardzo dużych nakładów finansowych, wymagało czasu i bardzo przekonującej argumentacji. W polskim środowisku naukowym ta wyraźna potrzeba skryształizowała się dopiero w ostatnim dziesięcioleciu. W moim przekonaniu decyzja Rządu dotycząca przyznania znacznych środków finansowych Uniwersytetowi Jagiellońskiemu na budowę polskiego synchrotronu, jest logicznym wynikiem naszych wcześniejszych trudnych negocjacji na wysokim szczeblu w KBN, które formowały pozytywne nastawienie w polskim środowisku nauk przyrodniczych w zakresie wsparcia w Polsce bardzo kosztownych badań z użyciem promieniowania synchrotronowego.

Równie ważnym celem statutowym było podnoszenie kwalifikacji naukowych członków Towarzystwa. Cel ten został w pełni osiągnięty przez bezpośredni kontakt członków i sympatyków PTPS w czasie organizowanych przez Towarzystwo szkół i sympozjów z czynnym udziałem wielu przedstawicieli różnych ośrodków synchrotronowych Europy, USA i Japonii z którymi współpracowali poprzednio członkowie Towarzystwa. Warto przypomnieć, że początki działalności Towarzystwa były niełatwe. Pierwsza Szkoła i Sympozjum została zorganizowana dla jeszcze nielicznej grupy członków Towarzystwa, z udziałem ponad 20 wykładowców z zagranicy, głównie kierowników grup badawczych z którymi współpracowali badacze z Polski. Entuzjazm organizatorów kolejnych Szkół oraz poziom i różnorodność tematyki sprawiał, że uczestnikami bywali również młodzi pracownicy naukowcy i studenci przysyłani z europejskich laboratoriów synchrotronowych. Tutaj należy przypomnieć bardzo aktywne i bezinteresowne włączenie się szeregu wybitnych przedstawicieli światowych ośrodków synchrotronowych w szkolenie polskiego środowiska

użytkowników promieniowania synchrotronowego i organizację naszych Szkół i Sympozjów. Wśród grona kilkudziesięciu aktywnych wykładowców pierwszych kilku Szkół i Sympozjum warto przypomnieć nazwiska kilkunastu, którzy pomagali nam najbardziej aktywnie. Wśród nich byli wybitni profesorowie Joseph. Norgren, i Per Olaf. Nilsson ze Szwecji, Jurgen Haertwig, Ruprecht Haensel i Ake Kvik, z ESRF Grenoble, Zbigniew Dauter, Klaus Einhorn i Ricardo Manzke z Niemiec; Emilio Burattini, Stefano Logomarsino, Giorgio. Margaritondo, Settimio Mobilio, Mario Piacentini i Paulo Perfetti z Włoch; Pierre Lagarde, Cecile Malgrange i Albert Renoprez, z Francji, Peter Fratzl i Peter Langner z Austrii, Fred Schlachter, i Franz Himpsel z USA oraz Akito Kakizaki i Masaki Taniguchi z Japonii. Oprócz swojej obecności rekomendowali oni i nakłaniali również do uczestniczenia w naszych Sympozjach wielu swoich współpracowników i uczniów. Udzielona pomoc przez wszystkich zagranicznych uczestników owocowała wysokim poziomem kolejnych Sympozjów. Wszystkim wymienionym i kilkudziesięciu niewymiennym z nazwiska wykładowcom i uczestnikom jesteśmy winni bardzo serdeczną wdzięczność. Myśląc o tym po latach, nie potrafię dociec skąd brała się z ich strony bezinteresowna determinacja pomocy polskimi użytkownikom promieniowania synchrotronowego.

Podsumowując ten wrywkowy obraz działalności PTPS, można spoglądać z uzasadnionym optymizmem w przyszłość naszego Towarzystwa. Z mojej perspektywy, widzę dalej PTPS jako bardzo ważny stymulator wartościowej działalności naukowej polskich użytkowników promieniowania synchrotronowego, a w szczególności również jako źródło zasilające programy badawcze budowanego polskiego synchrotronu. Przed budowniczymi synchrotronu stoi zadanie oddania obiektu do użytku. Jest to jednak tylko część zadania. Przed członkami PTPS i przyszłymi użytkownikami pozyskiwanymi pilnie z zagranicy stoi, nie zapisane żadną umową, wypełnienie w przyszłości treścią badawczą budowanej inwestycji. Wieloletnie moje doświadczenie badawcze dyktuje mi scenariusz, w którym zrzeszeni w PTPS aktywni użytkownicy promieniowania synchrotronowego odegrają kluczową rolę, niezależnie od aktualnej świadomości budowniczych i obecnego zaangażowania członków Towarzystwa w budowę przyszłych linii pomiarowych.

Na zakończenie życzę naszemu Towarzystwu dalszego rozwoju i wielu lat bardzo aktywnej działalności a członkom i sympatykom Towarzystwa życzę wartościowych rezultatów badawczych.

Dziękuję serdecznie za uwagę.

Andrzej Kisiel

Photographic impressions of the first International School and Symposium on Synchrotron Radiation in Natural Science, Jaszowiec, Poland, 13 – 21 May 1992.



Pierwszy rząd: (1) Marek Wołczyrz, (2) Kai Uwe Gawlik, (3) Grzegorz Kowalski, (4) Jerzy Gronkowski, (5) Paweł Serda, (6) Izabela Sosnowska, (7) Krystyna Ławniczak-Jabłońska, (8) Ewa Sobczak, (9) Leena Sisko Johansson, (11) Thomas Wroblewski, (12) Jacek Grochowski, (13) R. Markowski, (14) Cecile Malgrange;
 Drugi rząd: (1) Krzysztof Maurin, (2) Krzysztof Wieteska, (5) J. Szade, (6) Bogdan J. Kowalski, (7) Sonke Harm, (8) Bogusław Mierzwa, (10) Maria Lefeld Sosnowska, (11) Wojciech Wierzchowski, (12) Wojciech Paszkowicz, (13) Bronisław A. Orłowski, (14) Andrzej Burian, (16) Andrzej Kisiel, (17) Ruprecht Haensel, (19) Julian Auleytner, (20) Joseph Nordgren, (22) Giorgio Margaritondo, (25) Mariella Antonetti, (26) Ryszard Iwanowski, (28) Ake Kvik, (30) Jerzy Pielaszek, (31) Elżbieta Dynowska;
 Trzeci rząd: (1) Albert-Jean Renouprez, (3) Maciej Szymański, (4) Juerg Osterwalder, (8) Wojciech Kwiatek, (9) Andrzej Rodzik, (10) Marta Zimnal Starnawska, (11) Tomasz Harasimowicz.



Pierwszy rząd: Julian Auleytner, Andrzej Kisiel,
 Ewa Sobczak;
 Drugi rząd: Cecile Malgrange, Bronisław A. Orłowski



Jacek Grochowski, Andrzej Kisiel.

*Pomoc w uzupełnieniu identyfikacji uczestników mile widziana.

The 9th National Meeting of Synchrotron Radiation Users (Warsaw 2011)

The 9th National Meeting of Synchrotron Radiation Users was held in the Institute of Physical Chemistry of the Polish Academy of Science, Warsaw, on 26th – 27th of September 2011. The national meetings are organized biennially interlaced with International Schools and Symposia on Synchrotron Radiation in Natural Science. It gathered 80 participants (see photo below) who presented 13 invited lectures, 9 oral presentations and 37 posters. Most participants came from Polish scientific institutions although some represented foreign centers (Canada, Sweden and France). During the meeting two workshops were organized: one devoted to interpretation of XANES data, “X-ray Absorption Near Edge Structure — Muffin Tin Model and beyond” (Dr. Keisuke Hatada, Laboratori Nazionali di Frascati dell’INFN, Italy), the other was a tutorial to a popular crystallographic software suite JANA2006 (Prof. Václav Petříček, Institute of Physics, Prague ASCR, Czech Republic).

Among the invited lectures, the participants had an opportunity to listen about recent progress in construction of the first Polish synchrotron in Kraków (SOLARIS - the National Synchrotron Radiation Center at Jagiellonian University) as well as about a new Polish initiative POLFEL - free electron UV laser. On a purely scientific part, the participants could acquaint themselves with, e.g. a new approaches in protein crystallography structure solution (“The first crystal structure of monomeric retroviral protease solved by online game players”) as well as new developments in the coherent X-ray diffraction imaging technique. A number of review lectures covering, e.g. x-ray absorption, magnetic

spectroscopy/microscopy or presentations of interesting applications of diffraction experiments could serve as a valuable guide for students and less experienced researchers. Selected contributions to the meeting were published in *Acta Physica Polonica A* (4th issue of vol. 121, 2012), edited by W. Paszkowicz and Z. Kaszukur. The conference materials were printed within a special issue of the Polish Synchrotron Radiation Society (PSRS) bulletin “Synchrotron Radiation in Natural Science” (ISSN 1644 – 7190) — this part was edited under Pielaszek Research software providing also the conference web management.

The Meeting offered an opportunity to celebrate 20 years of the PSRS. It was marked by a special occasional session and a banquet in the evening. To celebrate the PSRS anniversary a team of its members, advanced users of synchrotron radiation, prepared for young colleagues a tutorial book (in Polish). It describes the techniques most frequently used by Polish synchrotron users to share the experience with newcomers. The book was presented to the public during the meeting. The Society plans to convert this tutorial into regular textbook after receiving sponsorship for professional editorial work.

The Meeting has received financial support from the Polish Ministry of Science and Higher Education as well as material support from Prevac and Bruker.

The organizers take this opportunity to thank all colleagues contributing to the organization and management of the event.

Zbigniew Kaszukur
(the Meeting Chairman)



Participants of KSUPS 2011.

Welcome to the 11th ISSRNS

On behalf of the Programme Committee of the 11th International School and Symposium on Synchrotron Radiation in Natural Science (ISSRNS) we are pleased to welcome you to this School and Symposium.

The ISSRNS is a series of meetings, organized every two years since 1992, devoted to recent advances and new techniques employing synchrotron radiation in physics, chemistry, materials science, biology and medicine. The aim of this conference is to propagate the newest possibilities and achievements of the synchrotron related science as well as to enable the participants to learn and share the knowledge. Among the invited speakers are usually the specialists from synchrotron centers and the experts in different applications of the synchrotron radiation. ISSRNS meetings owe their success mainly to the lecturers from various synchrotron and scientific centers in the world, in particular: J. Dove, V. Holý, G. Margaritondo, N. Mårtensson, G. Materlik, T.H. Metzger, D.L. Nagy, P.-O. Nilsson, J. Nordgren, B. Ravel, J.J. Rehr, W. Stirling, M. Taniguchi, E. Weckert, and many others.

This year the 11th ISSRNS is organized by Polish Synchrotron Radiation Society in cooperation with Henryk Niewodniczański Institute of Nuclear Physics Polish Academy of Sciences, Kraków, Poland and under Honorary Patronage by Mayor of the Royal City of Kraków Jacek Majchrowski, General Director of the Institute of Nuclear Physics PAN Marek Jeżabek, and Rector of the Jagiellonian University in Kraków Karol Musioł.

Since foundation stone ceremony for National Synchrotron Radiation Centre SOLARIS, will take place in May in Kraków the Board of Polish Synchrotron Radiation Society decided to organize the meeting in Kraków-Tyńiec. The conference venue is very close to the place where SOLARIS will be built.

... “The Royal City of Kraków, is the major center of education in Poland. More than ten university or academy-level institutions educate 170,000 students. Kraków, is now a city of culture and science, with 22 institutions of academic education, numerous theatres, cinemas, museums, galleries, music centers and cabarets. In 1978 Kraków was placed on the UNESCO list of world heritage. The town is located 219 m above sea level, on the Vistula River, 100 km from the Tatra Mountains and 300 km from Warsaw the recent capital of Poland. The historic centre of Kraków, the former capital of Poland (till the 17th century), is situated at the foot of the Royal Wawel Castle. The 13th-century merchants’ town has Europe’s largest market square and numerous historical houses, palaces and churches with their magnificent interiors. Further evidence of the town’s fascinating history is provided by the remnants of the 14th-century fortifications and the medieval site of Kazimierz with its ancient synagogues in the southern part of town, Jagiellonian University and the Gothic cathedral on the Wawel hill where the kings of Poland were buried” ...

The conference venue is in a comfortable hotel which is situated in the natural surroundings of the Royal City of Kraków. It is situated near the Benedictine Abbey in Tyńiec, by the Vistula River, next to a leisure center with a sports hall, an indoor swimming pool, fitness facilities and a state-of-the-art kayak and raft course.

We hope you will find 11th ISSRNS as a very successful and remarkable event that could combine scientific purpose with possible rest.

Wojciech M. Kwiatek
Chairman

11th International School and Symposium on Synchrotron Radiation in Natural Science (ISSRNS'2012)

May 20th – 25th, 2012
Kraków Poland



Organized by Polish Synchrotron Radiation Society
in cooperation with Institute of Nuclear Physics Polish Academy of Science
and under the honorary patronage of:



Mayor of the Royal City
of Kraków
Jacek Majchrowski



General Director of the Institute
of Nuclear Physics, Polish
Academy of Science
Marek Jeżabek



Rector of the Jagiellonian
University in Kraków
Karol Musioł

INTERNATIONAL ADVISORY BOARD

- Dieter Einfeld
– ALBA Synchrotron Light Facility, Barcelona, Spain
- Pawel Grochulski
– Canadian Light Source, University of Saskatchewan, Saskatoon, Canada
- Jürgen Härtwig
– European Synchrotron Radiation Facility, Grenoble, France
- Udo Heinemann
– Max-Delbrück-Centrum für Molekulare Medizin, Berlin, Germany,
- Krystyna Jabłońska
– Institute of Physics, Polish Academy of Sciences, Warszawa, Poland
- Marek Jeżabek
– Institute of Nuclear Physics, Polish Academy of Science, Kraków,
Poland
- Augusto Marcelli
– Laboratori Nazionali di Frascati, Frascati, Italy
- Václav Petříček
– Institute of Physics, Academy of Sciences of the Czech Republic, Praha,
Czech Republic
- Kenya Shimada
– Hiroshima University Hiroshima Synchrotron Radiation Center,
Hiroshima, Japan
- Hiromitsu Tomizawa
– RIKEN, SPring-8 Center, Kouto, Japan

ORGANIZING COMMITTEE

- Wojciech M. Kwiatek (Chairman)
 - Institute of Nuclear Physics, Polish Academy of Science, Kraków, Poland
- Czesława Paluszkiewicz (Secretary)
 - AGH University of Science and Technology, Kraków, Poland
- Wojciech Paszkowicz (Proceedings Editor)
 - Institute of Physics, Polish Academy of Science, Warszawa, Poland
- Jakub Bielecki
 - Institute of Nuclear Physics, Polish Academy of Science, Kraków, Poland, and Świerk Computing Centre Project, National Centre for Nuclear Research, Otwock-Świerk, Poland
- Joanna Czapla
 - Institute of Nuclear Physics, Polish Academy of Science, Kraków, Poland
- Maciej Kozak
 - Adam Mickiewicz University, Poznań, Poland
- Janusz Lekki
 - Institute of Nuclear Physics, Polish Academy of Science, Kraków, Poland
- Ewelina Lipiec
 - Institute of Nuclear Physics, Polish Academy of Science, Kraków, Poland
- Anna Zachara
 - Institute of Nuclear Physics, Polish Academy of Science, Kraków, Poland
- Arkadiusz Zarzycki
 - Institute of Nuclear Physics, Polish Academy of Science, Kraków, Poland

SPONSORS

Ministry of Science
and High Education



Hamamatsu Photonics

HAMAMATSU

BRUKER



NETZSCH

NETZSCH

Renishaw Sp. z o.o.

RENISHAW
apply innovation™

PANalytical B. V. Sp. z o.o.



Spectro-Lab

Spectro-Lab

Conference Schedule

SUNDAY 20th May 2012

| | | | |
|-------------|---|-----|----|
| 17.00–17.20 | Opening | | |
| 17.20–18.00 | Claus M. Schneider , Juelich, Germany Photoelectron spectromicroscopy — opportunities and challenges | L 1 | 24 |
| 18.00–18.40 | Wojciech Rypniewski , Poznań, Poland Working hard and in the cold: Chitinase from <i>M. marina</i> | L 2 | 27 |
| 19.00–21.00 | Welcome Grill | | |

MONDAY 21st May 2012

| | | | |
|--------------|--|-----|----|
| 7.30 – 8.45 | Breakfast | | |
| 9.00 – 9.40 | Paul Dumas , Cédex, France What role does synchrotron infrared micro-spectroscopy play in biomedical applications? | L 3 | 28 |
| 9.40 – 10.20 | Małgorzata Korbas , Saskatoon, Canada Shedding synchrotron light on mercury toxicity | L 4 | 29 |
| 10.20–10.40 | Joanna Chwiej , Juelich, Germany The progress of elemental anomalies of hippocampal formation in pilocarpine model of temporal lobe epilepsy — X-ray fluorescence microscopy study | O 1 | 31 |
| 10.40–11.00 | Joanna Czaplą , Kraków, Poland The chemical species of sulphur in prostate cancer cells studied by XANES | O 2 | 32 |
| 11.00–11.30 | Coffee Break | | |
| 11.30–12.10 | Beata Ziaja-Motyka , Hamburg, Germany European X-ray free electron laser: Status and applications | L 5 | 33 |
| 12.10–12.50 | Mirosław Gilski , Poznań, Poland Atomic resolution macromolecular crystallography with synchrotron radiation | L 6 | 34 |
| 12.50–13.10 | Zuzanna Pietralik , Poznań, Poland Complexation of nucleic acids by cationic gemini surfactant | O 3 | 35 |
| 13.10–13.30 | Justyna Kutorasinska , Kraków, Poland Investigation of differences in frequency of creatine inclusions within hippocampal formation between the acute and latent periods of pilocarpine model of TLE-SRFTIR microspectroscopy study | O 4 | 36 |
| 13.30–15.00 | Lunch | | |
| 17.00–19.00 | Special Session in City Hall | | |
| | Marek Stankiewicz , Kraków, Poland SOLARIS — new light for Polish research | L 7 | 37 |
| | Paweł Olko , Kraków, Poland National Centre for Hadron Radiotherapy — Bronowice Cyclotron Centre | L 8 | 38 |
| | Grzegorz Wrochna , Warszawa, Poland POLFEL — towards a THz FEL source in Poland | L 9 | 40 |
| 19.00–21.00 | Reception at City Hall | | |
| 21.00–22.30 | Kraków by night | | |

TUESDAY 22nd May 2012

| | | | |
|--------------|---|------|----|
| 7.30 – 8.45 | Breakfast | | |
| 9.00 – 15.00 | Conference Excursion | | |
| 15.00–16.20 | Lunch | | |
| 16.20–17.00 | Hiromitsu Tomizawa, Hyogo, Japan The features and design overview of state-of-the-art XFEL | L 10 | 41 |
| 17.00–17.40 | Christian Bressler, Hamburg, Germany Observing molecular reactions via simultaneous ultrafast X-ray spectroscopy and scattering | L 11 | 42 |
| 17.40–18.00 | Coffee Break | | |
| 18.00–18.40 | Giovanni Dietler, Lausanne, Switzerland Interplay between topology and statistical properties of DNA: A polymer physics approach | L 12 | 44 |
| 18.40–19.00 | Milen Gateshki, Almelo, The Netherlands High-energy X-ray scattering studies of nanomaterials using a laboratory system | 0 5 | 45 |
| 19.00–20.00 | Dinner | | |
| 20.00–22.00 | Poster Session / JANA2006 Workshop | | |

WEDNESDAY 23th May 2012

| | | | |
|--------------|---|------|----|
| 7.30 – 8.45 | Breakfast | | |
| 9.00 – 9.40 | Tadashi Togashi, Hyogo, Japan Seeding of extreme ultraviolet free electron laser with high-order harmonic | L 13 | 46 |
| 9.40 – 10.20 | Václav Petříček, Praha, Czech Republic Solving and refining difficult structures by the program package JANA2006 | L 14 | 47 |
| 10.20–11.00 | Carlo J. Bocchetta, Kraków, Poland Techniques and technologies for ultra bright synchrotron light sources | O 6 | 48 |
| 11.00–11.30 | Coffee Break | | |
| 11.30–12.10 | Petra Rudolf, Groningen, The Netherlands Graphene growth on Cu(111): Microscopic angle-resolved photoemission and scanning tunneling microscopy investigations | L 15 | 49 |
| 12.10–12.50 | Vladimir M. Kaganer, Berlin, Germany X-ray diffraction peak profiles from relaxed epitaxial films | L 16 | 50 |
| 12.50–13.10 | Andrzej Bartnik, Warsaw, Poland Luminescence of gases induced with EUV pulses from a laser plasma source | 0 7 | 51 |
| 13.10–13.30 | Przemysław W. Wachulak, Juelich, Germany Imaging in nanoscale using laser-plasma sources of extreme ultraviolet (EUV) | 0 8 | 53 |
| 13.30–15.00 | Lunch | | |
| 15.00–15.40 | Augusto Marcelli, Frascati, Italy X-ray CT scan of stratospheric micron-sized dust particles: An attempt to a non-destructive morphological reconstruction | L 17 | 54 |
| 15.40–16.20 | Hiroyuki Oyanagi, Tsukuba, Japan Nanocrystals and small clusters investigated by synchrotron radiation and microfluidics | L 18 | 55 |
| 16.20–16.40 | Jürgen Härtwig, Grenoble, France Measurement of residual strains with quantitative X-ray topography | 0 9 | 56 |
| 16.40–19.00 | Visit to Niepołomice Royal Castle | | |
| 19.00–22.30 | Conference Dinner | | |

THURSDAY 24th May 2012

| | | | |
|--------------|---|------|----|
| 7.30 – 8.45 | Breakfast | | |
| 9.00 – 9.40 | Christian Pettenkofer , Berlin, Germany Energy converting interfaces studied by synchrotron radiation | L 19 | 57 |
| 9.40 – 10.20 | Masaki Taniguchi , Hiroshima, Japan Electronic and spin structures of solids by means of synchrotron radiation photoemission | L 20 | 58 |
| 10.20–10.40 | Krystyna Lawniczak-Jablonska , Warsaw, Poland XMCD studies of the magnetic properties of nanoclusters in GaAs matrix | O 10 | 60 |
| 10.40–13.10 | Visit to Tyniec Monastery | | |
| 13.30–15.00 | Lunch | | |
| 15.00–15.40 | Charles S. Fadley , Berkeley, USA Probing the electronic and magnetic properties of bulk materials and buried layers and interfaces with standing-wave and hard-x-ray photoemission | L 21 | 61 |
| 15.40–16.00 | Marcin Sikora , Kraków, Poland Electronic structure of A ₂ FeReO ₆ double perovskites probed with Re 2p RXES | O 11 | 63 |
| 16.00–16.20 | Andrei Rogalev , Grenoble, France X-ray Magnetic Circular Dichroism under high magnetic field | O 12 | 64 |
| 16.20–16.40 | Paweł Zajdel , Katowice, Poland Valence of constituents of selected rare earth silicides — XANES and LAPW numerical study | O 13 | 65 |
| 16.40–17.00 | Aleksandra Szkudlarek , Krakow, Poland Studies of cobalt nanoconstrictions by scanning transmission X-ray microscopy and micromagnetic simulations | O 14 | 67 |
| 17.00–17.20 | Coffee Break | | |
| 17.20–19.00 | Poster Session | | |
| 19.00–20.00 | Dinner | | |
| 20.00–22.00 | PTPS Meeting | | |

FRIDAY 25th May 2012

| | | | |
|--------------|--|------|----|
| 7.30 – 8.45 | Breakfast | | |
| 9.00 – 9.40 | Czesław Kapusta , Krakow, Poland Study of magnetoresistive nanogranular films with X-ray spectroscopies | L 22 | 68 |
| 9.40 – 10.20 | Elżbieta Guziewicz , Warsaw, Poland Resonant photoemission of 4f electrons on clean semiconductor surfaces | L 23 | 69 |
| 10.20–10.40 | Jerzy Kubacki , Katowice, Poland Resonant photoemission studies of Fe doped SrTiO ₃ thin films | O 15 | 71 |
| 10.40–11.00 | Piotr Goryl , Kraków, Poland The Solaris concepts for the beamlines control systems | O 16 | 72 |
| 11.00–11.30 | Coffee Break | | |
| 11.30–11.50 | Maciej Kozak , Poznań, Poland Structural studies of covalently stabilised oligomers of human cystatin C | O 17 | 73 |
| 11.50–12.10 | Henryk Drozdowski , Poznań, Poland Structure and intermolecular interactions in selected binary solutions studied by X-ray methods | O 18 | 74 |
| 12.10–12.30 | Pisutti Dararutana , Bangkok, Thailand Characterization of ancient burnt rice excavated in Thailand archaeological sites | O 19 | 75 |
| 12.30–12.50 | Joanna Kowalska , Kraków, Poland Effect of AVE 0991 – angiotensin-(1-7) receptor agonist treatment on elemental and biomolecules distribution in atherosclerotic plaques of apoE-knockout mice | O 20 | 76 |
| 12.50–13.10 | Aldona Kubala-Kukuś , Kielce, Poland Synchrotron radiation based micro X-ray fluorescence analysis of the calibration samples used in surface sensitive TXRF and GEXRF techniques | O 21 | 78 |
| 13.10–13.30 | Closing Remarks | | |
| 13.30–15.00 | Lunch | | |

PHOTOELECTRON SPECTRONANOSCOPY — OPPORTUNITIES AND CHALLENGES

C.M. Schneider^{1,2*}, M. Patt¹, V. Feyer^{1,3}, C. Wiemann¹, I.P. Krug¹, F. Nickel¹,
D. Gottlob, and S. Cramm¹

¹Peter Grünberg Institute (PGI-6) and JARA-FIT, Research Center Jülich, D – 52425 Jülich, Germany

²Faculty of Physics and Center for Nanointegration Duisburg-Essen (CENIDE), Universität
Duisburg-Essen, D – 47048 Duisburg, Germany

³Sincrotrone Trieste S.C.p.A., S.S. 14, km 163.5 in Area Science Park, 34012 Basovizza, Trieste, Italy

Keywords: synchrotron radiation, spectromicroscopy, photoemission microscopy

*e-mail: c.m.schneider@fz-juelich.de

The progress in key technologies is intimately connected to the synthesis and understanding of new materials as well as the refinement and optimization of known material systems. Together with improving the functionality of a material system, however, often its structural, chemical and electronic complexity increases. A major challenge in understanding the properties of these complicated layered structures is the determination of the chemical state, electronic or magnetic state/structure in a layer or at an interface. With respect to the investigation of nanosized objects, a breakthrough has been achieved by establishing total yield x-ray photoemission electron microscopy (XPEEM) as a very versatile nanoscopy technique for static and dynamic problems [1, 2].

Even more information on the details of the electronic states is provided by direct photoelectrons. In order to discriminate these in the yield spectrum an energy-filtering in XPEEM must be used [3]-[5]. We will focus on a two specific approaches, which we have established during the last two years. The first one combines an electrostatic PEEM column with a double-hemispherical energy analyser to permit laterally resolved XPS studies. This instrument has been coined “NanoESCA” and has been recently installed at the soft x-ray nanospectroscopy beamline at the storage ring facility Elettra (Italy) [6]. The second approach employs an aberration-corrected LEEM/PEEM instrument [5], which has been installed at the Jülich soft x-ray beamline at BESSY-II (Berlin).

The NanoESCA instrument — The system at ELETTRA features a novel electrostatic lens system with 30 kV extraction voltage, a double-hemispherical energy filter [7], a single-event counting detector unit, and a 5-axis sample manipulator with liquid helium cooling. The system provides two operation modes: (i) spatially resolved photoelectron imaging with a lateral resolution of < 100 nm, and (ii) mapping of the photoelectron angular distribution (k-space microscopy). It is also equipped with a surface science preparation chamber and a load-lock system to introduce samples without breaking the UHV.

Soft XPS Imaging — A first test has been carried out on a grating-type sample with variable line

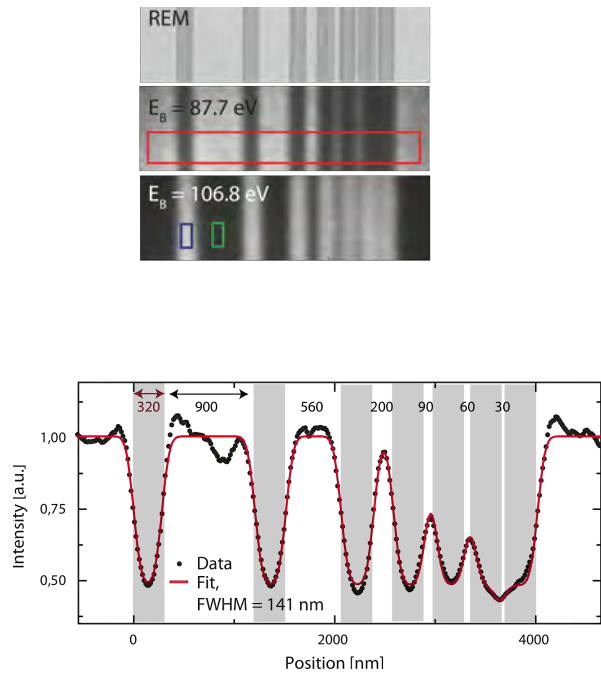
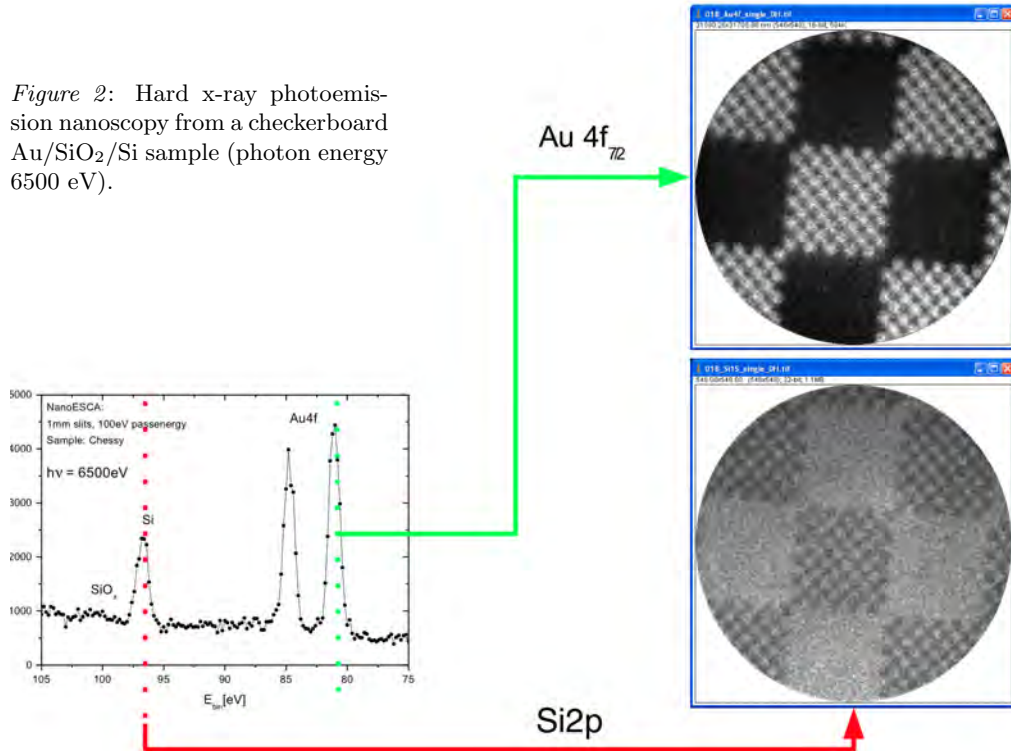


Figure 1: Soft x-ray photoemission nanoscopy from a grating-type Au/SiO₂/Si sample (photon energy 200 eV).

spacing. For this purpose, 320 nm wide grooves have been milled by a focused ion beam into a Au film on a SiO₂/Si template, leaving behind Au lines with widths ranging from 900 nm down to 30 nm. The data (Fig. 1) show a scanning electron microscope image compared to XPS images on the Au 4*f* ($E_B = 87.8$ eV) and Si 2*p* ($E_B = 106.8$ eV) photoemission lines. In the Si 2*p* line we can discern an image contrast even down to the smallest Au line. A quantitative analysis of the lateral resolution is obtained on the basis of a line scan across the Au pattern reproduced in the bottom part of the figure. This line scan is the average of horizontal pixel lines in the Au 4*f* image. Fitting the experimental data by a set of Lorentzians and step functions yields a value of 141 nm for the FWHM of the Lorentzians. This is a measure of the lateral resolution obtained in this experiment.

Hard XPS Imaging — Fig. 2 displays the first result obtained by hard x-ray nanoscopy from a Au/Si checkerboard calibration sample. The photon energy has been 6.5 keV. Because of the low photo-

Figure 2: Hard x-ray photoemission nanoscopy from a checkerboard Au/SiO₂/Si sample (photon energy 6500 eV).



emission cross section in hard x-ray photoemission and the resulting low signal levels, we operated the microscope with the largest available contrast aperture (500 μm), which limits the lateral resolution. The data demonstrate clearly that element-selective imaging on the Au 4*f* and Si 2*p* is feasible. In both cases the kinetic energy of the photoelectrons is more than 6.4 keV. The inelastic mean free path of the photoelectrons at this kinetic energy is about 10 nm, which is still well below the thickness of the Au layer. Therefore, we see a clear contrast inversion in the images when switching between the Au 4*f* and Si 2*p* photoemission signal. A further analysis of the images reveals a lateral resolution of about 450 nm, which agrees well with the expectations from electron-optical simulations for the chosen contrast aperture. We could also demonstrate that it is possible to image the interface in a Au/SrTiO₃ layer structure through the 10 nm thick Au top layer.

Reciprocal Space Mapping — By using a diffraction lens behind the objective the angular distribu-

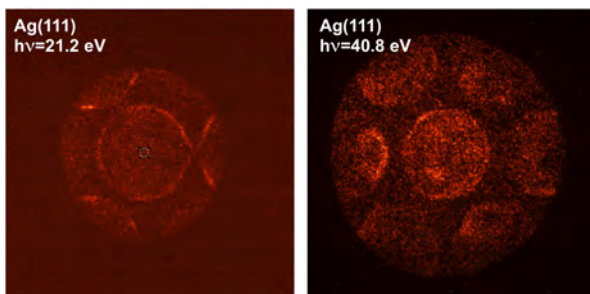


Figure 3: Fermi surface mapping from a Ag(111) surface at two different photon energies.

tion rather than the spatial distribution of the photoelectrons is mapped onto the image detector. By choosing appropriate kinetic energies of the photoelectrons this allows one to image a cut through the energy distribution curves. In particular, if the kinetic energy corresponds to the Fermi energy E_F we are able to directly map the Fermi surface. This is demonstrated in Fig. 3 for a Ag(111) surface. The photon energy of $h\nu = 21.2$ eV gives access to the first Brillouin zone (BZ) which is seen as a circle around the center of the image. In addition, small parts of the neighboring BZs are seen. The angular field of view is not limited by the microscope settings but the maximum k-vector transfer at this photon energy. This becomes obvious by increasing the photon energy to $h\nu = 40.8$ eV. Now the wave vector transfer allows one to probe a larger portion of the nearest neighbor BZs and to access also the next nearest neighbor BZs. This operation mode has also been employed to study topological insulators.

We will also report on first experiences with the aberration corrected PEEM/LEEM system at the synchrotron radiation source BESSY in Berlin. This instrument is mainly dedicated to time-resolved studies of magnetization dynamics with an emphasis on high lateral resolution rather than spectroscopic capabilities.

Acknowledgments: This work has been financially supported by the Deutsche Forschungsgemeinschaft through SFB 491, SFB 917 and the German Ministry of Education and Research BMBF (contract No. 05KS7UK1).

References

- [1] J. Feng and A. Scholl, *Photoemission Electron Microscopy in: Science of Microscopy, vol. I*, P.W. Hawkes and J.C.H. Spence, Eds. (Springer, Berlin, 2007).
- [2] G. Schönhense, H.J. Elmers, S.A. Nepijko, and C.M. Schneider, “Time-resolved photoemission electron microscopy,” *Adv. Im. El. Phys.* **142** (2006) 159.
- [3] A. Locatelli and E. Bauer, “Recent advances in chemical and magnetic imaging of surfaces and interfaces by XPEEM,” *J. Phys.: Cond. Matter* **20** (2008) 093002.
- [4] M. Escher, K. Winkler, O. Renault, and N. Barrett, “Applications of high lateral and energy resolution imaging XPS with a double hemispherical analyser based spectromicroscope,” *J. Electron Spectr. Rel. Phenom.* **178 - 179** (2010) 303.
- [5] R.M. Tromp, J.B. Hannon, A.W. Ellis, W. Wan, A. Berghaus, and O. Schaff, “A new aberration-corrected, energy-filtered LEEM/PEEM instrument. I. Principles and design,” *Ultramicroscopy* **110** (2010) 852.
- [6] C. Wiemann, M. Patt, I.P. Krug, N.B. Weber, M. Escher, M. Merkel, and C.M. Schneider, “A new nanospectroscopy tool with synchrotron radiation: NanoESCA@Elettra,” *e-J. Surf. Sci. Nanotech.* **9** (2011) 395.
- [7] M. Escher, N. Weber, M. Merkel, C. Zietzen, P. Bernhard, G. Schönhense, S. Schmidt, F. Förster, F. Reinert, B. Krömker, and D. Funnemann, “NanoESCA: A novel energy filter for imaging x-ray photoemission spectroscopy,” *J. Phys.: Cond. Matter* **17** (2005) S1329.

WORKING HARD AND IN THE COLD: CHITINASE FROM *M. marina*W. Rypniewski^{1*}, P.H. Małecki¹, and C.V. Vorgias²¹Institute of Bioorganic Chemistry PAN, Noskowskiego 12/14, 61-704 Poznań, Poland²Department of Biochemistry and Molecular Biology, National and Kapodistrian University of Athens, Panepistimiopolis-Zographou, 15784 Athens, Greece

Keywords: synchrotron radiation, macromolecular crystallography, chitinase, psychrophile

*e-mail: wojtekr@ibch.poznan.pl

A wide variety of microorganisms are present in cold environment, displaying a diverse range of adaptations. The major part of the marine biosphere is characterized by permanent low temperatures (-2 – 10°C) and therefore is a good source of cold-adapted marine bacteria, the so-called psychrophilic bacteria. Chitin is a very abundant insoluble biopolymer in the marine environment and is composed of linear chains of β -1,4-linked N-acetyl-D-glucosamine (NAG) residues that are highly cross-linked by hydrogen bonds. Chitin is abundant in nature, second after cellulose, as a crucial structural component of the cell walls of fungi and certain green algae, and as a major constituent of shells, cuticles and exoskeletons of worms, molluscs and arthropods, including crustaceans and insects. Chitin and its partially deacetylated derivative, chitosan, as well as other derivatives exhibit interesting properties and constitute a valuable raw material for biomedical, agricultural, cosmetics, and innovative biotechnological applications. In the aquatic biosphere, approximately 10^{11} tons of chitin are produced annually.

Chitinases (EC 3.2.1.14) hydrolyse the β -1,4-linkages in chitin. Chitinases produced by psychrophilic bacteria, responsible for degradation of the krill chitin, should have high catalytic activities under these low-temperature conditions and most often, if not always, exhibit high thermosensitivity. These properties can be very useful for various applications.

We report the crystal structure of a chitinase from the psychrophilic bacterium *Moritella marina*. The enzyme has been examined in complexes with the reaction intermediate, with the reaction product and in an unliganded form. The enzyme consists of 528 amino-acid residues arranged into four domains: a β/α -barrel that includes the substrate-binding and the active site, two elongated domains having an Ig-like fold, and a small chitin-binding

domain (Figure 1). The enzyme is active in the crystal form. It has reduced a NAG₄ substrate, added to the cryo-protecting solution, to an oxazolinium reaction intermediate. In another experiment it reduced NAG₃ to NAG₂. The results of its activity are clear in the electron density and have been examined in order to determine the basis of substrate recognition and the enzymatic activity.

Comparisons with related enzymes have been used to identify features that are conserved, and therefore are presumed to be essential, and those that have been evolving and are therefore likely to be the enzyme's response to the specific environment.

Psychrophilic enzymes have been proposed to possess some "additional flexibility" that allows them to function efficiently at low temperature. We have examined the crystal structure of the psychrophilic chitinase looking for such features.

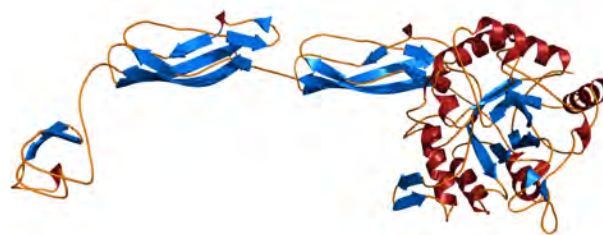


Figure 1: Ribbon diagram of chitinase from *M. marina*.

Acknowledgments: This work was supported by the Foundation for Polish Science and EU structural funds.

References

- [1] E. Stefanidi, C.E. Vorgias, "Molecular analysis of the gene encoding a new chitinase from the marine psychrophilic bacterium *Moritella marina* and biochemical characterization of the recombinant enzyme," *Extremophiles*. **12** (2008) 541.

WHAT ROLE DOES SYNCHROTRON INFRARED MICRO-SPECTROSCOPY PLAY IN BIOMEDICAL APPLICATIONS?

P. Dumas*

SOLEIL Synchrotron, BP48, 91192 Gif Sur Yvette Cédex, France

* e-mail: paul.dumas@synchrotron-soleil.fr

Synchrotron radiation is best known as a source of X-rays, but it is also a source for VUV to soft-X-rays photons. However, it was realised in the early 90's that this source can also be exploited in the infrared energy domain. Even if in some frequency regions (roughly 30 microns and below) the total photon flux emitted by the synchrotron source remains inferior to that of a thermal source, the brightness of a synchrotron largely exceeds that of a laboratory thermal source. Enhancement as high as three orders of magnitude has been achieved in terms of brightness (or brilliance or spectral radiance). This is essentially the feature that is most exploited in infrared spectroscopy and microscopy. Besides brightness, other characteristics like time structure (few picoseconds duration) and well-defined polarization states are being also exploited.

The main sources of infrared photons from storage rings are edge emission and bending magnet emission, and many recent infrared beamlines exploit both sources to double their experimental capacity.

Synchrotron infrared spectroscopy and micro-spectroscopy held a big promise in medical diagnosis. It is a powerful methodology to identify metabolic changes occurring at single cell level.

The brightness advantage, combined with a high beam stability (especially on recent third generation synchrotron), has resulted in fast data recording at high lateral resolution, with very good spectral quality (S/N). There exist several biological and biomedical applications which emphasize on the promising future of synchrotron infrared micro-spectroscopy in these scientific disciplines.

Among relevant examples, I will focus on the following:

- Urinary stone disease, constitutes a major health problem and is affecting an increasing number of people. Calcium oxalate, calcium phosphate, uric acid, ammonium hydrogen urate and magnesium ammonium phosphate are the main components of stones. Very

small crystals in the kidney biopsy sample, of 2.8-dihydroxyadenine (2.8-DHA) were identified, and this has direct relevant therapeutic implications. IR synchrotron microscopy is actually routinely used by doctors from Hospital for a rapid screening of kidney sections. This results in a direct implication in the patient therapy and recovery.

- The potential changes occurring in hematopoietic cells expressing BCR-ABL and BCR-ABL carrying T3151 mutation, conferring resistance to most tyrosine kinase inhibitors currently used has been evaluated using IR micro-spectroscopy. The use of the synchrotron is fully justified due to the small dimension of human leukemia cells.
- Stem cells research is a very important research topic nowadays. Several studies have shown that IR microscopy can determine the differentiation state of the stem cells. But more importantly, we have been able to show that synchrotron IR microscopy can assess unambiguously the reprogramming of stem cells, which is more difficult otherwise.
- Liver steatosis is a severe disease that can lead to hepatosteatosis, cirrhosis and cancer. The precise determination of the steatosis content during the liver transplant is crucial with recommendation to select livers exhibiting no more than 20% steatosis. This drastic recommendation contrasts with the incapacity of usual histological methods to rigorously provide an objective and non-biased assessment of steatosis. Synchrotron infrared microspectroscopy has helped determining the presence of micro vesicle with lipids content that can be directly related to the lipidomic HPLC tests. The database established with the synchrotron source is actually used to condition an IR thermal source based microscope, to be set up in hospital for direct diagnostic during liver transplant.

SHEDDING SYNCHROTRON LIGHT ON MERCURY TOXICITY

M. Korbas^{1*}, T.C. MacDonald^{2,3,4}, N.J. Sylvain⁴, I.J. Pickering²,
G.N. George^{2,3,4} and, P.H. Krone^{3,4}

¹Canadian Light Source Inc., Saskatoon, SK, Canada

²Molecular and Environmental Science Research Group, Department of Geological Sciences, University of Saskatchewan, Saskatoon, SK, Canada

³Toxicology Centre, University of Saskatchewan, Saskatoon, SK, Canada

⁴Department of Anatomy and Cell Biology, University of Saskatchewan, Saskatoon, SK, Canada

*e-mail: Gosia.Korbas@lightsources.ca

Mercury is among the most problematic toxicants to which human populations are exposed. The nature and the extent of mercury toxicity depend largely on its molecular form. Neurotoxic methylmercury (CH_3Hg^+) compounds are particularly insidious due to the latency in the onset of toxic symptoms. Low level but widespread human exposure to methylmercury occurs through consumption of fish and shellfish. The WHO has estimated that over one billion people worldwide depend on fish for daily nutrition and thus may be at higher risk. Despite public health concerns, relatively little is known about the biochemical mech-

anisms underlying the neurotoxicity of methylmercury.

To some extent, this gap in our knowledge is caused by a lack of techniques suitable to probe chemical form of mercury as well as its localization directly *in situ*. Two synchrotron-based methods offer great possibilities in this respect. Synchrotron X-ray absorption spectroscopy (XAS) can reveal chemical speciation of the elements of interest in intact biological tissues whereas synchrotron X-ray fluorescence imaging (XFI) can directly visualize distributions of these elements down to the cellular and even subcellular levels (Figure 1).

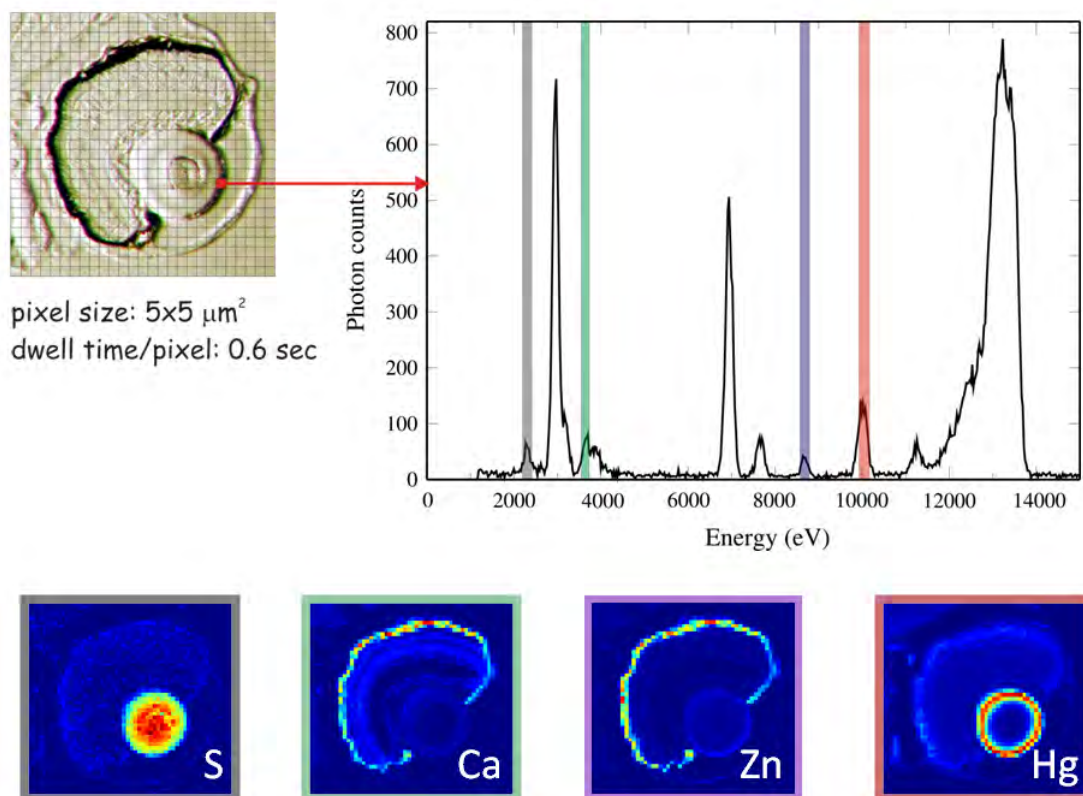


Figure 1: Principles of X-ray fluorescence imaging. The elemental distribution images (*lower panel*) are built by raster scanning a specimen, here, a 6 micron-thick section of a zebrafish larval eye (*upper panel, left*), in the synchrotron micro-beam and collecting the excited X-ray fluorescence signal (*upper panel, right*) from each irradiated spot. Maps are then obtained by filtering from each spectrum the X-ray fluorescence signal at the energies specific for the respective element.

To understand the molecular pathways by which mercury affects the function of the targeted organ, we have combined the zebrafish model system with synchrotron techniques. By taking advantage of the remarkably high elemental specificity and spatial resolution of XFI, we have revealed specific accumulation of methylmercury in the eye tissue (lens epithelium/fibers and retina) [1]-[3]. Recently, by taking advantage of a sub-micron X-ray beam spot size offered by the 2-ID-D beamline at the Advanced Photon Source (Argonne, USA), we have been able to pinpoint an exact cellular localization of methylmercury within the retina and other target organs.

In addition, using the same approach, we have also investigated the efficacy of two mercury chelators, meso-2,3-dimercaptosuccinic acid (DMSA) and alpha-lipoic acid (ALA), in treating mercury intoxication in developing zebrafish larvae following their acute exposures to organic and inorganic mercury toxicants.

This presentation will showcase some of the recent studies into the toxicology of mercury using synchrotron techniques. A main focus will be on the tissue and cell specific accumulation of different mercury compounds in developing vertebrates,

with a special emphasis on mercury uptake by sensory organs. The efficacy of the studied chelators in reducing mercury burdens will also be highlighted.

In addition, I will briefly introduce the BioXAS Facility, a currently constructed suite of three beamlines at the Canadian Light Source, which has been specifically tailored for biological and health-related studies of metals in living systems using XAS and XFI.

References

- [1] M. Korbas, S.R. Blechinger, I.J. Pickering, P.H. Krone, G.N. George "Localizing organomercury uptake and accumulation in zebrafish larvae at the tissue and cellular level," *Proc. Natl. Acad. Sci. U.S.A.* **105** (2008) 12108 – 12112.
- [2] M. Korbas, P.H. Krone, I.J. Pickering, G.N. George, "Dynamic accumulation and redistribution of methylmercury in the lens of developing zebrafish embryos and larvae," *J. Biol. Inorg. Chem.* **15** (2010) 1137 – 1145.
- [3] M. Korbas, T.C. MacDonald, I.J. Pickering, G.N. George, P.H. Krone, "Chemical form matters: Differential accumulation of mercury following inorganic and organic mercury exposures in zebrafish larvae," *ACS Chem. Biol.* **7** (2012) 411 – 420.

THE PROGRESS OF ELEMENTAL ANOMALIES OF HIPPOCAMPAL FORMATION IN PILOCARPINE MODEL OF TEMPORAL LOBE EPILEPSY — X-RAY FLUORESCENCE MICROSCOPY STUDY

J. Chwiej^{1*}, J. Kutorasinska¹, K. Janeczko², K. Gzielo-Jurek², L. Uram²,
K. Appel³, R. Simon⁴, and Z. Setkowicz²

¹AGH University of Science and Technology, Faculty of Physics and Applied Computer Science, Krakow, Poland

²Jagiellonian University, Faculty of Biology and Earth Sciences, Department of Neuroanatomy, Krakow, Poland

³Deutsches Elektronen-Synchrotron (DESY), Hamburg, Germany

⁴Institut für Synchrotronstrahlung, Research Centre Karlsruhe, Karlsruhe, Germany

Keywords: pilocarpine model of epilepsy, topographic and quantitative elemental analysis, X-ray fluorescence microscopy, synchrotron radiation

*e-mail: Joanna.Chwiej@fis.agh.edu.pl

Although epilepsy has been a serious problem of clinical neurology for many years, the mechanisms of its pathogenesis are still not fully understood. The analysis of nervous tissue from the period of epileptogenesis is possible based on the animal models of the disease. Animal models of epilepsy help better understand the mechanisms leading to spontaneous seizure activity, allow observations of the progress and character of seizures as well as evaluation of the action of new antiepileptic drugs [1, 2]. The most frequently occurring type of epilepsy in adults is the temporal lobe epilepsy (TLE) and the most frequently used and highly isomorphic with human cases of TLE animal model is one with seizures induced with pilocarpine.

Administration of pilocarpine in rats evokes sequential behavioral and electrographic changes that can be divided into three distinct periods: an acute period that builds up progressively into a limbic *status epilepticus* (24 h), a silent (latent) period with progressive normalization of EEG and behavior (from a few to a few dozen days) and a chronic period with spontaneous recurrent seizures [3].

The main purpose of the present investigations was the analysis of the dynamics of elemental changes observed in rat hippocampus as a result of pilocarpine induced seizures. For the topographic and quantitative elemental analysis of tissues, taken from animals 3 hours (SE3H group) and 1 (SE24H), 4 (SE4D) and 7 (SE7D) days from pilocarpine administration, X-ray fluorescence microscopy was applied. The measurements were carried out at HASYLAB beamline L and at ANKA beamline FLUO. The 17 keV beams focused using the polycapillary optics to 15 and 12 μm were used

for the study. The analysis of the differences in the hippocampal accumulation of S, K, Ca, Fe, Cu and Zn between the analyzed animal groups showed that seizure induced excitotoxicity, mossy fiber sprouting and iron induced oxidative stress are the mechanisms involved in the neurodegenerative processes which may finally lead to spontaneous seizures in the chronic period of pilocarpine model.

Acknowledgments: This work was supported by the Polish Ministry of Science and Higher Education and the following grants:

- Polish Ministry of Science and Higher Education grant IUVENTUS PLUS no. JP2010005370,
- HASYLAB experimental grant I-20110056 EC,
- ANKA experimental grant BIO-1.

References

- [1] W. Loscher, “Animals models of epilepsy for the development of antiepileptogenic and disease-modifying drugs. A comparison of the pharmacology of kindling and post-status epilepticus models of temporal lobe epilepsy,” *Epilepsy Res.* **50** (2002) 105 – 123.
- [2] A.K. Sharma, R.Y. Reams, W.H. Jordan, M.A. Miller, H.L. Thacker, P.W. Snyder, “Mesial temporal lobe epilepsy: pathogenesis, induced rodent models and lesions,” *Toxicol. Path.* **35** (2007) 984 – 999.
- [3] F.A. Scorza, R.M. Arida, M. da Graca Naffah-Mazzacoratti, D.A. Scerni, L. Calderazzo, E.A. Cavalheiro, “The pilocarpine model of epilepsy: What have we learned?,” *An. Acad. Bras. Cienc.* **81** (2009) 345 – 365.

THE CHEMICAL SPECIES OF SULPHUR IN PROSTATE CANCER CELLS STUDIED BY XANES

J. Czapla^{1*}, W.M. Kwiatek¹, J. Lekki¹, J. Dulińska², R. Steininger³, and J. Göttlicher³

¹*Institute of Nuclear Physics PAN, ul. Radzikowskiego 152, 31-342 Kraków, Poland*

²*Chair of Medical Biochemistry, Jagiellonian University Medical College, Kopernika 7, 31-034 Kraków, Poland*

³*Karlsruhe Institute of Technology, Institute for Synchrotron Radiation, Hermann-von-Helmholtz-Platz 1, D-76344 Eggenstein-Leopoldshafen, Germany*

Keywords: XANES, prostate cancer, sulphur

** e-mail: joanna.czapla@ifj.edu.pl*

The role of sulphur in prostate cancer progression may be significant for understanding the process of carcinogenesis. This work, based on XANES spectroscopy, is focusing on determination of sulphur chemical species occurring in prostate cancer cell lines. Changes in the ratio of oxidized and reduced sulphur forms may indicate changes in redox balance due to the oxidation stress. Oxidation stress, the biochemical condition characterized by an imbalance between cellular oxidizing and reducing species, provides unusual oxidizing conditions in vivo, characterized by the presence of reactive oxygen species that can cause oxidative damage to

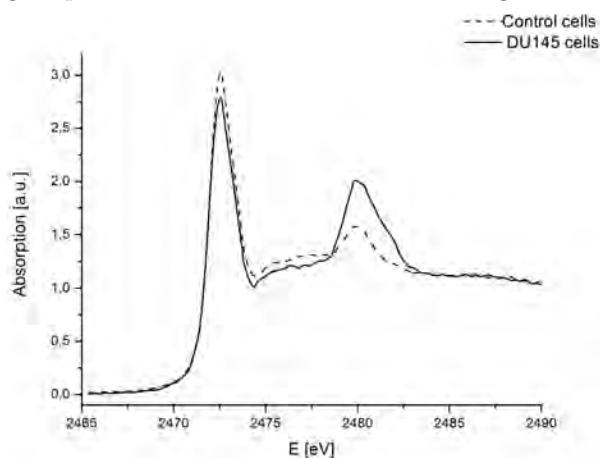


Figure 1: The k-edge XANES spectra of sulphur obtained from DU145 cells and control cells.

biomolecules [1]. Such a damage may lead to carcinogenesis and that is the reason of this type of studies.

The experimental material consisted of four commercially available cell lines: three from metastasized prostate cancer (PC3, LNCaP, DU145) and one from the peripheral zone of the prostate, used as a control (PZ-HPV-7). The experiment was performed at the SUL-X beamline of the synchrotron radiation source ANKA, Karlsruhe (Germany). The K-edge XANES spectra of sulphur were analysed in order to establish sulphur species that occur in prostate cancer cells and whether there are any differences between their content in the various cell lines. As an example the comparison between XANES spectrum from DU145 and control cell lines is presented in Fig. 1.

The results obtained are discussed in terms of the differences in cells morphology and sulphur biochemistry.

Acknowledgments: The research leading to these results has received funding from the European Community's Seventh Framework Programme (FP7/2007 – 2013) under grant agreement n° 226716 (proposal BIO-12). We acknowledge ANKA for support and granting beamtime in the proposal BIO-12.

References

- [1] C. Jacob, G.I. Giles, N.M. Giles, H. Sies, "Sulfur and selenium: the role of oxidation state in protein structure and function," *Angew. Chem. Int. Ed.* **42** (2003) 4742.

EUROPEAN X-RAY FREE ELECTRON LASER: STATUS AND APPLICATIONS

B. Ziaja-Motyka*

CFEL, DESY and INP, Kraków

* *e-mail*: beata.ziaja-motyka@desy.de

In my presentation a concise overview of the present status of the research with free-electron-lasers (FELs) will be given. I will explain the operating principle of FELs and present their potential applications to imaging of single particles and time-resolved studies of ultrafast dynamics in atomic,

condensed matter, plasma physics and in materials science in the context of experiments planned at the European X-ray FEL facility. Finally, I will discuss the basics on the interaction of FEL radiation with matter that has implications for all FEL applications.

ATOMIC RESOLUTION MACROMOLECULAR CRYSTALLOGRAPHY WITH SYNCHROTRON RADIATION

M. Gilski *

Department of Crystallography, Faculty of Chemistry, A. Mickiewicz University, Poznań, Poland
and Center for Biocrystallographic Research, Institute of Bioorganic Chemistry,
Polish Academy of Sciences, Poznań, Poland

Keywords: atomic resolution structures, X-ray crystallography, synchrotron radiation

* e-mail: mirek@amu.edu.pl

The recent developments at modern third-generation synchrotron radiation facilities with highly sensitive, fast and reliable detectors have a huge impact on macromolecular X-ray crystallography. High-brilliance synchrotron sources allow to determine macromolecule structures with atomic and subatomic resolution. In connection with a number of methodological improvements and new crystallographic software ranging from data processing to refinement [1], all it gave the opportunity to determination of the macromolecular structures with unprecedented extremely high resolution and quality, at a level traditionally reserved for small molecules.

At this resolution, individual atoms are clearly resolved and fine details of the structures become visible direct in the electron density maps.

The main importance of such structures is the possibility of having broader insights into macromolecule function. At very high resolution, hydrogen atoms can be seen in electron density maps and the detailed information about the protonation states of catalytically important residues can be studied, what often is critical for full understanding of molecular mechanisms.

The high data to parameter ratio permits the refinement of individual anisotropic atomic displacement parameters and the information on the mobility of a macromolecule and dynamic processes can be read from the crystal structure.

Atomic resolution gives the opportunity for clear definition of multiple conformations, although the proportion of disordered residues is higher at higher

resolution, and the disorder is seen as distinct alternative conformations.

Water in macromolecule crystal occupies 30 – 70 % of the unit cell and plays an important role in macromolecule's function and stabilization. Ultrahigh resolution data allows to refine water molecules with anisotropic displacement parameters and refine them with fractional occupancies. In this situation analysing the subtle hydrogen bond network, involving precisely located water molecules, is possible.

Atomic resolution structures can be refined without or with only weak stereochemical restraints. Macromolecular models refined at ultrahigh resolutions, for well ordered structures, can be used for validation and improvement of stereochemical restraint libraries [1, 2], commonly used during refinement of lower resolution structures.

References

- [1] M. Gilski, "Data processing programs for analysis of diffraction images of macromolecular crystals recorded using synchrotron radiation," *Acta Phys. Pol. A* **121**(4) (2012) 871 – 875.
- [2] M. Jaskolski, M. Gilski, Z. Dauter, A. Wlodawer, "Stereochemical restraints revisited: How accurate are refinement targets and how much should protein structures be allowed to deviate from them," *Acta Cryst.* **D63** (2007) 611 – 620.
- [3] M. Jaskolski, M. Gilski, Z. Dauter, A. Wlodawer, "Numerology versus reality: A voice in a recent dispute," *Acta Cryst.* **D63** (2007) 1282 – 1283.
- [4] K. Brzezinski *et al.*, "High regularity of Z-DNA revealed by ultra high-resolution crystal structure at 0.55 Å," *Nucleic Acids Res.* **39** (2011) 6238 – 6248.

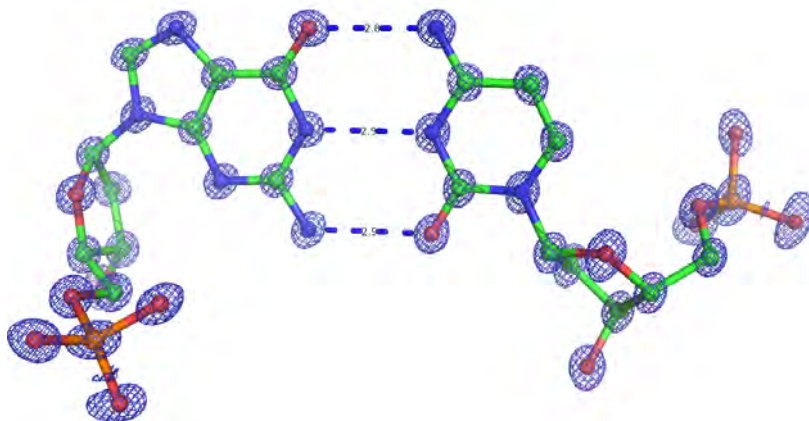


Figure 1: Fragment of electron density map of extremely high resolution structure of Z-DNA hexamer duplex d(CGCGCG) [4]. Cyt3-Gua10 base pair with the corresponding F_{obs} map at 1.5σ contour level, resolution 0.53 Å.

COMPLEXATION OF NUCLEIC ACIDS BY CATIONIC GEMINI SURFACTANT

Z. Pietralik and M. Kozak*

*Department of Macromolecular Physics, Faculty of Physics, Adam Mickiewicz
University, Umultowska 85, 61-614 Poznań, Poland*

Keywords: gene therapy, gemini surfactants

**e-mail: mkozak@amu.edu.pl*

Complexation of DNA is a great issue for drug delivery and gene therapy development [1]. Many amphiphilic compounds have been tested for possible applications in these fields, among them, gemini surfactants (consisting of 2 cationic head groups and 2 hydrophobic tails linked by a spacer group) appear to be very promising candidates because of their high transfection efficiency and low cytotoxicity [2].

The aim of this work was to investigate the interaction of DNA (from Salmon sperm) with cationic gemini surfactant 1,1'-(1,4 butane)bis-3-dodecyloxymethylimidazolium chloride and to determine the ability of this gemini surfactant to complexation of DNA molecules.

The ability of surfactant to complex DNA was evaluated by running the agarose gel electrophoresis. Circular dichroism (CD) experiments were carried out with Jasco J-815 CD spectrometer. A series of the SAXS data sets were collected at DESY, at the EMBL beam line X33 (Hamburg, Germany) [3], using synchrotron radiation with a wavelength 0.15 nm and Pilatus detector. Measurements were performed at 20°C for the scattering vector $0.05 < s < 5.0 \text{ nm}^{-1}$. All data sets were normalized to the incident beam intensity, corrected for detector response and scattering from the buffer was subtracted using PRIMUS [4].

CD spectrum shows that with increasing concentration of gemini surfactant, DNA undergoes conformational changes from native B-form to chiral

Ψ -phase. In this phase DNA has a highly condensed structure with surfactant in the outer layer. The SAXS measurements and agarose gel electrophoresis also indicated that the gemini surfactant studied forms stable complexes with DNA molecules.

Acknowledgments: The research was supported by research grant (UMO-2011/01/B/ST5/00846) from National Science Centre (Poland).

References

- [1] M. Cao, M. Deng, X-L. Wang, Y. Wang, "Decompaction of cationic Gemini surfactant-induced DNA condensates by β -cyclodextrin and anionic surfactant," *J. Phys. Chem. B* **112** (2008) 13648 – 13654.
- [2] P. Camilleri, A. Kremer, A. Edwards, K.H. Jennings, O. Jenkins, I. Marshall, C. McGregor, W. Nevelle, S.Q. Rice, R.J. Smith, M.J. Wilkison, A.J. Kirby, "A novel class of cationic Gemini surfactants showing efficient in vitro gene transfection properties," *Chem. Commun.* **14** (2000) 1252 – 1254.
- [3] M.W. Roessle, R. Klaering, U. Ristau, B. Robrahn, D. Jahn, T. Gehrman, P. Konarev, A. Round, S. Fiedler, C. Hermes, D.I. Svergun, "Upgrade of the small-angle X-ray scattering beamline X33 at the European Molecular Biology Laboratory, Hamburg," *J. Appl. Crystallogr.* **40** (2007) 190 – 194.
- [4] P.V. Konarev, V.V. Volkov, A.V. Sokolova, M.H.J. Koch, D.I. Svergun, "PRIMUS: A Windows PC-based system for small-angle scattering data analysis," *J. Appl. Crystallogr.* **36** (2003) 1277 – 1282.

INVESTIGATION OF DIFFERENCES IN FREQUENCY OF CREATINE INCLUSIONS WITHIN HIPPOCAMPAL FORMATION BETWEEN THE ACUTE AND LATENT PERIODS OF PILOCARPINE MODEL OF TLE-SRFTIR MICROSPECTROSCOPY STUDY

J. Kutorasinska^{1*}, Z. Setkowicz², K. Janeczko², C. Sandt³, P. Dumas³, and J. Chwiej¹

¹AGH-University of Science and Technology, Faculty of Physics and Applied Computer Science, Krakow, Poland

²Jagiellonian University, Faculty of Biology and Earth Sciences, Department of Neuroanatomy, Krakow, Poland

³SOLEIL, St Aubin, France

Keywords: epilepsy, creatine, synchrotron radiation, SR FTIR microspectroscopy

*e-mail: Justyna.Kutorasinska@fis.agh.edu.pl

Epilepsy is one of the most common neurological disorders and despite of the longtime history of researches under this disease the etiology of almost 70% of its cases is still unknown. The investigation under the pathogenesis of epilepsy are rarely carried out based on the human tissues, which can be obtained only post mortem or during the resection of epileptic foci. Therefore, different animal models of epileptic seizures are used.

Epidemiological studies shows that the most frequently occurring type of epilepsy in adults is temporal lobe epilepsy (TLE) and the main features of TLE are [1]:

1. localization of epileptic foci in the limbic system,
2. a seizure-free time interval following the precipitating injury,
3. the presence of hippocampal sclerosis leading to reorganization of neuronal networks [2].

Highly isomorphic with human cases of TLE is animal model of epilepsy with pilocarpine induced seizures. After pilocarpine administration in animals three distinct periods can be distinguished in their behaviors. They are as follows:

1. an acute period occurring during the first 24 hours after pilocarpine injection,
2. a silent period with progressive normalization of EEG and behavior and lasting from around 4 to 44 days,
3. a chronic period in which spontaneous recurrent seizures may occur [3].

The present work is the continuation of our previous research in frame of which the frequency of creatine inclusions in hippocampal formation was examined for rats in the acute period after pilocarpine injection. The comparison of epileptic animals with controls showed an increased accumulation of creatine deposits which were localized mainly in the dentate gyrus hippocampal area and in the multiform cell layer. What is more, obtained data pointed to statistically important correlation between the number of inclusions and the total time of seizure activity within the observation period [4].

The purpose of the present study was comparison of the number of creatine inclusions in hippocampal formation for the acute and latent periods after injection of pilocarpine. As in our previous research, synchrotron Fourier-transform infrared microspectroscopy (SRFTIR) was used for the detection of creatine in tissues. The measurements were done at SMIS beamline of SOLEIL. The use of synchrotron source of infrared radiation allowed us to carry out the research with the spatial resolution of 10 μm . Because SRFTIR microspectroscopy is non-invasive and nondestructive method we were able to verify obtained results with the use of Raman microspectroscopy [5].

Results of the present work showed that accumulation of creatine inclusions in the epileptic hippocampus is not only temporary but permanent effect of pilocarpine induced seizures.

Acknowledgments: This work was supported by Polish Ministry of Science and Higher Education and Polish National Science Centre grant: 2921/B/T02/2011/40. We acknowledge SOLEIL for provision of synchrotron radiation facilities (Proposal ID 20090749 and 20100664).

References

- [1] E.J. Pedley, *Epilepsy: A Comprehensive Textbook* (Williams & Wilkins, Philadelphia 2008).
- [2] G. Curia, D. Longo, G. Biagini, R.S.G. Jones, M. Avoli, "The pilocarpine model of temporal lobe epilepsy," *J. Neurosci. Meth.* **172** (2008) 143 – 157.
- [3] F.A. Scorza, R.M. Arida, M. Da Graca Naffah-Mazzacoratti, D.A. Scerni, L. Carderazzo, E.A. Cavalheiro, "The pilocarpine model of epilepsy: What have we learned?," *An. Acad. Cienc.* **81** (2009) 345 – 365.
- [4] J. Dulinska, Z. Setkowicz, K. Janeczko, C. Sandt, P. Dumas, L. Uram, K. Gzielo-Jurek, J. Chwiej "Synchrotron radiation Fourier-transform microspectroscopy study showed an increased frequency of creatine inclusions in the rat hippocampal formation following pilocarpine-induced seizures," *Anal. Bioanal. Chem.* **402** (2012) 2267 – 2274.
- [5] B. Stuart *Modern Infrared Spectroscopy* (ACOL University of Greenwich, UK 1996).

SOLARIS — NEW LIGHT FOR POLISH RESEARCH

Marek Stankiewicz*

*National Synchrotron Radiation Centre SOLARIS Jagiellonian University,
ul. Gronostajowa 7/P.1.6, 30–387 Kraków, Poland*

*e-mail: m.j.stankiewicz@uj.edu.pl

The current status of the Solaris project will be presented.

The first Polish synchrotron radiation facility Solaris is being built at the Jagiellonian University III-rd Campus in Krakow. The project named the National Centre of Electromagnetic Radiation for Research Applications was granted at the beginning of 2010 and is run by Jagiellonian University. It is financed from the European Structural Funds. The initiative has been supported by the strong community of few hundred Polish synchrotron radiation users collaborating with synchrotron facilities abroad. The project is based on an identical copy of the 1.5 GeV storage ring being concurrently built in Lund, Sweden, by MAX-laboratory. In December 2010 an agreement was signed between the Jagiellonian University and Lund University for the mutual cooperation and sharing of ideas and designs related to the construction of the two facilities.

At the first stage, the project will deliver the synchrotron radiation facility consisting of:

- Electron injection system including electron source and 400 – 700 MeV linear accelerator (this accelerator will have the option to be upgraded in the future to the full injection energy of 1.5 GeV);
- 96 m circumference, 1.5 GeV, 500 mA storage ring with 12 bending magnets separated by 3.5 m long straight sections;
- 1 bending magnet radiation based experimental beamline with a multi-grating monochro-

mator and VUV/Soft X-ray electron spectroscopy end-station;

- accommodating buildings.

The potential of the facility is vast. The project assumes and allows for a broad scope of future upgrades and development. The synchrotron will be capable of delivering radiation from both the bending magnets and insertion devices installed in the straight sections. Installation of up to 20 beamlines and corresponding experimental end stations is feasible and will provide research options for many research groups to work simultaneously. The building complex, apart from the synchrotron installation, will also accommodate all the necessary auxiliary facilities, e.g. workshops, preparatory laboratories, staff and administration offices.

The Polish synchrotron is going to be the first research infrastructure of such substantial size and potential constructed in this part of Europe. The synchrotron, being a large-scale, multi-user and multi-disciplinary facility represents a very efficient investment in research by providing state-of-the-art research opportunities for many research groups. The expected benefits are not limited only to the scientific community. The availability of such a technologically advanced facility also contributes to developments in such areas like enhancing education and training, stimulating hi-tech companies and services, providing new options for the research oriented industry, creation of new jobs.

NATIONAL CENTRE FOR HADRON RADIOTHERAPY — BRONOWICE CYCLOTRON CENTRE

P. Olko* and **M. Jeżabek**

Institute of Nuclear Physics PAN, Radzikowskiego 152, 31-342 Kraków, Poland

Keywords: proton radiotherapy, cancer

** e-mail: pawel.olko@ifj.edu.pl*

The basic factor which determines the success of radiotherapy is delivering the highest possible dose of ionizing radiation to the tumor volume while sparing the neighboring critical organs and healthy tissues. Protons with energies from about 60 MeV to 250 MeV are useful for cancer treatment because of the phenomenon of the Bragg peak i.e. increasing of energy deposition at the end of protons path in tissue. Therefore, the unwanted doses to healthy organs, particularly the entrance dose, are minimal as compared to MV X-rays used in conventional radiotherapy. This is of particular importance to pediatric patients in whom the probability of later radiation-induced cancer should be minimized.

In February 18, 2011 a series of proton irradiation of the first two patients has been completed at the Institute of Nuclear Physics (IFJ PAN) in Kraków, Poland. Later on, additional eleven patients suffering from eye melanoma, underwent a series of irradiation with 60 MeV proton beam using home-developed AIC-144 cyclotron. Physicists collaborated with physicians from the Clinic of Ophthalmology and Ophthalmic Oncology Collegium Medicum Jagiellonian University. The AIC-144 isochronous cyclotron was designed at IFJ PAN at the end of 80's and adapted to proton radiotherapy between 2008 and 2010. The beam delivery and the treatment room were also developed by IFJ

PAN engineers, technicians and software developers. The facility, first in Poland and in the neighboring Central-Eastern European countries, is able to satisfy all national needs of ocular melanoma therapy.

60 MeV protons travel in water at the depth of about 30 mm which is sufficient to treat eyes but cannot be used to cure the deeply seated tumors. On September 13, 2006 representatives of ten major Polish scientific and medical institutions established the consortium of The National Hadron Radiotherapy Centre (Polish acronym: NCRH) coordinated by the Institute of Nuclear Physics (IFJ PAN) in Kraków. Within its long-term strategy, the Consortium foresees a two-stage development: in its first stage, a 230 – 250 MeV proton accelerator with a horizontal experimental beam for research and a treatment beam with a proton gantry, will be installed at IFJ PAN in Kraków. In the second stage, a dedicated clinical centre, with proton and C-12 beams, will be established in Warsaw.

Poland, as a new member of European Union, received in years 2007 – 2013 support for reconstruction of its infrastructure. In 2009 – 2010 IFJ PAN received about 50 MEuro (85% from EU structural funds, 15% from Polish government) to finance the project of installation in Krakow the new Proteus C-235 230 MeV proton cyclotron from the Ion Beam Application (IBA), Belgium. On August 2, 2010



Figure 1: The architectural concept of the NCRH facility at IFJ PAN in Kraków. The centre will be operational in December 2012.

the contract between IFJ PAN and IBA has been signed for turn-key delivery of the 230 MeV Proteus C-235 proton cyclotron with a horizontal experimental beam for research and for the eye line. The energy selector will allow to use the proton beam in energy range from 70 MeV to 230 MeV. The construction of the facility at the premises of IFJ PAN at Bronowice started in March 2011 and the facility will be fully operational at the end of December 2012 (see Fig. 1).

In December 2011 the additional contract was signed for turnkey installation of the dedicated

proton gantry, its housing, and the medical building. The 0 – 360° proton gantry with the 3 mm and 9 mm scanning pencil beams, Patient Positioning System with robotic arm, remote positioning will be installed and put in operation in the mid of 2014.

Acknowledgments: This work was supported from the project “National Centre for Hadron Radiotherapy — Bronowice Cyclotron Centre” financed from the Operational Programme Innovative Economy.

POLFEL – POLISH FREE ELECTRON LASER FROM THz TO XUV**G. Wrochna^{1*}, J.B. Pełka², R. Nietubyć^{1,3}, R. Sobierajski² and J. Sekutowicz⁴**¹*National Centre for Nuclear Research, A. Soltana 7, PL 05-400 Otwock, Poland*²*Institute of Physics, Polish Academy of Sciences, al. Lotników 32/46, PL 02-668 Warsaw, Poland*³*National Synchrotron Radiation Centre “Solaris,” Jagiellonian University, Gronostajowa 7/p.1.6, PL 30-387 Kraków, Poland*⁴*Deutsches Elektronen Synchrotron, Notkestrasse 85, D-22607 Hamburg, Germany**Keywords: Free Electron Laser, THz sources, 4th generation sources*** e-mail: G.Wrochna@ncbj.gov.pl*

Free Electron Lasers (FEL) based on the effect of self-amplified spontaneous emission (SASE), break fundamental barriers that limit both usual optical lasers (in wavelength and tunability) and conventional synchrotron radiation sources (in coherence, pulse length and intensity). SASE-FELs can produce a monochromatic radiation in femtosecond pulses with a peak power up to several GW, in the wide spectral range from terahertz waves down to hard x-rays. Both the peak brilliance and a number of photons in the coherence volume exceeds that attainable with the best 3rd generation synchrotron beamlines by up to nine orders of magnitude. The unique SASE-FEL radiation properties open up previously unavailable opportunities of probing the condensed matter with atomic spatial and femtosecond temporal resolution.

In recent years, the ideas of many pioneering research methods making use of these new, 4th generation light sources, have been confirmed experimentally. The SASE-FELs have recently become indispensable complementary to the 3rd generation synchrotrons, demonstrating their key importance in addressing the challenges of modern science and technology.

Currently operating in Europe are only three SASE-FEL facilities (working in the wavelength range of VUV and shorter): FLASH in Hamburg, SPARC in Frascati and FERMI at ELETTRA

synchrotron in Trieste. Access to these devices is very limited, as compared to needs. Until 2016, only 3 or 4 new sources of this type will be built in Europe. In this number may be Polish free electron laser POLFEL, which construction in the coming years has been proposed. Apart from the SASE-FEL laser facility, POLFEL will also form a scientific center, focusing its activities on the development of experimental methods and operating electromagnetic radiation for basic research and technology purposes. It will be also involved in the development of new intense photon sources for technology and medicine. It is proposed to locate the facility at the National Centre for Nuclear Research in Świerk near Warsaw.

The lecture is aimed at the presentation of concept and applications of the Terahertz-FEL source which is proposed as the first stage of construction, thereafter, in the next steps, to be supplemented with XUV to soft x-rays emission capability.

The research capabilities of the powerful long-wavelength and tunable photon source, have been addressed to basic research in the wide range of disciplines: from medicine, biology, chemistry to atomic and high energy density physics and astrophysics. Proposed facility represents a unique tool for surface engineering and other processes which utilize the irradiation, as well as for substances identification for security-related applications.

THE FEATURES AND DESIGN OVERVIEW OF STATE-OF-THE-ART XFEL

Hiromitsu Tomizawa^{1,2*}

¹*Japan Synchrotron Radiation Research Institute, Kouto 1-1-1, Sayo, Hyogo 679-5198, Japan*

²*RIKEN, SPring-8 Center, Kouto 1-1-1, Sayo, Hyogo 679-5148, Japan*

Keywords: X-ray Free Electron Laser

**e-mail: hiro@spring8.or.jp*

In the last decade, XFELs (X-ray Free Electron Laser) [1]-[3] have been constructed and operated in the world as the next generation of 3rd-generation synchrotron radiation sources. The underlying theory of a high-gain FEL has existed for three decades [4]. For VUV and XFELs, contrary to conventional optical lasers, laser cavity mirrors can no longer be applied due to their low reflectivities in normal incidence geometry and high absorption of their materials in the VUV and X-ray regions. Since a single-pass SASE (Self Amplified Spontaneous Emission) FEL operates in the high-gain regime, it does not require any optical cavity and it can be lasing in the VUV and X-ray regime.

In this lecture, the basic physics of SASE FEL will be explained in comparison to conventional optical laser and synchrotron radiation sources. The FEL radiation is explained in classical physics as interactions between radiation and electrons, and even simpler than the physics of conventional optical lasers. Conversely, the XFEL machine has more varieties (complicated) in technology. The XFEL consists of a high-brightness injector, a linear-accelerator (LINAC) and a long undulator section. Since the electrons in the FEL are not bound to (“free” from) atoms, and not limited to specific transitions between levels, the wavelength of the FEL is tunable over a wide range depending on accelerator energy and undulator parameters. These three main components are required for all of XFEL machines, but can be modified depending upon technological choice for aiming user experiments. There are three XFEL machines: Euro-XFEL (EU), LCLS (USA), SACLA (Japan), and all three are already operating or under construction [1]-[3]. The different choice of technologies of each facility will be compared with the performance of the machine. For instance, SACLA uses thermionic electron gun and sub-harmonic bunchers, which have a very high bunching factor (~ 3000) with velocity bunching in the low energy region and magnetic bunching in the high energy. The other XFEL facilities use laser-excited photocathode RF guns without any velocity bunching system.

Recently, the second generation of XFEL comes up as a seeded FEL scheme to improve the longitudinal (temporal) coherency. The seeding scheme

has two major technologies. One is seeded directly with femtosecond-laser-driven HHG (Higher Harmonic Generation) [5]. It should be reliable for the soft X-ray region. The other is so-called “self-seeding,” seeded simply with narrow-band-filtered SASE generated at the upstream part of undulator section (monochromatization of $\sim 10^5$) [6]. It is feasible for the hard X-ray region at present.

In the near future, we will have three “extreme” light sources: petawatt-class conventional optical laser, 3rd-generation synchrotron radiation source, and full-coherent seeded XFEL. These light sources are a complementary trinity to discover the dynamical nature of a variety of different materials, including the nature of life in vivo. The synergy users experiments utilizing those light sources will be openly discussed.

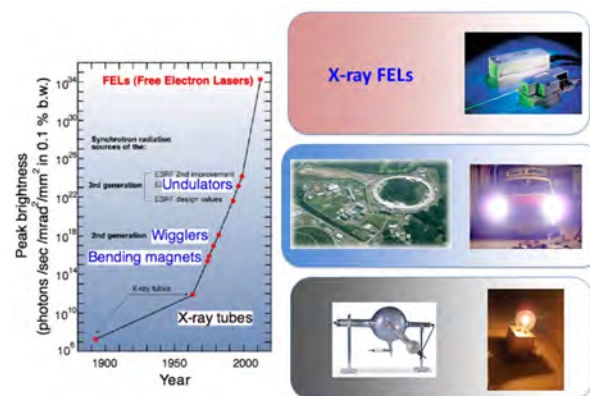


Figure 1: Historical developments of X-ray light source technologies.

References

- [1] *TESLA Technical Design Report*, DESY TESLA Report 2001 – 23, DESY TESLA-FEL 2001 – 05 (2001).
- [2] *Linac Coherent Light Source Design Study Report*, SLAC-R-593, UC – 414 (2002).
- [3] *SCSS XFEL Conceptual Design Report*, RIKEN Harima Institute/SPring-8 (2005).
- [4] R. Bonifacio *et al.*, *Opt. Commun.* **50** (1984) 373; K.-J. Kim, *Phys. Rev. Lett.* **57** (1986) 1871.
- [5] T. Togashi *et al.*, *Opt. Express* **19** (2011) 317.
- [6] G. Geloni *et al.*, DESY 10 – 053 (2010) 1.

OBSERVING MOLECULAR REACTIONS VIA SIMULTANEOUS ULTRAFAST X-RAY SPECTROSCOPY AND SCATTERING

A. Galler¹, W. Gawelda¹, K. Haldrup², K. Kjaer², T. van Driel², A.M. March³, G. Doumy³, E. Kanter³, D. Ray³, R. Dunford³, J. Uhlig⁴, S. Canton⁴, G. Smolentsev⁴, D. Fritz⁵, M. Cammarata⁵, H. Lemke⁵, U. Bergmann⁵, R. Alonso Mori⁵, N. Sás⁶, A. Bordage⁶, G. Vankó⁶, E. Gallo⁷, P. Glatzel⁷, K. Gaffney⁸, V. Sundström⁴, M.M. Nielsen², L. Young³, S. Southworth³, and C. Bressler^{1*}

¹European X-ray Free Electron Laser Facility, Hamburg, Germany

²Danish Technical University, Riso, Denmark

³APS, Advanced Photon Source, Argonne National Lab, Chicago, USA

⁴University of Lund, Lund, Sweden

⁵LCLS, Linear Coherent Light Source, Stanford, USA

⁶KFKI, Research Institute for Particle and Nuclear Physics, Budapest, Hungary

⁷ESRF, European Synchrotron Facility, Grenoble, France

⁸SLAC/PULSE, Stanford Linear Accelerator, Stanford, USA

Keywords: time-resolved, ultrafast, structural dynamics

*e-mail: christian.bressler@xfel.eu

Over the past decade ultrafast structural dynamics has been a rapidly growing field aiming to deliver unprecedented detail of understanding the initial steps in complex chemical reactions e.g. during light-induced spin switching, or during a photocatalytic event. Such processes play a vital role in chemistry and biology next to technological applications including efficient charge transport in solar energy converters and ultrafast switchable molecular magnets.

All these processes are either triggered on or occur on a femto- to picosecond timescale, therefore a pump probe technique exploiting ultrashort pulses is mandatory. The other prerequisite is an x-ray tool, which can determine the electronic, spin, and geometric degrees of freedom on the atomic length scale. Transition metal based spin crossover (SCO) systems are of particular interest due to their possible application in quantum-computers, but also in the quest for an efficient artificial solar energy cell. Light induced spin switching systems offer the advantage of an ultrafast trigger for studying their dynamic magnetic properties. In $[\text{Fe}(\text{bpy})_3]^{2+}$, the transition between the low spin (LS) ground and the high spin (HS) excited states is governed by a complex interplay of changes in the electronic and spin configuration next to geometric structural modifications [1]. New charge transfer materials also undergoes such complex processes, whose optimization is highly desirable for photocatalytic applications. We thus investigated a bi-metallic (Ru-Co) compound where the metal atoms are connected through a system of bipyridine (bpy) ligands. The detailed understanding of the charge transport from the Ru donor to the Co acceptor including oxidation (Ru), subsequent reduction (Co), next to geometrical structure changes, and finally the expected spin state changes on the acceptor ion is of high interest for both understanding the mechanism and

finding ways to improve its efficiency. We report on both ps and fs studies of different Fe-based spin transition compounds as well as on a bimetallic Ru-Co compound. These studies were carried out with high S/N, and combining – on a shot-to-shot basis – x-ray emission and x-ray diffuse scattering techniques.

Previous x-ray spectroscopic studies performed at kHz repetition rates yielded results with suitable signal to noise ratios (S/N) after rather long collection times at synchrotrons, which so far prevented a wide scale application of this method. Exploiting MHz laser sources is a straightforward improvement for a much faster data collection rate, and we performed benchmark experiments at the ESRF (ID26) and the APS (7ID) at pump-probe repetition rates up to that of the x-ray source. In order to unravel the complex behavior of photo-excited molecules we implemented a suite of different spectroscopic and scattering techniques. X-ray absorption spectroscopy (XAS) with its sensitivity to local electronic and geometric structural changes [2], 1s x-ray emission spectroscopy (XES) which as a direct probe of the spin state via the exchange interaction between $2p$ and $3d$ orbitals [3], and x-ray diffuse scattering (XDS), which yields complementary information about the local as well as the global structure of the studied molecule.

Among the investigated systems we focus here on $[\text{Fe}(\text{bpy})_3]^{2+}$ and the RuCo molecules. The fs XAS on $[\text{Fe}(\text{bpy})_3]^{2+}$ confirmed an earlier slicing result (using only 10 photons/pulse at 2 kHz) [4], including the switching time, which matches nicely the XES-derived spin switching time, thus determining the HS state formation of $[\text{Fe}(\text{bpy})_3]^{2+}$ directly. The limited time resolution (instrument response) of about 250 fs leaves the issue about the (sequential) order of the elementary steps in spin switching still unsettled.

These experiments were performed simultaneously to the x-ray diffuse scattering patterns (Fig 1.), which reveal a rich variety of changes on the fs, but also few ps time scales. In combination with our ps scattering results on this compound we can enrich our understanding of the geometric structural changes, but now including a first glimpse at the solvent cage dynamics.

While our dynamic studies on the RuCo system at synchrotron sources revealed an x-radiation induced conversion of the RuCo compound, we nevertheless unambiguously confirmed the electron transfer time to 200 ps. Utilizing ultrashort x-ray pulses from LCLS we confirmed this result, but interestingly also discovered a new ultrafast component for the electron transport time on the Co acceptor, which contributes to 1/3 of the total signal. Since

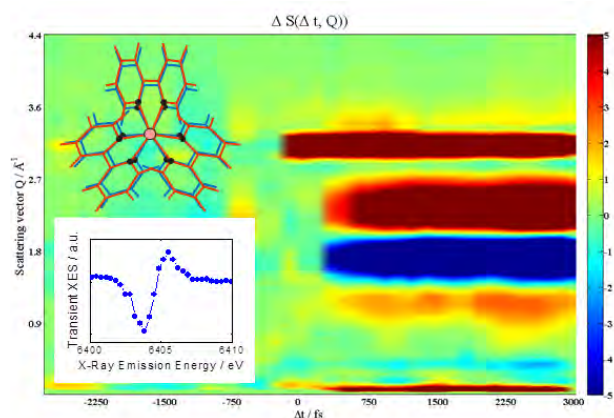


Figure 1: Simultaneous XDS and XES (lower inset) of photoexcited $[\text{Fe}(\text{bpy})_3]^{2+}$ (upper inset illustrating the geometry of low spin in blue and high spin in red) showing different femtosecond modulations for the scattering pattern scanning the pump probe delay and the transient $\text{K}^{\alpha 1}$ XES for a fixed pump probe delay of 500 fs.

we exploited the characteristic XES signal in the Co acceptor, this arrival time also includes an ultrafast SCO process.

Using XES in concert with XDS tools we have investigated a collection of spin transition systems, on both the ps and fs time scales, with hitherto unprecedented S/N. The analysis of these studies should flow into the analysis of more complex compounds, like the bpy-based bimetallic RuCo compound, which revealed at the LCLS its unusual temporal behaviour. As an outlook, these studies should allow a more mature investigation of the dynamic properties in complex molecular systems, which now can include dynamic guest-host interactions in the liquid phase.

Acknowledgments: This work was supported by the Deutsche Forschungsgemeinschaft (SfB925, TPA4), and by the European XFEL.

References

- [1] W. Gawelda *et al.*, "Structural determination of a short-lived excited iron(II) complex by picosecond X-ray absorption spectroscopy," *Phys. Rev. Lett.* **98** (2007) 057401.
- [2] C. Bressler and M. Chergui, "Molecular structural dynamics probed by ultrafast X-ray absorption spectroscopy," *Ann. Rev. Phys. Chem.* **61** (2010) 263.
- [3] G. Vankó *et al.*, "Picosecond time-resolved X-ray emission spectroscopy: Ultrafast spin-state determination in an iron complex," *Angew. Chem. Int. Ed.* **94** (2010) 5910.
- [4] C. Bressler *et al.*, "Femtosecond XANES study of the light-induced spin crossover dynamics in an iron(II) complex," *Science* **323** (2009) 489.

INTERPLAY BETWEEN TOPOLOGY AND STATISTICAL PROPERTIES OF DNA: A POLYMER PHYSICS APPROACH

Giovanni Dietler*

Laboratoire de Physique de la Matière Vivante, Ecole Polytechnique Fédérale de Lausanne (EPFL),
CH-1015 Lausanne, Switzerland

Keywords: DNA, Atomic Force Microscope, polymer physics

*e-mail: giovanni.dietler@epfl.ch

The talk will present how to use DNA of various topological forms (linear, circular and knotted DNA) in order to study polymer physics. On the other side, I will show the benefits of this approach for the study of DNA and its function inside the cell and what it can be gained from polymer physics.

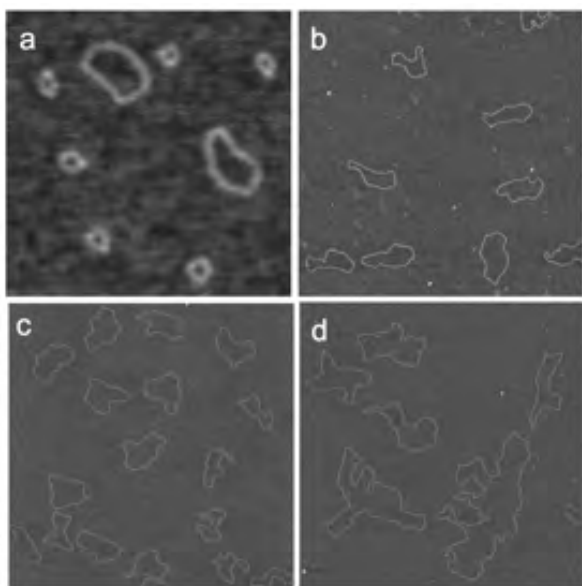


Figure 1: Circular DNA of various lengths imaged by Atomic Force Microscope. (a) 350 nm image size; (b) 2 μm image size; (c) 3 μm image size; (d) 2.5 μm image size.

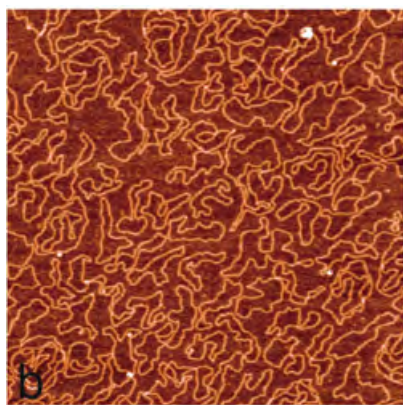


Figure 2: Concentrated “solution” of circular DNA.

Examples will be presented for linear DNA of various lengths, circular DNA as isolated molecules and in concentrated forms, and knotted DNA. For these studies, Atomic Force Microscopy (AFM) images of DNA were analyzed and interpreted using polymer physics concepts. It turns out that AFM images deliver a wealth of detailed data never available before and that now it is possible to compare theoretical predictions for linear, circular and knotted polymers with real polymers.

Acknowledgments: This work was supported by the Swiss National Science Foundation.

References

- [1] T. Sakaue, G. Witz, G. Dietler, and H. Wada, “Universal bond correlation function for two-dimensional polymer rings,” *EPL* **96** (2010) 68002.
- [2] F. Valle, M. Favre, P. de los Rios, A. Rosa, and G. Dietler, “Scaling exponents and probability distributions of DNA end-to-end distance,” *Phys. Rev. Lett.* **95** (2005) 158105.
- [3] E. Ercolini, F. Valle, J. Adamcik, R. Metzler, P. de los Rios, J. Roca, and G. Dietler, “Fractal dimension and localization of DNA knots,” *Phys. Rev. Lett.* **98** (2007) 058102.
- [4] G. Witz, K. Rechendorff, J. Adamcik, and G. Dietler, “Conformation of circular DNA in two dimensions,” *Phys. Rev. Lett.* **101** (2008) 148103.
- [5] K. Rechendorff, G. Witz, J. Adamcik, and G. Dietler, “Persistence length and scaling properties of single-stranded DNA adsorbed on modified graphite,” *J. Chem. Phys.* **131** (2009) 095103.
- [6] F. Drube, K. Alim, G. Witz, G. Dietler, and E. Frey, “Excluded volume effects on semiflexible ring polymers,” *Nano Lett.* **10** (2010) 1445.
- [7] J.-H. Jeon, J. Adamcik, G. Dietler, and R. Metzler, “Supercoiling induces denaturation bubbles in circular DNA,” *Phys. Rev. Lett.* **105** (2010) 208101.
- [8] J. Adamcik, J.-M. Jung, J. Flakowski, P. de los Rios, G. Dietler, and R. Mezzenga, “Understanding amyloid aggregation by statistical analysis of atomic force microscopy images,” *Nat. Nanotechnol.* **5** (2010) 423.

HIGH-ENERGY X-RAY SCATTERING STUDIES OF NANOMATERIALS USING A LABORATORY SYSTEM

M. Gateshki*, H. te Nijenhuis, D. Beckers, A. Kharchenko, and M. Fransen

PANalytical B.V., Almelo, The Netherlands

Keywords: X-ray diffraction, pair distribution function, nanocrystalline materials

**e-mail: milen.gateshki@PANalytical.com*

The increased interest in recent years regarding the properties and applications of nanomaterials has also created the need to characterize the structures of these materials. However, due to the lack of long-range atomic ordering, the structures of nanostructured and amorphous materials are not accessible by conventional diffraction methods used to study crystalline materials. One of the most promising techniques to study nanostructures using X-ray diffraction is by using the total scattering (Bragg peaks and diffuse scattering) from the samples and the pair distribution function (PDF) analysis. The pair distribution function provides the probability of finding atoms separated by a certain distance. This function is not direction-dependent; it only looks at the absolute value of the distance between the nearest neighbors, the next nearest neighbors and so on. The method can therefore also be used to analyze non-crystalline materials. From experimental point of view a typical PDF analysis requires the use of

intense high-energy X-ray radiation ($E \geq 20$ KeV) and a wide 2θ range.

After the initial feasibility studies regarding the use of standard laboratory diffraction equipment for PDF analysis [1] this application has been further developed to achieve improved data quality and to extend the range of materials, geometrical configurations and X-ray optical components that can be used for PDF experiments. Studies performed on different nanocrystalline and amorphous materials of scientific and technological interest, including organic substances, oxides, metallic alloys, etc. have demonstrated that PDF analysis with a laboratory diffractometer can be a valuable tool for structural characterization of nanomaterials.

References

- [1] J. te Nijenhuis, M. Gateshki, M.J. Fransen, *Z. Kristallogr. Suppl.* **30** (2009) 163.

SEEDING OF EXTREME ULTRAVIOLET FREE ELECTRON LASER WITH HIGH-ORDER HARMONIC

T. Togashi^{1*}, E.J. Takahashi², K. Midorikawa², M. Aoyama³, K. Yamakawa³, T. Sato^{4,5}, A. Iwasaki⁵, S. Owada⁵, K. Yamanouchi⁵, T. Hara^{4,1}, S. Matsubara¹, T. Ohshima⁴, Y. Otake^{4,1}, H. Tanaka^{4,1}, T. Tanaka⁴, H. Tomizawa^{4,1}, T. Watanabe¹, M. Yabashi^{4,1}, and T. Ishikawa⁴

¹Japan Synchrotron Radiation Research Institute, Kouto 1-1-1, Sayo, Hyogo 679-5198, Japan

²RIKEN Advanced Science Institute, Hirosawa 2-1, Wako, Saitama 351-0198, Japan

³Japan Atomic Energy Agency, Umemidai 8-1, Kizugawa, Kyoto 619-0215, Japan

⁴RIKEN, SPring-8 Center, Kouto 1-1-1, Sayo, Hyogo 679-5148, Japan

⁵The University of Tokyo, Hongo 7-3-1, Bunkyo-ku, Tokyo 113-0033, Japan

Keywords: free electron laser, high-order harmonics, extreme ultraviolet

*e-mail: tadashit@spring8.or.jp

Frontiers in optical science in the short-wavelength region have greatly been expanded by the advent of intense, single-pass free-electron lasers (FELs) based on a self-amplified spontaneous emission (SASE) scheme [1, 2]. However, their temporal profile and frequency-domain spectra are composed of random and uncontrollable spikes, exhibiting shot-to-shot fluctuation originating from the stochastic start-up process intrinsic to spontaneous radiation. The most straightforward method for improving the temporal coherence of FEL is to inject the high-order harmonic (HH) generated by a laser into an FEL amplifier. In this paper, we first demonstrate [3] the 13th harmonic (61 nm) [4] of a Ti:sapphire laser in the plateau region was injected as the SPring-8 Compact SASE Source test accelerator [2].

Figure 1 shows the recorded spectra of the FEL radiation in fifty successive shots both without (a) and with (b) the HH injection. They exhibit sharp increases in the spectral intensity for several shots shown as red lines in Fig. 1 (b). The small event-number ratio of the enhancement, which is typically ~ 10 shots per 1000 shots, is caused by the timing jitter between the seeding laser pulse and the electron bunch. In addition, we investigated the resonance effect by changing the deflection parameter, K , of the undulator (i.e., the central wavelength of undulator radiation) by varying the undulator gap. The high-intensity pulses are observable only in the vicinity of the conditions with the central wavelength of 61.2 nm, as shown in the inset of Fig. 1 (a). This resonance behavior can be regarded as an evidence of the successful operation of the seeded FEL in this EUV region.

When the amplification conditions were fulfilled, strong enhancement of the radiation intensity by a factor of 650 was observed. The random and uncontrollable spikes, which appeared in the spectra of the SASE based FEL radiation without the seeding source, were found to be suppressed drastically to form to a narrow-band, single peak profile at 61.2 nm. The properties of the seeded FEL radiation

were well reproduced by numerical simulations. We will discuss the future precept of the seeded FEL scheme to the shorter wavelength region.

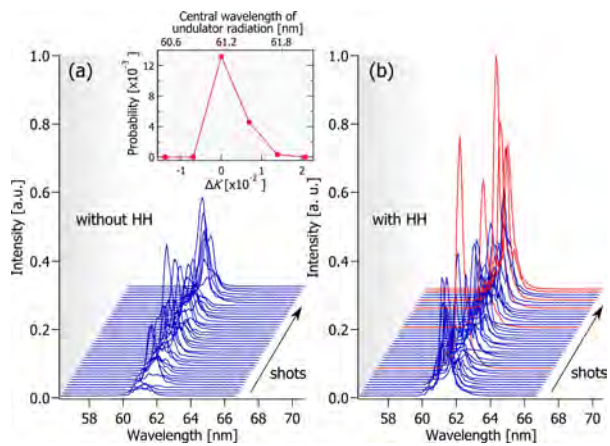


Figure 1: Spectra of FEL radiation in fifty successive shots without (a) and with (b) HH injection. The red lines in (b) show profiles that have higher intensities above the threshold level. The inset shows an appearance probability of the high-intensity condition as a function of the deviation of K -value, $\Delta K = K - 1.37944$ (lower axis), and the central wavelength of the undulator radiation (upper axis).

References

- [1] W. Ackermann *et al.*, "Operation of a free-electron laser from the extreme ultraviolet to the water window," *Nature Phot.* **1** (2007) 336.; P. Emma *et al.*, "First lasing and operation of an angstrom-wavelength free-electron laser," *Nature Photonics* **4** (2010) 641.
- [2] T. Shintake *et al.*, "A compact free-electron laser for generating coherent radiation in the extreme ultraviolet region," *Nature Phot.* **2** (2008) 555.
- [3] T. Togashi *et al.*, "Extreme ultraviolet free electron laser seeded with high-order harmonic of Ti:sapphire laser" *Opt. Express* **19** (2011) 317.
- [4] E. Takahashi *et al.*, "Generation of 10-uJ coherent extreme-ultraviolet light by use of high-order harmonics," *Opt. Lett.* **27** (2002) 1920.

SOLVING AND REFINING DIFFICULT STRUCTURES BY THE PROGRAM PACKAGE JANA2006

V. Petříček* and M. Dušek

*Institute of Physics, Academy of Sciences of the Czech Republic v.v.i.,
Na Slovance 10, 182 21 Praha 8, Czech Republic*

Keywords: structure analysis, modulated crystals, program Jana2006

**e-mail: petricek@fzu.cz*

The solution and refinement of crystal structures play a crucial role in very different branches of science dealing with crystalline solids. New experimental techniques, namely using of area detectors, make the procedure for describing of crystal structures much easier and more effective. Thus a standard crystal structure can be measured, solved and refined [1] within several hours. However, many other compounds cannot be characterized as standard ones as they are affected by twinning, modulations and disorder of different kinds. These effects not only complicate structure solution but in many cases they are strongly correlated with physical and chemical properties of the investigated materials. This fact is the main driving force for developing of the program package Jana2006 [2].

The system can be used to solve and refine regular, modulated and composite crystal structures against powder or single crystal data collected with X-ray laboratory diffractometers, synchrotron or neutron sources. The latest version allows so called joint-refinement in which several data sets can be combined together.

Probably the most common problem in crystal structure analysis is twinning in crystals. Several different examples including multiphase systems will be presented to show how to handle data and how to solve and refine such structures.

Modulated and composite crystals represent another category of complicated structures. The frequency of their occurrence has considerably grown up with increasing usage of modern CCD diffractometers, which give full information about the large portion of diffraction space. Thus detection of satellite reflections is simple as well as their integration, which is an option of the data processing software supplied with most diffractometers. Thus the way from experiment to the solution process is relatively straightforward.

The superspace theory, as developed by de Wolff, Janssen and Janner [3], is used to make a symmetry analysis which leads to the most probable superspace group. Recently developed technique called “charge flipping” [4] allows for *ab initio* solution

of aperiodic structures and opens the field for non-specialists.

Modulations in the crystal, affecting various structural parameters (site occupancies, atomic positions and also atomic displacement parameters), can be usually described as a combination of continuous harmonic functions. There are cases, however, when the modulation has a discontinuous character, which cannot be sufficiently described with the continuous harmonic model. Discontinuity in modulation can be recognized already in the diffraction pattern by presence of strong higher order satellites and needs for efficient description special modulation functions of crenel or saw-tooth shape [5]. These functions have been introduced in Jana program and recently a new algorithm has been developed that facilitates their application.

The lecture will be made as an introduction to the Jana2006 workshop.

Acknowledgments: This work was supported by Premium Academiae of the Czech Academy of Sciences.

References

- [1] G.M. Sheldrick, “A short history of SHELX,” *Acta Cryst. A* **64** (2008) 112 – 122.
- [2] V. Petříček, M. Dušek, L. Palatinus, *Jana2006 — the crystallographic computing system* (Praha, Czech Republic 2006).
- [3] P.M. de Wolff, T. Janssen, A. Janner, “The superspace groups for incommensurate crystal structures with a one-dimensional modulation,” *Acta Cryst. A* **37** (1981) 625 – 636.
- [4] L. Palatinus, G. Chapuis, “SUPERFLIP — a computer program for the solution of crystal structures by charge flipping in arbitrary dimensions,” *J. Appl. Cryst.* **40** (2007) 786 – 790.
- [5] V. Petříček, A. van der Lee, M. Evain, “On the use of crenel functions for occupationally modulated structures,” *Acta Cryst. A* **51** (1995) 529 – 535.
- [6] V. Petříček, Y. Gao, P. Lee, P. Coppens, “X-ray analysis of the incommensurate modulation in the 2:2:1:2 Bi-Sr-Ca-Cu-O superconductor including the oxygen atoms,” *Phys. Rev. B* **42** (1990) 387 – 392.

TECHNIQUES AND TECHNOLOGIES FOR ULTRA BRIGHT SYNCHROTRON LIGHT SOURCES

Carlo J. Bocchetta*

*Synchrotron Radiation Center SOLARIS, Jagiellonian University,
ul. Gronostajowa 7/P-1.6, 30-387 Kraków, Poland*

*e-mail: carlo.bocchetta@uj.edu.pl

The designs of the latest generation of synchrotron light sources, both under construction and planned, have the objectives of ultra-low emittance and low energy spread, extreme beam stability and full exploitation of photon energies in the range of a few electron-volts to hard X-Rays with excellent coherence and time structure. Recent developments on lattice design have brought the electron beam emittance to sub nmrad values. As a consequence the adopted hardware and software technologies have to match requirements and guarantee continued performance. When designing a synchrotron radiation source based on a storage ring there is the need to take into account the strong interdependence between many parameters: the photon energy is related to beam energy and the type of insertion device; the brightness of the source is related to the beam energy, the emittance, the circulating current, beam stability and insertion devices; source stability is related to the circulating current and consequent beam instabilities, to transmitted vibrations and the ability to stabilise passively and actively; the time structure of the source is related to bunch lengths, bunch currents and to the type of accelerator or slicing technique used.

Ultra low emittance accelerator designs for ring based light sources benefit from the use of many magnets in an achromat structure and/or the use of damping wigglers. Optimal designs of the of the magnet lattice require many families of sextupole magnets to maximise the transverse and momentum dynamic apertures, often with the use of octupole magnets. The use of conventional separated function magnets is often not the most favourable solution and magnets that have a combination of multipoles are more appropriate to reach the desired emittances. Such magnets should be compact, with small apertures and strong fields and have a low cost, both in production and operation. Modern industrial techniques are available for the production of exotic magnets having exceptional field properties. The small apertures necessitate narrow gap vacuum chambers which in turn require state-of-the-art solutions for pumping given the low vacuum conductance of the chambers. The design of the

vacuum chamber is strongly linked to the magnetic and mechanical design of the magnet. To reach a technologically feasible design, the adoption of Non-Evaporable Getter thin film technology is often the only means of pumping the vacuum chamber. Small bore vacuum chambers may in turn have adverse effects on the beam causing instabilities through generated wake-fields and will necessitate the implementation of Landau cavities and sophisticated feedback systems. Landau cavities additionally benefit machine operation by decreasing longitudinal bunch densities. This latter effect is particularly important given the very high electron bunch densities that can compromise the final emittance value because of intra-beam scattering.

Beam stability is of paramount importance in maintaining the ultra-bright characteristics of the photon beams. The accelerator and its housing have to be treated and designed together. Unavoidable cultural noise has to be isolated and damped. Care has to be taken in the design of all components of the infra-structure from magnet support stands to experimental floors, from water installations to the landscaping of areas around the facility. Ground vibration in the range of tens of nanometers can be amplified by supports and the magnetic lattice to levels that compromise facility performance. In addition to passive mechanisms towards beam stability many active systems are also required using state-of-the-art technology. Active systems can range from fast multibunch feedback systems (100's MHz) to top-up operations for thermal stability and improved feedback operational ranges. Top-up operation is essential to reach full performance and must be invisible to users. Operational ease of the facility is governed by the use of modern control systems that integrate a multitude of different systems and allow both operators and users transparent access to beam parameters and settings.

The talk will give a broad overview of state-of-the-art synchrotron light source design, both ring and linac based. Examples from on-going design and construction will be shown, together with examples of systems and solutions to technological requirements that guarantee performance.

GRAPHENE GROWTH ON CU(111): MICROSCOPIC ANGLE-RESOLVED PHOTOEMISSION AND SCANNING TUNNELING MICROSCOPY INVESTIGATIONS

P. Rudolf*

*Zernike Institute for Advanced Materials, University of Groningen,
Nijenborgh 4, NL-9747 AG Groningen, The Netherlands*

*e-mail: p.rudolf@rug.nl

The investigation of graphene grown on a copper foil by chemical vapor deposition has been widely explored in last few years. However, only in a very few experiments the graphene growth on highly-ordered copper surfaces (*i.e.* single crystals) has been studied. In these studies, graphene was grown in-situ under ultrahigh vacuum conditions.

Our studies focus on graphene on Cu(111) grown ex-situ in a vacuum furnace by chemical vapor deposition of methane. All investigations have been carried out in an ultrahigh vacuum environment while the samples were annealed at 400°C

in order to remove surface contaminants. Angle-resolved photoemission spectroscopy with a microscopic photon beam resulted in the detection of a clear band structure exhibiting a Dirac cone shape. Scanning tunneling microscopy experiments showed that the Cu surface is covered mainly by a single layer of graphene. Different rotational domains were detected, some showing a Moire pattern. In addition, the role of oxygen on the growth process and its contribution to the modification of the morphology of the copper/graphene is also presented.

X-RAY DIFFRACTION PEAK PROFILES FROM RELAXED EPITAXIAL FILMS

Vladimir M. Kaganer*

Paul Drude Institute for Solid State Electronics, Hausvogteiplatz 5–7, 10117 Berlin, Germany

Keywords: epitaxy, films, relaxation, dislocations

*e-mail: kaganer@pdi-berlin.de

Epitaxial films relax because of the lattice parameter mismatch between the film and the substrate. Misfit dislocations are formed at the interface, and threading dislocations go from the interface to the surface. The x-ray diffraction peak profiles are sensitive to the dislocation strain fields and contain information on the dislocation densities, Burgers vectors, and positional correlations of the dislocations. The aim of this talk is to discuss main features of the diffraction patterns due to dislocations in epitaxial films, and demonstrate possibilities of obtaining information on dislocation distributions from the x-ray diffraction experiments [1]-[5].

Dislocations develop positional correlations to reduce elastic energy of the relaxed epitaxial film. The minimum of elastic energy of misfit dislocations is reached for periodic dislocations. The edge (Lomer) dislocations glide along the interface and can approach this state, while the 60° dislocations that glide in the inclined planes have less possibility to order. The case of large dislocation densities, when the mean distance between misfit dislocations is much smaller than the film thickness, is most important experimentally and relatively easy for calculations. Positional correlations are described by a single parameter $g \leq$ which is the mean-squared fluctuation of the number of dislocations on a given interval [1, 5]. The case of low dislocation densities is more complex and involves the correlation function for dislocation positions [3].

The positional correlations of threading dislocations are directed to screen the long-range strain fields of the dislocations. The x-ray diffraction profiles from threading dislocations in GaN epitaxial films [3] are well described by the Krivoglaz-Wilkens correlation function $G(x) \propto \exp[-\rho x^2 \ln(R/x)]$, where ρ is the dislocation density and R is a screening distance. From the fits of the experimental profiles, this distance occurs comparable with the mean distance between dislocations, so that just neighbor dislocations screen each other.

If statistical properties of the dislocation distribution are known (or postulated), the x-ray scattered intensity can be calculated by the Monte Carlo method [3]-[5]. The Monte Carlo integration is

performed within the kinematical diffraction theory without any further simplifications or approximations. Dislocation positions are generated on random with desired positional correlations. The average over an ensemble of dislocations is performed by the Monte Carlo method. The spatial integration over the film can be performed either by the Monte Carlo method [3, 5] or by usual quadrature formulas [4].

The misfit dislocations are generated in the Monte Carlo calculations as Markov chains. A choice of the probability distribution for distances between neighbour dislocations allows a continuous variation from completely uncorrelated dislocations to almost periodic ones. The satellite reflections appear for highly enough correlations [3].

For threading dislocations, the screening of the long-range strain is provided by dislocation pairs with opposite Burgers vectors of two dislocations in the pair. The mean distance between dislocations serves as a screening distance. It can be larger than the mean distance between dislocations, so that the pairs overlap, rather than make separated dislocation dipoles [4].

Thus, the x-ray diffraction profiles can be evaluated for a wide class of distributions of misfit and threading dislocations in epitaxial films. A combination of the approximate calculations and the direct Monte Carlo modeling provides a solid ground for the dislocation density determination and the detailed description of dislocation distributions in relaxed epitaxial films.

References

- [1] V.M. Kaganer, R. Köhler, M. Schmidbauer, R. Opitz, and B. Jenichen, *Phys. Rev. B* **55** (1997) 1793.
- [2] V.M. Kaganer, O. Brandt, A. Trampert, and K.H. Ploog, *Phys. Rev. B* **72** (2005) 045423.
- [3] V.M. Kaganer and K.K. Sabelfeld, *Phys. Rev. B* **80** (2009) 184105.
- [4] V.M. Kaganer and K.K. Sabelfeld, *Acta Cryst. A* **66** (2010) 703.
- [5] V.M. Kaganer and K.K. Sabelfeld, *Phys. Status Solidi A* **208** (2011) 2563.

IMAGING IN NANOSCALE USING LASER-PLASMA SOURCES OF EXTREME ULTRAVIOLET (EUV)

P.W. Wachulak^{1*}, A. Baranowska-Korczyk², D. Pánek³, P. Brůža³, A. Bartnik¹, J. Kostecki¹, L. Węgrzyński¹, R. Jarocki¹, M. Szczurek¹, D. Elbaum², and H. Fiedorowicz¹

¹Institute of Optoelectronics, Military University of Technology, 2 Kaliskiego Str., 00-908 Warsaw, Poland

²Institute of Physics, Polish Academy of Sciences, 32/46 Aleje Lotników, 02-668 Warsaw, Poland

³Faculty of Biomedical Engineering, Czech Technical University, Nám. Síttná 3105, Kladno, Czech Republic

Keywords: nanoimaging, extreme ultraviolet EUV, microscopy, Fresnel zone plates

*e-mail: wachulak@gmail.com

Recent rapid developments of nanoscience and nanotechnology require nanometer scale resolution imaging tools and methods. One of the methods, extensively studied for the last few decades, is an extreme ultraviolet (EUV) and soft X-ray (SXR) microscopy, based on Fresnel zone plates. The introduction of compact sources of bright EUV and SXR radiation paved the way for the development of tabletop microscopes that can render images of nanoscale objects with exposures as short as a few seconds and spatial resolution approaching that of synchrotron-based microscopes [1, 2].

In this paper, we report on applications of a desk-top microscopy using a laser-plasma EUV source based on a gas-puff target for studies of morphology of thin silicon membranes coated with NaCl crystals and ZnO nanowires. Previously measured spatial resolution of this microscope, reaching 50 nm, allows for acquisition of images of various objects with high spatial resolution and field of view approaching $50 \times 50 \mu\text{m}^2$ in a very compact setup. Utilization of the short wavelength EUV radiation allows to demonstrate the intrinsic advantage of this radiation for extraction of additional information about the investigated object, which cannot be obtained directly from optical micrographs and SEM images. Moreover, this microscope does not require additional sample modification necessary for SEM microscopy.

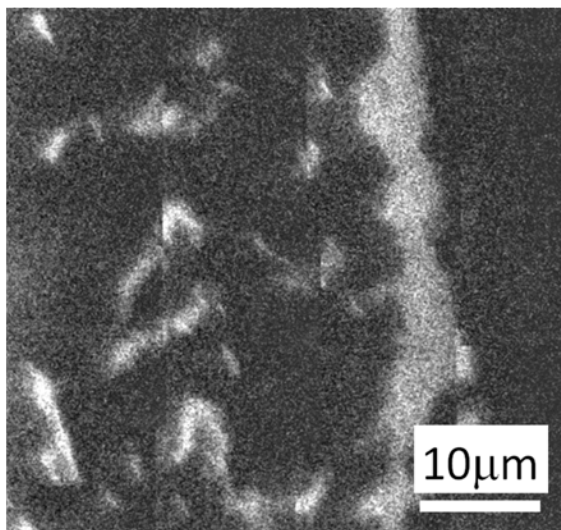


Figure 1: EUV image of the sample, $\sim 50 \times 50 \mu\text{m}^2$ with re-crystallized NaCl.

Both, NaCl coated membranes and ZnO coated polymer nanowires were imaged using an EUV microscopy setup, reported previously in [1, 2]. NaCl was crystallized on a 15 nm thick non-porous silicon membrane (SPI Supplies) with dimensions $0.07 \times 1.5 \text{ mm}^2$. The NaCl crystals were prepared from phosphate buffered saline (PBS) solution. During the process of re-crystallization stress was introduced to the membrane causing random cracks of various sizes to appear in the NaCl crystals and the silicon membrane. Sample EUV image of cracks in the membrane are presented in Fig. 1. ZnO coated polymer nanowires were prepared by electrospinning on top of a gold mesh. Later they were annealed at 500°C for 4 hours. Sample image of ZnO coated nanowires are presented in Fig. 2.

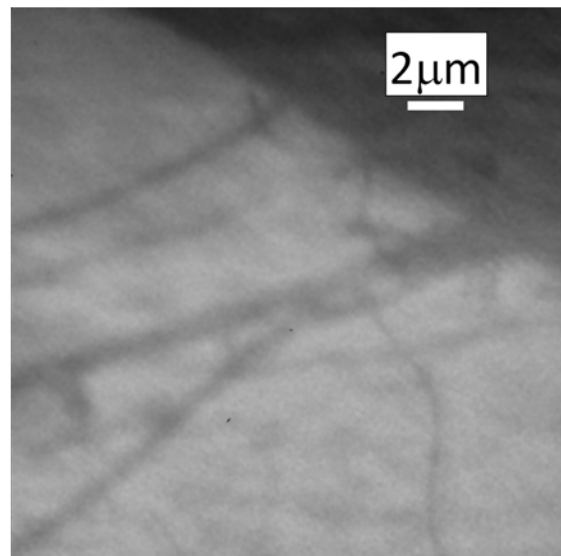


Figure 2: EUV image of the sample, $\sim 20 \times 20 \mu\text{m}^2$ with ZnO coated polymer nanowires.

Acknowledgments: The research was supported by the Foundation for Polish Science under the HOMING 2009 Programme (grant number HOM2009/14B), Military University of Technology project number 08-662, Also, the support of GA AV CR KAN300100702 project is gratefully acknowledged.

References

- [1] P.W. Wachulak, A. Bartnik, and H. Fiedorowicz, *Opt. Lett.* **35** (2010) 2337 – 2339.
- [2] P.W. Wachulak, A. Bartnik, H. Fiedorowicz, and J. Kostecki, *Opt. Express* **19** (2011) 9541 – 9550.

X-RAY CT SCAN OF STRATOSPHERIC MICRON-SIZED DUST PARTICLES: AN ATTEMPT TO A NON-DESTRUCTIVE MORPHOLOGICAL RECONSTRUCTION

A. Marcelli^{1,2*}, K. Zhang³, Z. Wu^{3,4}, V. Della Corte⁵, A. Rotundi⁵, G. Della Ventura⁶,
M. Ferrari⁵, F.J.M. Rietmeijer⁷, and E. Pace⁸

¹INFN - Laboratori Nazionali di Frascati, 00044 Frascati, Italy

²University of Science and Technology of China, CAS, Hefei 230026, P.R. China

³Beijing Synchrotron Radiation Facility, IHEP, CAS, Beijing 100049, P.R. China

⁴National Synchrotron Radiation Laboratory, University of Science and Technology of China,
Hefei, Anhui 230029, P.R. China

⁵Dipartimento Scienze Applicate, Università degli Studi di Napoli "Parthenope," Napoli 80134, Italy

⁶Dipartimento Scienze Geologiche, Università degli Studi Roma Tre, Roma 00146, Italy

⁷Department of Earth and Planetary Sciences, University of New Mexico, Albuquerque,
NM 87131-0001, USA

⁸Dipartimento Astronomia e Scienza dello Spazio, Università degli Studi di Firenze, Firenze, Italy

* e-mail: marcelli@lnf.infn.it

Aerosols and dust are key elements in many mineralogical, geochemical and physical processes. As an example, windblown mineral dust plays a key role in the climate system, and permits evaluation of climate and environmental phenomena. Similarly, interplanetary dusts are the building blocks from which planetesimals accreted in the early solar system lead to the formation of planets, comets and asteroids [1].

We will present in this contribution the status of the physical and chemical characterization of stratospheric micron-sized dust particles with sizes ranging from 0.3 to 20 μm . Collection of uncontaminated dust has been performed by the DUSTER instrument [2, 3] on board of stratospheric balloons flying at altitudes of 35–40 km. Preliminary characterization of grain morphology and size by Field Emission Scanning Electron Microscopy (FESEM), study of the mineralogy and the carbonaceous component by InfraRed (IR) micro-spectroscopy and Raman micro-spectroscopy have been performed at the Cosmic Physics Laboratory of the University of Naples "Parthenope" / INAF-OAC [4]. In addition, a synchrotron X-ray CT scan investigation of two grains from the DUSTER collection with micrometer size have been performed obtaining a full 3D reconstruction of these particles. Indeed, analytical capabilities in mineralogy, geochemistry and physics of organic/inorganic matter has undergone a tremendous development in the last few years, due to the availability of synchrotron-light based microscope-based techniques. Nano-CT experiments were performed with a full-field transmission x-ray microscope (TXM) in the range 5 to 12 keV at the Beijing Synchrotron Radiation Facility (BSRF) operating at 2.5 GeV with an available spatial resolution < 30 nm.

Results show that this non-destructive 3D X-ray imaging technique is unique and ideal to visualize hidden internal structures of these micron-sized grains collected in the stratosphere. Actually, experiments may simultaneously provide a detailed morphological and crystal-chemical characterization of dusts, contributing to the identification of their origin: terrestrial vs. extraterrestrial.

References

- [1] D.E. Brownlee, *The Origin and Role of Dust in the Early Solar System* (LPI Technical Report 94 – 02 for Lunar and Planetary Institute, Workshop on analysis of IDPs, December 1994).
- [2] A. Ciucci, P. Palumbo, R. Brunetto, V. Della Corte, S. De Angelis, A. Rotundi, F.J.M. Rietmeijer, E. Zona, L. Colangeli, F. Esposito, E. Mazzetta Epifani, V. Mennella, S. Inarta, S. Peterzen, S. Masi, R. Ibba, "DUSTER (Dust in the Upper Stratosphere Tracking Experiment and Retrieval) preliminary analysis," *Mem. S.A.It. Suppl.*, **16** (2011) 119 – 124.
- [3] V. Della Corte, P. Palumbo, S. De Angelis, A. Ciucci, R. Brunetto, A. Rotundi, F.J.M. Rietmeijer, E. Zona, E. Bussoletti, L. Colangeli, F. Esposito, E. Mazzotta Epifani, V. Mennella, S. Peterzen, S. Masi, R. Ibba, "DUSTER (Dust in the Upper Stratosphere Tracking Experiment and Return): A balloon-borne dust particle collector," *Mem. S.A.It.*, **16** (2011) 14 – 20.
- [4] S. De Angelis, V. Della Corte, G.A. Baratta, F.J.M. Rietmeijer, R. Brunetto, P. Palumbo, A. Ciucci, A. Rotundi, "Raman Micro-Spectroscopy performed on extraterrestrial particles," *Spectrosc. Lett.* **44** (2011) 549 – 553.

NANOCRYSTALS AND SMALL CLUSTERS INVESTIGATED BY SYNCHROTRON RADIATION AND MICROFLUIDICS

Hiroyuki Oyanagi*

Electronics and Photonics Research Institute, AIST, 1-1-1 Umezono, Tsukuba 305-8568, Japan

Keywords: synchrotron radiation, nanocrystal, small cluster, microfluidics, X-ray absorption spectroscopy

*e-mail: h.oyanagi@aist.go.jp

Recently, small clusters (SCs) formed by N atoms where $N < 50$ attract keen attention, associated with recent demands on understanding microscopic mechanisms of initial growth (nucleation) of nanocrystals (NC's) and state of "monomers". Combining synchrotron radiation and x-ray absorption spectroscopy (XAS) with microfluidics allows us to study the initial process within a limited volume ($v_0 < 1 \text{ mm}^3$) *in-situ*. Microfluidic cell [1] is a microchannel device along which a chemical reaction occurs in a lamellar flow [2]. For investigating time-dependent structures of NCs, "monomers" or SCs, a high-sensitivity is needed which is realized by high brilliance x-ray beam available from insertion devices at the 3rd generation facilities (*ca.* 10^{12} photons per sec) and modern x-ray detectors. Here, we describe *in-situ* XAS studies using microfluidics to illustrate the capability described above, demonstrated by a couple of applications, i.e., *i*) the structural and kinetics studies during the initial stage of CdSe NCs [3] and *ii*) copper SCs ($N = 13 - 19$) photo-induced by intense x-ray beam.

Colloidal semiconductor NCs, sometimes called quantum dots, became popular due to their size-tunable optical properties and a variety of industrial applications. We demonstrated that time-dependent EXAS (conventionally used as an average local probe) is informative on higher order structures, i.e., NC size and density if bond formation

kinetics is analyzed [4, 5]. The second application is copper SCs formed by a reducing reaction in organic solvent under photo-irradiation. The local structure of SCs prepared in organic solution by reducing Cu(II) hexafluoroacetylacetonate $[\text{Cu}(\text{hfac})_2]$ was studied *as-grown* by XANES and EXAFS. The Cu K-XANES spectra indicated the formation of copper SCs by ligand-exchange with oleylamine and a subsequent reducing by diphenylsilane. The multiple-scattering (MS) XANES calculation for various model SCs suggests that the SCs consist of 13 – 19 atoms that are characterized by a similar fcc-like local structure although the SCs are expected to be insulating based on the electronic state calculated by DFT on possible models.

Acknowledgments: The authors express his thanks to the collaborators; Z. H. Sun, Y. Jiang, M. Uehara, H. Nakamura, K. Yamashita, Y. Orimoto, L. Zhang, C. Lee, A. Fukano and H. Maeda.

References

- [1] H. Nakamura *et al.*, *Chem. Commun.* **2** (2002) 2844.
- [2] H. Holman *et al.*, *Anal. Chem.* **81** (2009) 8564.
- [3] M. Uehara *et al.*, *Appl. Phys. Lett.* **94** (2009) 063104.
- [4] Z. Sun *et al.*, *J. Phys. Chem. C* **113** (2009) 18608.
- [5] H. Oyanagi *et al.*, unpublished.

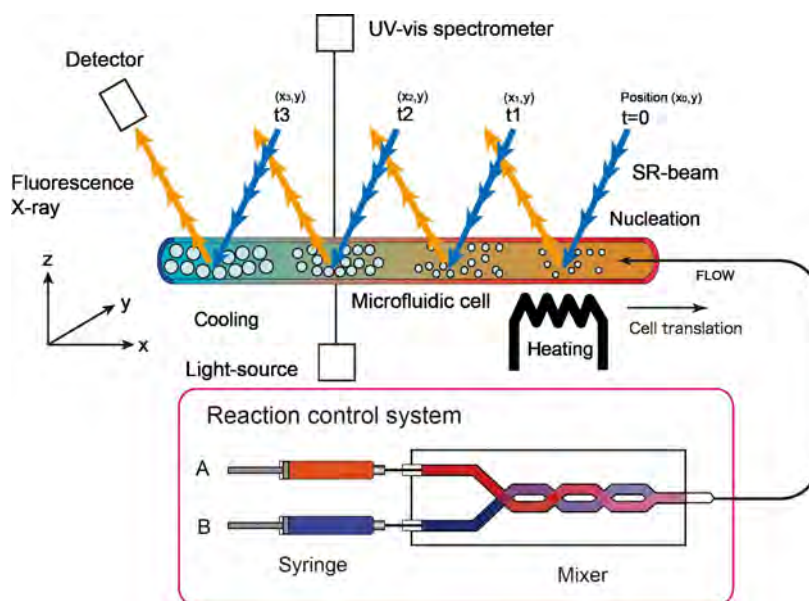


Figure 1: Schematic principle of *in-situ* XAS.

MEASUREMENT OF RESIDUAL STRAINS WITH QUANTITATIVE X-RAY TOPOGRAPHY

F. Masiello^{1,2}, S.H. Connell³, and J. Härtwig^{1*}

¹*European Synchrotron Radiation Facility, Grenoble, France*

²*PANalytical B.V., Almelo, The Netherlands*

³*University of Johannesburg, South Africa*

**e-mail: haertwig@esrf.fr*

Due to its excellent optical, thermal and mechanical properties synthetic single-crystalline diamond is a very well suited material for several X-ray optical elements to be used in 3rd generation X-ray sources. In the case of 4th generation X-ray sources like the XFEL in Hamburg it is probably the only possible material for some applications. Diamond is used for Bragg diffracting elements like monochromators, beam splitters or phase plates/polarisers. However, the beam quality should not be spoiled by those elements. Thus, a high perfection in the crystal bulk and very good surface quality are crucial.

In recent years, considerable progress has been made in the field of the HPHT synthesis methods (high-pressure high-temperature). This has allowed the growth of diamond crystals with linear dimensions of around 10 mm and with low nitrogen content (below 40 ppb instead of hundreds of ppm). The result is a material with extended areas (20 mm² and more) that are free of macroscopic defects like dislocations, stacking faults and inclusions. The residual strains in these areas may be on an extremely low level (smaller than 10⁻⁷), fulfilling the stringent requirements on crystal quality. The sources of residual strains are long range (over millimetres!) strain fields of still existing dislocations, or local variations of the impurity concentrations. Surface scratches, which may even not be visible under an optical microscope and other imperfections at

the surface, also play a role. Such low strain levels are far away from the detection limit of standard methods of X-ray diffraction. The classical measurement of the FWHM of rocking curves is far too insensitive. Even such popular X-ray topography methods like Lang topography (laboratory) or synchrotron white beam topography are not sufficiently sensitive to the levels of strain which are required to be measured, even by some orders of magnitude.

Our goal was twofold. On the one hand we wanted to push the detection limit for residual strains as far (low) as possible, and on the other hand, we wanted to obtain quantitative results with spatial resolution, based on X-ray topographs. Thus, to vary the strain sensitivity and to measure extremely low strain values, we had to use sophisticated non-dispersive double crystal diffraction topography methods (“plane” wave topography). The idea was to use a non-dispersive (*n*,*-m*)-setup with a bendable silicon monochromator, combined with high-order reflections and to also use rather high X-ray energies. In this way narrow rocking curves with extremely steep flanks could be obtained. This results in extreme strain sensitivity when using the steepest part of the flank. We were able to achieve detection limits even down to 10⁻⁹. Quantitative 2D-analysis of local strain was possible with two different experimental methods. We shall demonstrate this based on results obtained from diamond plates purchased from Element Six.

ENERGY CONVERTING INTERFACES STUDIED BY SYNCHROTRON RADIATION

C. Pettenkofer* and A. Hofmann

Helmholtz-Zentrum-Berlin, Albert-Einstein Str.15 12489 Berlin, Germany

Keywords: synchrotron radiation

*e-mail: pettenkofer@helmholtz-berlin.de

The electronic properties of interfaces in semiconductor devices are crucially dependent on the detailed atomic structure of the contact plane.

Most studies on solar cell interfaces are carried out on technologically prepared interfaces. In this study we start from idealized single crystalline interfaces prepared by MBE, MOMBE, ALD etc. under very well defined UHV conditions and investigated in situ by UPS, XPS, LEED, STM and XPEEM.

In particular we report on our attempts to model the junction in chalcopyrite thin films by well defined interfaces to clarify the influence of grain boundaries, lateral inhomogenities and chemical variations across and aside the contact plane. Chalcopyrites of the Type CuInX_2 ($X = \text{S}, \text{Se}$) were grown by MBE as single crystalline samples in various orientations and were studied by surface analytical tools like XPS, UPS, LEED, STM and XPEEM in situ. Especially the application of synchrotron radiation in photo emission experiments is an extremely powerful tool to gain insight into the morphology and structure of hetero contacts. In a single deposition experiment it is possible to determine the band alignment, band bending, chemical reacted interfaces and their crystalline structure with high accuracy. By following the development of the contact phase to ZnO, ZnSe, ZnS step by step in an UHV environment, all properties of the interface are determined on an atomic scale with high resolution. Beside the formation of an ordered vacancy compound of the absorber the existence of various interfacial layers are detected and their influence on the parameters of a cell is discussed.

For CuInSe_2 the formation of Cu poor interface layers is observed by SRXPS by the formation of the interface to ZnSe buffer layers. The development of Cu-poor surface phases was discussed by Zunger *et al.* and is here detected unambiguously.

To determine the band alignment valence band spectra have to be recorded to obtain the valence band onset. Here we will show that the right value can only be obtained by using synchrotron radiation as the correct position of the valence band in k-space has to be determined at the Γ -point.

Further details on interface properties will be given by presenting XPEEM results on energy converting interfaces.

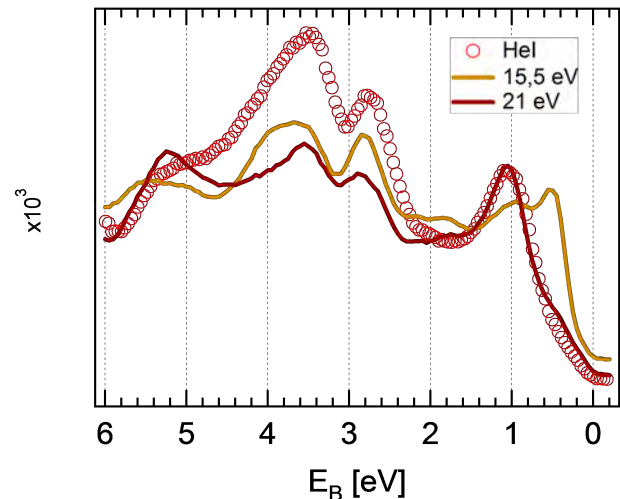


Figure 1: Valence band for CuInSe_2 (112) for different photon energies.

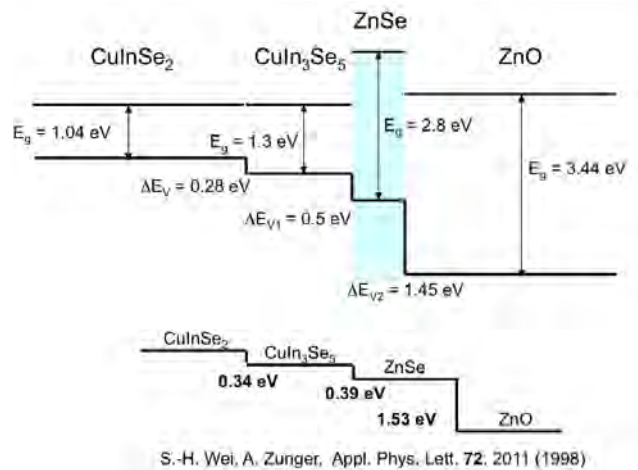


Figure 2: Valence band offsets in the $\text{CuInSe}_2/\text{ZnSe}/\text{ZnO}$ heterojunction as determined by photoemission data and the calculation of Wei and Zunger.

ELECTRONIC AND SPIN STRUCTURES OF SOLIDS BY MEANS OF SYNCHROTRON RADIATION PHOTOEMISSION

Masaki Taniguchi^{1,2*}

¹*Hiroshima Synchrotron Radiation Center, Hiroshima University, Kagamiyama 2-313,
Higashi-Hiroshima 739-0046, Japan*

²*Graduate School of Science, Hiroshima University, Kagamiyama 1-3-1,
Higashi-Hiroshima, 739-8526, Japan*

*Keywords: high-resolution ARPES, unconventional superconductor, topological insulator,
Rashba system, spin structure*

**e-mail: taniguch@hiroshima-u.ac.jp*

Synchrotron radiation photoemission is a powerful tool to directly clarify the electronic and spin structures of solids that are directly related to the physical properties. Angle-resolved photoemission spectroscopy (ARPES) with very high energy- and momentum-resolutions was successfully applied to investigations of many body interactions in single crystalline metals and unconventional superconductors. In addition, spin- and angle-resolved photoemission spectroscopy (SARPES), which can directly determine the spin-polarized band dispersions, was intensively employed for investigations on peculiar spin texture of surface states due to the spin-orbit interaction, such as surface Rashba spin splitting states or helical spin states of topological insulators.

In this talk, I will discuss electron-boson couplings in ruthenate superconductor Sr_2RuO_4 investigated by ARPES [1], and spin-polarized Dirac-cone like surface state with d character at $W(110)$ by SARPES [2]. I also report high performance SARPES apparatus developed at Hiroshima Synchrotron Radiation Center [3].

The Sr_2RuO_4 has attracted considerable attentions for several reasons such as unconventional superconductivity, a structural similarity to the cuprates, and a two-dimensional Fermi liquid behavior in the normal states. Furthermore, the multiband electronic structure is essential feature of Sr_2RuO_4 , which is contrast to the cuprates possessing a single band.

In order to resolve the complex electronic structure of Sr_2RuO_4 , it is indispensable to utilize the linear polarization of the synchrotron radiation. By changing the polarization direction of the incident light, it is possible not only to identify the wave function parity of the initial states with respect to a mirror plane of single crystals [4] but also to select the observable electronic states. Namely, the even-(odd-) symmetry initial states are only observable with p - (s -) polarization because of the dipole selection rule.

We have observed the fine quasiparticle dispersions of Sr_2RuO_4 using the high-resolution ARPES with tunable polarization. We found strong hybridization between the in-plane and out-of-plane quasiparticles via the Coulomb and spin-orbit inter-

actions [1]. This effect enhances the quasiparticle mass due to the inflow of out-of-plane quasiparticles into the two-dimensional Fermi surface sheet, where the quasiparticles are further subjected to the multiple electron-boson couplings. The result suggests that the spin-triplet p -wave superconductivity of Sr_2RuO_4 is phonon mediated.

Topological insulators and Rashba systems with spin-split surface states induced by strong spin-orbit interaction have attracted a great attention for the dissipationless spin current transport [5]. Such spin split surface states have been intensively studied by ARPES mainly for the surface of sp -electrons systems at heavy metals and topological insulators [6, 7].

A material with d -derived spin-splitting band remains yet to be explored. Possible strong correlation effects among d electrons in topological insulators and Rashba systems could be important scientific issue. We show the first experimental evidence of nearly massless and strongly spin-polarized surface states in a spin-orbit-induced symmetry gap of $W(110)$ [2]. Our SARPES study reveals that the spin polarization is antisymmetric with respect to zone center. The constant-energy cuts of this Dirac-cone-like state are found to be strongly anisotropic, which paves the way to the study of peculiar d -electron based topological properties with anomalous spin textures.

Finally, I report our newly developed highly efficient SARPES apparatus developed at Hiroshima Synchrotron Radiation Center [3]. By utilizing high-efficient spin detector based on very low energy electron diffraction (VLEED) [8] by ferromagnetic target ($\text{Fe}(001)p1 \times 1\text{-O}$) as the spin detector and combining it with high-resolution hemispherical analyzers (SCIENTA R4000), high-efficient and high-resolution SARPES experiment has been realized. Especially, the present machine was designed to improve the performance of the first prototype machine, and resolution of 7.5 meV in energy and $\pm 0.18^\circ$ in angle has been achieved with spin resolution [3]. One can observe both in-plane and out-of-plane spin components by a 90° electron deflector. In addition, the two-dimensional electron detector for conventional spin-integrated ARPES measure-

ment can realize quick and precise observation of the electronic band structure and Fermi surfaces. Therefore, one can find the specific electronic structure where is interested in to observe the spin structure quite efficiently and measure the spin structure with high-resolution.

Acknowledgments: These works have been done in collaboration with Dr. Iwasawa, Dr. Yoshida, Dr. Hase, Dr. Koikegami, Mr. Hayashi, Dr. Jiang, Prof. Shimada, Prof. Namatame, Dr. Aiura, Dr. Miyamoto, Prof. Kimura, Mr. Kuroda, Prof. Okuda, Prof. Donath, and Mr. Miyahara.

References

- [1] H. Iwasawa, Y. Yoshida, I. Hase, S. Koikegami, H. Hayashi, J. Jiang, K. Shimada, H. Namatame, M. Taniguchi, and Y. Aiura, *Phys. Rev. Lett.* **105** (2010) 226406.
- [2] K. Miyamoto, A. Kimura, K. Kuroda, T. Okuda, K. Shimada, H. Namatame, M. Taniguchi, and M. Donath, *Phys. Rev. Lett.* **108** (2012) 066808.
- [3] T. Okuda, K. Miyamaoto, H. Miyahara, K. Kuroda, A. Kimura, H. Namatame, and M. Taniguchi, *Rev. Sci. Instrum.* **82** (2011) 103302.
- [4] W. Eberhardt and F.J. Himpsel, *Phys. Rev. B* **21** (1980) 5572.
- [5] Y.A. Bychkov *et al.*, *JETP Lett.* **39** (1984) 78; S. Datta *et al.*, *Appl. Phys. Lett.* **56** (1990) 665.
- [6] M. Hoesch *et al.*, *Phys. Rev. B* **69** (2004) 241401(R); T. Hirahara *et al.*, *New J. Phys.* **10** (2008) 083038.
- [7] K. Kuroda *et al.*, *Phys. Rev. Lett.* **105** (2010) 146801; K. Kuroda *et al.*, *Phys. Rev. Lett.* **105** (2010) 076802.
- [8] D. Tillmann, R. Thiel, and E. Kisker, *Z. Phys. B* **77** (1989) 1.

XMCD STUDIES OF THE MAGNETIC PROPERTIES OF NANOCLUSTERS IN GaAs MATRIX

K. Lawniczak-Jablonska^{1*}, A. Wolska¹, M.T. Klepka¹, and V. Sessi²

¹*Institute of Physics, Polish Academy of Sciences, Al. Lotnikow 32/46, 02-668 Warsaw, Poland*

²*European Synchrotron Radiation Facility, 6 Rue Jules Horowitz, 38043 Grenoble, France*

Keywords: granular materials, magnetic moments, spintronics, XMCD

**e-mail: jablo@ifpan.edu.pl*

The failure in producing the room temperature (RT) ferromagnetic diluted magnetic semiconductors, resulted in the increasing interest in the granular materials which are ferromagnetic at room temperature. In the case of GaMnAs, granular material can be easily produced by thermal processing of the low temperature grown MBE layers. In such materials the ferromagnetic clusters which show RT magnetism are immersed in a semiconducting matrix. Recently the possibility to produce the magnetic tunnel junctions with active layer of GaMnAs with the small cubic cluster was demonstrated [1]. As a result, new questions aroused concerning the control of the nanoclusters' crystallographic structure, size distribution and magnetic properties.

In the series of our recent papers [2]-[5] we demonstrate that the cubic MnAs clusters do not exist. Instead the small cubic GaMnAs clusters are formed with much higher content of Mn than ever produced in GaMnAs layers with randomly distributed Mn atoms. The clusters with size larger than 8 nm already have the MnAs hexagonal structure. Moreover, the commonly accepted conditions that annealing of layer up to 500°C produces exclusively cubic clusters while annealing at 600°C or higher results in solely hexagonal clusters are not valid.

The recent studies of x-ray absorption spectra (XAS) and x-ray magnetic circular dichroism (XMCD) on the series of granular materials will be presented. From the performed studies result that the Mn position in the as grown samples (substitutional or interstitial) plays an important role in the formation of nanoclusters of given crystallographic structure. The XMCD investigation performed at the ESRF station ID08 showed the remarkable difference in the magnetic properties of cubic and hexagonal nanoclusters. Moreover, the small number of the hexagonal MnAs nanoclusters is sufficient to dominate the magnetic properties of the sample (see Fig. 1) and the shape of the XMCD signal. Nevertheless, in all granular samples the XMCD signal was observed at RT under the magnetic field while at 12 K the dichroic signal was also detected for the remanently magnetized samples.

Two detection mode were applied with different sensitivity. The surface sensitive total electron yield (TEY) and bulk sensitive total fluorescence yield

(TFY). The remarkable differences in the shape of both signal were detected (Fig.1) indicating variation in the spatial distribution of clusters with different structure. The dependence of the orbital and spin magnetic moment on the structure and size of observed clusters will be also discussed.

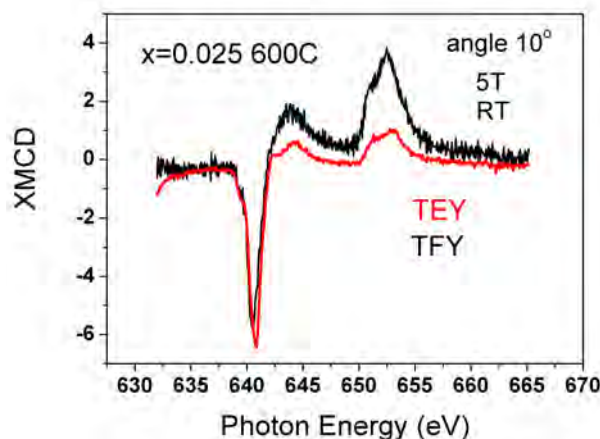


Figure 1: The XMCD at the $L_{2,3}$ edge of Mn measured at RT under field 5 T in two detection modes — total electron yield (TEY) and total fluorescence yield (TFY). The sample $\text{Ga}_{1-x}\text{Mn}_x\text{As}$ with $x = 0.025$ after annealing at 600°C has only small fraction of hexagonal nanoclusters which dominated the XMCD bulk signal. The surface signal is still characteristic for cubic clusters.

Acknowledgments: The measurements performed at HasyLab have received funding from the European Community's Seventh Framework Programme (FP7/2007 – 2013) under grant ELISA agreement no. 226716. The measurement at ESRF from special project ESRF/73/2006 from the Ministry of Science and High Education. Authors thank you J. Sadowski for providing the samples.

References

- [1] P.N. Hai *et al.*, *Nature* **458** (2009) 489.
- [2] K. Lawniczak-Jablonska *et al.*, *Phys. Status Solidi (RRL)* **5** (2011) 62.
- [3] K. Lawniczak-Jablonska *et al.*, *J. Solid State Chem.* **184** (2011) 1530.
- [4] K. Lawniczak-Jablonska *et al.*, *Phys. Status Solidi B* **248** (2011) 1609.
- [5] K. Lawniczak-Jablonska *et al.*, *Rad. Phys. Chem.* **78** (2009) S80.

PROBING THE ELECTRONIC AND MAGNETIC PROPERTIES OF BULK MATERIALS AND BURIED LAYERS AND INTERFACES WITH STANDING-WAVE AND HARD-X-RAY PHOTOEMISSION

C.S. Fadley

Department of Physics, University of California Davis Materials Sciences Division,
Lawrence Berkeley National Laboratory

*e-mail: fadley@physics.ucdavis.edu

In this lecture, I will discuss some new directions in soft x-ray photoemission (XPS, SXPS) and hard x-ray photoemission (HXPS, HAXPES, HIKE) by my group and its several collaborators [1]-[12], including experiments carried out at the ALS, BESSY, SPring8, Petra III, and SLS. These involve combined SXPS and HXPS studies of buried layers and interfaces in magnetic and transition-metal oxide multilayers [5, 6, 8, 10], hard x-ray photoemission studies of the bulk electronic structure of some spintronic materials [4, 7, 11]; including band-offset measurements in oxide multilayers [12]; the use of

standing waves from multilayer mirrors to enhance depth contrast in spectroscopy [5, 6, 10], as well as in angle-resolved photoemission (ARPES) [1, 5] and photoelectron microscopy [3]; and the prospects for carrying out bulk sensitive hard x-ray ARPES (HARPES) [9] and hard x-ray photoelectron diffraction (HXPD) [2].

Acknowledgments: This work was supported by the U.S. Department of Energy under Contract No. DE-AC02-05CH11231, the Army Research Office, under MURI Grant W911-NF-09-1-0398, and the Forschungszentrum Julich, Peter Grunberg Institute.

References

- [1] C.S. Fadley, "X-ray photoelectron spectroscopy: Progress and perspectives," *J. Electron. Spectrosc. Relat. Phenom.* **2** (2010) 178 – 179 (invited review).
- [2] A. Winkelmann, J. Garcia de Abajo, and C.S. Fadley, "High energy photoelectron diffraction: Model calculations and future possibilities," *New J. Phys.* **10** (2008) 113002.
- [3] F. Kronast, R. Ovsyannikov, A. Kaiser, C. Wiemann, S.-H. Yang, D.E. Bürgler, R. Schreiber, F. Salmassi, P. Fischer, H.A. Dürr, C.M. Schneider, W. Eberhardt, and C.S. Fadley, "Depth-resolved soft x-ray photoelectron emission microscopy in nanostructures via standing-wave excited photoemission," *Appl. Phys. Lett.* **93** (2008) 243116; A.X. Gray, F. Kronast, C. Papp, S.H. Yang, S. Cramm, I.P. Krug, F. Salmassi, E.M. Gullikson, D.L. Hilken, E.H. Anderson, P.J. Fischer, H.A. Dürr, C.M. Schneider, and C.S. Fadley, "Standing-wave excited soft x-ray photoemission microscopy: Application to nanodot Co magnetic arrays," *Appl. Phys. Lett.* **97** (2010) 062503.
- [4] Z. Boekelheide, A.X. Gray, C. Papp, B. Balke, D.A. Stewart, S. Ueda, K. Kobayashi, F. Hellman, and C.S. Fadley, "Band gap and electronic structure of an epitaxial, semiconducting $\text{Cr}_{0.80}\text{Al}_{0.20}$ thin film," *Phys. Rev. Lett.* **105** (2010) 236404.
- [5] A.X. Gray, C. Papp, B. Balke, S.-H. Yang, M. Huijben, E. Rotenberg, A. Bostwick, S. Ueda, Y. Yamashita, K. Kobayashi, E.M. Gullikson, J.B. Kortright, F.M.F. de Groot, G. Rijnders, D.H.A. Blank, R. Ramesh, and C.S. Fadley, "Interface properties of magnetic tunnel junction $\text{La}_{0.7}\text{Sr}_{0.3}\text{MnO}_3/\text{SrTiO}_3$ superlattices studied by standing-wave excited photoemission spectroscopy," *Phys. Rev. B* **82** (2010) 205116; and A.X. Gray *et al.*, to be published.
- [6] S. Döring, F. Schönbohm, U. Berges, R. Schreiber, D.E. Bürgler, C.M. Schneider, M. Gorgoi, F. Schäfers, C. Papp, B. Balke, C.S. Fadley, C. Westphal, "Hard x-ray photoemission study using standing-wave excitation applied to the MgO/Fe interface," *Phys. Rev. B* **83** (2011) 165444; and S.H. Yang, B. Balke, C. Papp, S. Döring, U. Berges, L. Plucinski, C. Westphal, C.M. Schneider, S.S.P. Parkin, and C.S. Fadley, "Determination of layer-resolved magnetic and electronic structure of Fe/MgO by soft x-ray standing-wave core- and valence- photoemission," *Phys. Rev. B* **84** (2011) 184410.
- [7] A.X. Gray, J. Karel, J. Minar, C. Bordel, H. Ebert, J. Braun, S. Ueda, Y. Yamashita, L. Ouyang, D.J. Smith, K. Kobayashi, F. Hellman, and C.S. Fadley, "Hard X-ray photoemission study of near-heusler $\text{Fe}_x\text{Si}_{1-x}$ alloys," *Phys. Rev. B* **83** (2011) 195112.
- [8] A.X. Gray, A. Janotti, J. Son, J.M. LeBeau, S. Ueda, Y. Yamashita, K. Kobayashi, A.M. Kaiser, R. Sutarto, H. Wadati, G.A. Sawatzky, C.G. Van de Walle, S. Stemmer, C.S. Fadley, "Insulating state of ultrathin epitaxial LaNiO_3 thin films detected by hard x-ray photoemission," *Phys. Rev. B* **84** (2011) 075104.
- [9] C. Papp, A. Gray, B. Balke, S. Ueda, K. Kobayashi, S. Sakai, H. Yoshikawa, Y. Yamashita, S.L. He, E. Ylvisaker, L. Plucinski, C. Schneider, J. Minar, J. Braun, H. Ebert, W.E. Pickett, C.S. Fadley, "Probing bulk electronic structure with hard X-ray angle-resolved photoemission," *Nature Materials* **10** (2011) 759; see also companion News and Views article: D.L. Feng, *Nature Materials* **10** (2011) 729-730.

- [10] A.M. Kaiser, A.X. Gray, G. Conti, J. Son, A. Greer, A. Perona, A. Rattanachata, A.Y. Saw, A. Bostwick, S. Yang, S.-H. Yang, E.M. Gullikson, J.B. Kortright, S. Stemmer, and C.S. Fadley, "Suppression of near-Fermi level electronic states at the interface in a $\text{LaNiO}_3/\text{SrTiO}_3$ superlattice," *Phys. Rev. Lett.* **107** (2011) 116402.
- [11] C. Caspers, M. Müller, A.X. Gray, A.M. Kaiser, A. Gloskovskii, C.S. Fadley, W. Drube, and C.M. Schneider, "Chemical stability of the magnetic oxide EuO directly on silicon observed by hard X-ray photoemission spectroscopy," *Phys. Rev. B* **84** (2011) 205217.
- [12] G. Conti, A.X. Gray, A.M. Kaiser, A. Greer, J. Karel, S. Ueda, Y. Yamashita, A. Gloskovskii, A. Jannotti, C. G. Van de Walle, K. Kobayashi, W. Drube, S. Stemmer, and C.S. Fadley, "Determination of band offsets in complex oxide thin-film heterostructures by hard X-Ray photoelectron spectroscopy", to be published.

ELECTRONIC STRUCTURE OF $A_2\text{FeReO}_6$ DOUBLE PEROVSKITES PROBED WITH Re 2p RXES

M. Sikora*

AGH University of Science and Technology, Av. Mickiewicza 30, 30–059 Kraków, Poland

Keywords: electronic structure, rhenium compounds, magnetoresistive double perovskites, RXES, RIXS

*e-mail: marcin.sikora@agh.edu.pl

Ordered double perovskites $A_2BB'O_6$ (A = alkaline earth metals, $B = 3d$ transition metal, and $B' = 3d, 4d$, or $5d$ transition metal) reveal extraordinary properties in terms of their potential application in magnetoelectronics, namely large spin polarization of the electrical carriers, significant magnetoresistance at room temperature and high Curie temperature [1]. The $B = \text{Re}$ double perovskites show strong magneto-structural coupling as well as an unexpected increase in the Curie temperature with decreasing $B-O-B'$ angle and, thus, a reduction in the effective d -electron hopping integral. Such behavior, that is in contrast to other transition-metal oxides, is attributed to the interplay between structural degrees of freedom with unquenched Re orbital moment [2], giving rise to a competition between the octahedral ligand field and the strong spin-orbit coupling in the $5d$ orbitals.

Here we show an attempt to verify these assumptions employing high resolution X-ray spectroscopy

to probe the element specific electronic structure of double perovskites and its evolution upon decreasing $B-O-B'$ angle, i.e. going from $A = \text{Ba}$, through Sr to Ca. $2p$ Resonant X-ray Emission Spectroscopy (RXES) and $2p5d$ Resonant Inelastic X-ray Scattering (RIXS) have been applied providing us with detailed information on electronic structure of core levels and valence band, respectively, with bulk sensitivity.

We observe that Re-probed electronic structure of core levels, even the shallow ones, is insensitive to local environment. Also the bandwidth of valence band does not show significant differences among the compounds studied. However, the splitting of the features in unoccupied electronic structure as well as intensity and fine structure of the spectral features reveal gradual evolution upon decreasing of $B-O-B'$ angle (Fig. 1). Detailed analysis of the spectral shape of $2p5d$ RIXS will be performed following the approach of Nikolay Smolentsev *et al.* [3].

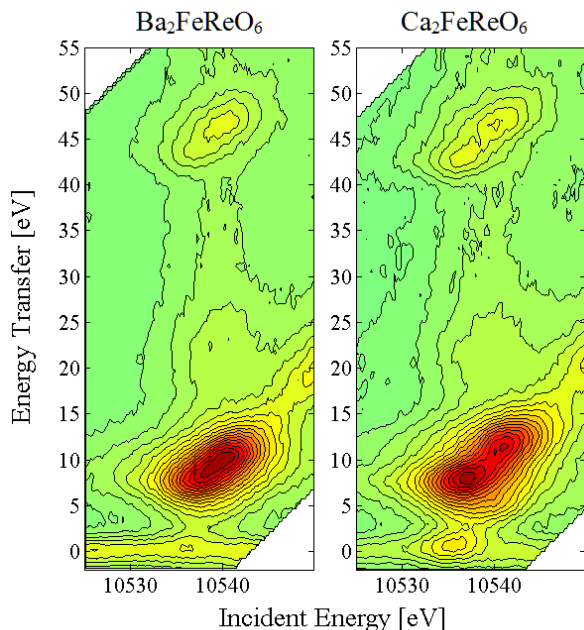


Figure 1: Contour plots of the $2p5d$ RIXS in $\text{Ba}_2\text{FeReO}_6$ (left) and $\text{Ca}_2\text{FeReO}_6$ (right) probed at Re L_3 -edge.

Acknowledgments: European Synchrotron Radiation Facility, Grenoble, is acknowledged for provision of beamtime. We thank the ID26 staff for help in setting up the experiment. Financial support from the Polish Ministry of Science and Higher Education, grants ESRF/73/2006 and N N202 071539, is acknowledged.

References

- [1] D. Serrate, J.M. De Teresa, M.R. Ibarra, "Double perovskites with ferromagnetism above room temperature," *J. Phys.: Condens. Matter* **19** (2007) 023201.
- [2] M. Sikora, O. Mathon, P. van der Linden, J.M. Michalik, J.M. de Teresa, Cz. Kapusta, S. Pasquarelli, "Field-induced magnetostructural phase transition in double perovskite $\text{Ca}_2\text{FeReO}_6$ studied via x-ray magnetic circular dichroism," *Phys. Rev. B* **79** (2009) 220402.
- [3] N. Smolentsev, M. Sikora, A.V. Soldatov, K.O. Kvashnina, P. Glatzel, "Spin-orbit sensitive hard x-ray probe of the occupied and unoccupied $5d$ density of states," *Phys. Rev. B* **84** (2011) 235113.

X-RAY MAGNETIC CIRCULAR DICHOISM UNDER HIGH MAGNETIC FIELD

A. Rogalev* and **F. Wilhelm**

European Synchrotron Radiation Facility, 6, rue Jules Horowitz, 38000 Grenoble, France

Keywords: X-ray spectroscopy, circular polarization, magnetism

**e-mail: rogalev@esrf.fr*

X-ray Magnetic Circular Dichroism (XMCD) spectroscopy is a well-established experimental tool to study the microscopic origin of magnetism allowing one to determine separately spin and orbital magnetic moments of each element in both amplitude and direction. So far, XMCD has been extensively used to investigate mainly ferro- or ferromagnetic materials, and only very few studies have been performed on paramagnetic compounds. This is partly because a sufficiently high magnetic field for magnetizing paramagnetic or antiferromagnetic materials was not available at synchrotron facilities. Fields of 1 – 2 T are generally used for conventional XMCD experiments, and even the highest field using a large superconducting magnet has been limited to 10 T.

In this presentation we describe first a new experimental set-up dedicated to high field XMCD measurements that has been recently installed at the ESRF beamline ID12. Static magnetic field of up to 17 Tesla is generated by a superconducting solenoid. The sample is mounted on a cold finger of a He constant flow cryostat allowing to vary the

temperature from 2.2 K to 300 K. Spectra are measured using total fluorescence yield detection mode with a Si photodiode mounted on a liquid nitrogen shield of the magnet.

Performances of this set-up are illustrated with results of thorough XMCD studies of a variety of magnetic systems:

- Metamagnetic phase transitions under high magnetic field have been studied in antiferromagnets with large magnetic anisotropy like PrCo_2Ge_2 and CeRu_2Si_2 ;
- The existence of an intrinsic magnetic moment in gold nanoparticles grown onto naturally thiol-containing proteinaceous archaeal surface layer has been evidenced by XMCD at the Au $L_{2,3}$ -edges;
- Curie and van Vleck magnetic susceptibilities have been measured on paramagnetic insulators ($\text{Gd}_3\text{Ga}_5\text{O}_{12}$ and $\text{Eu}_3\text{Ga}_5\text{O}_{12}$) using an intense XMCD signal at the L -edges of the rare-earth.

VALENCE OF CONSTITUENTS OF SELECTED RARE EARTH SILICIDES — XANES AND LAPW NUMERICAL STUDY

P. Zajdel^{1*}, A. Kisiel², A. Szytuła², P. Starowicz², J. Goraus¹, J. Konior², A. Banaś³,
A. Balerna⁴, G. Cinque⁴, and A. Grilli⁴

¹University of Silesia, Institute of Physics, ul. Uniwersytecka 4, 40-007 Katowice, Poland

²Jagiellonian University, Institute of Physics, ul. Reymonta 4, 30-059 Kraków, Poland

³Singapore Synchrotron Light Source, National University of Singapore, 5 Research Link Singapore 117603

⁴Laboratori Nazionali di Frascati, INFN, Via E. Fermi 40, I-00044 Frascati, Italy, Lab DAFNE-Light

Keywords: XAS, rare earth, silicides

*e-mail: pawel.zajdel@us.edu.pl

The intermetallic rare earth (RE) silicides bring out a lot of attention due to their uranium based members, frustrated geometry and interesting magnetism. Although the electronic structure and magnetism are primarily determined by the rare earth and the RE-Pd/Rh hybridization it is interesting to verify a role of silicon as a “passive” spacer.

Here we report on the investigation of the chemical environment and electronic structure of Si and Pd using X-Ray Absorption Fine Structure in two different families. The XAS experiments were performed at the DAFNE-Light Laboratory of the Laboratori Nazionali di Frascati, Italy. Data were collected at room temperature, in the transmission mode.

Two families of silicides were chosen for the study. First, we elucidated similarities and differences caused by different rare earth in the same matrix for RE₂PdSi₃ series, where RE=Ce, Nd, Td, Dy, Ho, Er. The compounds crystallize in an AlB₂-type structure (space group P6/mmm). The RE ions occupy the Al-equivalent positions, while non-magnetic Pd and Si atoms should be statistically distributed on B sites. However, recent study has hinted to the existence of additional order between Pd/Si layers, which coexists with the disorder [1].

Figure 1. presents Si K edges (some are omitted for clarity) of Ce, Dy and Er based compounds as

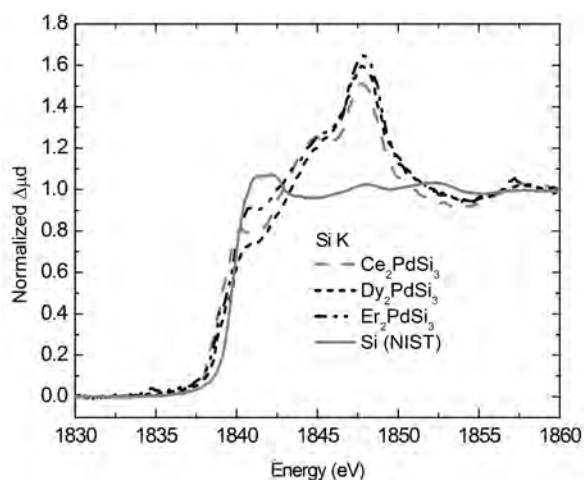


Figure 1: Si K edges of selected compounds of R₂PdSi₃ series.

well as pure silicon.

The Si K edges of the silicides are shifted to lower energies by about 0.5 eV, relative to pure Si and this shift decreases with filling of the 4*f*-shell of the RE. Such trend is consistent with the weak anionic character of Si, which is reduced by the increased screening and contraction of the radius of the lanthanide.

The Pd *L*_{III} edges were recorded with worse quality due to weak signal in the transmission mode. Figure 2. presents the edges of the respective compounds with the presented error bar estimated from the raw spectra.

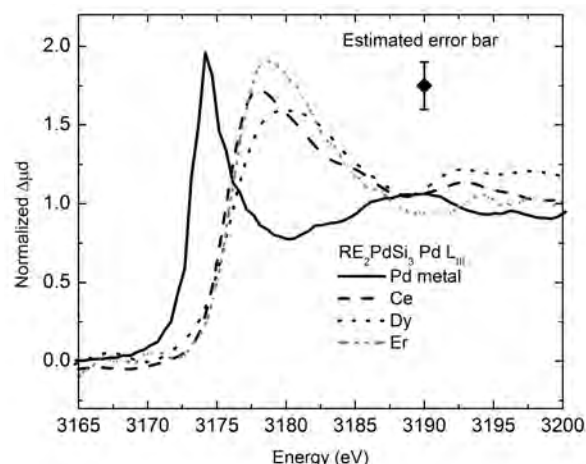


Figure 2: Smoothed Pd *L*_{III} edges of R₂PdSi₃ series.

Contrary to the Si *K*, all of the Pd *L*_{III} edges are shifted to higher energies in accordance with the cationic character of the metal. Due to significant noise, it was impossible to observe any systematic effect with the increasing atomic number of the rare earth.

The second part of the study was based on the HoRh_{*x*}Pd_{2-*x*}Si₂ series of compounds, which crystallize in the tetragonal ThCr₂Si₂-type crystal structure (space group I4/mmm). Here, the charge equilibrium of the system was imbalanced on the transition metal site by substitution of the palladium ([Kr]4*d*10) with rhodium ([Kr]4*d*85*s*1). Figure 3. presents Si *K* edges of the selected members of the family.

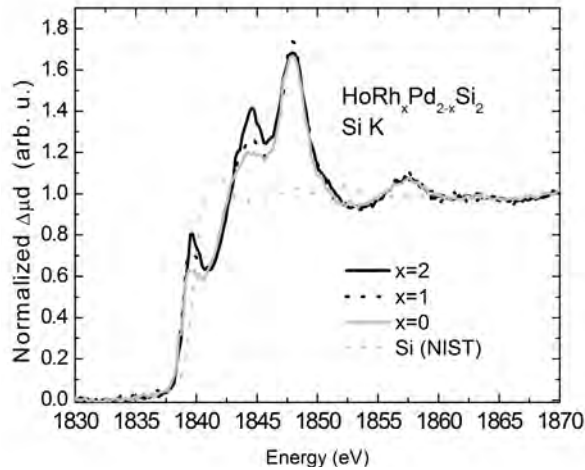


Figure 3: Si K edges of selected compounds of the $\text{HoRh}_x\text{Pd}_{2-x}\text{Si}_2$ series.

They are also shifted to lower energies in agreement with slight anionic character of the silicon. However, no change in the edge position is observed with Pd/Rh substitution. On the other hand, a clear trend can be observed in the amplitude of the edge structures situated at 1840 eV and 1845 eV, which decreases with larger Pd content. Such behaviour can be understood in term of the hybridisation between TM d and Si p states. As the TM $4d$ states are filling up and are pulled down below the Fermi's energy, they drag a part of spectral density away from the silicon $3p$ band.

In order to better comprehend the properties of both families, we concentrated on the holmium ones as the common rare earth [2, 3] and calculated theoretical densities of states using Wien2K'09 code with LDA+U formalism. Figure 4. shows that the Si K edge of HoPd_2Si_2 is well reproduced

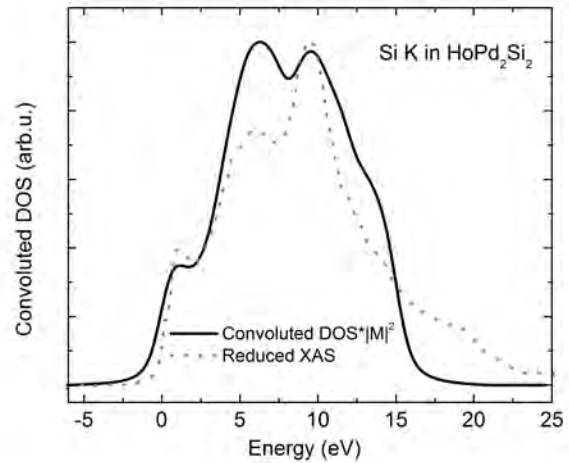


Figure 4: Comparison of calculated and experimental Si K edge in HoPd_2Si_2 .

up to 15 eV above the edge where our approximation breaks down. All features are reproduced both in the edge and its derivative.

Acknowledgments: This work was done under a EU TARI XANES-EXAFS project no 19. HPRI-CT-1999-00088.

References

- [1] C. Richter, T. Leisegang, M. Zschornak, R. Mitrach, D. Novikov, and D. C. Meyer, *Desy report* (2009) 2009775.
- [2] A. Szytuła, M. Hofmann, B. Penc, M. Ślaski, S. Majumdar, E.V. Sampathkumaran, and A. Zygmunt, *J. Magn. Magn. Mater.* **202** (1999) 365.
- [3] A. Szytuła, T. Jaworska-Gołab, S. Baran, B. Penc, J. Leciejewicz, M. Hofmann, and A. Zygmunt, *J. Phys.: Condens. Matter* **13** (2001) 8007.

STUDIES OF COBALT NANOCONSTRICTIONS BY SCANNING TRANSMISSION X-RAY MICROSCOPY AND MICROMAGNETIC SIMULATIONS

A. Fernández-Pacheco^{2,3*}, A. Szkudlarek^{1*}, L.E. Serrano-Ramón², T. Tyliszczak⁴,
Cz. Kapusta¹, M.R. Ibarra³, and J.M. De Teresa^{2,3}

¹AGH University of Science and Technology, Faculty of Physics and Applied Computer Science,
Department of Solid State Physics, Adama Mickiewicza 30, 30-059 Krakow, Poland

²Instituto de Ciencia de Materiales de Aragón (ICMA), Departamento de Física de la Materia
Condensada, Universidad de Zaragoza-CSIC, Pedro Cerbuna 12, 5009 Zaragoza, Spain

³Laboratorio de Microscopías Avanzadas (LMA), Instituto de Nanociencia de Aragón (INA), Universidad
de Zaragoza, Mariano Esquillor 50018 Zaragoza, Spain

⁴Advanced Light Source, Lawrence Berkeley National Laboratory, 1 Cyclotron Road Berkeley, CA, USA

Keywords: magnetic nanoconstriction, Scanning Transmission X-Ray Microscopy (STXM),
micromagnetic simulations

*e-mail: af457@cam.uk.co

High magnetoresistance values reported in literature have attracted a lot of attention to nanomagnetic contacts. However, the physical phenomena which are ruled mainly by the magnetization in the regions adjacent to the nanoconstriction [1], might be masked by artifacts [2]. In order to investigate the character of magnetization reversal process the structures with asymmetric contact shape were

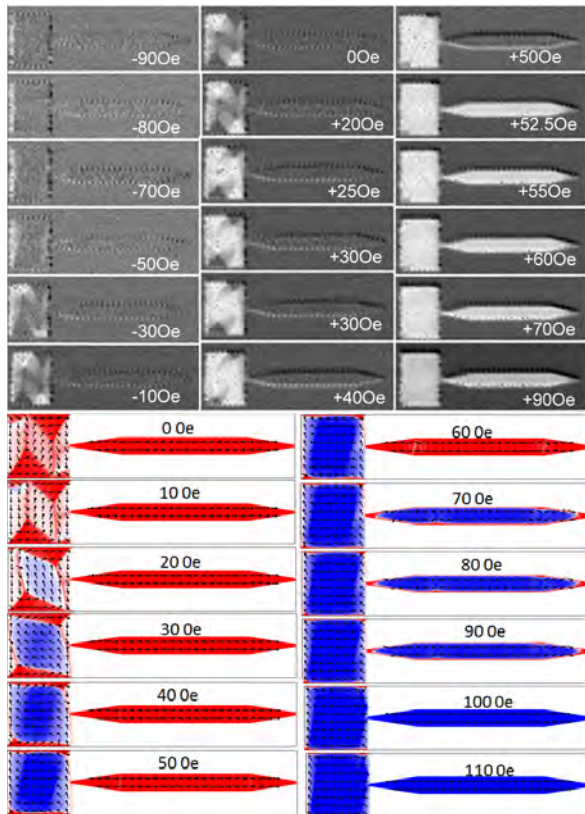


Figure 1: Room temperature STXM images of the structure as a function of the external magnetic field compared with micromagnetic simulations. Values of the x -component of the field are shown.

fabricated. The samples consist of a $4 \mu\text{m} \times 4 \mu\text{m}$ square pad and a $8 \mu\text{m} \times 1 \mu\text{m}$ rectangular wire, which are joined together by a constriction. The minimum size of the contact areas studied is $80 \times 10 \text{ nm}^2$. The structures were fabricated by focused-electron-beam-induced deposition (FEBID) — a novel single step lithography technique, which allows to obtain high purity polycrystalline cobalt deposit using the $\text{Co}_2(\text{CO})_8$ precursor.

The magnetization reversal was investigated by Scanning Transmission X-ray Microscopy (STXM) at the Advance Light Source in Berkeley. The advanced magnetic imaging by X-Ray Circular Dichroism allows to obtain a unique insight into the process with a spatial resolution of about 40 nm. The analysis of images explains well the experimentally observed magnetoresistance (MR), basing on the theory of anisotropic (AMR) in the diffusive electrical transport regime, i.e. derived from the y -component of the magnetization. The micromagnetic simulations, complementary to MR and STXM measurements, correspond very well to the STMX images.

STXM images show a different magnetization structure during reversal as a function of the electrode thickness and constriction size, which is also confirmed by micromagnetic simulations.

The measured MR values are compared with those obtained from simulations.

References

- [1] G. Sarau, C.M. Schneider, *J. Appl. Phys.* **102** (2007) 083907.
- [2] B. Doudin and M. Viret, *J. Phys.: Condens. Matter* **20** (2008) 083201.
- [3] A. Fernández-Pacheco *et al.*, *Nanotechnology* **23** (2012) 105703.

STUDY OF MAGNETORESISTIVE NANOGRANULAR FILMS WITH X-RAY SPECTROSCOPIES

Cz. Kapusta^{1*}, M. Sikora¹, J. Przewoźnik¹, J. Żukrowski¹, J. Fedotova², and J. Kasiuk²

¹AGH University of Science and Technology, Faculty of Physics and Applied Computer Science, Krakow, Poland

²NC PHEP BSU, 220040 Minsk, Belarus

Keywords: X-ray absorption spectroscopies, nanogranular composite films, tunnel magnetoresistance

*e-mail: kapusta@agh.edu.pl

Granular films composed of nanometer size particles of magnetic metals such as Fe, Co and their alloys in an insulating matrix such as Al₂O₃, ZrO₂ or SiO₂ have recently attracted a great deal of interest. This is due to their magnetoresistive properties and prospective application in magnetic sensors, information storage media and high frequency electronic devices. Relatively easy and flexible synthesis routes using sputtering techniques make possible tailoring of their magnetic and electrical properties in a wide range by varying composition and metal/insulator fraction ratio.

In the lecture the application of the X-ray absorption spectroscopy to the study of the (FeCoZr)-(Al₂O₃) and (FeCoZr)-(CaF₂) sputtered nanogranular composite thin films will be addressed. The spectra in the XANES and EXAFS ranges of the materials with different metal-to-insulator ratios prepared in the inert gas atmosphere and under oxidizing conditions will be presented and discussed. A relation to the results of X-ray diffraction, magnetometry, Mössbauer spectroscopy and electrical transport as well as magnetoresistivity measurements will be given.

In the Fig. 1 an example of the Fe and Co *K*-edge X-ray absorption spectra in the XANES range for fully oxidized (FeCoZr)₆₄(Al₂O₃)₃₆ film, pure FeCoZr film and a partly oxidized film of intermediate composition, are presented. Both, Fe and Co absorption edges of the FeCoZr film are similar to each other and resemble those of elemental Fe and Co. Much different shapes of absorption edges are revealed in the spectra of the nanocomposite films.

Surprisingly, the Fe spectrum for (FeCoZr)_{56.5}(Al₂O₃)_{43.5} indicates a larger oxide contribution, in contrast to that of Co, which is closer to pure alloy spectrum. It shows that oxidation process is not spatially uniform, but favors

oxidation of iron prior to cobalt.

The results of combined studies will be discussed in terms of their relation to the enhancement of the TMR effect in the “core-shell” granular structures through spin accumulation and filtering processes.

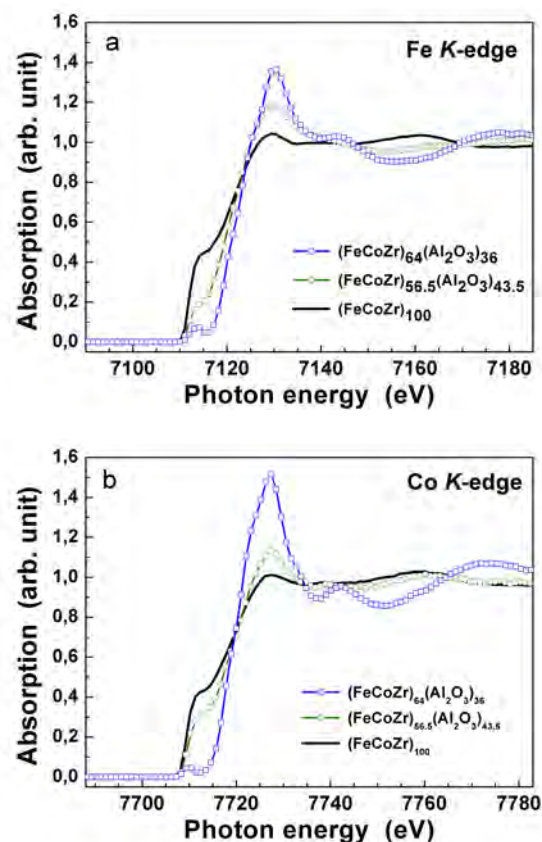


Figure 1: The Fe (a) and Co (b) *K*-edge XANES spectra of (FeCoZr)-(Al₂O₃) thin films.

RESONANT PHOTOEMISSION OF $4f$ ELECTRONS ON CLEAN SEMICONDUCTOR SURFACES

E. Guzewicz^{1*}, B.A. Orlowski¹, A. Reszka¹, L. Wachnicki¹, S. Gieraltowska¹, M. Godlewski¹, I.A. Kowalik¹, B.J. Kowalski^{1,2}, and R.L. Johnson²

¹*Institute of Physics, Polish Academy of Sciences, Al. Lotników 32/46, 02-668 Warsaw, Poland*

²*Institut für Experimentalphysik, Universität Hamburg, Luruper Chausee 149, 22761 Hamburg, Germany*

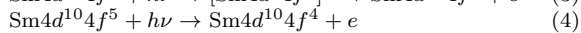
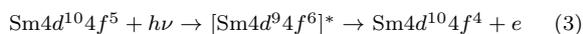
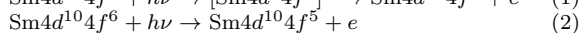
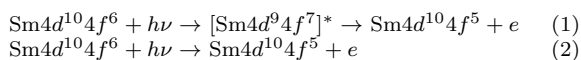
Keywords: synchrotron radiation, samarium, zinc oxide, gallium nitride, cadmium telluride, semimagnetic semiconductors

**e-mail: guzel@ifpan.edu.pl*

Wide band-gap semiconductors doped with rare-earth (RE) elements have experienced attention as materials for optoelectronic devices. The $4f$ electrons of RE ions are usually highly localized and in the electronic structure of the host material and thus the $4f^n$ electrons are only slightly perturbed compared to free ion energy levels. As a consequence, the wavelength of RE-related light emission is atomic like and almost insensitive to temperature, which usually is an attractive attribute for light-emitting devices. Because of that RE doped wide band semiconductors are attractive candidates for optoelectronic and thin film electroluminescent devices [1]-[1].

However, for some RE elements, for which the ionization energy of the $4f$ shell is close to the chemical potential, a mixed-valence state occurs. This regime may arise for samarium compounds, where $4f^6$ (Sm^{2+}) and $4f^5$ (Sm^{3+}) configurations are close to the Fermi level and almost degenerate. Therefore even small changes of the chemical environment cause changes in the samarium $4f$ configuration and thus influences the Sm valence and light emission, because Sm^{2+} and Sm^{3+} ions produce quite different photoluminescence spectra [4, 5].

In the paper we present resonant photoemission results for samarium doped wide band gap semiconductor surfaces like cadmium telluride (CdTe), gallium nitride (GaN) and zinc oxide (ZnO). Samarium is a very rewarding subject for resonant photoemission (RPES) studies because its divalent and trivalent electron configurations can be characterized by distinct and well-resolved photoemission spectral features. In resonant photoemission the emission from the $\text{Sm}4f$ shell is resonantly enhanced when photon energy is tuned to the $\text{Sm}4d \rightarrow \text{Sm}4f$ energy threshold. For the Sm^{2+} ($4f^6$) and Sm^{3+} ($4f^5$) configurations, two RPES processes can be expressed as follows:



where * denotes an excited state. Equations (1) and (2) describe resonant and classical photoemission path for Sm^{2+} , while equations (3) and (4) express these processes for a Sm^{3+} configuration.

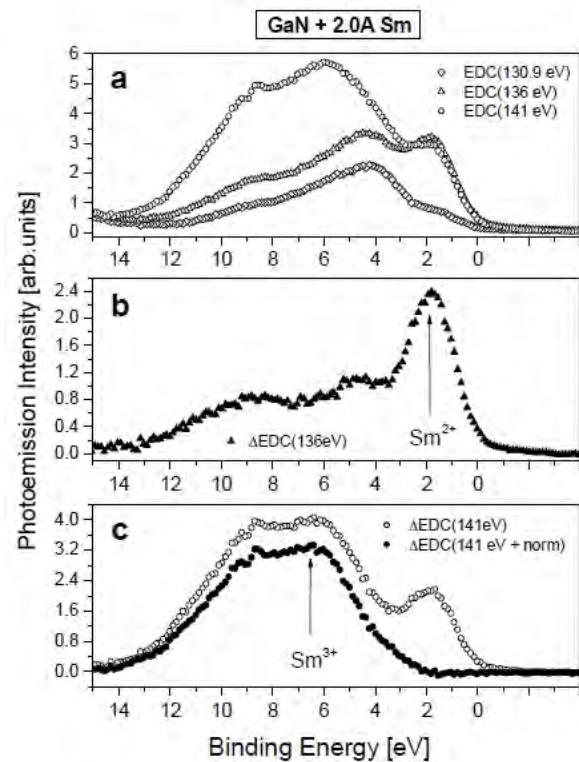


Figure 1: Valence band EDCs of the Sm/GaN system (a) taken for $h\nu = 141$ eV, 136 eV and 130.9 eV and difference spectra ΔEDC showing the $4f$ contributions for Sm^{2+} (b) and Sm^{3+} (c).

In the synchrotron radiation experiments we sequentially deposited small amounts of samarium atoms on clean semiconductor surfaces (CdTe, GaN, ZnO) and via the RPES experiment we observed variations in the electronic band structure of the semiconductor systems. All experiments were performed at the Flipper II beamline in the HASYLAB synchrotron radiation laboratory (Germany). The resonant enhancement in the photoemission intensity was observed at photon energy of 141 eV (for Sm^{3+} valence) and 136 eV (for Sm^{2+} valence), while the anti-resonance was observed at 131 eV. The difference between resonant and antiresonant photoemission spectra provides information about the $\text{Sm}4f$ contribution to the electronic band structure of the investigated system. Valence band EDCs of the Sm/GaN system taken for $h\nu = 141$ eV, 136 eV and 130.9 eV (a) are shown in Fig. 1 together

with the difference spectra, Δ EDCs, showing the $4f$ contributions for Sm^{2+} (b) and Sm^{3+} (c). Analogous results for the Sm/ZnO are presented in Fig. 2.

Resonant photoemission results provide a unique possibility to observe the variation in Sm valence after subsequent steps of samarium deposition onto clean semiconductor surfaces. It will be shown that samarium reacts in different ways with clean ZnO, GaN and CdTe surfaces. For CdTe and GaN the interaction of samarium with semiconductor surface is rather strong. In case of CdTe it leads to creation of Sm-CdTe compound that inhibits further diffusion of samarium atoms into the bulk [6]. In case of the Sm/GaN system [7] some Ga atoms are released

and segregated. When samarium is deposited onto the clean zinc oxide surface a metallic shoulder at the Fermi level is observed even after deposition of the first Sm monolayer, but it disappears after 30 minutes annealing at 300°C and than the Sm^{3+} valence is strongly privileged.

It will be shown that thanks to the Resonant Photoemission experiment we can extract information on subtle changes in chemical environment of the measured semiconducting systems.

Acknowledgments: The research was partially supported by the European Union within the European Regional Development Fund, through grant Innovative Economy (POIG.01.01.02-00-008/08). The authors acknowledge support by MSHE of Poland research Projects DESY/68/2007 and by the European Community via the Research Infrastructure Action under the FP6 “Structuring the European Research Area” Programme (through the Integrated Infrastructure Initiative “Integrating Activity on Synchrotron and Free Electron Laser Science”) at DESY.

References

- [1] S.A.M. Lima, M.R. Davolos, *Appl. Phys. Lett.* **90** (2007) 023503.
- [2] C.C. Yang, S.Y. Cheng, H.Y. Lee, S.Y. Chen, *Ceramics Int.* **32** (2006) 37.
- [3] D. Kouyate, J.-C. Ronsard-Haret, J. Kossanyi, *J. Mater. Chem.* **2** (1992) 727.
- [4] C.T.M. Ribeiro, F. Alvarez, A.R. Zanatta, *Adv. Mat.* **14** (2002) 1154.
- [5] J. Qiu, K. Miura, K. Nouti, *et al.*, *Solid State Commun.* **113** (2000) 341.
- [6] E. Guziewicz, K. Szamota-Sadowska, B.J. Kowalski, B.A. Orlowski, J. Ghijsen, R.L. Johnson, *Appl. Surf. Science* **166** (2000) 231.
- [7] E. Guziewicz, B.J. Kowalski, B.A. Orlowski, *et al.*, *Surf. Science* **551** (2004) 132.

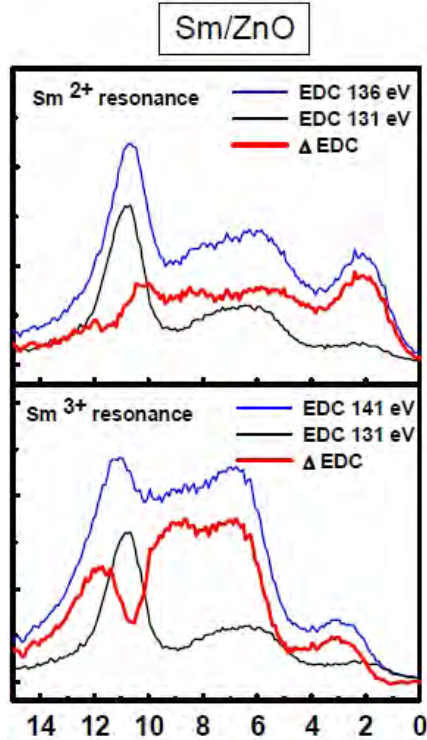


Figure 2: Valence band EDCs of the Sm/ZnO system taken for $h\nu = 141$ eV, 136 eV and 131 eV and difference spectra Δ EDC showing the $4f$ contributions for Sm^{2+} (upper) and Sm^{3+} (lower). EDC spectra at the Sm^{2+} and Sm^{3+} resonance (141 eV and 136 eV, respectively).

RESONANT PHOTOEMISSION STUDIES OF Fe DOPED SrTiO₃ THIN FILMS

J. Kubacki^{1*}, D. Kajewski¹, J. Szade¹, A. Köhl², Ch. Lenser²,
R. Dittmann², K. Szot^{1,2}, and K. Schulte³

¹A. Chelkowski Institute of Physics, University of Silesia, Uniwersytecka 4, 40-007 Katowice, Poland

²Peter Grünberg Institute, Research Centre Jülich, 52428 Jülich, Germany

³Lund University, MAX-lab, Ole Römers väg 1. SE-223 63 Lund, Sweden

Keywords: synchrotron radiation, thin films, X-ray absorption, photoelectron spectroscopy

*e-mail: jerzy.kubacki@us.edu.pl

Doping is one of the methods to control the properties of a model perovskite SrTiO₃ (STO) which is an insulator with the band gap of 3.2 eV. One of the interesting cases is Fe doping. Several exciting effects have been reported for Fe doped crystals, especially electrical degradation connected with electrocoloration. Fe doped STO thin films exhibit promising switching properties with possible application in memristive memories [1]. The main feature determining these properties is modification of the electronic structure where the role of the in-gap states is crucial [2]. To get insight into the contribution of Fe and main components to the electronic structure we have performed X-Ray Absorption Spectroscopy and Resonant Photoemission studies.

The epitaxial Fe doped STO films with thickness of about 20 nm were obtained by PLD (Pulsed Laser Deposition) method on the Nb doped SrTiO₃ single crystal substrate. Three samples were studied — films doped with 2% Fe, 5% Fe and the undoped SrTiO₃ film. The samples were annealed in UHV conditions prior to study at 150°C, 300°C and 630°C.

The XAS spectra on L_{2,3} edge of titanium and iron and K edge of oxygen were obtained with the use of two methods — total electron yield (TEY) measured by the drain current and Auger electron yield (AEY). The methods have different surface sensitivity.

The valence band spectra were obtained for the photon energies corresponding to in- and off-resonance of iron, titanium and oxygen. It enabled to separate the contributions from those elements to valence band and especially to the region of the STO energy gap. It appeared that Fe is present in two oxidation states Fe²⁺ and Fe³⁺ in the films. It turned out from the XAS spectra that the content of Fe ions in two different valence states was the same for both nominal doping levels and it varied with the annealing temperature. The content of 2+ Fe was higher in the surface region what can be related with the concentration of oxygen vacancies.

We were able to distinguish contribution from both Fe oxidation states to the valence band. For Fe³⁺ the electronic states are located mostly above the top of the valence band whereas for Fe²⁺ there are distributed within the gap forming a relatively broad structure.

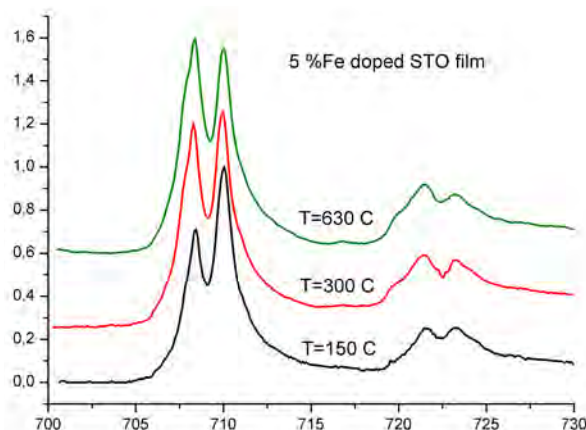


Figure 1: XAS spectra of the 5% Fe doped SrTiO₃ film obtained with the use of TEY mode at various temperatures.

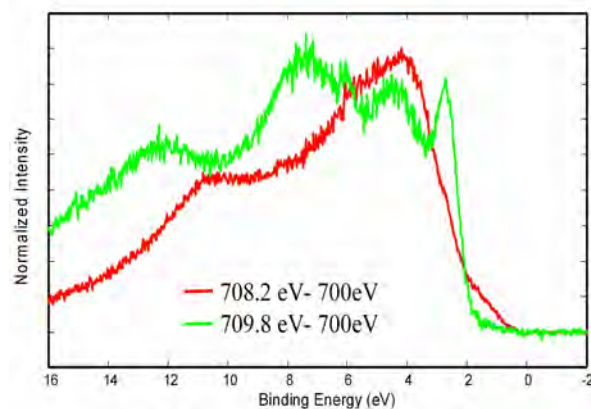


Figure 2: Partial density of Fe 3d states (PDOS) obtained from the on- and off-resonance photoemission spectra for photon energies corresponding to two peaks in the Fe L₃ absorption edge ($h = 708.2$ eV (on-resonance), $h = 709.8$ eV (on-resonance) and $h = 700$ eV (off-resonance)), 2% Fe doped SrTiO₃ film.

References

- [1] K. Szot, R. Dittmann, W. Speier, R. Waser, "Nanoscale resistive switching in SrTiO₃ thin films," *Phys. Status Solidi — Rapid Res. Lett.* **1** (2007) R86.
- [2] J. Szade, K. Szot, M. Kulpa, J. Kubacki, Ch. Lenser, R. Dittmann, R. Waser, "Electronic structure of epitaxial Fe-doped SrTiO₃ thin films," *Phase Transitions* **84** (2011) 489.

THE SOLARIS CONCEPTS FOR THE BEAMLINES CONTROL SYSTEMS

P. Goryl^{1*}, C.J. Bocchetta¹, M.J. Stankiewicz¹, A.I. Wawrzyniak¹, K. Wawrzyniak¹,
M. Zajac¹, Ł. Żytiniak¹, and D. Spruce²

¹National Synchrotron Radiation Centre 'Solaris', Jagiellonian University,
ul. Gronostajowa 7/P.1.6, 30-387 Kraków, Poland

²MAX IV Laboratories, Lund, Sweden

Keywords: synchrotron radiation, control, software, instrumentation, Solaris

*e-mail: piotr.goryl@uj.edu.pl

An overview will be given of activities and decisions taken in relation to the IT and the control infrastructure. This includes current status, software and hardware choices, a computer network design [1] and services provided by the Solaris. A guideline for the beamlines control systems will be presented, too.

A control system and IT infrastructure for the Solaris machine is in design and development. The design will have impact on the beamlines design and operation. The control system for both the machine and beamlines should follow a standard to ensure it is cost effective, manageable and possible to maintain [2].

The TANGO [3] control system and its dedicated tools have been chosen for the integration layer. TANGO has been implemented at several laboratories in Europe and found to be both reliable and mature.

Each beamline should have an autonomous control system that is nonetheless capable to exchange data with the main machine control system and the IT infrastructure to the extent it is necessary for both the beamline and the storage ring being operated. This means that the beamline control system should have as low as possible impact on the other part of the facility and vice-versa.

The control system development will be developed by the control group provided with the necessary resources from the beamline budget. This approach ensures that knowledge used for the control system development will last at the facility and makes later maintenance feasible [2].

A typical beamline contains three major parts: an insertion device, a frontend to exit slit part, an end-station. Each of those requires different level of interaction between the machine control system and the beamline CS (CS = Control System):

- The insertion device is a part of the storage ring and it should be controlled by the machine CS. The Tango Device Server, along with necessary GUI should be provided and should be available in the control room. Beamline should have an access to this as a TANGO client.
- The frontend to exit slit part is more the beamline than the storage ring. However, it is connected to the machine and it should be

possible to access it as a client from the machine CS. Additionally, it shall provide the interlock system integrated with the machine one. This is due to ensure the radiation safety and the vacuum safety.

- The end station is the solely part of the beamline. The only case it is necessary to make it direct communicate with the machine is if it provides any hazard to the ambient.

In addition to the above physical (horizontal) distinction, the control system could be regarded as four layers in a logical (vertical) plane:

- The hardware layer. It includes the physical equipment like mirrors, motors, vacuum valves etc.
- The local layer. It includes: acquisition/actuating electronics, the interlock PLC system and low level control equipment
- The integration layer. It consists of the Tango device servers, the Tango Host and the computer network.
- The Operator/Supervisory layer — GUI applications, the computational software, the archiving. The Tango standard applications and the Taurus [4] library will be used for the GUI applications, wherever possible. The Sardana [5] is a tool to be used for the experiments' sequencing.

Acknowledgments: Work supported by the European Regional Development Fund within the frame of the Innovative Economy Operational Program: POIG.02.01.00-12-213/09.

References

- [1] P. Goryl *et al.*, *Solaris project status and challenges* (ICALEPCS'13, MOPMU008 2011).
- [2] P. Goryl, *The guideline for the Solaris beamlines' control systems* (Solaris, CS-BL-001 2012).
- [3] Tango Community., Tango website, <http://www.tango-controls.org>.
- [4] ALBA., *Taurus's documentation*, <http://www.tangocontrols.org/static/taurus/latest/doc/html/index.h>
- [5] ALBA., *SARDANA — Instrumentation and Data Acquisition Control System*, <http://computing.cells.es/services/collaborations/sardana>.

STRUCTURAL STUDIES OF COVALENTLY STABILISED OLIGOMERS OF HUMAN CYSTATIN C

M. Kozak^{1*}, M. Taube¹, M. Murawska¹, V. Lindström², and A. Grubb²

¹Department of Macromolecular Physics, A. Mickiewicz University, Poznan, Poland

²Department of Clinical Chemistry and Pharmacology, Lund University Hospital Lund, Sweden

Keywords: synchrotron radiation, cystatin, amyloid

*e-mail: mkozak@amu.edu.pl

Human cystatin C (HCC) is a small protein (MW 13.4 kDa), acting as an inhibitor of cysteine proteases. In pathological conditions HCC undergoes oligomerisation via the domain swapping mechanism. Oligomerization of HCC leads to formation of amyloid deposits in brain arteries [1]. This protein was also found as codeposits in the amyloid plaques of Alzheimer's disease or Down's syndrome. So far two crystal structures of full length (native) dimeric forms of HCC and monomer-stabilized with an engineered disulfide bond (Leu47Cys)-(Gly69Cys) have been solved by X-ray crystallography [2]-[4].

The aim of this study was the characterization of native protein and covalently stabilized monomers and oligomers (dimers, trimers, dodecamers and icosatetramers) of human cystatin C in solution using small angle X-ray scattering (SAXS).

Combination of synchrotron radiation and SAXS method in structural analysis of macromolecules in solution enables not only determination of the basic structural parameters (the radius of gyration, the maximum size of particle or molecular weight) but also permits a verification of the crystal structure of biomacromolecules with the scattering data collected in solution and provides information on the possible conformational changes taking place in solution. Detailed analysis of SAXS data including the *ab initio* shape-determination algorithms provides also the information on the envelope (the shape) of the protein molecules in solution.

The SAXS data were obtained using synchrotron radiation in MAXLab (beam line 9-11-4, MAXII storage ring) and DESY (beam line X33). Using shape determination program DAMMIN [5] the low resolution models in solution of native HCC and covalently stabilized HCC oligomers (monomer, dimer and trimer). Native monomeric HCC irradiated by synchrotron radiation undergoes dimerisation in solution. Dimeric native HCC form in solution a dimer with elongated shape. The conformations of HCC molecules (monomeric and dimeric forms) in solution were evaluated by the use of CRY SOL [6]. Monomeric HCC and both dimeric crystal struc-

tures (cubic and tetragonal) were compared with SAXS data. This comparison clearly indicated that the preferred conformation of native dimeric HCC occurring in solution is the conformation of extended dimer observed in the tetragonal form.

Also the processes of formation of oligomers of native HCC in different pH and temperature conditions were monitored using SAXS in 1h time steps. The structures of HCC oligomers were also characterized by microscopic methods.

Acknowledgments: This research was supported in part by research grant (No N N202 127237) from the Ministry of Science and Higher Education (Poland). The data collection was supported by European Community — EMBL Hamburg Outstation, contract number: RII3-CT-2004-506008.

References

- [1] A.O. Grubb, "Cystatin C — properties and use as diagnostic marker," *Adv. Clin. Chem.* **35** (2000) 63 - 99.
- [2] R. Janowski, M. Kozak, E. Jankowska, Z. Grzonka, A. Grubb, M. Abrahamson, M. Jaskolski, "Human cystatin C, an amyloidogenic protein, dimerizes through three-dimensional domain swapping," *Nature Struct. Biol.* **8** (2001) 316 - 320.
- [3] R. Janowski, M. Kozak, A. Grubb, M. Abrahamson, M. Jaskolski, "3D domain-swapped human cystatin C with amyloidlike intermolecular beta-sheets," *Proteins: Struct. Funct. Bioinf.* **61** (2005) 570 - 578.
- [4] R. Kolodziejczyk, K. Michalska, A. Hernandez-Santoyo, M. Wahlbom, A. Grubb, M. Jaskolski, "Crystal structure of human cystatin C stabilized against amyloid formation," *FEBS J.* **277** (2010) 1726 - 1737.
- [5] D.I. Svergun, "Restoring low resolution structure of biological macromolecules from solution scattering using simulated annealing," *Biophys. J.* **76** (1999) 2879 - 2886.
- [6] D. Svergun, C. Barberato, M.H.J. Koch, "CRY SOL — a program to evaluate x-ray solution scattering of biological macromolecules from atomic coordinates," *J. Appl. Cryst.* **28** (1995) 768 - 773.

STRUCTURE AND INTERMOLECULAR INTERACTIONS IN SELECTED BINARY SOLUTIONS STUDIED BY X-RAY METHODS

H. Drozdowski, A. Romaniuk, and Z. Błaszczak

Department of Optics, Faculty of Physics A. Mickiewicz University,
ul. Umultowska 85, 61-614 Poznań, Poland

Keywords: binary solution, intermolecular interactions, X-ray diffraction in liquid solutions

* e-mail: riemann@amu.edu.pl

X-ray structural results for liquid *ortho*-nitrotoluene and *ortho*-nitrotoluene C₇H₇NO₂ in 1,4-dimethylbenzene are reported. The measurements were performed using the transmission technique (Figure 1).

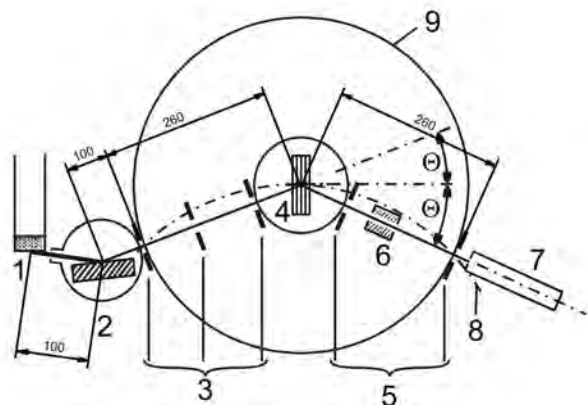


Figure 1: The focusing of the beam passing through the monochromator and goniometer with the preparation studied: 1 – X-ray lamp anode, 2 – monochromator, 3 – a system of input slits of the goniometer, 4 – cuvette with the liquid solution studied, 5 – a system of output slits, 6 – Soller slits, 7 – radiation counter, 8 – Rowland circle, 9 – goniometer circle; distances expressed in mm [1].

Averaged scattered X-ray angular distribution for 10% solution of *ortho*-nitrotoluene in 1,4-dimethylbenzene was determined (Figure 2).

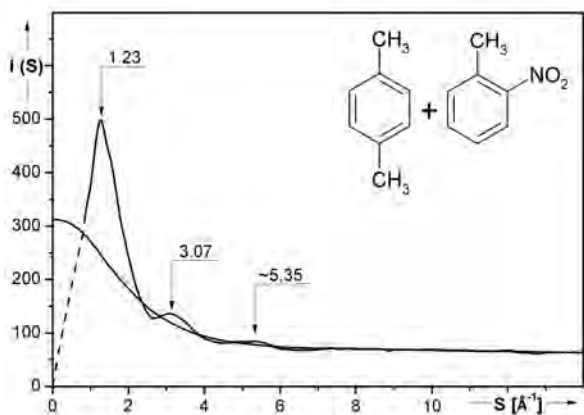


Figure 2: The mean angular distribution of the scattered radiation intensity for binary solution studied.

Radial electron density distribution function was obtained from a modified Warren, Krutter and Morningsstar equation [2] (Figure 3).

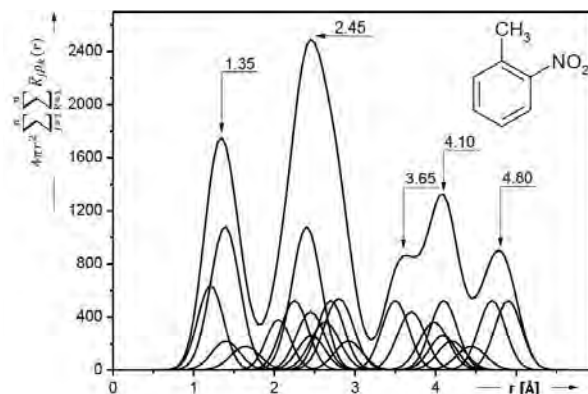


Figure 3: The electron-density radial-distribution function (EDRDF) of the *ortho*-nitrotoluene is a sum of the curves of the Gauss normal distribution.

To the maxima of $I(S)$, EDRDF, interatomic and intermolecular distances are assigned [3]. The experimental results were used to plot models of the most highly probable mutual disposition of the molecules in liquid *ortho*-nitrotoluene and its solution (Figure 4).

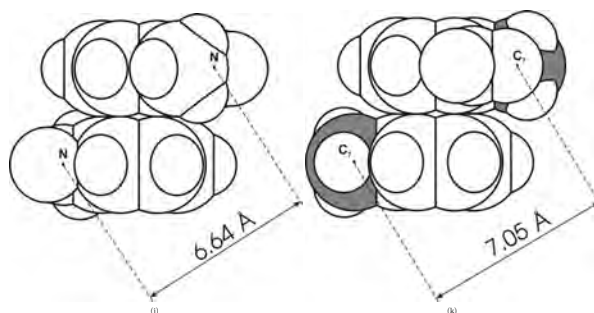


Figure 4: Model of the most highly probable mutual disposition of molecules in 10% solution of *ortho*-nitrotoluene in 1,4-dimethylbenzene.

References

- [1] K. Nowakowski, H. Drozdowski, "X-ray method structural study of liquid cyclohexanol," *Copern. Lett.* **1** (2010) 100 – 105.
- [2] H. Drozdowski, K. Nowakowski, Z. Błaszczak, "X-ray diffraction investigation of cyclohexane derivatives at 293 K," *Rad. Phys. Chem.* **80** (2011) 1058 – 1063.
- [3] H. Drozdowski, A. Mansfeld, "X-ray analysis of intermolecular interactions in solution of *ortho*-nitroanisole C₇H₇NO₃ in 1,4-dimethylbenzene," *Phys. Chem. Liq.* **46** (2008) 255 – 262.

CHARACTERIZATION OF ANCIENT BURNT RICE EXCAVATED IN THAILAND ARCHAEOLOGICAL SITES

K. Won-in¹, T. Sako², W. Pattanasiriwisana³, S. Tancharakorn³, and P. Dararutana^{4*}

¹Department of Earth Sciences, Faculty Science, Kasetsart University, Bangkok 10900 Thailand

²The 3rd Regional Office of Fine Arts, Phra Nakhon Sri Ayuttaya 10300 Thailand

³Synchrotron Light Research Institute, Nakhon Ratchasima 30000 Thailand

⁴The Royal Thai Army Chemical Department, Bangkok 10900 Thailand

Keywords: ancient Thai burnt rice, SRXRF, SEM-EDS

*e-mail: pisutti@hotmail.com

Rice is the main foodstuff for about half of the world's population, especially in Asia [1]. In Thailand, it is the essence of life. Archaeological evidence which based on the paddy rice revealed that rice has been planted in northeastern area of Thailand more than 5,500 years ago. The burnt rice grains were found in various archaeological sites in Thailand which related with the religious ceremony and the home prosperity [2]. In this work, the ancient burnt rice from Nakorn Nayok, Suphan Buri and Prachin Buri Provinces was elementally analyzed using micro-beam XRF based on synchrotron radiation. SEM-EDS was carried out to characterize the structure and composition. IR spectroscopy was also used to study the chemical composition and bio-molecular structure. The grains were oblique in shape with a rough surface. It was found that major elements contained C, Si, Ca and Al. Other trace elements such as Ti, Mn, Fe, Cu and Zn were also

detected. The IR spectra gave some information about the presence of molecular bonds.

Acknowledgments: This work was supported by the Faculty of Science at Kasetsart University (Bangkok). The Thailand Regional Office of Fine Arts (the 2nd at Suphun Buri, the 3rd at Phra Nakhon Sri Ayuttaya and the 5th at Prachin Buri) were thanked for samples. The Thailand Synchrotron Light Research Institute at Nakhon Ratchasima and Maejo University at Chiang Mai were also thanked for providing microbeam-XRF and SEM-EDS, respectively.

References

- [1] K.A. Gomez, *Rice, the grain of culture* (Lecture of the Thai Rice Foundation at the Siam Society, Bangkok, Thailand 2001).
- [2] T. Sako, *Archaeological excavation: Dong Lakon* (The Fine Arts Department, Bangkok, Thailand 2008).

EFFECT OF AVE 0991 – ANGIOTENSIN-(1-7) RECEPTOR AGONIST TREATMENT ON ELEMENTAL AND BIOMOLECULES DISTRIBUTION IN ATHEROSCLEROTIC PLAQUES OF APOE-KNOCKOUT MICE

J. Kowalska^{1*}, M. Gajda², W.M. Kwiatek¹, K. Appel³, and P. Dumas⁴

¹*Institute of Nuclear Physics, Polish Academy of Sciences, Radzikowskiego 152, 31-342 Kraków, Poland*

²*Department of Histology, Jagiellonian University Medical College, Kopernika 7, 31-034 Kraków, Poland*

³*HASYLAB, Deutsches Elektronen Synchrotron, Notkestraße 85, D-22607 Hamburg, Switzerland*

⁴*SOLEIL, L'Orme des Merisiers, Saint Aubin – BP 4, 91-192 Gif-sur-Yvette CEDEX, France*

Keywords: atherosclerosis, iron, zinc, copper, phosphorus, calcium, protein secondary structure, phospholipids saturation level, micro SRFTIR, micro-XRF

*e-mail: joanna.kowalska@ifj.edu.pl

Atherosclerosis is a multietiological inflammatory disease involving large and medium-sized arteries with growing incidence in westernized populations. Despite of many intense studies the pathomechanism of this disease is still not fully understood. Gene-targeted, apolipoprotein E – knockout (apoE-KO) mice display early and advanced vascular lesions (including lipid deposits and inflammatory cell infiltration as well as valvular calcifications), therefore became a reliable model to investigate the pathomechanism and treatment of this disease.

The aim of the present study was to investigate the changes in the distribution of selected pro- and anti-inflammatory trace elements as well as biomolecules in atherosclerotic plaques of apoE-KO mice fed chow diet supplemented or not with AVE 0991 — angiotensin-(1-7) receptor agonist (a potential candidate for atherosclerosis treatment). In this study both synchrotron radiation based micro XRF (X-ray Fluorescence) and micro FTIR (Fourier Transform InfraRed) spectroscopy were applied and combined with histological stainings.

Based on histological staining more advanced atherosclerosis expressed by total area occupied by lipids was observed (oil-red-O staining). Moreover higher enzymatic activity and larger area by metalloproteinases was observed in the control group of animals as compared to the AVE 0991 treated ones (zymographically with fluorescein-gelatin) [1].

All micro-XRF measurements were carried out at beamline *L* of the storage ring DORIS III (HASYLAB, Hamburg). The primary photon energy was set to 17.5 keV and the beam was focused to the final size of 15 μm in diameter using a polycapillary half-lens. All emitted spectra were recorded with a Vortex SDD detector. Two types of measurements were performed:

- a) 2D maps acquired from lesional areas of aortic root with surrounding cardiac muscle (15 μm step, 5 s/point),
- b) precise point spectra from morphologically defined areas (15 μm resolution, 300 s/point) [2].

The distribution of P, Cl, Ca, Fe, Cu and Zn corresponded well with histological structures of the atherosclerotic lesions. Iron as a proatherogenic element appeared mostly in the region of atheroma as compared to other tissue structures and there was no significant difference in the concentration of this element in both studied groups. On the other hand Zn a hypothetically antiatherogenic element occurred mainly in peripheral regions of the aortic cross section and its concentration was higher in the control group as compared to the AVE 0991 treated one. Similar observation were seen in case of Cu distribution and concentration. Some spots of high Ca and P concentration (both considered as a relatively late event in the progression of atherosclerosis) were visible in the area of high lipids deposition.

Micro-FTIR measurements were performed at SMIS beamline at synchrotron SOLEIL facility equipped with a Nicolet Nexus 5700 spectrometer coupled with a Continuum XL IR microscope and a 50 μm MCT/A detector. All spectra were taken in transmission mode using a 12 μm FWHM beam size, with a 4 cm^{-1} spectral resolution and repetition of 128 scans in order to get a good statistics. Two types of measurements were performed like in case of XRF analysis.

The biomolecular analysis was mostly focused on the phospholipids saturation level (2930 cm^{-1} / 2960 cm^{-1}) and lipid to protein ratio (1730 cm^{-1} / 1660 cm^{-1}). Both of this parameters were lower in case of AVE 0991 group as compared to the control one, which may imply the influence of the applied pharmaceutical on the lipid oxidation process in atherosclerosis. Moreover, the protein secondary structure was studied based on the composition on the amide I band (1660 cm^{-1}) demonstrating the higher percentage content of β -sheet structure as compared to the α -helix one in both groups and also some switches in the bands positions, which may indicate the changes in protein structure.

Acknowledgments: The research leading to these results has received funding from the European Community's Seventh Framework Programme (FP7/2007 – 2013) under grant agreement n° 226716. The data were ob-

tained during the realization of DESY D-II-20100089 and SOLEIL 20100901 projects.

References

- [1] J. Toton-Zuranska, M. Gajda, G. Pyka-Fosciak, K. Kus, M. Pawlowska, A. Niepsuj, P. Wolkow, R. Olszaniecki, J. Jawien, R. Korbut, "AVE 0991 – angiotensin-(1-7) receptor agonist, inhibits atherogenesis in apoE-knockout mice," *J. Physiol. Pharmacol.* **61** (2010) 181.
- [2] M. Gajda, J. Kowalska, A. Banas, K. Banas, W.M. Kwiatek, J. Jawien, R. Olszaniecki, K. Appel, *Effect of AVE 0991 – angiotensin-(1-7) receptor agonist on element al distribution in atherosclerotic plaques of apoE-knockout mice* (HasyLab Users Report 2010).

SYNCHROTRON RADIATION BASED MICRO X-RAY FLUORESCENCE ANALYSIS OF THE CALIBRATION SAMPLES USED IN SURFACE SENSITIVE TXRF AND GEXRF TECHNIQUES

A. Kubala-Kukus^{1,2*}, D. Banaś^{1,2}, M. Pajek¹, J. Szlachetko^{1,3}, J.-Cl. Dousse⁴, J. Hoszowska⁴, Y. Kayser⁴, S. Nowak⁴, P. Jagodziński⁵, J. Susini⁶, and M. Salomé⁶

¹*Institute of Physics, Jan Kochanowski University, Świętokrzyska 15, 25-406 Kielce, Poland*

²*Department of Physical Methods, Holycross Cancer Center, Artwińskiego 3, 25-734 Kielce, Poland*

³*Paul Scherrer Institute, Swiss Light Source, CH-5232 Villigen, Switzerland*

⁴*Department of Physics, University of Fribourg, Chemin du Musée 3, CH-1700 Fribourg, Switzerland*

⁵*Department of Physics, Kielce University of Technology, Al. Tysiaclecia PP 7, 25-314 Kielce, Poland*

⁶*European Synchrotron Radiation Facility (ESRF), Jules Horowitz 6, 38000 Grenoble, France*

Keywords: micro x-ray fluorescence analysis, calibration standards, TXRF, GEXRF, censoring

** e-mail: aldona.kubala-kukus@ujk.edu.pl*

The x-ray fluorescence techniques, with widely used the total-reflection x-ray fluorescence (TXRF) method [1], offer unique possibilities to study the concentrations of a wide range of trace elements in various types of samples. These techniques can be used for detailed surface studies of different materials, including ultra-low concentration contamination, the lateral and depth distributions of elements in the micrometer and nanometer scales. TXRF method is commonly employed in the semiconductor industry for determination of contaminants on silicon wafer surfaces [1]. An alternative method to TXRF is the grazing emission x-ray fluorescence (GEXRF) technique [3]. In the GEXRF method the x-ray fluorescence is observed at a small, grazing emission angle below a critical angle, being usually lower than 1° , depending on the energy of the emitted characteristic x-ray. The grazing emission geometry results in suppression of x-ray fluorescence from the bulk material, which for grazing emission angles is limited to the evanescent x-ray waves propagating along the surface. In this way the x-ray fluorescence from the substrate is limited to the very shallow surface layer of about few nm, which results in a relative enhancement of the characteristic fluorescence emission from surface impurities with respect to emission from the bulk. The GEXRF is an “inverse” of the total reflection x-ray fluorescence (TXRF) method and both techniques have similar detection limits.

In a series of experiments performed at the ESRF beamline ID21 we have demonstrated that the grazing emission x-ray fluorescence (GEXRF) technique combined with synchrotron radiation excitation and high-resolution x-ray detection offers attractive possibilities for application of synchrotron radiation to study the distribution elements on the surface of materials in nanoscale [4]-[7]. One of possible application is determination of the low-level impurities concentration on silicon [4, 5].

Both TXRF and GEXRF techniques provide qualitative and quantitative results. Calibration procedure normally used involves placing a microdroplet ($\sim \mu\text{l}$) of the standard solution onto a silicon

wafer. After evaporation of the solvent, the residual amount of elements on the wafer is used as a reference standard [4, 5, 8]. However, usually a distribution of residue material on the substrate surface is not known accurately and consequently, such calibration method is burdened with uncertainty whether the calibration sample is of the pure particle type, which is usually assumed for evaluation purposes, or whether forms a film type layer. In the latter case, the relationship between the elements concentration on the wafer surface and the resulting fluorescence intensity deviates from that of the particle case, and thus leads to invalid calibration factors.

In the present work the investigation of the lateral distribution of elements in the multielemental calibrating samples by using the synchrotron radiation based micro X-ray fluorescence is presented. The studies have been performed at the European Synchrotron Radiation Facility (ESRF) at the ID21 X-ray microscopy beamline. The goal of this project was the investigation of a uniformity of the elemental distributions and determination of the residuum morphology, especially in the context of application different temperatures in drying process. In data analysis the censoring approach [9] will be also applied. This statistical approach allows on the data corrections in case of the presence of “nondetects”. i.e. the measurements in which the concentration is not measured directly due to the actual value of detection limit.

The performed investigation of the lateral distribution of elements in the multielemental calibrating samples combined with the application of the censoring approach to “nondetects” can results in substantial improvement of calibration procedures for surface sensitive TXRF and GEXRF techniques, used for determination of contaminants on semiconductor surfaces.

References

- [1] R. Klockenkämper, *Total Reflection X-ray Fluorescence Analysis* (Wiley, New York 1997).

- [2] D. Hellin, S. De Gendt, N. Valckx, P.W. Mertens, Ch. Vinckier, "Trends in total reflection X-ray fluorescence spectrometry for metallic contamination control in semiconductor nanotechnology," *Spectrochim. Acta B* **61** (2006) 496 – 514.
- [3] H.P. Urbach, P.K. de Bokx, "Calculations of intensities in grazing-emission x-ray fluorescence," *Phys. Rev. B* **53** (1996) 752.
- [4] J. Szlachetko *et al.*, "Application of the high-resolution grazing emission x-ray fluorescence method for impurities control in semiconductor nanotechnology," *J. Appl. Phys.* **105** (2009) 086101.
- [5] A. Kubala-Kukuś *et al.*, "Observation of ultralow-level Al impurities on a silicon surface by high-resolution grazing emission x-ray fluorescence excited by synchrotron radiation," *Phys. Rev. B* **80** (2009) 113305.
- [6] Y. Kayser *et al.*, "Depth profiles of Al impurities implanted in Si wafers determined by means of the high resolution grazing emission x-ray fluorescence technique," *Spectrochim. Acta B* **65** (2010) 445 – 449.
- [7] Y. Kayser *et al.*, "Depth profiling of dopants implanted in Si using the synchrotron radiation based high-resolution grazing emission technique," *X-Ray Spectrom.* **41** (2012) 98 – 104.
- [8] A. Kubala-Kukuś, J. Braziewicz, M. Pajek, "Total-reflection X-ray fluorescence studies of trace elements in biomedical samples," *Spectrochim. Acta B* **59** (2004) 1283 – 1289.
- [9] M. Pajek, A. Kubala-Kukuś, J. Braziewicz, "Censoring: A new approach for detection limits in TXRF," *Spectrochim. Acta B* **59** (2004) 1091 – 1099.

REVERSIBLE VALENCY TRANSITIONS OF EUROPIUM IN MBE GROWN Eu-Mn THIN FILMS

K. Balin^{1,2*}, **J. Szade**¹, and **Z. Celinski**²

¹*A. Chelkowski Institute of Physics, University of Silesia, Katowice, 40-007, Poland*

²*Center for Magnetism and Magnetic Nanostructures, University of Colorado at Colorado Springs, Colorado Springs, CO 80918, USA*

Keywords: europium valency, reversible valency transitions, intermetallic alloys, thin films

**e-mail: katarzyna.balin@us.edu.pl*

The examination of formation of unknown ordered Eu-Mn compounds and the valency of europium in MBE grown thin films were the main point of our interest. We considered that such Eu-based materials, in which the control of the valency of Eu would be possible, may be applied into new classes of spin-based sensor, memory or logic devices.

Europium may exist in two valency states; metallic europium is divalent, in alloys or intermetallic compounds it may be in a divalent, trivalent or intermediate-valency state. Magnetic properties of europium are directly connected to its valency state; Eu^{3+} is non-magnetic ($J = 0$) while the Eu^{2+} has a large pure spin moment ($J = 7/2$). The ability of controlling of the Eu valency and consequently switching between the non-magnetic and the magnetic states of europium led us for study the Eu-Mn system. Such ability would be highly useful nowadays when microelectronic devices are being substituted by devices which using spin properties instead of charge degrees of freedom.

We used a MBE system to grow $\sim 10 - 40$ nm thick Eu-Mn films assuming that structural effects at interfaces in a multilayer system may be helpful in formation of new phases. The films were deposited on polycrystalline Mo buffer layer grown on Si or GaAs substrates. The *in situ* XPS measurements were performed during the controlled alloying between neighboring layers and after that process. This allowed carrying out studies in several different directions. The first one was aimed at monitoring the reaction of the film constituent elements.

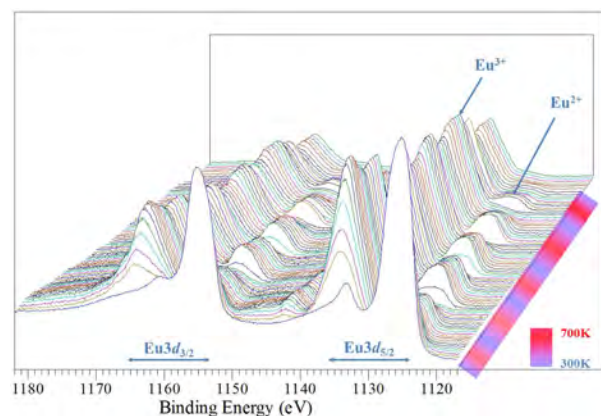


Figure 1: Valency transitions of europium.

It turned out (chemical shifts and relative changes in the intensity ratio) that within the examined system the elements are inter-mixing at elevated temperatures. The second one was directed to changes in the valency of europium. The changes associated to the reaction with surrounding transition metal lead to valency transition of europium $\text{Eu}^{2+} \leftrightarrow \text{Eu}^{3+}$. Europium may remain in a divalent state (EuMn_2) [1], may change the valency to trivalent or show intermediate valence state ($\text{Eu}_2\text{Mn}_{17}$). The third one was the observation of reversible valence transitions of europium which was found to be forced by heat treatment or change of the interface resulting from covering the surface of the film.

Annealing at elevated temperatures leads to increase of the intensity of the Eu^{2+} states while the reverse “cooling down” process causes opposite $\text{Eu}^{2+} \leftrightarrow \text{Eu}^{3+}$ transition. The excitation of the Eu^{2+} states tends to decrease with the temperature increase but the reversible changes even after annealing at high temperatures do not disappear.

Such behavior, taking into account published report [2], is probably an individual property of the thin layer of Eu or its oxide in some unique environment.

Due to results obtained for MBE grown EuF_3 thin films presented in ref. 3, where X-ray absorption (XAS) and resonant photoemission (RESPE) have been used for the investigations of europium valency, we attempt to solve the issue of europium valency in Eu-Mn with the use of those techniques.

Acknowledgments: This work was supported by NSF DMR 0907053.

References

- [1] K. Balin *et al.*, “Electronic structure, crystallographic, magnetic, and transport characterization of EuMn_2 films,” *Appl. Phys.* **107** (2010) 09E154.
- [2] J.A.D. Matthew *et al.*, “Silicide formation and valence switching at the Eu-Si interface monitored by electron energy loss spectroscopy in the reflection mode,” *J. Phys.: Condens. Matter* **4** (1992) 8489.
- [3] J. Szade, W. Burian, Z. Celiski, T. O’Keevan, M. Zangrando, F. Bondino, E. Magnano, “Resonance induced divalent Eu states in EuF_3 ultrathin layer,” *Surf. Sci.* **580** (2005) 163.

STUDY OF ABSORPTION PROPERTIES OF CHEMICALLY MODIFIED HALLOYSITE SAMPLES WITH X-RAY FLUORESCENCE AND X-RAY POWDER DIFFRACTION METHODS

D. Banaś^{1,2}, J. Braziewicz^{1,2}, A. Kubala-Kukus^{1,2*}, U. Majewska^{1,2}, M. Pajek¹, J. Wudarczyk-Moćko², K. Czech³, M. Garnuszek³, P. Słomkiewicz³, and B. Szczepanik³

¹*Institute of Physics, Jan Kochanowski University, Świętokrzyska 15, 25-406 Kielce, Poland*

²*Department of Physical Methods, Holycross Cancer Center, Artwińskiego 3, 25-734 Kielce, Poland*

³*Institute of Chemistry, Jan Kochanowski University, Świętokrzyska 15, 25-406 Kielce, Poland*

Keywords: X-ray fluorescence, X-ray powder diffraction, halloysite samples

**e-mail: aldona.kubala-kukus@ujk.edu.pl*

Halloysite is a clay mineral, chemically similar to kaolin, typically formed by hydrothermal alteration of aluminosilicate minerals [1]. On the microscopic scale halloysite usually occurs as nanotubes, which average diameter is a few dozen of nanometers and lengths is in the range of few micrometers. Sometimes, depending on deposit, these nanotubes split open and unroll to form laths or spatula shapes [2]. Halloysite nanotubes are much cheaper and easier available than carbon nanotubes, have high mechanical and chemical strength and as a result they are very well suited for nanotechnology. Additionally, because of biocompatibility of the halloysite they are frequently used in environmental protection and industry for example as sorptive material in biofilters or coagulant for water and sewage treatment plants. Surprisingly, despite of common exploiting, the chemistry of the halloysite nanotubes, inner and outer surfaces of their nanoscale volumes are not yet well studied [2]. Recently growing applications of the halloysite stimulate many research studies on properties, possible chemical modifications of their structure [3, 4] and technological applications [5, 6].

The aim of the measurements presented here was study of the absorption properties in the halloysite nanotubes. The analysed halloysite samples come from strip mine “Dunino” in the vicinity of Legnica (Poland). The measurements were performed in the Institute of Physics of Jan Kochanowski University (UJK) in Kielce (Poland) in collaboration with Institute of Chemistry UJK.

The samples were analysed with three different complementary X-ray spectrometry techniques: X-ray powder diffraction (XRPD) [7], classical X-ray fluorescence (XRF) [8] and its modification total reflection X-ray fluorescence (TXRF) [9]. The XRPD technique was used for determination of concentration of halloysite mineral and chemical composition of the raw and chemically modified samples. With classical, wavelength dispersive x-ray fluorescence (WDXRF) method, changes of the elemental composition in the sample as a results of treatment with different concentration of sulphuric acid were measured. With total reflection X-ray flu-

orescence technique (TXRF) concentrations of the trace elements absorbed by halloysite nanotubes in filtration process were determined. As a result it has been shown that application of the complementary X-ray spectrometry techniques allows on observation of changes of the sample composition caused by chemical modifications of the halloysite samples and studies of their absorption properties.

In this work the experimental setups, sample preparation procedures and obtained results will be presented and discussed in details.

Acknowledgments: This work was supported by ESF Human Capital Operational Programme under Grants No. 6/1/8.2.1./POKL/2009 (K.Cz.) and WND-POKL.08.02.01-26-007/11 (M.G.).

References

- [1] E. Hope, J. Kittrick, “Surface tension and the morphology of halloysite,” *Am. Mineral.* **49** (1964) 859 – 863.
- [2] E. Joussein, S. Petit, J. Churchman, “Halloysite clay minerals — a review,” *Clay Miner.* **40(4)** (2005) 383 – 426.
- [3] C.T. Johnston, “Probing the nanoscale architecture of clay mineral,” *Clay Miner.* **45(3)** (2010) 245 – 279.
- [4] J. Matusik, A. Gawel, E. Bielanska, W. Osuch, and K. Bahranowski, “The effect of structural order on nanotubes derived from kaolin-group minerals,” *Clays Clay Miner.* **57(4)** (2009) 452 – 464.
- [5] M.L. Lipowski, P.M. Słomkiewicz, J.A. Zdenkowski, patent PL – 178092.
- [6] M.L. Lipowski, P.M. Słomkiewicz, J.A. Zdenkowski, patent PL – 197737.
- [7] V.K. Pecharsky, P.Y. Zavalij, *Fundamentals of Powder Diffraction and Structural Characterization of Materials* (Springer, New York 2009).
- [8] J.P. Willis, A.R. Duncan, *Understanding XRF Spectrometry* (PANalytical B.V., Almelo 2008).
- [9] R. Klockenkämper, *Total-Reflection X-Ray Fluorescence Analysis* (Wiley Interscience, John Wiley & Sons, New York 1997).

ANALYSIS OF SYNCHROTRON RADIATION INDUCED X-RAY EMISSION SPECTRA WITH R ENVIRONMENT

K. Banas^{1*}, A.M. Banas¹, M. Gajda², W.M. Kwiatek³, B. Pawlicki⁴, and M.B.H. Breese^{1,5}

¹*Singapore Synchrotron Light Source, National University of Singapore, 5 Research Link, 117603 Singapore*

²*Department of Histology, Jagiellonian University Medical College, Kopernika 7, 31-034 Kraków, Poland*

³*Institute of Nuclear Physics PAN, Radzikowskiego 152, 31-342 Kraków, Poland*

⁴*Gabriel Narutowicz Hospital, Prądnicka 37, 31-202 Kraków, Poland*

⁵*Physics Department, National University of Singapore, 2 Science Drive 3, 117542 Singapore*

Keywords: synchrotron radiation, XRF, fluorescence spectroscopy, R platform, multivariate analysis

**e-mail: slskb@nus.edu.sg*

Life sciences have seen a huge increase in the amount and complexity of data being collected with every experiment. Scientists today are faced with increasingly difficult task to extract vital information from the vast amount of numbers. Software used for this purpose should be sufficiently powerful and flexible to handle large and complex data sets. On the other hand it should allow the user to exactly follow what is being calculated – black-box type of software should be avoided.

R Platform [1] for statistical analysis nicely fits these requirements. With its rapidly expanding user community is quickly becoming the most important tool in statistical analysis of data in biology, geology, genetics, physics and chemistry to name just few of them. The most important feature of R is the package system, allowing users to address specific problems with dedicated package and even for more advanced users to contribute software for their own fields. At this moment there are 3705 packages at CRAN — The Comprehensive R Archive Network [2] (state for 15.03.2012). R is available free of charge for most of contemporary operating systems including Windows, MacOS and wide variety of UNIX based platforms.

In this presentation application of the R platform for the spectral preprocessing as well as univariate and multivariate statistical analysis is shown. One of the advantages of using R is high

quality graphics that could be produced in various formats: bitmap files (jpg and png) and vector graphics (postscript and pdf).

Analysis of the spectral data obtained from the experiment usually includes: baseline correction, normalization, sometimes subtracting common for every spectrum component, removing artifacts like spikes or glitches, offset correction etc. All these procedures could be implemented in R. One of the packages for this kind of analysis is hyperSpec [3].

In order to reduce the amount of variables in the spectral datasets multivariate approach like cluster analysis and principal component analysis [4] is extremely useful. In this poster results of univariate analysis (concentration distribution maps for selected elements) are compared with multivariate way of spectral data treatment.

Acknowledgments: This work was partially performed under NUS Core Support C-380-003-003-001.

References

- [1] R platform <http://www.r-project.org/>.
- [2] CRAN <http://cran.r-project.org/>.
- [3] hyperSpec package <http://hyperspec.r-forge.r-project.org/>.
- [4] W. Hardle and L. Simar, *Applied Multivariate Statistical Analysis* (Springer, 2007).

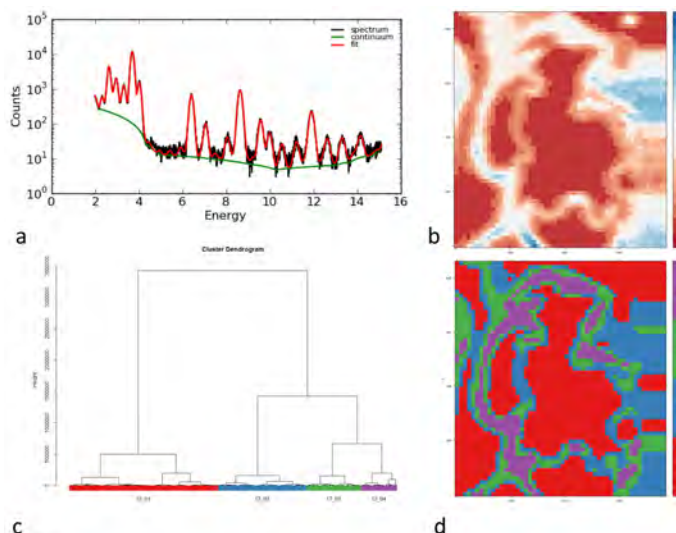


Figure 1: Typical SRXES spectrum of biological sample (a), spatial distribution of zinc (b), dendrogram calculated for spectral distance (c), spatial distribution of four clusters (d).

STRUCTURAL STUDIES OF MAGNETIC Fe DOPED ZnO NANOFIBERS

A. Baranowska-Korczyk*, K. Fronc, J.B. Pełka, K. Sobczak, P. Dłużewski, and D. Elbaum

Institute of Physics, Polish Academy of Sciences, al. Lotników 32/46, PL-02668 Warsaw, Poland

Keywords: electrospinning, ZnO nanofibers, ZnFeO

*e-mail: akorczyk@ifpan.edu.pl

Although many growth techniques were employed to produce magnetic oxides, electrospun magnetic nanofibers are still novel nanostructures. Electrospinning is gaining more attention due to its versatility and low cost operation. The room temperature ferromagnetic nanofibers were obtained by electrospinning and calcinations in air. Our previous work was aimed to join the extensive studies on these magnetic, electrospun Fe doped ZnO nanofibers [1].

Based on the new data, we discuss structural properties of our nanofibers. The X-ray (XRD) structural characterization was performed using synchrotron radiation at the W1 beamline at DESY-HASYLAB. The data were collected with 2θ scan in the glancing incidence geometry ($\lambda = 1.54056 \text{ \AA}$). No clear evidence of the second phase can be confirmed, as could be expected according to the atomic ratio of Fe to Zn, of about 0.1. This was consistent with previously reported results for similar size of ZnO nanocrystals doped with Co and Mn ions [2, 3]. The low activation energy and relatively fast growth of the crystal allowed a large amount of doped ions to be build-in the ZnO crystals. The activation energy for ZnO crystals growth in our nanofibers was estimated to be about 12 kJ/mol, one order of magnitude lower than the value for the bulk ceramics ZnO.

We showed that incorporating iron ions into ZnO did not affect the crystal structure of the host based on Electron Energy Loss Spectroscopy (EELS) analysis. We did not observe any precipitates from the second phase with resolution of about 1.5 nm. The sizes of crystals responsible for magnetic properties, as results of zero field cooled and field cooled measurements, were diameters between 3 and 10 nm [1]. It implies that the magnetic signal comes from Fe ions build-in ZnO crystals, because we do not observe other crystals (besides ZnO crystals) in this range of sizes. However, presence of the additional crystals in the ZnO matrix, e.g. Fe_2O_3 , FeO, ZnFe_2O_4 with diameter below 1.5 nm not detectable by XRD and EELS techniques is possible.

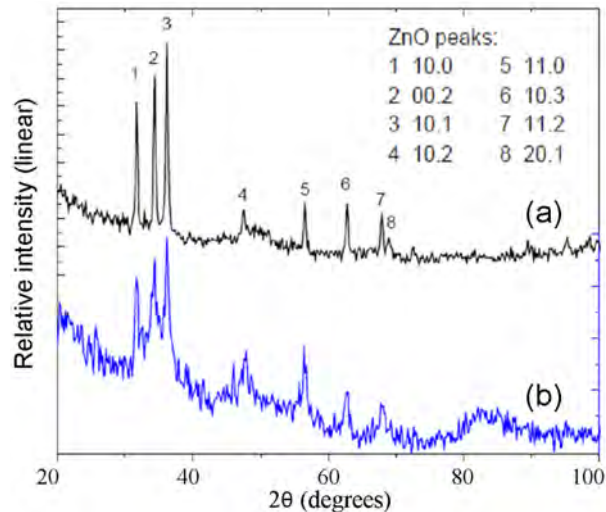


Figure 1: Typical X-ray diffraction patterns of Fe doped ZnO nanofibers: the higher (a) and the lower (b) density of nanofibers.

Acknowledgments: The research was partially supported by the European Union within European Regional Development Fund, through Grant Innovative Economy (POIG.01.01.02-00-008/08) and by the Ministry of Science and Higher Education (Poland) through Grant No. N518 424036.

References

- [1] A. Baranowska-Korczyk, A. Reszka, K. Sobczak, B. Sikora, P. Dziawa, M. Aleszkiewicz, Ł. Kłopotowski, W. Paszkowicz, P. Dłużewski, B.J. Kowalski, T.A. Kowalewski, M. Sawicki, D. Elbaum, K. Fronc, "Magnetic Fe doped ZnO nanofibers obtained by electrospinning," *J. Sol-Gel Sci. Technol.* **61** (2012) 494 – 500.
- [2] B.B. Straumal, A.A. Mazilkin, S.G. Protasova, A.A. Myatiev, P.B. Straumal, B. Baretzky, "Increase of Co solubility with decreasing grain size in ZnO," *Acta Mater.* **56** (2008) 6246 – 6256.
- [3] B. Straumal, B. Baretzky, A. Mazilkin, S. Protasova, A. Myatiev, P. Straumal, "Increase of Mn solubility with decreasing grain size in ZnO," *J. Eur. Ceram. Soc.* **29** (2009) 1963 – 1970.

SOLARIS — NATIONAL SYNCHROTRON RADIATION CENTRE, PROJECT PROGRESS, MAY 2012

**M.R. Bartosik^{1*}, C.J. Bocchetta², P. Goryl², M.J. Stankiewicz^{1,2}, P. Tracz², Ł. Walczak²,
A.I. Wawrzyniak^{1,2}, K. Wawrzyniak², J. Wiechecki², M. Zajac², and Ł. Żytniak²**

¹*Institute of Physics, Jagiellonian University, ul. Reymonta 4, 31-059 Krakow, Poland*

²*National Synchrotron Radiation Centre Solaris, Jagiellonian University,
ul. Gronostajowa 7/P-1.6, 30-387 Krakow, Poland*

Keywords: synchrotron, synchrotron radiation, Solaris project

**e-mail: marcin.bartosik@uj.edu.pl*

The current status and plans for the future development of the recently granted National Synchrotron Radiation Centre — Solaris will be presented. The layout and basic design parameters of the accelerator will be shown and described.

The project is run by Jagiellonian University. The Centre will be situated within the Campus of the 600th Anniversary of the Jagiellonian University Revival area, the new location for the Science Faculties and the site of the Jagiellonian Centre of Innovation. The building was designed and is being built by the ALPINE Construction Polska Sp. z o. o. / Lęprzem Sp. z o. o. Consortium with whom the contract was signed on the 24th of March 2011.

The synchrotron radiation facility will consist of:

- An electron injection system including thermionic RF gun, 550 MeV S-band linear accelerator and transfer line.

- A low emittance 1.5 GeV storage ring with a circumference of 96 m and 500 mA circulating current. The storage ring will have 12 double bend achromats (DBA) separated by 3.5 m long straight sections [1].
- One bending magnet based experimental beamline with Photoelectron Emission Microscope (PEEM) with band-pass filtering.

The main parameters of the machine are shown in Table 1 and the layout is visualized in Fig. 1.

Novel concepts have been applied to the system design which is based on the integrated magnets technology developed by Mikael Eriksson's team at MAX-lab in Lund University, Sweden with whom in December 2010 Jagiellonian University signed a relevant Cooperation Agreement [2]. The innovative design of the device allows the realization of a powerful scientific instrument at a very competitive price and the participation of experts from MAX-lab is essential to the project.

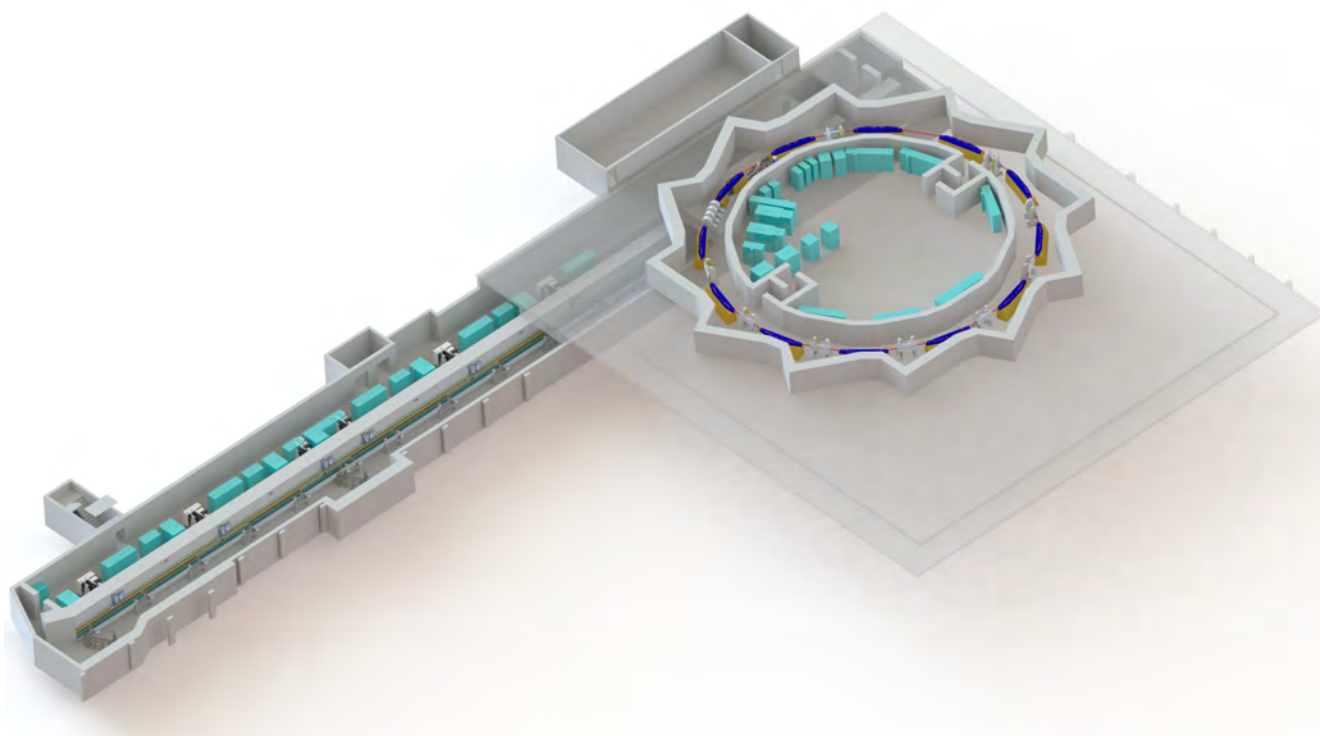


Figure 1: Layout of the Solaris synchrotron.

Table 1. Storage ring main parameters.

| | |
|---|-------------------|
| Horizontal tune ν_x | 11.22 |
| Vertical tune ν_y | 3.15 |
| Natural horizontal chromaticity ξ_x | -22.964 |
| Natural vertical chromaticity ξ_y | -17.154 |
| Momentum compaction (linear) α_C | $3.055 * 10^{-3}$ |
| Horizontal damping partition J_x | 1.464 |
| Bare lattice emittance ε_0 | 5.982 nm rad |

The funded project includes one experimental beamline and the search for funds for the full range of beamlines and endstations has started. Radiation sources for future beamlines can be from bending magnets and undulators, which may include a superconducting wiggler, mounted on one of ten free straight sections. The first beamline will be based on bending magnet radiation. Due to experimental interest (Soft x-ray absorption spectroscopy)

and existing instrumentation (PEEM) the planned beamline will be designed for the soft X-ray photon energy range. The spectroscopy chamber and the PEEM microscope will be exchangeable. Already two external applications for funding additional experimental liners have been submitted. They include Ultra Resolution Angle Resolved Photoemission Spectroscopy (UARPEs) and X-ray photoemission spectroscopy (XPS) beamlines, both based on undulators.

References

- [1] C.J. Bocchetta *et al*, *Project status of the Polish Synchrotron Radiation facility Solaris* (Proceedings of IPAC2011, San Sebastián, Spain).
- [2] M. Eriksson, *The MAX IV synchrotron light source* (Proceedings of IPAC2011, San Sebastián, Spain).

FIRST-PRINCIPLE APPROACH TO INTERPRETATION OF CHANGES IN IR SPECTRA OF CELLULAR DNA

J. Bielecki^{1*}, E. Lipiec², and W.M. Kwiatek²

¹*Świerk Computing Centre Project, National Centre for Nuclear Research, Soltana 7, 05-400 Otwock-Świerk, Poland*

²*Institute of Nuclear Physics, Polish Academy of Sciences, Radzikowskiego 152, 31-342 Kraków, Poland*

Keywords: synchrotron radiation, SR-FTIR, DFT, ab-initio, DNA

**e-mail: jakub.bielecki@ncbj.gov.pl*

The Fourier Transform Infrared Microspectroscopy (μ FTIR) has been proven to be a powerful tool for detecting changes in biomolecules such as cellular DNA [1]. However only Synchrotron Radiation-based techniques (e.g. μ SR-FTIR) provide sufficient signal-to-noise ratio to conduct vibrational analysis at the single cells level [2]. Nevertheless large molecules such a DNA are likely to yield IR spectra with many close lying peaks what makes a systematic analysis of the spectra quite difficult. Thus an accurate first-principles-based calculations are required for interpretation of the spectra changes due to radiation damage.

Development of modern high performance computing (HPC) systems together with the improvement of numerical methods as well as more common utilization of graphics processing units (GPU) for scientific calculations enables conducting large-scale computations of molecular vibrational spectra with high level of accuracy (e.g. within density functional theory (DFT) with B3LYP exchange-correlation functional and $6-31+G(d)$ or $6-31+G(d,p)$ basis set).

This work aims to provide a comparison of experimentally obtained μ SR-FTIR spectra of cellular DNA (PC-3 cells line) damaged by particle radiation with the calculated spectra in order to provide comprehensive interpretation of damage mechanisms. The PC-3 cells were irradiated by horizontal focused proton microbeam (16 μ m in diameter at the irradiated spot) from the Van de Graaff accelerator (Single Proton Hit Facility at IFJ PAN, Krakow [3]). Irradiation process was conducted with single cells at protons energies of 1 MeV, 1.5 MeV and 2 MeV and five different doses were delivered for each energy (50, 200, 400, 2000, 4000 protons per cell). The experiment control group consisted of untreated cells.

The influence of possible radiation damage of DNA segments such as: (*i*) strand breaks, (*ii*) base

removing from backbone, (*iii*) base damage on experimentally obtained spectra was verified by DFT B3LYP calculations. Energy thresholds for different types the DNA damage as well as IR spectra of modified DNA structures were calculated. Development was performed at Świerk Computing Centre - National Centre for Nuclear Research [4] while computations were carried out with the use of PL-Grid infrastructure [5].

Acknowledgments: This work is co-financed under the Operational Programme Innovative Economy 2007 – 2013 (agreement No. POIG.02.03.00–00–013/09). The experimental research leading to these results has received funding from the European Community's Seventh Framework Programme (FP7/2007 – 2013) under grant agreement No. 20110351. The research was also partially supported by PL-Grid Infrastructure.

References

- [1] E. Lipiec, J. Kowalska, J. Lekki, A. Wiechec, and W.M. Kwiatek, "FTIR microspectroscopy in studies of DNA damage induced by proton microbeam in single PC-3 cell," *Acta Phys. Pol. A* **121** (2012) 506 – 509.
- [2] M. Diem, M. Romeo, C. Matthaues, M. Miljkovic, L. Miller, P. Lasch, "Comparison of Fourier transform infrared (FTIR) spectra of individual cells acquired using synchrotron and conventional sources infrared," *Infrared Phys. Technol.* **45** (2004) 331 – 338.
- [3] W. Polak, O. Veselov, J. Lekki, Z. Stachura, M. Zazula, R. Ugenskiene, M. Polak, J. Styczeń, "Irradiating single cells using Kraków microprobe facility," *Nucl. Instr. Meth. B* **249** (2006) 743 – 746.
- [4] <http://www.cis.gov.pl/en>.
- [5] <http://www.plgrid.pl/en>.

X-RAY ABSORPTION AND EMISSION SPECTROSCOPY OF TITANIUM DIOXIDE WITH MODIFIED ANIONIC SUBLATTICE

K. Biernacka^{1*}, M. Sikora¹, Cz. Kapusta¹, A. Brudnik², K. Zakrzewska², and M. Radecka³

¹Faculty of Physics and Applied Computer Science, AGH University of Science and Technology, 30, Mickiewicza Av, 30-059 Krakow, Poland

²Faculty of Electrical Engineering, Automatics, Computer Science and Electronics, AGH University of Science and Technology, 30, Mickiewicza Av, 30-059 Krakow, Poland

³Faculty of Materials Science and Ceramics, AGH University of Science and Technology, 30, Mickiewicza Av, 30-059 Krakow, Poland

Keywords: titanium dioxide, photoelectrolysis, hydrogen, XANES, XES

*e-mail: biernack@agh.edu.pl

TiO₂ based thin films are very promising materials for an efficient conversion of solar energy into hydrogen in the process of water photolysis. Hydrogen is considered as a prospective energy carrier to replace traditional fossil fuels. TiO₂ with modified anionic sublattice is considered for potential applications as photoanode for hydrogen generation due to its reported photocatalytic activity in the visible light [1, 2].

Modification of anionic sublattices presented in this work consists in deviation from stoichiometric composition towards oxygen deficiency and nitrogen doping. Thin films of TiO_{2-x} and TiO_{2-x}:N were deposited by dc pulsed magnetron sputtering under

trollable technological parameter I/I_0 related to the sputtering rate. The efficiency of solar energy conversion into chemical energy is determined by the intrinsic properties of the photoanode material.

The aim of this work is to study local atomic environment and its changes upon doping of titanium dioxide by N as well as to understand the structural changes in nonstoichiometric TiO_{2-x} caused by oxygen deficiency. HERFD-XANES measurements at the Ti *K*-edge measurements give direct information on the location of N dopant in the TiO₂ structure. Spectra show a significant change in the pre-edge structure and shift of the edge to lower photon energy upon increasing nitrogen flow [3]. A significant evolution of the *Kβ* satellite region from valence-to-core Ti *Kβ* XES measurements is attributed to evolution in the local structure around Ti species and change in the character of electronic structure. The spin value and valence state have been derived from *Kβ* main emission lines that were correlated to the energy shift of respective *K* absorption edge (Fig. 1). The results from synchrotron measurements are correlated with XRD and optical measurements in order to obtain the full interpretation of the changes in local atomic/ionic structure and their influence on photo-electrical and optical properties.

Acknowledgments: The financial support of the Polish Ministry of Science and Higher Education (2009–2012) within the project NN515 080 637 is highly acknowledged. K.B. has been partly supported by the EU Human Capital Operation Program, Polish Project No. POKL.04.0101-00-434/08-00.

References

- [1] A. Brudnik *et al.*, "Microstructure and optical properties of photoactive TiO₂:N thin films," *Vacuum* **82** (2008) 936 – 941.
- [2] S. Sakthivel *et al.*, "Photocatalytic and photoelectrochemical properties of nitrogen-doped titanium dioxide," *Chem. Phys. Chem.* **4** (2003) 487 – 490.
- [3] A. Braun *et al.*, "Nitrogen doping of TiO₂ photocatalyst forms a second *e_g* state in the oxygen 1s NEXAFS pre-edge," *J. Phys. Chem.* **114** (2010) 516 – 519.

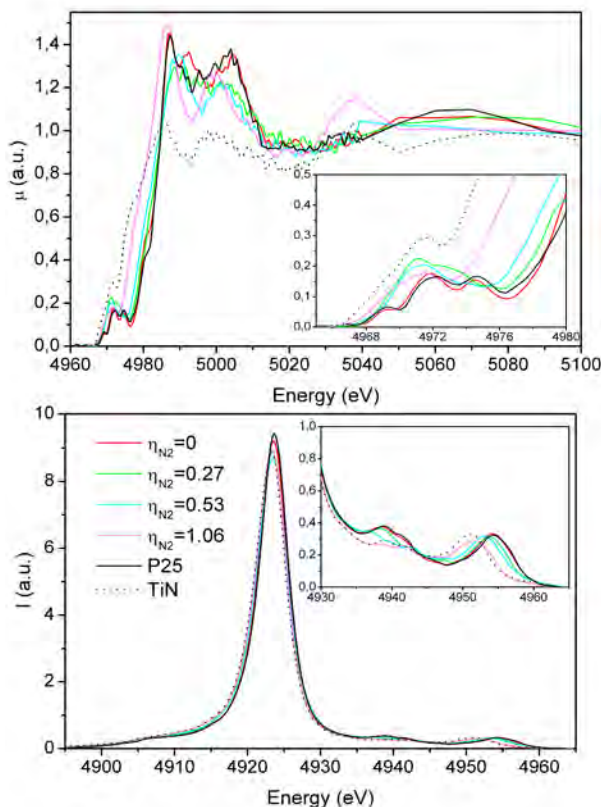


Figure 1: HERFD-XANES (upper) and XES (lower) spectra of TiO_{2-x}:N thin films and reference samples (TiO₂ P25, TiN) at Ti-K-edge and K β emission line, respectively. Insets show the close-up of the pre-edge and K β satellite regions.

optical emission spectroscopy as a function of con-

COMPTON PROFILE OF Mg SINGLE CRYSTAL: HIGH RESOLUTION EXPERIMENT AND THEORY

M. Brancewicz^{1*}, A. Andrejczuk¹, E. Żukowski¹, L. Dobrzyński², Y. Sakurai³, and M. Itou³

¹Faculty of Physics, University of Białystok, ul. Lipowa 41, 15-424 Białystok, Poland

²National Centre for Nuclear Research, ul. Andrzeja Soltana 7, 05-400 Otwock-Swierk, Poland

³Japan Synchrotron Radiation Research Institute, Mikazuki, Sayo, Hyogo 679-5198, Japan

Keywords: synchrotron radiation, Compton scattering, inelastic scattering, Compton profile, Mg

* e-mail: brancew@alpha.uwb.edu.pl

Compton scattering is a very powerful method for investigating the electronic structure in condensed matter physics. The spectrum of inelastically scattered monoenergetic photons in a target is related through Doppler effect to momentum density distribution $\rho(\mathbf{p})$, which is directly connected with the electron wave function in reciprocal space $\chi(\mathbf{p})$ and hence with Fourier transform of the wave function in real space $\psi(\mathbf{r})$:

$$\rho(\mathbf{p}) = |\chi(\mathbf{p})|^2 = \left| \int \psi(\mathbf{r}) e^{i\mathbf{p}\mathbf{r}} d^3\mathbf{r} \right|^2$$

Thus the Compton scattering technique is the most direct test of solid state theories, where electron wave functions are calculated from the first principles.

The final result of single Compton scattering experiment is the Compton profile $J(p_z)$ (CP), which is a one-dimensional projection (double integral) of the electron momentum density $\rho(\mathbf{p})$ onto the scattering vector direction (usually chosen as z axis):

$$J(p_z) = \int_{-\infty}^{+\infty} \int_{-\infty}^{+\infty} \rho(\mathbf{p}) dp_x dp_y$$

To test theoretical calculations, one usually shows differences between CPs measured in two directions (CPs anisotropies) [1, 2]. This approach has many advantages because some systematic errors in experimental data can be cancelled and sharp features connected with the anisotropy of electron momentum density are emphasized.

The directional Compton profiles of Mg single crystal have been measured along [100], [110], [001] and [310] directions using high resolution Compton spectrometer at SPring-8 (beamline BL08W) [3]. Preliminary results of this experiment were published in [1]. Apart from standard data analysis procedures taking into account a number of energy dependent corrections applied to the raw data, final results were prepared with the use of some modified algorithms. The experimental data

were compared with the Korringa-Kohn-Rostoker (KKR) semi-relativistic calculations and previous medium resolution Compton profile measurements [2]. Medium and high resolution CPs anisotropies show good agreement with theoretical KKR calculations, except the low momentum region where the agreement is worse, suggesting a need for revision of theoretical calculations.

It was observed later that the experimental CPs anisotropies of Mg agree slightly better with the old CP calculations performed with the use of APW theory [4]. It can be simply explained by almost free character of the valence electrons in Mg. In KKR theory electron wave functions outside the muffin-tin spheres are described by the linear combination of spherical harmonics. In the APW theory this is realized by the superposition of the plane waves (like in the case of free electrons).

The new theoretical band structure calculations for hexagonal Mg should take into account suggested almost free character of valence electrons and describe their behavior as a linear combination of plane wave like functions.

References

- [1] M. Brancewicz, A. Andrejczuk, Y. Sakurai, M. Itou, L. Dobrzyński, E. Żukowski, S. Kaprzyk, "Electron momentum density of hexagonal magnesium studied by high-resolution Compton scattering," *Rad. Phys. Chem.* **78** (2009) 137 – 139.
- [2] M. Brancewicz, H. Reniewicz, A. Andrejczuk, L. Dobrzyński, E. Żukowski, and S. Kaprzyk, "Electron momentum density of hexagonal magnesium studied by Compton scattering," *Solid State Phenom.* **112** (2006) 123 – 132.
- [3] Y. Sakurai, M. Itou, "A Cauchois-type X-ray spectrometer for momentum density studies on heavy-element materials," *J. Phys. Chem. Solids* **65** (2004) 2061 – 2064.
- [4] S. Wakoh, "Momentum density distribution in magnesium for Compton scattering and positron annihilation," *J. Phys. Soc. Jpn.* **50** (1981) 490 – 497.

DETECTION OF X-RAY ABSORPTION ANISOTROPY USING FLUORESCENCE RADIATION FOR ATOMIC RESOLVED IMAGING

K.M. Dąbrowski^{1*}, D.T. Dul¹, M. Tolkiehn², D.V. Novikov², and P. Korecki¹

¹*Institute of Physics, Jagiellonian University, Reymonta 4, 30-059 Kraków, Poland*

²*DESY, Notkestrasse 85, D-22603 Hamburg, Germany*

Keywords: X-ray absorption, atomic structure determination, polycapillary optics

**e-mail: karol.dabrowski@uj.edu.pl*

X-ray absorption anisotropy (XAA) recorded using a white synchrotron beam contains an unique information about local atomic structure. For a crystal, fine-structures in absorption pattern measured for various incident angles of the incident beam can be considered as distorted real-space projections of close packed atomic planes and directions.

Until recently, white beam XAA experiments used total electron yield to probe the absorption. In [1] it was shown that white-beam XAA can be recorded using x-ray fluorescence. In principle, fluorescence detection of XAA allows element sensitivity and enables experiments in a presence of an electric or magnetic field. Since XAA signal is very weak (0.1% of the background), experiments require high counting rates.

In this work we present results of XAA experiments performed for a LiNbO₃ (001) wafer using a hard x-ray wiggler on BW5 beamline at DORIS III (DESY/Hamburg). The white beam had a mean energy of 64 keV and FWHM of 36 keV.

Fluorescence detection of XAA was performed in two configurations. In the first geometry, x-ray fluorescence was detected using an avalanche photo diode (APD). The moderate energy resolution of the APD was sufficient to separate x-ray fluorescence signal from Compton and Bragg scattered radiation and to obtain XAA patterns with a quality allowing a direct observation of the projection of the LiNbO₃ structure (Figure 1).

The quantitative analysis of XAA was performed using wavelets [2] and reproduced local structure of Nb atoms inside a 10 Å sphere. Because of a weak scattering, direct visualization of oxygen atoms was impossible. However, their location could be determined indirectly, by examination of a distortion in the shape of Nb peaks.

In the second experimental geometry, preliminary test of polycapillary optics for recording of XAA patterns were performed. A polycapillary element was used simultaneously as a collimating device and a low-pass energy filter.

While, the quality of the XAA pattern recorded using APD was higher than for the setup with polycapillary optics, laboratory-based measurements

showed that the later configuration seems to be more promising for future application. For example, achieving of a two order of magnitude increase in count rate is likely with polycapillary optics optimized for white beam XAA experiments.

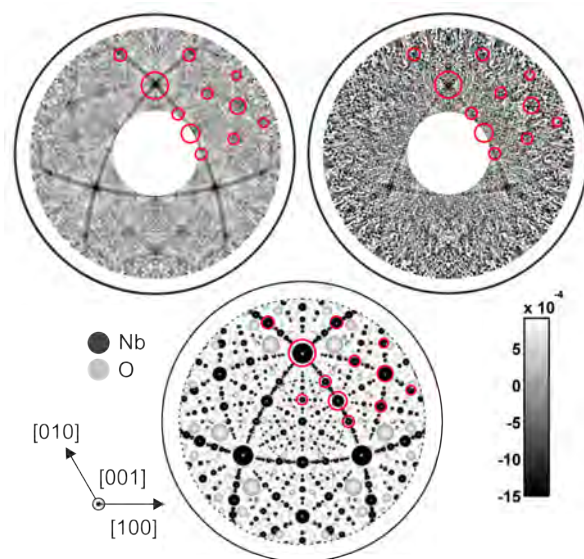


Figure 1: White beam x-ray absorption anisotropy patterns recorded for a LiNbO₃ sample using two different experimental geometries. Left: using APD. Right: using polycapillary optics and a PIN diode. Bottom: geometrical projection of the local structure of LiNbO₃.

Acknowledgments: This work was supported by Polish National Science Center (DEC-2011/01/B/ST3/00506) and by grant No. 226716 funded by European Community's Seventh Framework Programme (FP7/2007 – 2013).

References

- [1] P. Korecki, D.V. Novikov, M. Tolkiehn, "Projections of local atomic structure revealed by wavelet analysis of x-ray absorption anisotropy," *Phys. Rev. B* **80** (2009) 014119.
- [2] P. Korecki, M. Tolkiehn, K.M. Dabrowski, D.V. Novikov, "Fluorescence detection of white beam x-ray absorption anisotropy: Towards element sensitive projections of atomic structure," *J. Synchrotron Radiat.* **18** (2011) 851.

ELECTRONIC STRUCTURE OF IRRADIATED CdO THIN FILMS

I.N. Demchenko^{1*}, R. Minikayev¹, T. Tyliszczak², M. Chernyshova³, K.M. Yu²,
J.D. Denlinger², D. Speaks^{2,4}, and W. Walukiewicz²

¹*Institute of Physics PAS, al. Lotnikow 32/46, 02-668, Warsaw, Poland*

²*Lawrence Berkeley National Laboratory, 1 Cyclotron Rd, Bldg4R0230, Berkeley, CA 94720-8235, USA*

³*Institute of Plasma Physics and Laser Microfusion, 23 Hery Street, 01-497 Warsaw, Poland*

⁴*Department of Materials Science and Engineering, University of California, Berkeley, CA 94720, USA*

Keywords: synchrotron radiation, X-ray absorption, X-ray emission

**e-mail: demch@ifpan.edu.pl*

There has been an increasing interest in group II-oxides, a class of semiconductors analogous to the very extensively studied and commercially successful group III-nitrides. In spite of thoroughly investigated ZnO less attention has been paid to other group-II oxides. One of them, cadmium oxide, being synthesized by different methods, has still not very well established properties [1]-[6]. Up to date there is controversy regarding the type, direct or indirect, of the fundamental band gap of this material. Recent studies have shown that the Fermi energy on the free CdO surface is pinned at about 1.15 eV above the conduction band edge (E_C) [7]. This resembles the extensively studied case of InN where the Fermi energy was found to be pinned deeply in the conduction band at $E_C + 0.9$ eV. It is significant to note that, as in InN, the surface Fermi level pinning energy for semiconductors is expected to be like the bulk Fermi level stabilization energy in heavily damaged materials [8, 9]. In a striking contrast, a recent study has shown that intentional introduction of native point defects using irradiation with 1 MeV He⁺ ions led to stabilization of the bulk Fermi energy at about $E_C + 0.4$ eV in CdO [10] which is almost 3 times lower than the surface Fermi level pinning energy.

To better understand the properties of native defects in CdO, we have studied the effects of high concentration of native point defects on CdO electronic structure. The defects were generated by high energy Ne ions bombardment. Significant differences between experimental NEXAFS spectra gathered in total fluorescence yield (TFY, bulk sensitive) and total electron yield (TEY, rather surface sensitive) detection modes are observed. Such an observation confirms the fact that irradiation process drastically modifies the surface layer of investigated films. An interpretation of NEXAFS spectra at the *K*-edge of oxygen in “*as-grown*” and “*irradiated*” CdO films, within the *ab initio* DFT formalism will be shown. Different models with point defects (oxygen

vacancy) in the host CdO matrix were considered and respective theoretical spectra were calculated. Comparison of the experimental (“*irradiated*” versus “*as grown*”) and theoretical data allows concluding that electronic levels of defects push the Fermi level into the conductive band and shift the absorption threshold to a higher energy. The observed leading edge differences of TFY and TEY spectra could be likely explained basing on electron accumulation at the surface of *n*-type CdO due to the presence of positively charged donor-type surface states. Our conclusions are confirmed by optical absorption measurements.

Acknowledgments: The Advanced Light Source is supported by the Director, Office of Science, Office of Basic Energy Sciences, of the U.S. Department of Energy under Contract No. DE-AC02-05CH11231.

References

- [1] D. Ma, Z. Ye, L. Wang, *et al.*, *Mater. Lett.* **58** (2003) 128.
- [2] P.H. Jefferson, S.A. Hatfield, T.D. Veal, *et al.*, *Appl. Phys. Lett.* **92** (2008) 022101.
- [3] G. Phatak and R. Lal, *Thin Solid Films* **245** (1993) 17.
- [4] T.K. Subramanyam, B.S. Naidu, and S. Uthanna, *Appl. Surf. Sci.* **169** – **170** (2001) 529.
- [5] X. Li, Y. Yan, A. Mason, *et al.*, *Electrochem. Solid-State Lett.* **4** (2001) C66.
- [6] J.C. Boettger, *Int. J. Quantum Chem.* **107** (2007) 2988.
- [7] L.F.J. Piper, L. Colakerol, P.D.C. King, *et al.*, *Phys. Rev. B* **78** (2008) 165127.
- [8] W. Walukiewicz, *Phys. Rev. B* **37** (1988) 4760.
- [9] S.X. Li, K.M. Yu, J. Wu, *et al.*, *Phys. Rev. B* **71** (2005) 161201.
- [10] P.D.C. King, T.D. Veal, P.H. Jefferson, *et al.*, *Phys. Rev. B* **79** (2009) 035203.

SEARCHING FOR THE DIFFERENCES BETWEEN *TRICHINELLA SPIRALIS* AND MOUSE THYMIDYLATE SYNTHASES: A QUEST FOR SPECIES-SPECIFIC DRUGS

A. Dowiecjal^{1*}, A. Jarmuła¹, W.R. Rypniewski², T. Frączyk¹, P. Wilk¹, and W. Rode¹

¹Nencki Institute of Experimental Biology, Polish Academy of Sciences,
3 Pasteur Str., 02-093 Warszawa, Poland

²Institute of Bioorganic Chemistry, Polish Academy of Sciences,
12/14 Noskowskiego Str., 61-704 Poznań, Poland

Keywords: thymidylate synthase, *Trichinella spiralis*, parasitic nematode, selective inhibitor, synchrotron radiation

*e-mail: a.dowiecjal@nencki.gov.pl

The enzyme thymidylate synthase [TS: 2.1.1.45] catalyzes the multi-step reaction of methylation of dUMP, leading to dTMP, in the presence of the cofactor, N^{5,10}-methylenetetrahydrofolate. As indispensable component in all known proliferating systems, thymidylate synthase is an important molecular target for anticancer, antifungal, antiviral and antibacterial drugs.

Trichinella spiralis infection is responsible for trichinellosis, a serious disease, occurring regularly also in Poland. In view of high thymidylate synthase activity found throughout the parasite developmental cycle, the enzyme appears a potential target for chemotherapeutic drugs [1].

TS is one of the most conservative enzymes known, with the amino acid sequence identity for human and *E.coli* TSs' being 51% and similarity amounting to 67%; the corresponding values for the human and mouse enzymes are 88% and 93%, respectively. The high sequence similarity between TSs' of different origin results in a high degree of similarity of their spatial structures, as confirmed by large numbers of TS crystal structures deposited in the PDB database.

In view of this close structural similarity of different TS's, and particularly their active centers, inhibitors designed as substrate/cofactor analogues are beyond hope as candidates for species-selective inhibitors of the pathogen *vs.* mammalian enzyme. A possible solution, successfully applied to search for a specific inhibitor of bacterial *vs.* human TS [2], is virtual selection of an inhibitor, based on comparison of the 3D structures of pathogen and human

enzyme proteins, aimed at non-conservative protein fragments differing between both proteins.

In order to take advantage of such an approach, we made an attempt to find structural differences between TS of the parasitic nematode *Trichinella spiralis* and the mammalian enzyme. It is worthwhile to mention that thus far PDB does not contain any model of invertebrate TS.

Therefore we undertook crystallization of *Trichinella spiralis* TS complexed with the substrate, dUMP. Having obtained suitable monocrystals, we collected the diffraction data to the 1.9 Å resolution using synchrotron radiation at BESSY in Berlin. Preliminary analysis of solved structure of the parasitic nematode thymidylate synthase, compared to the mouse enzyme, points to at least two structural differences.

Acknowledgments: This work was supported by the National Science Centre Grant No. 2011/01/B/NZ6/01781.

References

- [1] M. Dąbrowska, E. Jagielska, J. Cieśla, A. Płucienniczak, J. Kwiatkowski, M. Wranicz, P. Boireau, W. Rode, "Trichinella spiralis thymidylate synthase: cDNA cloning and sequencing, and developmental pattern of mRNA expression," *Parasitology* **128** (2004) 209 – 221.
- [2] B.K. Shoichet, R.M. Stroud, D.V. Santi, I.D. Kuntz, K.M. Perry, "Structure-based discovery of inhibitors of thymidylate synthase," *Science* **259** (1993) 1445 – 1450.

A MOLECULAR STRUCTURE STUDY OF 1,3,5-TRICHLOROBENZENE

H. Drozdowski*, T. Hałas, and Z. Błaszczak

Department of Optics, Faculty of Physics A. Mickiewicz University,
ul. Umultowska 85, 61-614 Poznań, Poland

Keywords: molecular structure, 1,3,5-trichlorobenzene, internal ordering degree

* e-mail: riemann@amu.edu.pl

The paper presents the structure and molecular correlations in liquid 1,3,5-trichlorobenzene $C_6H_3Cl_3$ determined for the first time by the X-ray diffraction method [1]. Trichlorobenzene characterized by the melting point of 338 K and boiling point of 481 K ($M = 181.45$ g/mol). This paper reports the first studies of liquid trichlorobenzene performed by the counter method for the range of the angular measurements intensity extended to the value of $\theta = 60^\circ$ (Fig. 1). Trichlorobenzene samples of 99% purity were purchased from Aldrich-Chemie (Germany).

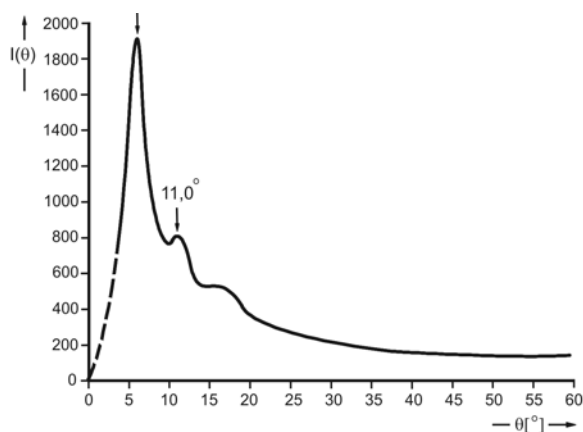


Figure 1: Mean angular distribution of the scattered intensity for pure 1,3,5-trichlorobenzene $C_6H_3Cl_3$.

From the position of the main maximum $I(\theta)$ of the east intermolecular distance, which is also the radius of the first coordination sphere, was determined.

The attractive dipole interaction between neighbouring molecules can favour the plane arrangement of molecules one over another in antiparallel arrangement (Fig. 2 and Fig. 3 — for liquid chlorobenzene). The distance between the centres of two neighbouring molecules is defined by van der Waals atomic radii.

The physical sense of the molecular packing coefficient [2] and its role in solving the near-range ordering in liquids chlorobenzene is explained.

On the basis of the differential radial distribution functions (DRDFs) it is possible to conclude about the mutual orientations of the functional groups ($-Cl$) of molecules with respect to the benzene rings of the neighbouring molecules. The antiparallel arrangement of the molecules dipole moments is indicated by the positions of the maxima on the functions and the size of the molecules. Because of the supposed role of the benzene ring and functional group ($-Cl$) attached to it at the *ortho*-, *meta*-, *para*-position, for mutual configurations of molecules in liquids studied, it seems very probable that the proposed models of local arrangements can also hold for other derivatives of benzene in the liquid phase.

The use of short-wave radiation $Mo K_\alpha$ enabled determination of the shortest interatomic distances within the benzene ring.

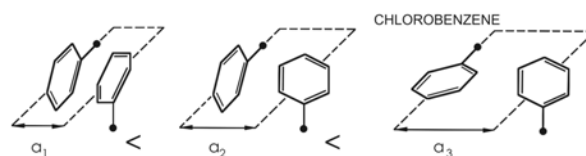


Figure 2: The model of probable configuration of molecules in chlorobenzene C_6H_5Cl .

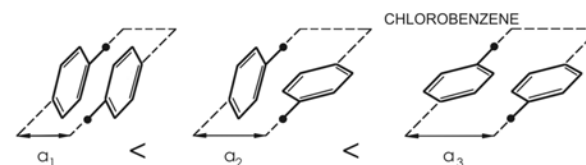


Figure 3: The arrangement of molecules in liquid chlorobenzene.

References

- [1] T. Hałas, H. Drozdowski, "Determination of local ordering in 1,3,5-trichlorobenzene $C_6H_3Cl_3$," *Polish Crystallogr. Meeting Wrocław* **53** (2011) 255.
- [2] H. Drozdowski, "The packing coefficient of liquid 2-phenylnaphthalene molecules at 396 K," *Phys. Chem. Liq.* **40** (2002) 421 – 434.

THE DETERMINATION OF MOLECULAR STRUCTURE OF CHLOROANISOLES BY X-RAY DIFFRACTION

H. Drozdowski*, A. Romaniuk, and Z. Błaszczak

Department of Optics, Faculty of Physics A. Mickiewicz University,
ul. Umultowska 85, 61-614 Poznań, Poland

Keywords: molecular function of structure, chloroanisoles, van der Waals atomic radii

*e-mail: riemann@amu.edu.pl

For the first time the method of reduction proposed by Mozzi-Warren with modifications introduced by the Drozdowski [1] has been applied to verify the assumed models of the molecules studied and to separate the intra- from intermolecular interactions. Analysis of intramolecular interactions between pairs of atoms and intermolecular interactions has been made.

The molecular function of structure was calculated from the modified Debye formula [2]:

$$i_m(S) = \left[\sum_{i=1}^n f_i(S) \right]^{-2} * \left[\sum_{j,s}^n \sum_{i \neq j}^n f_i f_j \exp\left(-\frac{\bar{u}_{ij} S^2 \sin(S\bar{r}_{ij})}{2 S\bar{r}_{ij}}\right) \right],$$

which describes the scattering by a single molecule.

The values of the function $Si(S)$ were calculated from equation [3]:

$$Si(s) = \frac{1}{r} \int_{S_1}^{S_2} \left[\sum_{j,k}^n \bar{K}_j 4\pi r^2 \rho_k(r) - \sum_j^n \bar{K}_j 4\pi r^2 \rho_0 \right] \sin(Sr) dr,$$

where r is the distance from an atom or molecule selected as scattering centre, $\rho_k(r)$ the function of radial electron density, \bar{K}_j — the effective mean atomic numbers. The calculations were performed for a finite range of S values from $S_1 = 0.430 \text{ \AA}^{-1}$ to $S_2 = 14.311 \text{ \AA}^{-1}$. The modified method of Blum-Narten reductions was applied to verify the correctness of the assumed models of the molecules and to permit a separation of the intra- and intermolecular interactions. Analysis of the functions of the experimental $i(S)$ and the calculated $i_m(S)$ for the model proposed.

The molecular structural function $i_m(S)$ was calculated from the equation of Debye for the Bragg

angle θ changing in the range $0^\circ - 60^\circ$. Having determined $i(S)$ and $i_m(S)$, the so-called distinct structure function [3] was obtained from equation:

$$i_d(S) = i(S) - i_m(S),$$

where $i_m(S)$ is the molecular structure function describing the scattering by a single molecule and $i_d(S)$ is the distinct structure function providing the information about intermolecular correlations from the experimental data. The dependencies of $i(S)$, $i_m(S)$ and $i_d(S)$ on S are presented in Fig. 1.

The method of reduction proposed by Mozzi-Warren with the modifications introduced by the Drozdowski [1]-[3] applied in analysis of the scattered radiation intensity permitted establishment of the correct models of the molecules chloroanisoles [4].

References

- [1] H. Drozdowski, "Structure of liquid 1-chloronaphthalene at 293 K," *J. Mol. Struct.* **526** (2000) 391.
- [2] H. Drozdowski, "Vibrations in atoms in liquid 1,4-dimethylbenzene," *Phys. Chem. Liq.* **44** (2006), 21.
- [3] H. Drozdowski, "The molecular structure of liquid 1-phenylnaphthalene by X-ray diffraction," *Acta Phys. Slovaca* **51** (2001) 163.
- [4] H. Drozdowski, A. Romaniuk, Z. Błaszczak, "Short-range ordering in ortho-chloroanisole at 293 K by X-Ray diffraction," *Bull. Synchr. Radiat. Nat. Science* **8** (2009) 38.

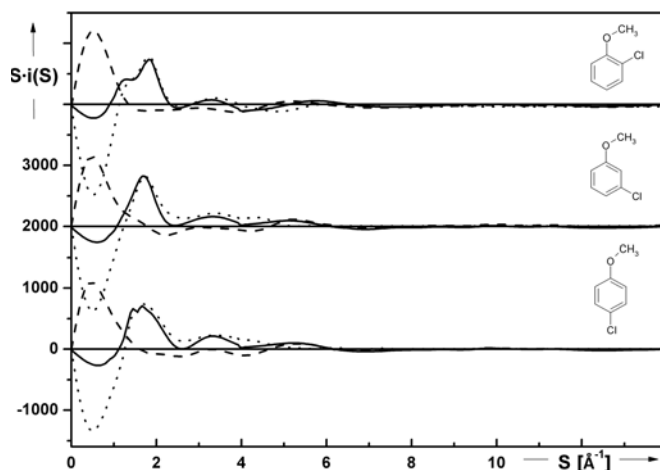


Figure 1: Curves - continuous lines — the experimental structure functions $Si(S)$. Curves - broken lines — the molecular structure functions $i_m(S)$ calculated according to Debye. Curves - dotted lines — subtraction of the calculated curves from the experimental structure functions.

DISTRIBUTION OF BIOMOLECULES IN THE ADRENAL GLAND TUMORS — FTIR RESULTS COMPARED WITH HISTOLOGICAL VIEW OF SAMPLES

J. Dudala^{1*}, M. Szczerbowska-Boruchowska¹, M. Lankosz¹, and M. Bialas²

¹AGH University of Science and Technology, Faculty of Physics
and Applied Computer Science, Krakow, Poland

²Chair and Department of Pathomorphology, Collegium Medicum, Jagiellonian University, Krakow, Poland

Keywords: infrared microspectroscopy, adrenal gland tumors, biochemical analysis

* e-mail: Joanna.Dudala@fis.agh.edu.pl

The aim of the presented study was to show the distribution of biomolecules in the adrenal gland tumors obtained by FTIR microspectroscopy in the light of histological structure of samples.

The adrenal glands are the endocrine organs located at the bottom pole of each kidney. Anatomically they are divided into the adrenal cortex (outer part) and the medulla (inner part). Both of them differ each other structurally and functionally. The adrenal gland tumors are often incidentally detected by chance (hence they are named incidentallomas) while diagnostic imaging is used for the reasons other than the endocrine disease indications [1]. Most of incidentallomas do not give any specific clinical symptoms nevertheless their disclosure often implies quite new direction of diagnosis and further patient treatment.

In the presented work three types of tumors were taken into consideration: adrenal cortical adenoma and adrenal cortical hyperplasia — both types derive from adrenal cortical cells; pheochromocytoma comes from chromaffin cells of the adrenal medulla.

The aim of presented investigations, performed for studied samples, was to find if there is any dependence between the biochemical structure and the type of tumor. Furthermore the determination of biomolecular composition of the adrenal gland tumors may be important for knowledge of tumor pathogenesis. In addition there is a strong need for identification of specific IR spectral biomarkers differentiating adrenal gland tumor type. Up to now the evaluation of the tumor type is possible on the base of histopathological examination after adrenalectomy. The conducted researches has the preliminary character but they might give the fundamentals for new diagnostic method, based on Fourier Transform Infrared Microspectroscopy, enables to differ the tumor type preoperatively.

The tissue samples were taken intraoperatively from patients with different type of the adrenal cortical gland tumors. The specimens were cryosectioned into the 10 μm thick slices, mounted on silver coated sample supports (Low-e MirrIR, Kevley Technologies) and freeze-dried at -80°C .

The studies were carried out at the Faculty of Physics and Applied Computer Science at the AGH University of Science and Technology in Krakow in co-operation with the Department of Pathomorphology, Collegium Medicum, Jagiellonian University in Krakow.

The measurements were performed using the IR microscope (Nicolet Continuum - Thermo Scientific) coupled with FTIR spectrometer (Nicolet 8700 - Thermo Scientific). The scientific instrumentation is equipped with ceramic infrared radiation source (the range of $20 \div 9600 \text{ cm}^{-1}$) and the MCT detector (mercury cadmium telluride, HgCdTeO_2) liquid nitrogen cooled. The beam was defined by the aperture size of $20 \mu\text{m} \times 20 \mu\text{m}$. The reflection mode was applied to collect the absorption IR spectra. Raster scanning of the samples enabled two-dimensional chemical mapping of tissue samples. The spectral analysis were carried out using OMNIC software (version 8.0). Distribution of functional groups of lipids, proteins, nucleic acids and carbohydrates were determined.

Since the studied tumors originated from different parts of adrenal gland tissue it was predictable that they might differ in biomolecular composition. The main difference was observed in the lipid functional groups. It turned out that level of lipids is higher in the adenoma samples comparing than in pheochromocytomas. Since the studied samples are different each other it is important to consider their histological structure while interpreting the IR microspectroscopy results. The further investigation is in progress.

Acknowledgments: This work was supported by the Polish Ministry of Science and Higher Education.

References

- [1] H.E. Turner, N.R. Moore, J.V. Byrne, J.A.H. Wass, "Pituitary, adrenal and thyroid incidentallomas," *Endocrine-Related Cancer* **5** (1998) 131 – 150.

WAVELET ANALYSIS OF X-RAY ABSORPTION ANISOTROPY: ACCURACY AND LIMITATIONS OF ATOMIC STRUCTURE IMAGING

D.T. Dul* and P. Korecki

Institute of Physics, Jagiellonian University, Reymonta 4, 30-059 Kraków, Poland

Keywords: X-ray absorption anisotropy, wavelet transform, atomic structure

*e-mail: dawid.tadeusz.dul@uj.edu.pl

X-ray absorption anisotropy (XAA) is a holographic-like imaging method that originates from the interference of an incident plane wave with spherical waves scattered from atoms inside the sample. Because of this interference the total x-ray field at the atomic absorbing sites is modified, and thus the absorption cross section changes with the relative orientation of the incident beam and the sample. The usage of broad-band polychromatic x-ray radiation enables one to interpret XAA patterns as quasi-real space projections of the local atomic structure.

As a holographic method, XAA solves the phase problem common in the traditional diffractive x-ray experiments and, in principle, allows one to obtain element sensitivity. However, analysis of XAA patterns still presents a challenge for experimenters. Some current reconstruction methods involve direct comparison of data with the geometrical projections of the crystallographic structure or a tomographic algorithm. The first approach gives only qualitative information as projections of atomic planes and directions are distorted by remnant diffraction. The second technique is on the other hand limited to cubic samples. Recently, a new approach was proposed in [1, 2], where the use of the continuous spherical wavelet transform was presented. This approach is constantly under development.

In this work we present a detailed study of the application of the spherical wavelet transform to the analysis of simulated, white-beam XAA patterns. Simulations have been performed for the hardest x-ray wigglers in operation. A new approximation to the x-ray spectrum (based on the Gumbel distribution) was proposed which accounts for its strongly skewed nature. Analytic formulas were derived for the wavelet filter and the resolution in both the radial and angular directions from the absorber.

As an example, it was shown that the wavelet filter can be effectively used to determine the projections of the local atomic structure in the GaN crystal (Figure 1). Potential applications of XAA

such as polarity determination or imaging of local structure around magnetic ions in the GaN matrix were thoroughly investigated.

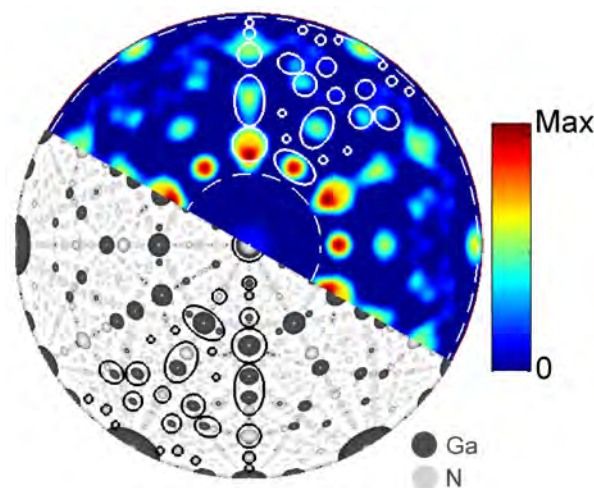


Figure 1: Projection of the local atomic structure around Ga atoms in the GaN crystal obtained with the wavelet transform filter from a simulated XAA pattern (top right), crystal view from the inside (bottom left). Circles and ellipses mark the nearest surrounding of Ga atoms.

Acknowledgments: This work was supported by the Polish National Science Center (DEC-2011/01/B/ST3/00506).

References

- [1] P. Korecki, D.V. Novikov, M. Tolkiehn, "Projections of local atomic structure revealed by wavelet analysis of x-ray absorption anisotropy," *Phys. Rev. B* **80** (2009) 014119.
- [2] P. Korecki, M. Tolkiehn, K.M. Dabrowski, D. V. Novikov, "Fluorescence detection of white beam x-ray absorption anisotropy: Towards element sensitive projections of atomic structure," *J. Synchrotron Radiat.* **18** (2011) 851.

STRUCTURAL CHARACTERIZATION OF THE CORE-SHELL ZnTe/ZnMgTe NANOWIRES

E. Dynowska^{1*}, J.Z. Domagała¹, P. Romanowski¹, E. Janik¹, P. Wojnar¹, and W. Caliebe²

¹*Institute of Physics, Polish Academy of Sciences, al. Lotników 32/46, PL-02668 Warszawa, Poland*

²*HASYLAB at DESY, Notkestr. 85, D-22603 Hamburg, Germany*

Keywords: synchrotron radiation, X-ray diffraction, nanowires, MBE, II-VI compounds

**e-mail: dynow@ifpan.edu.pl*

Semiconductor nanowires (NWs) can be used to build effective nanosensors and photovoltaic devices due to their extremely large the surface-to-volume ratio. On the other hand, the surface defects, especially surface states, significantly reduce the carrier lifetime and degrade the optoelectronic device performance. Therefore, a surface passivation is of a great importance, especially for ZnTe NWs which oxidize easily. Such passivation can be achieved by forming a shell of a large band gap material around the NW so the surface states are moved away from the charge carriers confined in the core.

In this work we present the results of structural characterization of seven samples of the core-shell ZnTe/Zn_{1-x}Mg_xTe NWs grown by MBE technique on the GaAs(111) substrate. The ZnTe NWs were grown at the temperature of about 470°C according to the procedure described in [1]. The Zn_{1-x}Mg_xTe shells were produced immediately after the growth of the ZnTe cores. In order to produce such shells the substrate temperature was reduced to the value (260 – 320°C) which stops the axial growth of NWs and forces the radial growth of Zn_{1-x}Mg_xTe shell.

The X-ray measurements were performed using synchrotron radiation at the W1 beamline at DESY-HASYLAB. The monochromatic X-ray beam of wavelength $\lambda = 1.54056 \text{ \AA}$ was used. Two modes of measurement were applied: symmetrical $2\theta - \omega$ scan and coplanar 2θ scan in the glancing incidence geometry [2]. The results of measurements in $2\theta - \omega$ mode confirmed that the crystallographic orientation of the substrate forces the orientation of NWs — three orders of reflections from (111) lattice planes from GaAs substrate and from NWs are visible. The measurements in the glancing incidence geometry show the relatively thin polycrystalline layer grown on the substrate between NWs. The peaks originate from ZnTe and Zn_{1-x}Mg_xTe phases, respectively. A zoom of the symmetrical patterns in the vicinity of 333 NW peaks allows to notice their splitting. This splitting indicates the

monocrystalline character of the Zn_{1-x}Mg_xTe shell with the same crystallographic orientation as that of the ZnTe core. The lattice parameters of ZnTe core and Zn_{1-x}Mg_xTe shell have been calculated from the position of the peaks related to the core and shell, respectively. For all samples, the lattice parameter of the ZnTe core was larger than that for the uncovered ZnTe NWs [3]. It is the result of the strain induced in the core by the lattice mismatched shell. Schematic model of the strain induced in the core is proposed.

Acknowledgments: This work was supported by the European Community-Research Infrastructure Action under the FP6 “Structuring the European Research Area” Programme (through the Integrated Infrastructure Initiative “Integrating Activity on Synchrotron and Free Electron Laser Science,” Contract RII3-CT-2004-506008), the European Union within European Regional Development Fund through Innovative Economy grant (POIG.01.01.02-00-008/08) and National Centre of Science (Poland) grant DEC-2011/01/D/ST5/05039.

References

- [1] E. Janik, P. Dłużewski, S. Kret, A. Presz, H. Kirmse, W. Neumann, W. Zaleszczyk, L.T. Baczewski, A. Petrouchik, E. Dynowska, J. Sadowski, W. Caliebe, G. Karczewski, T. Wojtowicz, “Catalytic growth of ZnTe nanowires by molecular beam epitaxy: Structural studies,” *Nanotechnology* **18** (2007) 475606.
- [2] E. Dynowska, W. Szuszkiewicz, J.Z. Domagała, E. Janik, M. Wiater, G. Karczewski, T. Wojtowicz, W. Caliebe, *Structural characterization of MBE grown ZnTe nanowires* (HASYLAB Annual Reports 2006 p756).
- [3] E. Dynowska, W. Szuszkiewicz, J.Z. Domagała, E. Janik, A. Presz, T. Wojtowicz, G. Karczewski, W. Caliebe, “X-ray characterization of catalytically grown ZnTe i ZnMgTe nanowires,” *Radiat. Phys. Chem.* **78** (2009) 120.

OBSERVATION OF EXTREMELY SLOW ORDERING EFFECTS
IN Co-IMPLANTED ZnOE. Dynowska^{1*}, W. Paszkowicz¹, P. Aleshkevych¹, L. Gładczuk¹, W. Szuszkiewicz¹,
S. Müller², C. Ronning³, and W. Caliebe⁴¹*Institute of Physics, Polish Academy of Sciences, al. Lotników 32/46, 02–668 Warszawa, Poland*²*II. Physikalisches Institut, Universität Göttingen, Friedrich-Hund-Platz 1, 37077 Göttingen, Germany*³*Institut für Festkörperphysik, Universität Jena, Max-Wien-Platz 1, 07743 Jena, Germany*⁴*Hasylab at DESY, Notkestr. 85, D–22603 Hamburg, Germany**Keywords: synchrotron radiation, X-ray diffraction, ZnO, implantation, cobalt***e-mail: dynow@ifpan.edu.pl*

The partial substitution of the nonmagnetic Zn ions in ZnO by magnetic transition metal (TM) ions (Fe, Mn, Co and Ni) was predicted to be a way towards room temperature ferromagnetism. One of the methods for the incorporation of TM into ZnO is ion implantation. However, for recovering the radiation-damaged ZnO lattice, post-implantation annealing is needed. In the case of relatively high TM doses such annealing can cause the formation of secondary phase precipitates which may have interesting magnetic properties as noted in Ref. [1].

In previous reports [1]–[3] we described the results of studies of TM containing ZnO layers formed by implantation of TM ions (TM = Mn, Fe, Co and Ni) into ZnO single crystals, with intentional atomic ratio $x = \text{TM}/(\text{Zn} + \text{TM} + \text{O})$ of 0.04 to 0.16, annealed at 700°C [1] and 900°C [1, 2], respectively. In this presentation we concentrate on the structural aspects of those studies with special consideration of ZnO sample implanted with Co ($x = 0.16$) annealed at 900°C in air for 15 – 30 min.

The X-ray structural characterization was performed using synchrotron radiation at the W1.1 beamline at DESY-Hasylab. The monochromatic X-ray beam of wavelength $\lambda = 1.54056 \text{ \AA}$ was used. Magnetization measurements were made with a superconducting quantum interference device (SQUID) at temperatures 5 and 300 K.

The results of the first measurements performed with the use of synchrotron radiation in 2008 were presented in [1, 2]. According to the cited results, the existence of secondary phases ZnMn_2O_4 , ZnFe_2O_4 and $\text{Ni}_{0.8}\text{Zn}_{0.2}\text{O}$ was confirmed for the samples implanted with Mn, Fe and Ni, respectively. In the case of Co-implanted samples, the X-ray diffraction did not reveal any secondary phase.

However, the measurements cyclically repeated during two years for the Co-implanted crystal, with a period of about 6 months revealed that new relatively strong reflections appear and grow with elapsing time (for Mn, Fe and Ni implanted samples, no time evolution is observed). The observed new diffraction peaks indicate a development of a new,

monocrystalline or quasi-monocrystalline phase in the implanted area. The lattice planes of this phase (with spacing 10.747 Å) are oriented in parallel to the (0001) planes of ZnO host. This means that new, oriented phases form not only for Mn, Fe, and Ni implanted ZnO, but also for Co implanted ZnO. The difference is that for Co-implanted ZnO, the phase formation process is very slow, in the month timescale. Generally, the presence of a set of diffraction peaks from an oriented layer does not allow unambiguous identification of a phase. Nevertheless, the attempts of understanding of the implanted layer structure led to finding a possible solution of the problem, which will be presented and discussed.

Acknowledgments: This work was supported by the European Community — Research Infrastructure Action under the FP6 “Structuring the European Research Area” Programme (through the Integrated Infrastructure Initiative “Integrating Activity on Synchrotron and Free Electron Laser Science,” Contract RII3-C-2004-506008) and by the Polish Ministry of Science and Higher Education from funds for science for 2009 – 2012 years, under a research project (0809/B/T02/2009/37).

References

- [1] M. Schumm, M. Koerdel, S. Müller, C. Ronning, E. Dynowska, Z. Gołacki, W. Szuszkiewicz, J. Geurts, “Secondary phase segregation in heavily transition metal implanted ZnO,” *J. Appl. Phys.* **105** (2009) 083525.
- [2] E. Dynowska, W. Szuszkiewicz, C. Ziereis, J. Geurts, S. Müller, C. Ronning, J. Domagala, P. Romanowski, W. Caliebe, “Structural studies of heavily transition metal implanted ZnO,” *8th National Symposium of Synchrotron Users, Poland, Synchr. Radiat. Nat. Sci.* **8** (2009), No. 1 – 2, 47.
- [3] J. Geurts, M. Schumm, M. Koerdel, C. Ziereis, S. Müller, C. Ronning, E. Dynowska, Z. Gołacki, W. Szuszkiewicz, “Annealing effects and generation of secondary phases in ZnO after high-dose transition metal implantation,” *Phys. Stat. Sol. B* **247** (2010) 1249.

XANES EVALUATION OF IRON LOCAL STRUCTURES IN MONOMER AND DIMERISED FORMS OF PORPHYRINS

K. Dziedzic-Kocurek* and J. Stanek

M. Smoluchowski Institute of Physics, Jagiellonian University, Reymonta 4, 30-059 Kraków, Poland

Keywords: synchrotron radiation, XANES, porphyrins

**e-mail: k.dziedzic-kocurek@uj.edu.pl*

There is a great deal of evidence that the biological function of the heme proteins is determined by the convoluted conformational and electronic properties of the heme group. Various spectroscopic methods have supplied valuable information about the active site of the heme proteins, but they cannot by themselves yield a detailed and consistent description at the molecular level. In no other class of proteins so much effort has been devoted to find a relationship between structure, function and the properties of the active constituent [1]-[3]. Starting from the preparation stage, the variety of slightly differing porphyrin complexes, in respect of their energetic form, causes basic complications in their analysis. Each of the prepared / synthesized complexes is individual, and the properties depend on the details of the preparation. One of the most interesting features of porphyrins is how small variations of the basic structural tetrapyrrolic macrocycle lead to a wide diversity of biochemical functions.

The aim of the project is to study iron local states in compounds that reveal slightly different structures. The crucial compound in performed analysis was protoporphyrin IX, its monomer and dimerised form substituted with iron. Iron substituted PPIX (protoporphyrin IX) is a “real part” of the heme, while mostly heme-model investigations are based on TPP (tetraphenylporphyrin) that in fact differs from an actual heme-building compound (differences in ligands). The EXAFS and XANES analysis of the PPIX-based compounds have been already reported [4].

However, due to the complex structure of a studied dimerised form of Fe-PPIX (it is a synthesized compound, that contains partially monomer admixture) it was important to compare obtained results with a pure monomer and dimerised compounds. As the standard compounds TPP derivatives has been selected. Nevertheless, provides information on Fe-PPIX-Cl and its dimerised derivatives, which are the most adequate model compound for the haemoglobin.

The dimerisation reduces the *s*-electron density at the Fe nuclei and shifts the absorption edge as

measured by the XANES spectra (Fig. 1). Also, a different rising edge respect to dimerised compound, suggesting a different and larger charge transfer of the samples containing Fe-O-Fe bridges, has been shown. Additionally, supporting Mössbauer spectroscopy studies have been also performed.

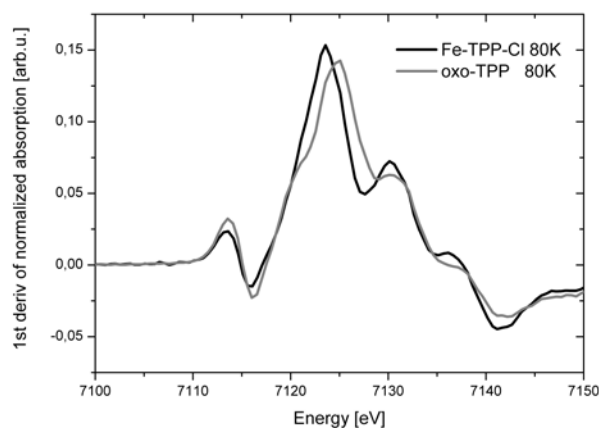


Figure 1: The first derivative of the edge region of the XANES spectra.

Acknowledgments: This work has been supported by HASYLAB-DESY under the contract RII3-CT-2004-506008 and by EC (FP7/2007 – 2013) under grant agreement n° 312284 (DESY, Hamburg).

References

- [1] J.E. Penner-Hahn, K.O. Hodgson, *Iron Porphyrins, Part III* (VCH Publishers, New York 1989).
- [2] A. Bianconi *et al.*, “XANES study of iron displacement in heam of myoglobin,” *FEBS Lett.* **178** (1884) 165 – 170.
- [3] P. D’Angelo *et al.*, “X-Ray absorption spectroscopy of hemes and hemeproteins in solution: Multiple scattering theory,” *Inorg. Chem.* **47** (2008) 9905 – 9918.
- [4] K. Dziedzic-Kocurek, J. Stanek, K. Burda, “Dynamics of iron in Fe-porphyrin aggregates studied by X-ray absorption and Mössbauer spectroscopy,” *Hyperfine Interact.* **185** (2008) 87 – 93.

ELASTIC PROPERTIES OF PRASEODYMIUM ORTHOVANADATE

O.N. Ermakova^{1,2*}, R. Minikayev¹, H. Dabkowska³, C. Lathe^{4,5},
J. de Groot⁶, and W. Paszkowicz¹

¹*Institute of Physics, Polish Academy of Sciences, Al. Lotnikow 32/46, 02-668 Warsaw, Poland*

²*Institute of Solid State Chemistry, Russian Academy of Sciences,
Pervomayskaya 91, 620990 Ekaterinburg, Russia*

³*Department of Physics, McMaster University, Hamilton, Ontario, L8S 4M1 Canada*

⁴*HASYLAB am DESY, Notkestrasse 85, D-22603 Hamburg, Germany*

⁵*Helmholtz Centre Potsdam, GFZ German Research Centre for Geosciences,
Telegrafenberg, 14473 Potsdam, Germany*

⁶*Institut für Festkörperforschung, JCNS, and JARA-FIT, Forschungszentrum
Jülich GmbH, 52425 Jülich, Germany*

Keywords: synchrotron radiation, rare-earth orthovanadates, bulk modulus, equation of state

**e-mail: Ermak@ifpan.edu.pl*

Rare-earth orthovanadates (RVO₄) are known to be applicable as laser materials. Their physical properties lead to applications in other optical devices, gas sensors, phosphors, polarizers, etc.; they are also useful in catalysis [1]-[6]. At ambient conditions RVO₄ adopt the zircon structure (space group $I4_1/amd$), except for LaVO₄ exhibiting polymorphism depending on preparation conditions. In the 5 – 10 GPa pressure range these materials undergo a phase transition from zircon to scheelite-type structure.

The aim of the present investigation was to determine the elastic properties of PrVO₄ at pressures from ambient up to 5 GPa, using the synchrotron beam, and to verify whether the zircon-scheelite phase transition occurs at the applied conditions. For this purpose, energy dispersive data at high-pressure conditions were collected using white synchrotron radiation at the F2.1 beamline Hasylab/DESY (Hamburg, Germany). The in-situ powder-diffraction experiments were carried out using the MAX80 X-ray diffraction press. The data were collected using a germanium solid-state detector. The diffraction angle was fixed at angle 3.793°. For calibration of the applied pressure NaCl powder was used. Unit cell parameters for PrVO₄ were refined using the Le Bail method. Bulk modulus was calculated from fitting of the second order Birch-Murnaghan equation of state.

The studied needle-shaped single crystal was grown by slow cooling of the molten PbO/PbF₂ flux. For high-pressure powder diffraction experiment, this crystal was finely ground in an agate mortar. In order to reduce strains in the diffraction experiment, the obtained powder was mixed with vaseline in volume proportion 1:1.

At ambient conditions, the lattice parameters of the studied zircon-type PrVO₄ crystal are in good agreement with literature data. In pressure range from ambient up to 5 GPa, the observed lattice

parameters smoothly decrease with increasing pressure; the total decrease of the unit-cell volume is at the level of 4.5%. Phase transition to scheelite structure is not observed within the studied pressure range.

Acknowledgments: The measurements performed at Hasylab have received funding from the 7th Framework Programme (FP7/2007 – 2013) of European Community under ELISA grant agreement No. 226716.

References

- [1] R.A. Fields, M. Birnbaum, and C.L. Fincher, "Highly efficient Nd: YVO diode-laser end-pumped laser," *Appl. Phys. Lett.* **51** (1987) 1885.
- [2] A.I. Zagumennyi, V.G. Ostroumov, I.A. Shcherbakov, T. Jensen, J.P. Meyen, and G. Huber, "The Nd: GdVO₄ crystal: A new material for diode-pumped lasers," *Sov. J. Quantum Electron.* **22** (1992) 1071.
- [3] A.A. Kaminskii, K. Ueda, H.J. Eichler, Y. Kuwano, H. Kouta, S.N. Bagaev, T.H. Chyba, J.C. Barnes, G.M.A. Gad, T. Murai, and J. Lu, "Tetragonal vanadates YVO₄ and GdVO₄ - new efficient $\chi^{(3)}$ -materials for Raman lasers," *Optics Commun.* **194** (2001) 201.
- [4] E.V. Tsipis, M.V. Patrakeev, V.V. Kharton, N.P. Vyshatko, J.R. Frade, "Ionic and p-type electronic transport in zircon-type Ce_{1-x}A_xVO_{4±δ} (A = Ca, Sr)," *J. Mater. Chem.* **12** (2002) 3738.
- [5] M. Yu, J. Lin, S.B. Wang, "Effects of x and R³⁺ on the luminescent properties of Eu³⁺ in nanocrystalline YV_xP_{1-x}O₄:Eu³⁺ and RVO₄:Eu³⁺ thin-film phosphors," *Appl. Phys. A: Mater. Sci. Proc.* **80** (2005) 353.
- [6] F. Chen, X. Wang, S. Li, G. Fu, K. Wang, Q. Lu, D. Shen, R. Nie, and H. Ma, "Low-loss optical planar waveguides in YVO₄ produced by silicon ion implantation at low doses," *J. Appl. Phys.* **94** (2003) 4708.

SIMULATIONS OF X-RAY TRANSMISSION IN POLYCAPILLARIES FOR SYNCHROTRON RADIATION APPLICATIONS

P. Jagodziński^{1*}, M. Pajek², D. Banaś², A. Kubala-Kukuś², J. Szlachetko^{2,3}, J.-Cl. Dousse⁴,
J. Hoszowska⁴, Y. Kayser⁴, and S. Nowak⁴

¹*Department of Physics, Kielce University of Technology, Tysiąclecia PP 7, 25–314 Kielce, Poland*

²*Institute of Physics, Jan Kochanowski University, Świętokrzyska 15, 25–406 Kielce, Poland*

³*Swiss Light Source, Paul Scherrer Institute (PSI), 5232 Villigen, Switzerland*

⁴*Department of Physics, University of Fribourg, Chemin du Musée 3, CH–1700 Fribourg, Switzerland*

Keywords: Monte-Carlo simulations, ray-tracing, X-ray polycapillary optics, external total reflection, synchrotron radiation

* e-mail: jagodzin@tu.kielce.pl

Polycapillary optics is a widely used technology for forming and guiding X-ray beams. In recent years the development of the polycapillary optics has become an active direction for X-ray research due to its wide potential applications in many fields, such as X-ray diffraction and fluorescence techniques and X-ray focusing optics for synchrotron radiation. The polycapillary consists of thousands of hexagonal glass tubes curved and arranged in the space. The incident X-rays can be transmitted in polycapillary by multiple total reflections on the internal surface of the tubes occurring at glancing angle smaller than the critical angle of total external reflection [1].

The main parameters describing the polycapillary properties are the transmission efficiency, the divergence of outgoing photon beam, the focal distance and spot size. The polycapillaries can be used for focusing a parallel beam, e.g. a synchrotron radiation beam, and for forming a parallel beam of photons emitted from a localized (e.g. point-like) X-ray source. Generally, the properties of the X-rays beam transmitted through a polycapillary depend on the source size and the energy of the X-rays as well as a shape of the polycapillary, length, focal distance and the sizes of its entrance and exit openings (Fig. 1). The other factors affecting the transmission process include the capillary material quality and surface roughness.

The influence of the above mentioned factors on the polycapillary properties were studied in the present work by using the Monte-Carlo simulation technique. The aim of this research was to develop the software to predict and visualize the process of propagation of X-rays through a polycapillary optical system. The present calculations can predict a distribution of X-rays transmitted by a polycapillary at arbitrary position behind its exit plane. In the Monte-Carlo calculations different properties of a transmitted photon beam were discussed in details. Consequently, the transmission efficiency, photon beam divergence, sizes of focal distance and spot were calculated for various X-ray energies in the range 1 – 10 keV. Generally, the Monte-Carlo simulations predict reasonable well the main char-

acteristics of the polycapillary and the parameters of the outgoing photon beam.

Performed calculations were compared with experimental results concerning the application of polycapillary X-ray optics for focusing of synchrotron radiation and excited in the sample X-ray fluorescence. In particular, simulations of the properties of a polycapillary based flat-crystal X-ray wavelength dispersive spectrometer (WDS) [2] installed at the ESRF ID21 X-ray Micro-spectroscopy Beamline and, in second case, a polycapillary used for focusing of the synchrotron radiation beam for grazing emission X-ray fluorescence (GEXRF) experiments [3] at ID21 beamline using a high-resolution von Hamos spectrometer [4] will be described in details. Finally, the results obtained using discussed polycapillary X-ray optics will be presented.

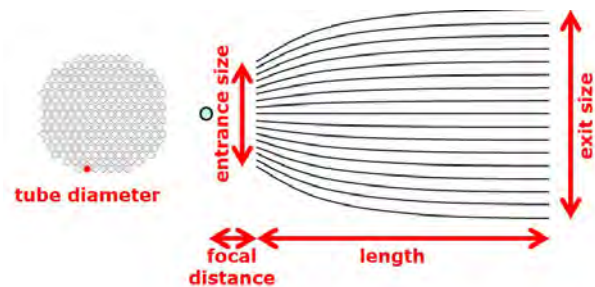


Figure 1: Input parameters for polycapillary simulations.

References

- [1] R. Klockenkämper, *Total-Reflection X-ray Fluorescence Analysis* (Wiley Interscience, John Wiley & Sons, USA, 1997).
- [2] J. Szlachetko *et al.*, “Wavelength-dispersive spectrometer for X-ray micro-fluorescence analysis at the X-ray Microscopy beamline ID21 (ESRF),” *J. Synchrotron Rad.* **17** (2010) 400 – 408.
- [3] Y. Kayser *et al.*, “Depth profiling of low energy P, In and Sb implants using synchrotron radiation based high-resolution micro-GEXRF,” EGAS 2011 conf.
- [4] J. Hoszowska *et al.*, “High Resolution von Hamos Crystal X-ray Spectrometer,” *Nucl. Instrum. Methods Phys. Res.* **A 376** (1996) 129 – 138.

CRYSTAL STRUCTURES OF MOUSE THYMIDYLATE SYNTHASE IN BINARY COMPLEX WITH A STRONG INHIBITOR, N(4)-OH-dCMP, AND TERNARY COMPLEX WITH N(4)-OH-dCMP AND THE COFACTOR PRODUCT, DIHYDROFOLATE

A. Jarmuła^{1*}, A. Dowierciał¹, P. Wilk¹, W.R. Rypniewski², B. Kierdaszuk³, and W. Rode¹

¹Nencki Institute of Experimental Biology, Polish Academy of Sciences,
3 Pasteur Str., 03–092 Warszawa, Poland

²Institute of Bioorganic Chemistry, Polish Academy of Sciences,
12–14 Noskowskiego Str., 61–704 Poznań, Poland

³Institute of Experimental Physics, Warsaw University, 93 Żwirki i Wigury Str., 02–089 Warszawa, Poland

Keywords: synchrotron radiation, inhibitor, thymidylate synthase, enzyme-ligand-cofactor complex

* e-mail: a.jarmula@nencki.gov.pl

Thymidylate synthase (TS; EC 2.1.1.45), an enzyme serving as a target in chemotherapy, catalyzes the conversion of 2'-deoxyuridine-5'-monophosphate (dUMP) to 2'-deoxythymidine-5'-monophosphate (dTMP), involving the reductive methylation of N(5,10)-methylene tetrahydrofolate (mTHF), functioning as both methyl donor and reducing agent.

N(4)-OH-dCMP is a substrate analogue, being a potent mTHF-dependent, thus mechanism-based, slow-binding inhibitor of TS ($K_i \sim 50$ nM). Incubated with the enzyme and the cofactor, N(4)-OH-dCMP was shown to form a ternary complex, similar to the classical TS inhibitor, FdUMP. However, when N(4)-OH-[5-³H]dCMP replaced dUMP in the reaction mixture, ³H abstraction from the uracil C(5) atom was not apparent, suggesting the reaction to be inhibited at an earlier stage than with FdUMP. In solution the equilibrium between rotamers around the C(4) = N(4) bond is significantly shifted toward the *syn* rotamer, but surprisingly only the *anti-imino* form, with the -OH group on the side of C(5), appeared to be the active inhibitor form.

In order to learn more about the inhibition mechanism, X-ray crystallographic studies of TS complexes with N(4)-OH-dCMP were undertaken. Structures of three mouse TS (mTS) complexes with the inhibitor were solved, based on crystals formed by the enzyme protein in the presence of either only N(4)-OH-dCMP (measured to 1.75 Å resolution) or both N(4)-OH-dCMP and mTHF (two crystals measured to resolutions of 1.35 Å and 1.17 Å). The structure of the mTS-N(4)-OH-dCMP complex was found to be closely similar to the corresponding structure of the native complex, mTS-dUMP. The both other structures showed the enzyme to be involved in a ternary complex with N(4)-OH-dCMP and non-covalently bound dihydrofolate (DHF), instead of expected mTHF, suggesting the inhibition to be a consequence of an abortive enzyme-catalyzed reaction, involving a transfer of

the one-carbon group to an as yet unknown site and reduction of mTHF to DHF. The structures showed no indication of proton release from the C(5) inhibitor atom. Instead, both the C(5) and C(6) atoms showed an *sp*³ hybridization, suggesting reduction and subsequent presence of second proton at C(5). In accord with our previous results, in all three complexes the molecule of N(4)-OH-dCMP was found in the *anti* rotameric form, with the latter probably playing a role in the mechanism of ligand recognition by TS.

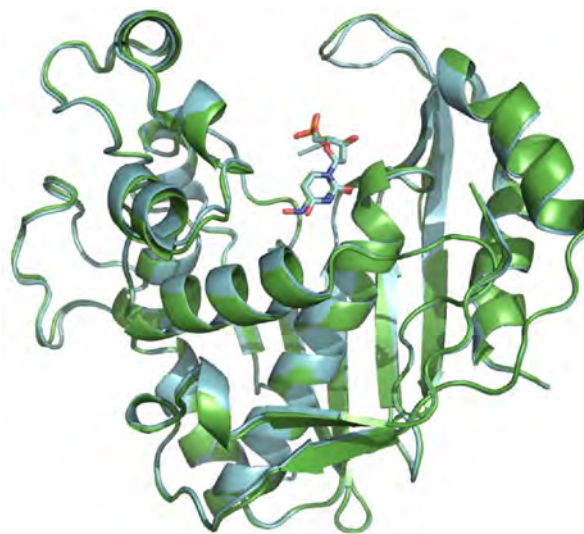


Figure 1: Superimposition of the subunits A of the crystal structures of the complexes between mTS and N(4)-OH-dCMP (green), and mTS and dUMP (light blue). The atoms of nitrogen, oxygen and phosphorus in the ligands are colored blue, red and orange, respectively.

Acknowledgments: Supported by the National Science Centre (grant No. 2011/01/B/NZ6/01781) and the Ministry of Science and Higher Education (grant No. N301 3948 33).

LINAC AND STORAGE RING MAGNETS FOR SOLARIS SYNCHROTRON

M. Johansson¹, R. Nietubyc^{2,3*}, and A. Wawrzyniak²¹Max IV Laboratory, Ole Römers väg 1, S-22100 Lund, Sweden,²National Synchrotron Radiation Centre "Solaris", Jagiellonian University, Gronostajowa 7/p.1.6, PL-30387 Kraków, Poland³National Centre for Nuclear Research Świerk, ul. Sołtana 7, PL-04400 Otwock, Poland

Keywords: linac, storage ring, magnetic lattice

*e-mail: robert.nietubyc@uj.edu.pl

The most desired feature of the electron accelerators feeding modern synchrotron radiation sources is a low emittance of an electron beam, because it enables brightness and coherence of the generated photon beam. Low emittance can be achieved with the enhancement of the focusing. Max IV [1]-[4] concept followed by the Solaris, offers the strong focusing of the stored beam achieved for relatively small dimension of the ring. Each of twelve symmetric, doubly bent achromats, contains thirteen magnets. Six of them produce magnetic fields having mixed harmonics: dipole with quadrupole and quadrupole with sextupole, respectively. For each achromat, the electromagnetic radiation is extracted from the first 15°-bending dipole through the photon beamlines led out with the angles of 3° and 7.5°. The yokes and poles of all achromat magnets are cut from a single, 5 m long block of iron. That solution assures high accuracy and stability in mutual positioning of particular magnet units. That, in turn, enables the small apertures, 20 mm × 40 mm and 28 mm × 56 mm, and thus a strong magnetic field. Strong field is advantageous not for electron optics only, but for insertion devices as well. On the other hand, possible interaction between magnets is to be analysed. For the entire ring, all magnets of the same type are powered from the same power supply.

Solaris linac includes three sections: pre-injector, linear accelerator and transfer line. In the pre-injector, two gradient dipoles settled together with flanking quadrupoles on both sides of the energy slit, perform the energy filtration and compression of the freshly emitted electron bunch. In the linear accelerator the beam is controlled with the system of focusing and defocusing quadrupoles inserted between accelerating modules. Eventually, the beam is elevated up to the ring plane with

the doubly bent transfer line containing septa and dipoles in the turns, and quadrupoles in the straight section.

Solaris linac will differ from that of Max IV in the number of accelerating modules and in distribution and excitation of magnets, however it will be built from the same magnets models. In the first phase of operation, low electron energy provided by the linac will be ramped in the ring. In such a case, the achromat magnets will work in the magnetic field magnitudes corresponding to the electron energy ranged from 550 MeV up to 1500 MeV. That invokes the analysis of possible saturation effects.

Preparation of magnetic design included iterative two-dimensionally magnetic field calculations performed using final elements code FEMM. Obtained results, were used as an input for the three-dimensional modeling with the Opera software. The poles shapes and apertures of particular magnets and magnets positions providing the desired optical parameters of the lattice were calculated and optimized taking into account mechanical constraints imposed by the vacuum system and reasonable machining tolerances. The coils were designed and, for water cooled magnets in the achromats, requirements for the cooling circuit were determined.

References

- [1] A.I. Wawrzyniak *et al.*, *Injector Layout and Beam Injection into Solaris*. San Sebastian: IPAC'11, 2011. THPC 123.
- [2] S.C. Leemann, MAX-lab Internal Note 20120313, Updates to the MAX IV 1.5 GeV Storage Ring Lattice.
- [3] M. Johansson, Private Communication.
- [4] A.I. Wawrzyniak, Internal report, Solaris injector, v.4.2, 19.04.2012.

XRD STUDY OF UNIFORMITY AND INTERDIFFUSION IN PdCo AND PdAg NANOALLOYS

Zbigniew Kaszkur*

Institute of Physical Chemistry PAS, Kasprzaka 44/52, 01-224 Warszawa, Poland

* e-mail: zbig@ichf.edu.pl

Nanoalloys of PdCo and PdAg may have a very interesting physical and chemical properties. PdCo can be ferromagnetic as Pd nanocrystals alone may become ferromagnetic and Co doping stabilizes this property, leading to a potential applications in magnetic storage media and electrical spin injection [1]. On the other hand both nanoalloys are known as a good catalyst e.g. in formic acid oxidation to be applied in formic acid fuel cells [2, 3]. PdAg is effective as a catalyst in hydrogenation and hydrodechlorination reactions [4]. Palladium contents within the alloy offers a simple way to test uniformity of the studied material. Exposition of the sample to hydrogen at RT leads to transition of Pd and its diluted alloys to a hydride phase with the lattice constant increase dependent on concentration. Any observation of a broad, structured XRD reflection may indicate presence of microvolumes of alloy with different metal-companion concentration (Figure 1). A gas-phase controlled temperature-programmed experiment may reveal information on sintering kinetics as well as kinetics of segregation.

For all practical applications phenomena of surface segregation and phase thermal stability is of fundamental importance. From the first observation of the Kirkendall effect [5] it is believed that the random walk metal transport phenomena proceed through vacancy mechanism. For nanocrystals the vacancy disappearance rate can be higher due to surface effect and this may affect the diffusion rate. Surface segregation in alloys is a special case of

interdiffusion moving up the concentration gradient thus violating the first Fick law. Kinetics of a surface segregation in solids could be estimated on the basis of Auger Electron Spectroscopy data [e.g. 6 for Ag in Cu]. The in situ XRD offers a unique opportunity to observe its time evolution e.g. when reversal of segregation is induced by chemisorption.

We present several experimental results shedding some light on the uniformity of the studied alloys as well on the interdiffusion rate for several 20 wt.% Pd₃Co supported on carbon (samples courtesy of prof. KuanWen Wang, Taiwan) and Pd₇Ag₃ supported on silica and metallic sponge sample.

References

- [1] D.B. Roa, I.D. Barcelos, A. de Siervo, K.R. Pirota, R.G. Lacerda, and R. Magalhães-Paniago, *Appl. Phys. Lett.* **96** (2010) 253114.
- [2] D. Morales-Acosta, M.D. Morales-Acosta, L.A. Godinez, L. Alvarez-Contreras, S.M. Duron-Torres, J. Ledesma-Garcia, L.G. Ariaga, *J. Power Sources* **196** (2011) 9270.
- [3] Yizhong Lu, Wei Chen, *ACS Catalysis* **2** (2012) 84.
- [4] B. Heinrichs, F. Noville, J-P. Schoebrechts, J-P. Pirard, *J. Cat.* **192** (2000) 108.
- [5] A.D. Smigelskas, E.O. Kirkendall, *Trans. AIME* **171** (1947) 130.
- [6] C. Girardeaux, G. Clugnet, Z. Erdelyi, J. Nyeki, J. Bernardini, D. Beke, A. Rolland, *Surf. Interface Anal.* **34** (2002) 389.

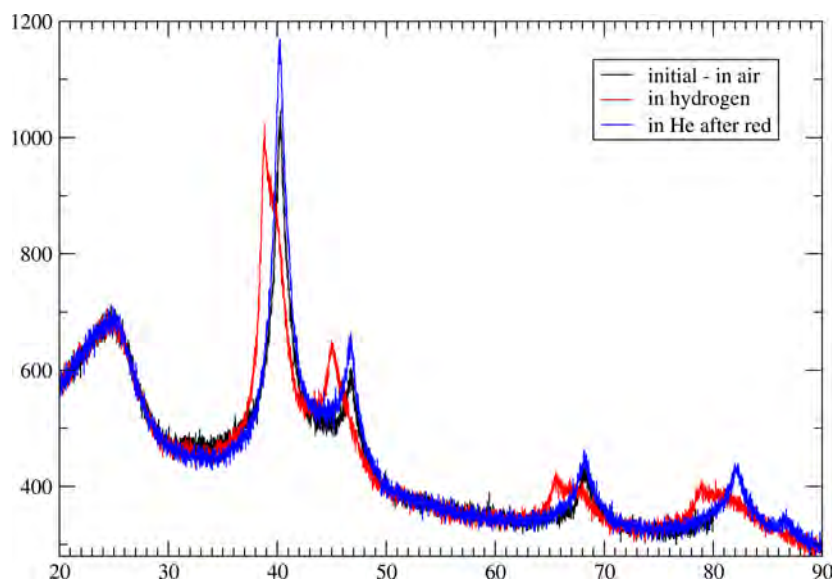


Figure 1: XRD in situ patterns of a sample of Pd₃Co/C. Intensity vs. scattering angle (CuK α).

INFLUENCE OF GEMINI SURFACTANTS WITH DIFFERENT CHAIN LENGTH ON THE STRUCTURE OF DPPC BILAYERS

W. Kida and M. Kozak*

Department of Macromolecular Physics, Faculty of Physics, Adam Mickiewicz University,
Umultowska 85, 61-614 Poznań, Poland

Keywords: gemini surfactants, phospholipids, FTIR

*e-mail: mkozak@amu.edu.pl

The miscibility properties of different lipids and formation of hydrated bilayer belong to fundamental problems in biotechnology and biology. Physical and functional properties of biomembranes are closely related to the miscibility of various kinds of lipids in them [1, 2]. Dipalmitoylphosphatidylcholine (DPPC) belongs to phospholipids, which make a class of lipids and are major components of all cell membranes as they are able to form lipid bilayers. One of the major substances that can strongly interact with phospholipids and change their structural behavior are gemini surfactants. Gemini surfactants are characterised with dimeric architecture of molecules made of two hydrophobic tails and two hydrophilic (polar) head groups [3, 4].

The study reported was undertaken to examine the influence of quaternary alkyl-derivatives of bisimidazolium with different spacers and alkyl chain lengths at various concentrations on the structure and phase stability of dipalmitoylphosphatidylcholine in aqueous solutions.

The data presented were collected using CONFOCHECK system. This system is based on FTIR Bruker spectrometer TENSOR 27 equipped with an AquaSpec micro transmission cell. The FTIR data were collected in the temperature range from 277 to 329 K using a HAAKE DL30 thermostat. For each spectrum, 128 scans in the spectral range 4000 – 950 cm^{-1} were collected with the resolution of 2 cm^{-1} . The original FTIR spectra were smoothed using the Savitzky-Golay method.

The surfactants studied disturbed the lamellar phase typical of DPPC and finally, for the highest

surfactant concentration, the formation of unilamellar vesicles - bicelles. With increasing length of the acyl chain the temperature of the main phase transition was shifted towards lower temperatures. The same effect was caused by increasing surfactant concentration [5].

Acknowledgments: The study was supported by a research grant from the Ministry of Science and Higher Education (Grant No. N N204 135738).

References

- [1] Tohru Inoue, Yoshinori Nibu, "Miscibility of binary phospholipid mixtures under hydrated and non-hydrated conditions. IV. Phosphatidylglycerols with different acyl chain length," *Chem. Phys. Lipids* **76** (1995) 181 – 191.
- [2] M. Bloom, E. Evans, O.G. Mouritsen, "Physical properties of the fluid-bilayer component of cell membranes: A perspective," *Q. Rev. Biophys.* **24** (1991) 293 – 297.
- [3] S.P. Moulik, "Micelles: self-organized surfactant assemblies," *Curr. Sci.* **71** (1996) 368 – 376.
- [4] P. Tyagi, R. Tyagi, "Synthesis, structural properties and applications of gemini surfactants: A review," *Tenside, Surfactants, Deterg.* **46** (2009) 373 – 382.
- [5] J. Krzaczkowska, E. Szcześniak, S. Jurga, "Phase behaviour of dipalmitoylphosphatidylcholine / surfactant / water systems studied by infrared spectroscopy," *J. Mol. Struct.* **794** (2006) 168 – 172.

DAMAGE OF TWO-COMPONENT MATERIALS SUCH AS GaAs, ZnO, SiO₂ CREATED BY ULTRA-SHORT VUV LASER PULSES

D. Klinger^{1*}, R. Sobierajski¹, J. Pelka¹, E. Lusakowska¹, D. Żymierska¹, W. Wierzchowski², K. Wieteska³, T. Balcer², J. Chalupský⁴, V. Hájková⁴, T. Burian⁴, A.J. Gleeson⁶, L. Juha⁴, K. Tiedtke⁷, S. Toleikis⁷, L. Vyšín⁴, H. Wabnitz⁷, and J. Gaudin⁵

¹*Institute of Physics, PAS, 32/46, Al. Lotników Str, 02-668 Warsaw, Poland*

²*Institute of Atomic Energy POLATOM, 05-400 Świerk-Otwock, Poland*

³*Institute of Electronic Materials Technology, 133, Wólczyńska Str, 01-919 Warsaw, Poland*

⁴*Institute of Physics, Academy of Sciences of the Czech Republic, Na Slovance 2, 182 21 Prague 8, Czech Republic*

⁵*European XFEL, DESY, Notkestr., 85 D-22607 Hamburg, Germany*

⁶*CCRLC Daresbury Laboratory, Warrington, Cheshire WA4 4AD, United Kingdom*

⁷*HASYLAB/DESY, Notkestr., 85 D-22607 Hamburg, Germany*

* e-mail: dorota.klinger@ifpan.edu.pl

The investigations of the basic processes taking place in the two-component materials affected by ultra-short laser pulses of VUV range are presented. Those sources give new possibilities for studying matter structure and physical processes dynamics due to a specific combination of radiation parameters — photon energy, ultra-short pulse time and a high power of laser beam. Radiation intensity values many times higher than the values obtained so far allow obtaining an extreme state of matter — warm and dense plasma. Shortening pulse time to femtoseconds caused a change of time frame for phenomena occurring in material — chemical reactions, phase changes as well as near-surface processes in a time frame comparable to periods of natural atom oscillation [1, 2].

First experiments were already carried out, using free-electron-laser for irradiating materials at an experimental station in DESY/Hamburg (results under preparation). A further phase of experiments, which will compare physical processes occurring in materials irradiated by VUV range radiation of time pulse varied from a few up to several femtoseconds generated by free-electron-lasers was conducted in Spring8/Osaka. In order to compare optical parameters (among others: absorption length, irradiation diffusion path) ablation experiments, using single femtosecond pulses of a few up to a few dozen nanometers wavelength.

The present work concentrates on the ablation dynamics in materials, GaAs, SiO₂ and ZnO. For example ZnO is an important wide-bandgap semiconductor, which has many applications, such as piezoelectric transducers and transparent conducting films. It has received extensive attention because of the technological applications in

short-wavelength light-emitting devices and semiconductor spin electronics [3]-[6].

Observations of ablation final result by using compatible methods will allow determining dynamics of ablation process in micron scale. The structural change in the near-surface layer by X-ray diffraction and reflectometry and structure morphology, ablation crater depth and structures created by hydrodynamic movement height study will be carried out using polarizing-interference microscope and atomic force microscope.

Knowing the phenomena occurring in materials under influence of ultra-short radiation pulses of an extreme UV range, explanation of crystal matter change dynamics for femtosecond pulses could make a base for anticipating results of attosecond pulses influence.

References

- [1] S.K. Sundaram, E. Mazur, "Inducing and probing non-thermal transitions in semiconductors using femtosecond laser pulses," *Nature Mater.* **1** (2002) 217.
- [2] L. Jiang, H.L. Tsai, "Energy transport and material removal in wide bandgap materials by a femtosecond laser pulse," *Int. J. Heat Mass Tran.* **48** (2005) 487.
- [3] T. Monteiro, C. Boemare, M.J. Soares, E. Rita, E. Alves, *J. Appl. Phys.* **93** (2003) 8995.
- [4] D.C. Look, D.C. Reynolds, J.W. Hemsley, R.L. Jones, J.R. Sizelove, *Appl. Phys. Lett.* **75** (1999) 811.
- [5] D.C. Look, *Mater. Sci. Eng.* **B 80** (2001) 383.
- [6] H. Yoshikawa, S. Adachi, *Jpn. J. Appl. Phys.* **36** (1997) 6237.

PHOTOEMISSION STUDY OF AMORPHOUS AND CRYSTALLINE GeTe AND (Ge,Mn)Te SEMICONDUCTORS

W. Knoff^{1*}, M.A. Pietrzyk¹, A. Reszka¹, B.A. Orłowski¹, T. Story¹, and R.L. Johnson²

¹*Institute of Physics, Polish Academy of Sciences,
Al. Lotników 32/46, 02-668 Warsaw, Poland*

²*Institute of Experimental Physics, University of Hamburg,
Luruper Chaussee 149, D-22761 Hamburg, Germany*

Keywords: synchrotron radiation, semiconductor, phase change material

*e-mail: knoff@ifpan.edu.pl

IV-V (Ge,Mn)Te diluted magnetic semiconductor is one of promising material in spintronics which exhibits carrier-induced ferromagnetism (described by RKKY mechanism) and ferroelectric properties depending on carrier and magnetic Mn ions content. Also, this material obtained in amorphous form offers possibility to ultra fast switching from amorphous to polycrystalline phase by applying laser beam or electric current. (PCM material). The scope of our project is to investigate and compare electron density of states of GeTe and (Ge,Mn)Te

in amorphous and monocrystalline form using Tunable VUV and photoelectron spectrometer.

These materials were grown on insulating BaF₂ by molecular beam epitaxy technique (MBE) employing effusion cells with GeTe, Te₂ and Mn content. To achieve monocrystalline GeTe and (Ge,Mn)Te semiconductors substrate temperature was kept at $T = 250^\circ\text{C}$. For GeTe and (Ge,Mn)Te in amorphous form at room temperature.

XRD measurements performed at room temperature revealed monocrystalline (111)-oriented rhomboedrical structure of GeTe and GeMnTe semiconductors. No evidence of crystalline phase was experimentally observed in amorphous semiconductors. In our investigation we compare photoemission spectra obtained at photon energy range $h\nu = 45 - 60$ eV which corresponds to experimentally observed three-peak structure valence band states in GeTe (Fig. 1a), and Fano resonance corresponding to Mn 3*p*-3*d* transition in GeMnTe (Fig. 1b) at the same range of photon energy. The contribution of Mn3*d* electrons was determined as located in valence band with binding energy 3.8 eV below Fermi level.

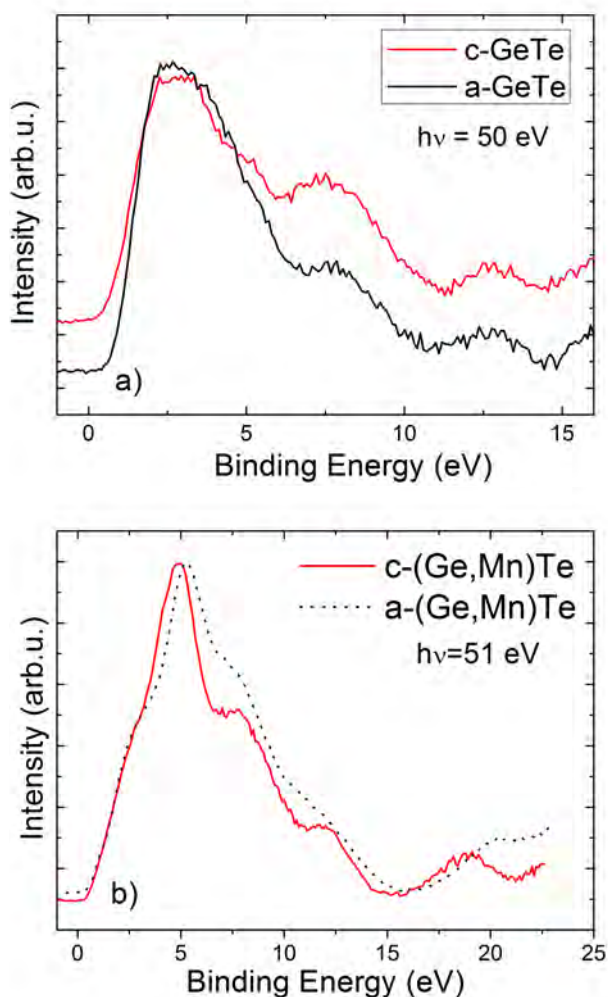


Figure 1: The valence band photoemission spectra of amorphous and crystalline GeTe (a) and (Ge,Mn)Te (b). The spectrum of (Ge,Mn)Te was measured at the energy corresponding to the Mn 3*p*-3*d* threshold.

Acknowledgments: The authors acknowledge support by MSHE of Poland research Projects DESY/68/2007 and by the European Community via the Research Infrastructure Action under the FP6 “Structuring the European Research Area” Programme (through the Integrated Infrastructure Initiative “Integrating Activity on Synchrotron and Free Electron Laser Science”) at DESY. Partially supported by European Union within the European Regional Development Fund, through an Innovative Economy grant (POIG.01.01.02-00-108/09) and (POIG.01.01.02-00-008/08). This work is also supported by the NCN (Poland) research project UMO 2011/01/B/ST3/02486.

References

- [1] N.J. Shevchik, J. Tejada, W.W. Langer, M. Cardona, *Phys. Rev. Lett.* **30** (1973) 659.
- [2] B.J. Kowalski, M.A. Pietrzyk, W. Knoff *et al.*, *Physics Procedia* **3** (2010) 1357.
- [3] M.A. Pietrzyk, B.J. Kowalski, B.A. Orłowski *et al.*, *Acta Phys. Pol.* **A 112** (2007) 275.

CHANGES IN CHEMICAL AND PHYSICAL STRUCTURE OF POLYMERS UNDER EUV RADIATION

B. Korczyk*, A. Bartnik, J. Kostecki, and H. Fiedorowicz

Institute of Optoelectronics, Military University of Technology, Kaliskiego 2, 00–908 Warsaw, Poland

Keywords: extreme ultraviolet radiation, polymer surface modification

**e-mail: b.korczyk@gmail.com*

Number techniques using excimer lasers [1] or synchrotron radiation [2] are employed for modification of polymers. Changing a chemical structure of the surface layer under the influence of extreme ultraviolet radiation is accompanied by a significant changes in its morphology. In this work poly(methyl methacrylate) (PMMA) and polyethylene terephthalate (PET) was irradiated with extreme ultraviolet. Radiation in the range from 5 to 70 nm wavelength was produced using a laser-plasma EUV source based on a double-stream gas-puff target. Depending on a susceptibility of the samples for EUV radiation parameters, different surface structures are created. In this experiment PMMA was irradiated with EUV photons in a spectral range selected with aluminum filter, while PET

was irradiated directly. Effects, range and nature of these interactions were investigated by high-resolution scanning electron microscopy. Cross sections were performed using a focused ion beam.

References

- [1] J. Lawrence, L. Li, “Modification of the wettability characteristics of polymethyl methacrylate (PMMA) by means of CO₂, Nd:YAG, excimer and high power diode laser radiation,” *Mater. Sci. Eng. A* **303** (2001) 142 – 149.
- [2] Y. Sato, D. Yamaguchi, T. Katoh, S. Ikeda, Y. Aoki, A. Oshima, Y. Tabata, M. Washio. “Surface modification of polytetrafluoroethylene by synchrotron radiation,” *Nucl. Instrum. Methods Phys. Res. B* **208** (2003) 231 – 235

ELECTRONIC STRUCTURE AND MAGNETISM OF (Zn,Co)O FILMS: A SOFT X-RAY SPECTROSCOPY STUDY

**I.A. Kowalik^{1*}, M.I. Lukasiewicz¹, E. Guzewicz¹, M. Godlewski¹, F.J. Luque²,
M.A. Nino³, A. Zakharov⁴, and D. Arvanitis⁵**

¹*Institute of Physics, Polish Academy of Sciences, al. Lotników 32/46, 02-668 Warsaw, Poland*

²*Depto. Física Materia Condensada, University Autónoma de Madrid, E-28049, Madrid, Spain*

³*IMDEA; Facultad de Ciencias Modulo C-IX, Madrid, Spain*

⁴*MAX-Lab; Lund University, P.O. Box 118, SE-22100 Lund, Sweden*

⁵*Department of Physics and Astronomy, Uppsala University, P.O. Box 516, 751 20 Uppsala, Sweden*

Keywords: synchrotron radiation, soft x-rays, XAS, XMCD, PEEM

**e-mail: ikowalik@ifpan.edu.pl*

ZnCoO is an important model material for spintronics applications. Here we exploit the element specificity of soft x-ray based spectroscopy and microscopy to characterize spontaneous nanocrystals formation at the interface of ZnCoO films grown on Si substrates. The samples are grown by means of Atomic Layer Deposition. Selected samples are subsequently sputtered, leading to a crater in the central region, to allow for a particular area of the ZnCoO close to the Si interface to be exposed.

Here we show *in situ* results for a sample at both the crater region as well as outside, under quasi-identical experimental conditions. X-ray Absorption Spectroscopy (XAS) and X-ray Magnetic Circular Dichroism (XMCD) measurements were performed at the EPU based I1011 beamline, at the MAX-lab synchrotron radiation facility in Lund, Sweden [1]. The measurements were performed in the total electron yield (TEY) mode. The presented spectra were taken in the non sputtered region as well as in the Si/ZnCoO interface region within the crater obtained by ion sputtering. These results are complemented by means of X-PEEM at the beam line I311 of MAX-lab.

By using the elemental specificity of XAS the composition of the ZnCoO sample is probed for these two sample regions [2]. The sample measured as grown in the first few nanometers contains about 6% of Co ions, however the amount of Co is inhomogeneous. The fine structure of the Co white lines exhibits differences for the as grown sample, as a function of the depth from the sample outer surface. The Co *L*-edges for the as grown film and around the crater show the typical multiplet shape observed for ZnCoO magnetically diluted samples [3]. However within the crater both the Co *L*-edge and O *K*-edges exhibit differences and indicate both a different stoichiometry as well as different electronic state for the O and Co ion cores probed by XAS. The shape of XAS spectra obtained for the Co *L*-edge indicates that in the interface region the metallic Co is the dominant phase but not the only one, we observe the superposition with some CoO [4]. The difference in the electronic state of the Co atoms in the surface and the interface region manifests also in the large variation in the number of holes of Co atoms in these two regions of the sample, illustrated as a

difference in the area under the *L*₃ XAS white line. The number of holes for Co atoms in the surface region is about 7, in the crater is about 3.5, when for metallic Co this value is 2.8 [2]. This result confirms the difference in the hybridization of Co with neighboring atoms. Inside the crater we not only observe a small amount of Co but also a small amount of Zn. We observe also that the electronic state of the Zn atoms in the interface region is different than in the surface region.

A small XMCD dichroic difference is found in the interface region at room temperature, when a magnetic field of 350 Gauss is applied in the surface plane. The dichroic response is much more pronounced at the *L*₃ white line indicating that the orbital moment carried by the Co atoms is much stronger than for Co bulk. By means of the X-PEEM measurements Co rich nanocrystals are identified. A discussion of the XAS, XMCD, and X-PEEM data both for the outer interface and the inner interface will be presented. The formation of nanocrystals in the inner interface evidenced here may be of general character and therefore allow to clarify discrepancies of the magnetic response of ZnCoO films in the literature.

Acknowledgments: We acknowledge the Swedish Research Council, the EC Seventh Framework Programme (FP7/2007 – 2013) under grant Nr 226716 (ELISA) for access to MAX-lab and the European Regional Development Fund, through Grant Innovative Economy (POIG.01.01.02-00-008/08).

References

- [1] I.A. Kowalik *et al.*, “Description of the new I1011 beamline for magnetic measurements using synchrotron radiation at MAX-lab,” *J. Phys.: Conf. Ser.* **211** (2010) 012030.
- [2] M. Sawicki *et al.*, “Homogenous and heterogeneous magnetism in (Zn,Co)O,” arXiv:1201.5268.
- [3] M. Kobayashi *et al.*, “Antiferromagnetic interaction between paramagnetic Co ions in the diluted magnetic semiconductor Zn_{1-x}Co_xO,” *Phys. Rev.* **B 81** (2010) 075204.
- [4] A.M. Mulders *et al.*, “On the interface magnetism of thin oxidized Co films: Orbital and spin moments,” *J. Phys.: Condens. Mat.* **21** (2009) 124211.

RESONANT AND ANGLE-RESOLVED PHOTOEMISSION SPECTROSCOPY OF $\text{Ga}_{1-x}\text{Mn}_x\text{Sb}$

B.J. Kowalski^{1*}, **R. Nietubyc**^{2,3}, and **J. Sadowski**^{4,1}

¹*Institute of Physics Polish Academy of Sciences, Al. Lotników 32/46, 02-668 Warsaw, Poland*

²*National Synchrotron Radiation Centre SOLARIS, Jagiellonian University,
ul. Gronostajowa 7/P-1.6, 30-387 Kraków, Poland*

³*National Centre for Nuclear Research, Andrzeja Sołtana 7, Otwock-Świerk, Poland*

⁴*MAX-lab, Lund University, Box 118, SE-22100 Lund, Sweden*

Keywords: synchrotron radiation, photoelectron spectroscopy, diluted magnetic semiconductors

**e-mail: kowab@ifpan.edu.pl*

$\text{Ga}_{1-x}\text{Mn}_x\text{Sb}$ is a diluted magnetic semiconductor exhibiting ferromagnetic properties, although at relatively low temperatures ($T_C = 2$ K [1]). However, it attracts interest due to the opportunity to study the interactions of magnetic ions with charge carriers in a host with anions chemically different than in $\text{Ga}_{1-x}\text{Mn}_x\text{As}$. The interaction between manganese atoms and surrounding anions influences strongly the details of the valence band structure. $\text{Ga}_{1-x}\text{Mn}_x\text{Sb}$ has also the band structure particularly suitable for making a novel device (like a ferromagnetic resonant interband tunneling diode [2]).

Resonant and angle-resolved photoelectron spectroscopies were applied in order to reveal the contribution of the Mn 3d states to the valence band of $\text{Ga}_{1-x}\text{Mn}_x\text{Sb}$. Since both techniques are based on use of synchrotron radiation, the experiments were carried out at the beamline 41 in the MAXlab synchrotron radiation laboratory of Lund University (Sweden).

The $\text{Ga}_{1-x}\text{Mn}_x\text{Sb}$ layers with Mn contents in the range of 1 to 3 %, were grown on GaSb(100) substrates by molecular beam epitaxy (MBE) at low substrate temperature of about 230°C. The growth was monitored by Reflection High Energy Electron Diffraction (RHEED). The 2-dimensional diffraction patterns (streaks) and distinct RHEED oscillations were observed throughout the growth of the $\text{Ga}_{1-x}\text{Mn}_x\text{Sb}$ layers up to their final thicknesses of 50 to 300 Å depending on the sample. The (100) surfaces of the layers exhibited also the Low Energy Electron Diffraction (LEED) patterns corresponding to the asymmetric (1 × 3) reconstruction.

No manifestations of secondary phases (like MnSb nanocrystals [3]) were detected on RHEED images after the growth. The absence of MnSb precipitates in the investigated samples was confirmed also by a comparative study (including the samples containing the precipitates) by scanning electron microscopy.

The resonant photoemission experiment, carried out for photon energy range from 37 to 60 eV

(covering the Mn 3p-3d resonance), allowed us to identify the spectral feature corresponding to emission from the Mn 3d states. The angle-resolved photoemission experiment, for photon energies from 50 to 106 eV enabled us to scan the band structure along the [100] direction (in the normal emission mode) as well as along the [011] direction (in the off-normal emission mode). The comparison of the experimental band structure diagram with the result of the resonant photoemission measurement showed that Mn 3d states contributed to a dispersionless structure at the binding energy of 3.9 eV (with respect to the Fermi energy), revealed against a background of the host semiconductor bands corresponding well to those reported in the literature for GaSb [4].

Acknowledgments: This research has received funding from the European Community's Seventh Framework Programme (FP7/2007-2013) under grant agreement no. 226716.

References

- [1] F. Matsukura, E. Abe, H. Ohno, "Magnetotransport properties of (Ga,Mn)Sb," *J. Appl. Phys.* **87** (2000) 6442.
- [2] I. Vurgaftman, J.R. Meyer, "Ferromagnetic resonant interband tunneling diode," *Appl. Phys. Lett.* **82** (2003) 2296.
- [3] K. Lawniczak-Jablonska, A. Wolska, M.T. Klepka, S. Kret, J. Gosk, A. Twardowski, D. Wasik, A. Kwiatkowski, B. Kurowska, B.J. Kowalski, J. Sadowski, "Photoemission and scanning-tunneling-microscopy study of GaSb(100)," *J. Appl. Phys.* **109** (2011) 074308.
- [4] G.E. Franklin, D.H. Rich, A. Samsavar, E.S. Hirschorn, F.M. Leibsle, T. Miller, T.-C. Chiang, "Magnetic properties of MnSb inclusions formed in GaSb matrix directly during molecular beam epitaxial growth," *Phys. Rev. B* **41** (1990) 12619.

APPLICATION OF THE X-RAY FLUORESCENCE ANALYSIS AND X-RAY DIFFRACTION IN GEOCHEMICAL STUDIES OF TILL SAMPLES

**A. Kubala-Kukus^{1,2*}, M. Ludwikowska-Kędzia³, D. Banaś^{1,2}, J. Braziewicz^{1,2},
U. Majewska^{1,2}, M. Pajek¹, and J. Wudarczyk-Moćko²**

¹*Institute of Physics, Jan Kochanowski University, Świętokrzyska 15, 25-406 Kielce, Poland*

²*Department of Physical Methods, Holycross Cancer Center, Artwińskiego 3, 25-734 Kielce, Poland*

³*Institute of Geography, Jan Kochanowski University, Świętokrzyska 15, 25-406 Kielce, Poland*

Keywords: X-ray fluorescence, X-ray powder diffraction, geochemical composition, till samples

**e-mail: aldona.kubala-kukus@ujk.edu.pl*

The elemental analysis of soil samples is in the interest of many fields of science as for example agriculture, biology or geography. One of the main and often concerned topic of this analysis is an influence of the environmental pollution on the soil heavy metals concentration. Knowledge of the soil elemental composition can be also essential for understanding of the soil genesis. In investigations of the elements concentration and mineral composition of the soil samples many X-ray spectrometry techniques have been successfully employed. One of the most known methods of X-ray spectrometry are wavelength dispersive X-ray fluorescence analysis (WDXRF) [1, 2] and X-ray powder diffraction (XRPD) method [3]. The XRPD technique gives information about the chemical composition of the analyzed samples while the WDXRF studies allowed on the fast elemental analysis, simultaneously in wide range of elements and broad range of the determined concentration (from tens of $\mu\text{g/g}$ to tens of percent). The WDXRF method is also very effective for the analysis of the samples with a very rich composition.

In presented work WDXRF and XRPD techniques have been applied in the geochemical studies of the till samples. The till samples were collected from region of Holy Cross Mountains — a mountain range located in central Poland. These Polish mountains, being one of the oldest mountains in Europe, are still not unambiguously described in the context of the geochemical studies of the quaternary sediments. The position of till from which the samples were taken is located in the west part of the Holy Cross Mountains, in the nature reserve Słopiec. The analysis was concentrated on the geochemical composition of the till samples both for materials occurring on the surface, which are characterized by continuous weathering processes, and for samples taken from bore-hole Słopiec which depth was 60 m. These X-ray fluorescence analysis and X-ray diffraction studies of the till samples are complementary research program to comprehensive sedimentologi-

cal studies of the till and sediment samples from different part of Holy Cross Mountains. The studies were concentrated both on the methodological aspect and general interpretation of the obtained results.

As the results of WDXRF measurements performed with AXIOS spectrometer the concentration of 36 elements (from oxygen to lead) were determined in till samples. The range of the measured concentrations were very broad: from about $10 \mu\text{g/g}$ to 40%. The XRPD analysis of the chemical composition of the till samples was done by using X'Pert PRO diffractometer. The obtained results have shown changes in geochemical composition of the samples depending on the its localization. Geochemical depth profile was compared with the sedimentological properties.

The concentrations of main elements were also used for analysis of oxides: Al_2O_3 , CaO , Na_2O and K_2O , which levels define chemical alternation index (CIA) and chemical weathering index (CIW) [4]. The CIA and CIW factors describe the weathering processes in the sediments, which can well reconstruct till samples genesis and geo-history.

In the presented work the experimental setups, sample preparation procedures, measurements program and first results will be discussed in details.

References

- [1] R.E. Van Grieken, A.A. Markowicz (eds.), *Handbook of X-ray Spectrometry* (Marcel Dekker, New York 1993).
- [2] J.P. Willis, A.R. Duncan, *Understanding XRF Spectrometry* (PANalytical B.V., Almelo 2008).
- [3] V.K. Pecharsky, P.Y. Zavalij, *Fundamentals of Powder Diffraction and Structural Characterization of Materials* (Springer, New York 2009).
- [4] Chao Li, Shouye Yang, "Is chemical index of alteration (CIA) a reliable proxy for chemical weathering in global drainage basins?," *Am. J. Sci.* **310** (2010) 111 – 127.

THE X-RAY ABSORPTION STUDIES OF THE Ti-Si-C FILMS STOICHIOMETRY IN FUNCTION OF THE TECHNOLOGICAL PARAMETERS

K. Lawniczak-Jablonska^{1*}, M.T. Klepka¹, A. Wolska¹, and M.A. Borysiewicz²

¹*Institute of Physics Polish Academy of Sciences, Al. Lotnikow 32/46, PL-02668 Warsaw, Poland*

²*Institute of Electron Technology, Al. Lotnikow 32/46, PL-02668 Warsaw, Poland*

Keywords: High Electron Mobility Transistors, metallisations, EXAFS, MAX phases

**e-mail: jablo@ifpan.edu.pl*

During the recent years significant interest was devoted to materials which fulfil requirements of technology to produce high frequency and high power electronic devices. Among them there are new materials for metallisation in High Electron Mobility Transistors (HEMT) produced on the base of group III nitrides. Due to the wide band gap these transistors are suitable to work under high voltages. The high current transported by metallic contacts induces a significant internal heat leading to a fast degradation of the conventional Ti/Al ohmic and Ni/Au Schottky contacts. Due to the unique combination of metallic electro-thermal conduction and the ceramic resistance to oxidation, and thermal stability [1, 2], the $M_{n+1}AX_n$ phases are chosen as the material potentially applicable to metallisation in these kind of devices. In the formula above M stands for transition metal, A for an element from group IIIA or IVA and X for carbon or nitrogen.

The MAX phases on one hand exhibit properties of metals, showing good thermal and electrical conductivity, machinability, high hardness. On the other hand they show properties of ceramics with damage tolerance, oxidation resistance, and thermal stability even at temperatures as high as 1000°C [3, 4]. These particular properties are related to the nanolaminate structure of MAX phases [4, 5]. A monocrystalline MAX phase consists of MX monolayers intertwined with monoatomic A layers. Among the M_3AX_2 phases very promising for applications in metallisations to III-N compounds is the Ti_3SiC_2 phase. In the presented paper the attempts to grow thin and monocrystalline films of the Ti_3SiC_2 phase by means of high-temperature magnetron sputtering from three independent cathodes are reported and the problems with achieving the stoichiometric phase are discussed. In the first step the structural characterisation of the deposited films was carried out in a standard way, by means of x-ray diffraction (XRD). In many cases the XRD peaks were broad and asymmetric. We demonstrate that in such a case the constructive conclusions for technology can be provided by the x-ray absorption (XAS) technique. The XAS as an atomic sensitive probe is the most suitable technique to examine the atomic order around Ti atoms as a function of

technological parameters. Due to the lack of long range crystalline order in the samples this information cannot be delivered by XRD. First the EXAFS studies were performed for one set of samples and suggestion for the change of technology were given. According to them the second set of samples were produced with stoichiometry very close to Ti_3SiC_2 compound. The dependence of the numbers of Ti, C and Si atoms on the ratio of power provided at the Ti and Si cathodes is presented in Fig. 1.

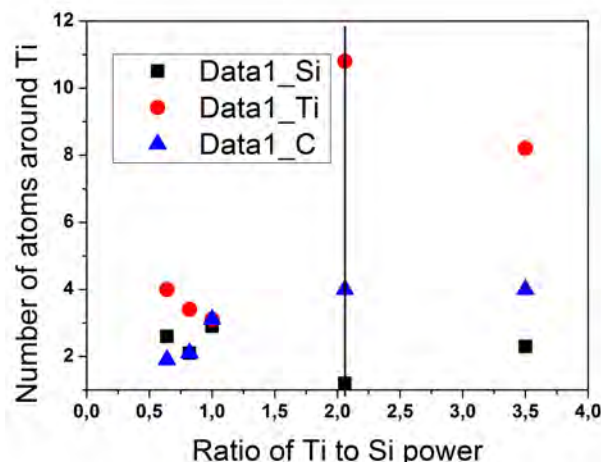


Figure 1: The number of C (triangles), Si (squares) and Ti (circles) atoms around central Ti atom in function of the ratio of powers at the Ti and Si cathode. The line indicates the values for stoichiometric Ti_3SiC_2 phase (Ti-10.8, Si-1.2 and C-4).

Acknowledgments: Research in part financed by the European Union within the European Regional Development Fund-project InTechFun. The measurements performed at synchrotron have received funding from the European Community's Seventh Framework Programme (FP7/2007 – 2013) under grant agreement n° 226716.

References

- [1] M.E. Lin *et al.*, *Appl. Phys. Lett.* **64** (1994) 1003.
- [2] J.S. Kwak *et al.*, *Semicond. Sci. Technol.* **15** (2000) 75.
- [3] M.W. Barsoum *Prog. Solid St. Chem.* **28** (2000) 201.
- [4] J. Emmerlich *et al.*, *Acta Mater.* **55** (2007) 1479.
- [5] W. Jeitschko *et al.*, *Monatsh. Chem.* **94** (1963) 672.

FIRST APPROACH OF THE FTIR MICROSPECTROSCOPY FOR STUDYING THE EFFECT OF IONISING RADIATION IN SINGLE CELLS

E. Lipiec^{1*}, G. Birarda², J. Lekki¹, L. Vaccari², A. Wiecheć¹, and W.M. Kwiatek¹

¹The Henryk Niewodniczanski Institute of Nuclear Physics, PAN, Kraków, Poland

²ELETTRA Synchrotron Light Laboratory, Area Science Park, 34012 Basovizza, Trieste, Italy

Keywords: FTIR microspectroscopy, DNA damage, single cell irradiation, DU-145

*e-mail: Ewelina.Lipiec@ifj.edu.pl

The application of microprobe [1] made a very important development in studies of the response of biological systems to radiation exposure. Research on the well localized radiation dose-dependent biological effects (such as DNA double strand breaks — the most important DNA damage produced by ionizing radiation) enhances the understanding of the mechanisms leading to cell death [2]. Among many experimental techniques applied in this field, optimization of FTIR microspectroscopy to study radiation damage in single cells allows fast detection of damage in lipids, proteins and nucleic acids on molecular level at the same time. Therefore, the aim of this study was the application of SR-FTIR microspectroscopy to investigate the DNA damage in single cells exposed to proton microbeam.

The DNA damage in single cells was induced by 1 MeV protons from the focused horizontal microbeam generated by the Van de Graaff accelerator at the Institute of Nuclear Physics PAN in Kraków, Poland. The prostate cancer cells DU-145 were irradiated by the specific number (50, 200, 400, 2000, 4000) of protons per cell. Cell FTIR spectra were obtained using both: *a*) the synchrotron radiation source at SISSI beamline at ELETTRA with the Mercury-Cadmium-Telluride (MCT) detector and *b*) global source with the Focal Plane Array (FPA) also at ELETTRA Laboratory, Trieste, Italy. In the presented study, experimental FTIR data obtained from both measurements were analyzed separately to investigate the changes in DNA backbone spectral range ($950\text{ cm}^{-1} - 1250\text{ cm}^{-1}$) of irradiated and control (untreated by ionizing radiation) cells. The results were then compared in order to evaluate the experimental approach for this study.

To show the structure in the relationships between the data and to detect the bands, which are different for the each group of spectra, the Principal Component Analysis (PCA) of the spectral region $950\text{ cm}^{-1} - 1250\text{ cm}^{-1}$ was performed using Statistica 8.0 software. The results showed distinct clusters for all groups of cells spectra, even for those

irradiated by the smallest dose of protons. The cellular spectral bands (about 20 for every FTIR spectrum, derived from proteins, nucleic acids and lipids [3, 4]) were fitted in spectral range $950\text{ cm}^{-1} - 1250\text{ cm}^{-1}$ with Gaussian-Lorentzian curves after the Mie scattering effect correction [5]. In both cases (cell spectra collected using MCT and FPA detector) the fitting analysis produced comparable results. The dose-dependent changes in the relative intensities of DNA peaks: 960 cm^{-1} (ribose-phosphate skeletal motions), and 1095 cm^{-1} (symmetric and stretching of O-P-O band), as well as shape and intensity modification of the 1105 cm^{-1} peak (symmetric stretching of P-O-C band) were observed.

Acknowledgments: This work was supported by European Community's Seventh Framework Programme (FP7/2007-2013) under grant agreement No. 20110367.

References

- [1] K.M. Prise, G. Schettino, M. Folkard, and K.D. Held, "Held New insights on cell death from radiation exposure," *Lancet Oncol.* **6** (2005) 520 – 528.
- [2] R. Ugenskiene, J. Lekki, W. Polak, M. Prise, M. Folkard, O. Veselov, Z. Stachura, W.M. Kwiatek, M. Zazula, J. Stachura, "Double strand breaks formation as a response to X-ray and targeted proton irradiation," *Nucl. Instr. and Meth. in Phys. Res. B* **260** (2007) 159 – 163.
- [3] G. Socrates *Infrared Characteristic Group Frequencies* (Wiley & Sons, New York, 2004).
- [4] B. Stuart *Infrared Spectroscopy: Fundamental and Applications* (John Wiley & Sons 2004).
- [5] P. Bassan, A. Kohler, H. Martens, J. Lee, H.J. Byrne, P. Dumas, E. Gazi, M. Brown, N. Clarke, P. Gardner, "Resonant Mie scattering (RMieS) correction of infrared spectra from highly scattering biological samples," *Analyst* **135** (2010) 268 – 277.

SINGULAR VALUE DECOMPOSITION ANALYSIS OF TIME-RESOLVED POWDER DIFFRACTION DATA

A.F. Mabied^{1*}, S. Nozawa², M. Hoshino^{3,4}, A. Tomita², T. Sato², and S. Adachi^{1,2,5}

¹Department of Materials Structure Science, School of High Energy Accelerator Science (KEK),
The Graduate University for Advanced Studies (Sokendai), Tsukuba, 305-0801, Japan

²Photon Factory, High Energy Accelerator Research Organization (KEK), Tsukuba, 305-0801, Japan

³Department of Chemistry and Materials Science, Tokyo Institute of Technology, Meguro-ku, Japan

⁴CREST, Japan Science and Technology Agency (JST), Japan

⁵PRESTO, Japan Science and Technology Agency (JST), Japan

Keywords: synchrotron radiation, SVD, time-resolved, powder diffraction, photodimerization

*e-mail: mabied@post.kek.jp

Singular value decomposition (SVD) analysis has proved efficiency for treating time dependant crystallographic and spectroscopic data revealing important information [1, 2]. SVD method can factorize an experimental data matrix into several components matrices, which can be written mathematically as follow; for an A m -by- n real matrix ($m \geq n$) can be decomposed into three matrices ($A = USV^T$) U is an m -by- n orthogonal matrix, S is an n -by- n diagonal matrix with positive or zero elements and V^T is the transpose of an orthogonal n -by- n matrix V . Physically, the columns of U matrix represents the measurements base spectrum and S elements give its singular values, which indicate the significant of U spectrum. V matrix separates the time dependant vectors of U elements [2].

In our work, we present the first example of the SVD analysis of the photodimerization time-resolved powder diffraction data of 1-chloroanthracene (1-chA) and 9-methylanthracene (9-MA), in order to add useful information about their photodimerization reaction dynamics. Anthracene derivatives have important applications in modern technology, such as fabrication of photo-switchable devices [3]. The powder data were set into m -by- n matrix its columns are the diffraction

intensity at the 2 theta angle points (details in ref. [4]).

The SVD results showed that, in case of 1-chA only one significant singular value was obtained (S_1). The u_1 spectrum vector accompanying to S_1 referred to the original spectrum of 1-chA monomer phase, which mean that the reaction did not occur. For 9-MA, three significant S components were obtained. Figure 1 illustrates the global fitting analysis of V time dependant spectra. It was successfully fitted to double exponential function, giving two time dependant components. Fast decay component assigned to dimerization process and slow decay component can be interpreted that a small amount of monomer still did not react, which in agreement with the reported in ref [5]. UV-Vis and IR spectroscopic measurements supported the results.

Acknowledgments: The synchrotron X-ray experiment at KEK, Japan was approved by the Photon Factory Program Advisory Committee (PF-PAC No. 2004S2-001).

References

- [1] Y. Zhao, M. Schmidt, "New software for the singular value decomposition of time-resolved crystallographic data," *J. Appl. Cryst.* **42** (2009) 734 – 740.
- [2] E.R. Henry, J. Hofrichter, "Singular value decomposition application to analysis of experimental data," *Methods Enzymol.* **210** (1992) 129 – 192.
- [3] P. Zhao, C.F. Fang, C.J. Xia, Y.M. Wang, D.S. Liu, S.J. Xie "A possible anthracene-based optical molecular switch driven by a reversible photodimerization reaction," *Appl. Phys. Lett.* **93** (2008) 013113.
- [4] T. Oka, N. Yag, T. Fujisawa, H. Kamikubo, F. Tokunaga, M. Kataok, "Time-resolved X-ray diffraction reveals multiple conformations in the MN transition of the bacteriorhodopsin photocycle," *Proc. Natl. Acad. Sci.* **97**(26) (2000) 14278 – 14282.
- [5] K. Takegoshi, S. Nakamura, T. Terao, "Solid-state photodimerization of 9-methylanthracene as studied by solid-state C13 NMR," *Solid State Nucl. Magn. Reson.* **11**(1998) 189 – 19.

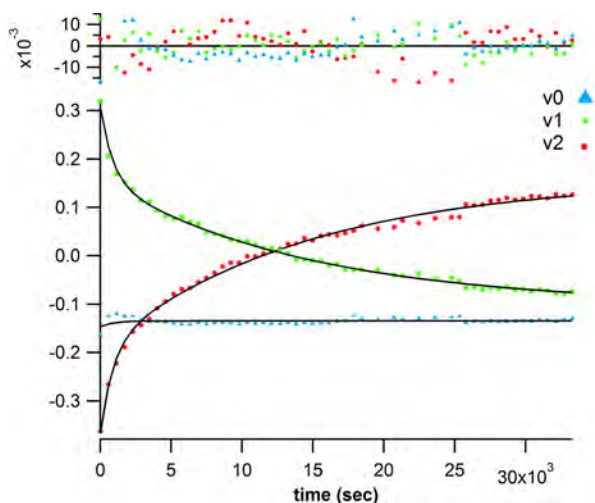


Figure 1: Global fitting results of 9-MA time dependant v spectra of SVD analysis.

CRYSTALLISATION OF POLYMER PHASES AND ITS INFLUENCE ON STRUCTURE AND MECHANICAL PROPERTIES OF MULTILAYERED POLYMER SYSTEMS

M. Małachowski¹ and M. Kozak^{2*}

¹Technological Department, Podanfol S.A

²Department of Macromolecular Physics, A. Mickiewicz University, Poznań, Poland

Keywords: multilayered packing materials, polymer crystallisation, polyamide, polyethylene

*e-mail: mkozak@amu.edu.pl

Thanks to their numerous advantageous features multilayered polymer systems have found a wide range of applications, in particular in food industry. Their structural and mechanical stability can be controlled by proper choice of parameters of their production [1]-[3].

The aim of the study was to check the influence of cooling process of a polymer melts on the structure of the crystalline phase and mechanical properties of the multilayered structures.

The materials studied were obtained by co-extrusion of low density polyethylene (LDPE) and polyamide 6 (PA6). The process of production could be divided into four stages: extrusion, cooling, orientation and structural stabilisation.

In the process the cooling medium was in direct contact only with the external polymer layer, while the other layers were isolated. The subsequent stage is mechanical orientation of the structure, which is sensitive and difficult as the structure improperly prepared can prove too flexible or too brittle and susceptible to cracking.

The crystalline structure of the polymer samples was studied by the wide angle X-ray diffraction

method (WAXS). Morphology of particular polymer layers was investigated under a scanning electron microscope (SEM). Mechanical properties of the samples were examined in a series of tests.

The samples studied were three and four-layer structures PA6/LDPE/PA6 and PA6/LDPE/PA6/LDPE. No binding polymers were used so that the layers could be easily separated and each layer could be studied separately.

Results provided by WAXS method permitted the observations of changes in the crystallinity degree in particular polymers and verification of changes in the crystal phase structure.

References

- [1] H. Shanak, K.H. Ehses, W. Gotz, P. Leibenguth, R. Pelster, *J. Mater. Sci.* **44** (2009) 655 – 663.
- [2] T.D. Fornes, D.R. Paul, *Polymer* **44** (2003) 3945 – 3961.
- [3] N. Vasanthan, *J. Polym. Sci. B: Pol. Phys.* **41** (2003) 2870 – 2877.

XAS/XMCD STUDIES OF Pt/Co/Pt NANOSTRUCTURES WITH OUT-OF-PLANE MAGNETIZATION INDUCED BY Ga⁺ IONS LOW FLUENCE IRRADIATION

P. Mazalski^{1*}, Z. Kurant¹, A. Maziewski¹, M.O. Liedke², J. Fassbender², L.T. Baczewski³, A. Wawro³, A. Rogalev⁴, and F. Wilhelm⁴

¹Laboratory of Magnetism, Faculty of Physics, University of Białystok, Lipowa 41, 15-424 Białystok, Poland

²Helmholtz-Zentrum Dresden-Rossendorf, Bautzner Landstrasse 400, 01328 Dresden, Germany

³Institute of Physics, Polish Academy of Science, Aleja Lotników 32, 02-668 Warszawa, Poland

⁴European Synchrotron Radiation Facility, 6 Rue Jules Horowitz, 38043 Grenoble Cedex, France

Keywords: synchrotron radiation, irradiation, magnetooptics

*e-mail: piotrmaz@uwb.edu.pl

Magnetic properties of ultrathin films are usually tuned by varying the film thickness, chemical composition or structure (see e.g. [1, 2]). It has been demonstrated that magnetic properties of thin films with perpendicular magnetic anisotropy of interfacial origin may be also tuned by ions irradiation [3]. A Pt/Co/Pt trilayer irradiated by different ions exhibits the out-of-plane to in-plane magnetization reorientation phase transition. Moreover, it was shown that an ion irradiation-driven intermixing and disordering at the Co-Pt interfaces was inducing a reduction of the anisotropy, coercivity, and Curie temperature.

In our recent paper [4] we have presented a new effect — remarkable change of a magnetic

anisotropy in the Pt/Co(2.6 nm)/Pt (deposited by sputtering technique) induced by an uniform low fluence Ga⁺ ion irradiation at 30 keV. With increasing fluence D magnetization rotates from in-plane to out-of-plane state and then back to in-plane state. Very recently the second up-turn of the magnetization was observed at the higher irradiation fluence [5]. Low dose Ga-ion irradiation creation of out-of-plane magnetization branch is illustrated in Fig. 1.

We propose that the origin of the observed out-of-plane magnetization state induced by ions irradiation is due to creation of strongly anisotropic Co-Pt L1₀ phase. This hypothesis is supported by measurement of K -edge X-ray absorption (XAS) and X-ray Magnetic Circular Dichroism (XMCD) on the ID12 ERSF beamline. The measurements were performed on: Pt/Co/Pt samples both as deposited film and irradiated one with the fluence creating the out-of-plane magnetization state and a reference sample of L1₀ Co_{0.5}Pt_{0.5} thin film. The XMCD spectrum of the irradiated sample is interpreted as the superposition of pure Co and L1₀ CoPt alloy contributions. TRIDYN [6] simulations, for different Ga⁺ ion fluence, were performed in order to corroborate these findings.

Acknowledgments: This work was supported by the following projects: SPINLAB — EU program Innovative Economy, Priority 2.2, SPIRIT European Community — contract no. 227012, ESRF/73/2006.

References

- [1] M. Kisielewski, *Phys. Rev. Lett.* **89** (2002) 87203.
- [2] A. Stupakiewicz, *Phys. Rev. Lett.* **101** (2008) 217202.
- [3] C. Chappert, *Science* **280** (1998) 1919.
- [4] J. Jaworowicz, *Appl. Phys. Lett.* **95** (2009) 022502.
- [5] A. Maziewski, *Phys. Rev.* **B 85** (2012) 054427.
- [6] W. Möller, *Comp. Phys. Commun.* **51** (1988) 355.

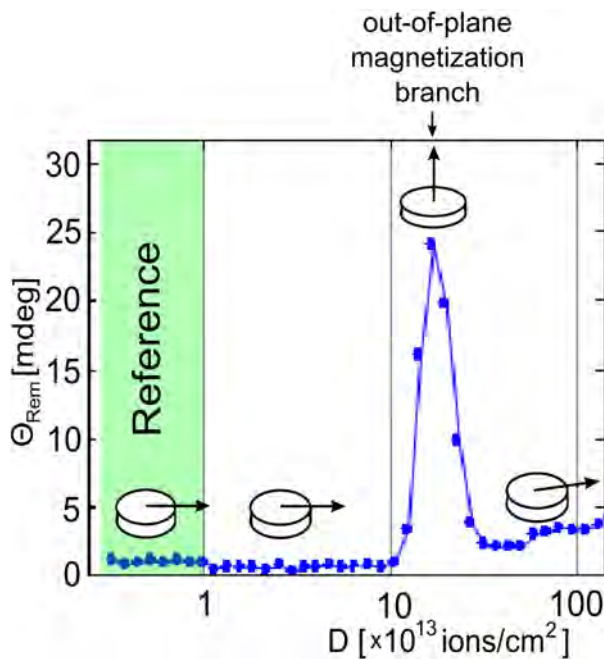


Figure 1: Remnant polar Kerr rotation θ_{REM} of Pt/Co(3.3 nm)/Pt film as a function of Ga⁺ irradiation fluence D . Green region — non-irradiated sample. Arrows show schematically the magnetization direction.

DIFFERENCES AND SIMILARITIES IN ROOTS OF THE NICKEL HYPERACCUMULATING AND NON-ACCUMULATING GENOTYPES OF *SENECIO CORONATUS* FROM SOUTH AFRICA

J. Mesjasz-Przybyłowicz^{1*}, A. Barnabas¹, I. Yousef², P. Dumas², F. Jamme², Ch. Sandt²,
F. Guillon³, P. Sechogela¹, and W. Przybyłowicz^{1,4}

¹Materials Research Department, iThemba LABS, Somerset West 7129, South Africa

²Soleil Synchrotron BP 48 F91192 Gif sur Yvette Cedex, France

³UR1268 Biopolymères, Interactions, Assemblages INRA F-44316 Nantes, France

⁴on leave from the Faculty of Physics and Applied Computer Science, University
of Science and Technology, Krakow, Poland

Keywords: synchrotron radiation, *Senecio coronatus*, Asteraceae, ultramafic soil, nickel hyperaccumulation,
infrared microspectroscopy, X-ray microanalysis, root, cytology, chemotaxonomy

*e-mail: mesjasz@tlabs.ac.za

Hyperaccumulation of heavy metals by a small number of certain plant species is a unique and fascinating phenomenon of great interest from a physiological point of view. The uptake mechanism is still not well understood, despite increasing number of investigations concentrating on different aspects of hyperaccumulation.

Senecio coronatus (Thunb.) Harv. Asteraceae (Hilliard 1977), is a very interesting example of a plant's adaptation to different ecological conditions. The species is widespread in grasslands in South Africa but is also found on ultramafic outcrops. Populations of *S. coronatus* occurring on ultramafic soils differ in terms of Ni uptake and represent Ni-hyperaccumulating and non-hyperaccumulating genotypes. The aim of the present study was to investigate the cytology of the roots of both genotypes, their Ni content and tissue distribution, and to ascertain whether there was a cytological basis for the differential uptake of Ni.

Light and fluorescence microscopy together with histochemical methods and TEM were used to study root cytology. X-ray microanalysis by means of a nuclear microprobe [particle-induced X-ray emission (PIXE) and proton backscattering (BS) techniques] was utilized to determine the concentration and distribution of Ni and other elements in freeze-dried root cross-sections (iThemba LABS, South Africa).

Synchrotron Infrared Microspectroscopy was used to get a deeper insight of biochemical differences between the nickel hyperaccumulating and non-accumulating genotypes. The experiment was performed at the SOLEIL synchrotron facility, France (Beam-line SMIS equipped with a Nicplan IR microscope coupled to a Nicolet Magna 860 FT-IR spectrometer (Thermo Scientific, Nicolet-USA). Results were evaluated using statistical approaches (Principal Component Analysis PCA).

Results from investigations on *S. coronatus* genotypes showed interesting cytological differences in the inner cortical region and exodermis of the

roots. Distinct groups of specialized cells with an organelle-rich cytoplasm that produced copious numbers of spherical bodies, occurred in the inner cortical region of the hyperaccumulator [1, 2]. Such distinct cell groups were absent from the inner cortex of the non-accumulator. Histochemical tests identified a mixture of lipids, alkaloids and terpenoids within the specialized groups of cells. Casparian bands were identified in exodermal cell walls of both genotypes but the bands fluoresced more intensely in the non-accumulator suggesting differences in chemical composition and probably also in apoplastic barrier efficiency. Results from infrared microspectroscopy showed significant differences between the specialized cells as well as cortex and pith regions of the Ni-hyperaccumulator roots compared to the same regions of the non-accumulator.

Further studies of the apoplastic barriers, specialized cells and secreted material in roots of both populations of *S. coronatus* are continued in order to gain a better understanding of their functions.

Acknowledgments: The authors greatly acknowledge Mpumalanga Parks Boards, SAFCOL and SAPPI Forestry for permission to access sites and all assistance. This work is based upon research supported by the South African National Research Foundation. Any opinion, finding, conclusion or recommendation expressed in this material are those of the authors and therefore the NRF does not accept any liability in regards thereto.

References

- [1] J. Mesjasz-Przybyłowicz, A. Barnabas, W.J. Przybyłowicz, "Comparison of cytology and distribution of nickel in roots of Ni-hyperaccumulating and non-accumulating genotypes of *Senecio coronatus*," *Plant and Soil* **293** (2007) 61 – 78.
- [2] J. Mesjasz-Przybyłowicz, A. Barnabas and W. Przybyłowicz, "Root ultrastructure of *Senecio coronatus* genotypes differing in Ni uptake," *Northeast. Nat.* **16** (Special Issue 5) (2009) 351 – 365.

DISTRIBUTION AND SPECIATION OF NICKEL IN HYPERACCUMULATING PLANTS FROM SOUTH AFRICA

J. Mesjasz-Przybylowicz¹, E. Montargès-Pelletier², A. Barnabas¹, G. Echevarria³,
V. Briois⁴, P. Sechogela¹, S. Groeber³, and W. Przybylowicz^{1,5*}

¹Materials Research Department, iThemba LABS, Somerset West 7129, South Africa

²Laboratoire Environnement et Minéralurgie, CNRS Université de Lorraine,
F-54500 Vandoeuvre les Nancy, France

³Laboratoire Sols et Environnement, INRA Université de Lorraine,
F-54505 Vandoeuvre-les-Nancy cedex, France

⁴SOLEIL, SAMBA beamline, l'Orme des Merisiers, Saint Aubin, 91192 Gif sur Yvette cedex, France

⁵on leave from the Faculty of Physics and Applied Computer Science, University
of Science and Technology, Krakow, Poland

Keywords: synchrotron radiation, speciation, nickel, hyperaccumulation, *Senecio coronatus*, *Berkheya coddii*, Asteraceae, ultramafic soil, microspectroscopy, XANES, EXAFS, X-ray fluorescence, x-ray microanalysis, micro-PIXE

* e-mail: przybylowicz@tlabs.ac.za

Hyperaccumulation is an unusual plant response to soils enriched with heavy metals such as Ni, Co, Zn, and Cd. Most plants growing on these metal-rich soils exclude metals from their shoots as excessive accumulation of heavy metals is toxic to the majority of them. However, about 2% of plants inhabiting these soils take up and accumulate large quantities of heavy metals in their shoots: a phenomenon known as hyperaccumulation. It has been reported for more than 450 species, mainly Ni accumulating species (about 400).

The uptake mechanism is still not well understood, despite increasing number of investigations concentrating on different aspects of hyperaccumulation. The mechanisms underlying the process of hyperaccumulation have been studied in relatively few species, all of which belong to the *Brassicaceae* family, known to be primarily of European/Mediterranean origin. Most of the results so far are from model plants like *Thlaspi* sp. and *Alyssum* sp., but the diversity within hyperaccumulating plant species suggests that several mechanisms are responsible for this phenomenon.

Two South African Ni-hyperaccumulating plants from the *Asteraceae*: *Berkheya coddii* Roessler and *Senecio coronatus* (Thunb.) Harv. were collected from their native habitat on ultramafic soils in the Barberton area (Mpumalanga Province, South Africa). Bulk elemental analyses of different plant parts and related soil were done using AA and ICP. Plant samples were cryo-fixed in liquid propane and freeze-dried. Microanalyses of elemental concentration and distribution were performed using particle induced X-ray emission (PIXE), complemented by simultaneously used proton backscattering for matrix corrections (nuclear microprobe at iThemba LABS, South Africa). Elemental localization was also examined with SEM-EDXS and micro-PIXE on frozen hydrated material. Plant anatomy and

cytology were studied using light and electron microscopy.

Spatially resolved X-ray absorption experiments were performed on SAMBA beamline to investigate nickel distribution and speciation within cross-sections of leaves, stems and roots. Incident X-ray beam was reduced in size using a pinhole for a first series of experiments, and using a monocapillary for a second series of experiments. Regions of interest were selected within the different plant tissues by direct visualisation, with the support of elemental profiles and maps acquired by X-ray fluorescence. XAS spectra were then collected at Ni *K*-edge, at room temperature.

Furthermore, in order to check the preservation of nickel status within freeze-dried plant samples, bulk X-ray absorption spectra obtained on frozen-hydrated and freeze-dried plant specimens were compared. XAS data were then collected at liquid N₂ temperature.

The results show that Ni is predominantly complexed by weak or middle-strong organic ligands, through the presence of carboxylate groups in the first sphere of coordination. Chelation could be definitely excluded from major accumulation mechanism. Spectroscopic signals strongly support the predominance of citrate and malate, low molecular weight ligands, for nickel transport and storage in the hyperaccumulators *S. coronatus* and *B. coddii*, growing in their natural environment.

Acknowledgments: This work is based upon research supported by the South African National Research Foundation and the French Ministries of Research and Foreign Affairs. Any opinion, finding, conclusion or recommendation expressed in this material are those of the authors and therefore the NRF does not accept any liability in regards thereto. The authors greatly acknowledge Mpumalanga Parks Boards, SAFCOL and SAPPI Forestry for permission to access sites and all assistance.

X-RAY STUDIES OF THERMAL PROPERTIES OF $\text{Pb}_{1-x}\text{Cd}_x\text{Te}$ SOLID SOLUTION IN A BROAD TEMPERATURE RANGE

R. Minikayev^{1*}, E. Dynowska¹, T. Story¹, A. Szczerbakow¹,
A.M.T. Bell², D. Trots³, and W. Szuszkiewicz¹

¹*Institute of Physics, Polish Academy of Sciences, Al. Lotników 32/46, PL-02668 Warsaw, Poland*

²*HASYLAB at DESY, Notkestr. 85, D-22607 Hamburg, Germany*

³*Universität Bayreuth, Universitätsstr. 30, D-95440 Bayreuth, Germany*

Keywords: synchrotron radiation, thermal expansion, structure refinement, high temperature, low temperature

**e-mail: minik@ifpan.edu.pl*

The $\text{Pb}_{1-x}\text{Cd}_x\text{Te}$ solid solution constitutes an attractive system for developing of the mid-IR optoelectronic or the thermo-electric devices based on quantum dots. These applications are powered by extremely low solubility of both materials [1] resulting from the difference in their crystal structure — rock salt (RS) for PbTe and zinc-blende (ZB) for CdTe. However, it was difficult to get a $\text{Pb}_{1-x}\text{Cd}_x\text{Te}$ uniform composite and only recently the metastable single crystals were obtained by self-selecting vapour growth (SSVG) method followed by a rapid quenching of resulting solid solutions [2, 3]. An access to new materials of high-quality made it possible to perform the X-ray diffraction measurements in a wide temperature range.

The previously performed high-temperature diffraction studies permitted us to correct a part of the relevant phase diagram [4]. Because of a huge difference between the expansion coefficient for CdTe [5] and PbTe [6] resulting from their different crystal structure the structure properties of $\text{Pb}_{1-x}\text{Cd}_x\text{Te}$ crystals in a broad temperature range were also of great interest. The goal of the present work was to study the structure properties of $\text{Pb}_{1-x}\text{Cd}_x\text{Te}$ solid solution at low and high temperatures and to get also new information about the temperature behavior of lattice parameters, and the thermal expansion coefficient values.

Single bulk $\text{Pb}_{1-x}\text{Cd}_x\text{Te}$ crystals (with $x \leq 0.11$) obtained by SSVG method at the Institute of Physics of the Polish Academy of Sciences in Warsaw were the object of present investigations. *In situ* low- and high-temperature X-ray diffraction measurements were performed at the B2 beamline (Hasylab/DESY), using the Debye-Scherrer geometry. The samples were prepared as a mixture of powdered $\text{Pb}_{1-x}\text{Cd}_x\text{Te}$ crystals and fine diamond powder (in the capacity of an internal standard), and placed in a thin-wall quartz or glass capillary, rotating inside a graphite heater or the cryostat during measurements. The Rietveld method, was used for the structural analysis.

The analysis of the results accomplished with the Rietveld refinement demonstrated a monotonous evolution of the lattice parameter with temperature. Thermal expansion of $\text{Pb}_{1-x}\text{Cd}_x\text{Te}$ crystals with the rock salt structure has been measured and analyzed for the first time at low temperatures.

Temperature evolution of the linear expansion coefficient of $\text{Pb}_{1-x}\text{Cd}_x\text{Te}$ is similar to that corresponding to PbTe and its value is positive at all temperatures under investigation. Linear expansion coefficient increases with increasing Cd content in $\text{Pb}_{1-x}\text{Cd}_x\text{Te}$ in comparison to relevant values corresponding to PbTe. Information concerning the $\text{Pb}_{1-x}\text{Cd}_x\text{Te}$ solid solution phase diagram and CdTe solubility limit in PbTe for $x < 0.1$ and $T < 1100$ K will also be shown and discussed.

Acknowledgments: This work has been partially supported by the European Community's Seventh Framework Programme (FP7/2007 – 2013) under grant agreement no. 226716 and by the European Union within the European Regional Development Fund, through grant Innovative Economy (POIG.01.01.02-00-108/09).

References

- [1] T. Schwarzl, E. Kaufmann, G. Springholz, K. Koike, T. Hotei, M. Yano, and W. Heiss, "Temperature-dependent midinfrared photoluminescence of epitaxial PbTe/CdTe quantum dots and calculation of the corresponding transition energy," *Phys. Rev. B* **78** (2008) 165320.
- [2] M. Szot, A. Szczerbakow, K. Dybko, L. Kowalczyk, E. Smajek, V. Domukhovski, E. Łusakowska, P. Dziawa, A. Mycielski, T. Story, M. Bułaka, M. Galicka, P. Sankowski, R. Buczek, and P. Kacman, "Experimental and theoretical analysis of PbTeCdTe solid solution grown by physical vapour transport method," *Acta Phys. Pol. A* **116** (2009) 959.
- [3] A. Szczerbakow and K. Durose, "Self-selecting vapour growth of bulk crystals – principles and applicability," *Prog. Cryst. Growth Character. Mater.* **51** (2005) 81.
- [4] R. Minikayev, E. Dynowska, E. Kamińska, A. Szczerbakow, D. Trots, T. Story, and W. Szuszkiewicz, "Evolution of $\text{Pb}_{1-x}\text{Cd}_x\text{Te}$ solid solution structure at high temperatures," *Acta Phys. Pol. A* **119** (2011) 699.
- [5] D. Bagot, R. Granger, and S. Rolland, "Thermal expansion coefficient and bond strength in $\text{Hg}_{1-x}\text{Cd}_x\text{Te}$ and $\text{Hg}_{1-x}\text{Zn}_x\text{Te}$," *Phys. Stat. Sol. (b)* **177** (1993) 295.
- [6] S.I. Novikova and N.Kh. Abrikosov, *Fiz. Tverd. Tela* **5** (1963) 1913 (in Russian); *Sov. Phys. Solid State* **5** (1964) 1397.

THERMAL EXPANSION OF GALLIUM NITRIDE

R. Minikayev¹, W. Paszkowicz^{1*}, P. Piszora², M. Knapp³, C. Bächtz⁴, and S. Podsiadło⁵¹*Institute of Physics PAS, al. Lotnikow 32/46, 02-668 Warsaw, Poland*²*Faculty of Chemistry, A. Mickiewicz University, ul. Grunwaldzka 6, 60-780 Poznan, Poland*³*Karlsruhe Institute of Technology, KIT (Germany), IAM-ESS Institute for Applied Materials — Energy Storage Systems, Karlsruhe, Germany*⁴*ESRF, B.P. 220, 38043 Grenoble, France*⁵*Faculty of Chemistry, Warsaw University of Technology, ul. Noakowskiego 3, 00-664 Warsaw, Poland**Keywords: gallium nitride, thermal expansion, lattice parameter*** e-mail: paszk@ifpan.edu.pl*

III-V nitrides such as GaN and InN and their solid solutions are basic components of modern optoelectronic devices. Physical properties of nitride films are strongly strain-dependent. The knowledge on lattice constants at high temperatures and on thermal expansion for the bulk material is helpful in optimizing the growth conditions and in reducing the thermal strain. The existing literature data on lattice parameters and thermal expansion of gallium nitride exhibit a scatter; most often these data were determined for limited temperature intervals. In the present study, we have used a single instrument in

order to determine the thermal behavior of polycrystalline gallium nitride in a broad temperature range. Diffraction measurements for gallium nitride fine powder were carried out at a high-resolution X-ray powder diffractometer (B2 beamline at HASYLAB) equipped with a helium cryostat and a graphite-heated furnace. Debye-Scherrer geometry with rotating capillary was applied. A smooth experimental dependence of lattice parameter of gallium nitride was obtained permitting for deriving a reliable temperature variation of thermal expansion coefficient.

SMALL ANGLE X-RAY SCATTERING (SAXS) STUDIES OF MONOMERIC HUMAN CYSTATIN C IN SOLUTION

M. Murawska¹, A. Grubb², and M. Kozak^{1*}

¹*Department of Macromolecular Physics, A. Mickiewicz University, Umultowska 85, 61-614 Poznań, Poland*

²*Department of Clinical Chemistry, Lund University, Lund, Sweden.*

Keywords: BioSAXS, human cystatin C

**e-mail: mkozak@amu.edu.pl*

Human cystatin C (HCC) is an inhibitor of cysteine proteases. This protein is present in many body fluids like blood, urine, saliva, cerebrospinal fluid, pleural fluid and in tissues such as cerebral cortex. Cystatin C is used as an important marker of kidney function with better correlation with mortality and cardiovascular problems than the other common markers like creatinine or glomerular filtration rate. This protein was observed as coprecipitate of pathological amyloid fibrils in the brains of patients with Alzheimer's disease. Especially a lot of cystatin C was present in the cerebrospinal fluid. For correct functioning in this role cystatin should occur in the form of monomers.

In the crystal, native HCC forms dimers via the domain swapping mechanism. This mechanism can be directly related to the cystatin tendency towards formation of amyloid deposits. Rarely, a naturally occurring mutation HCC (Leu68Gln) results in massive amyloidosis, cerebral haemorrhage and ultimately to death at a young age.

The study presented was aimed at developing low-resolution structure of monomeric form of human cystatin C in solution, stabilized by disulfide bonds against domain swapping, and comparing this structure with the crystal structure of monomeric human cystatin C (PDB: 3GAX).

The X-ray scattering data were obtained using synchrotron radiation and SAXS camera (beam line BLi911-4 [4], MAXII storage ring of the MAX-Lab Lund, Sweden; $\lambda = 0.091$ nm). Low-resolution structure of the monomeric human cystatin C in solution was restored by a computer simulation in program DAMMIN [5]. Independently, the SAXS data were directly compared using CRY SOL [6] with the theoretical scattering curve obtained on the basis of

crystal structure. This comparison clearly indicated that the preferred conformation of HCC occurring in solution is almost identical with the crystal structure.

Acknowledgments: The present study was carried out with financial support from the Ministry of Science and Higher Education (grant nr N N202 127237).

References

- [1] R. Janowski, M. Kozak, E. Jankowska, Z. Grzonka, A. Grubb, M. Abrahamson, M. Jaskolski, "Human cystatin C, an amyloidogenic protein, dimerizes through three dimensional domain swapping," *Nature Struct. Biol.* **8** (2001) 316 – 320.
- [2] M. Orlikowska, E. Jankowska, R. Kołodziejczyk, M. Jaskolski, A. Szymańska, "Hinge-loop mutation can be used to control 3D domain swapping and amyloidogenesis of human cystatin C," *J. Struct. Biol.* **173** (2011) 406 – 413.
- [3] A. Grubb, "Cystatin C — properties and use as diagnostic marker," *Adv. Clin. Chem.* **35** (2000) 63 – 99.
- [4] C.B. Mammen, T. Ursby, Y. Cerenius, M. Thunnissen, J. Als-Nielsen, S. Larsen, and A. Liljas, "Design of a 5-station macromolecular crystallography beamline at MAX-lab," *Acta Phys. Pol.* **A 101** (2002) 595 – 602.
- [5] D.I. Svergun, "Restoring low resolution structure of biological macromolecules from solution scattering using simulated annealing," *Biophys. J.* (1999) 2879 – 2886.
- [6] D.I. Svergun, C. Barberato, and M.H.J. Koch, "CRY SOL — a program to evaluate X-ray solution scattering of biological macromolecules from atomic coordinates", *J. Appl. Cryst.* **28** (1995) 768 – 773.

ROD-LIKE MORPHOLOGY OF SILVER NANOPARTICLES PRODUCED IN CATIONIC GEMINI SURFACTANTS SYSTEMS

M. Murawska¹, K. Smolarek¹, A. Skrzypczak², and M. Kozak^{1*}

¹Department of Macromolecular Physics, A. Mickiewicz University,
Umultowska 85, 61-614 Poznań, Poland

²Faculty of Chemical Technology, Poznań University of Technology, Piotrowo 3, 60-965 Poznań, Poland

Keywords: Au nanoparticles, gemini surfactants

*e-mail: mkozak@amu.edu.pl

Silver nanoparticles have found a wide range of applications. Thanks to their bactericidal properties they are used in a special lining of refrigerators, as components of cleaning agents, in water filters in the countries with problems in access to clean water [1]. Other applications of silver nanoparticles include their catalytic use [2], the use in real-time optical sensor [3] or as components of bionanosensors.

A typical reaction for the synthesis of silver nanoparticles in solution is similar to the Turkevich method [4]. The method proposed is a modification of the above method — we used Silver nitrate (AgNO_3) as a silver precursor and trisodium citrate ($\text{Na}_3\text{C}_6\text{H}_5\text{O}_7$) as a reducer [5], with addition of a gemini surfactant 1,1'-(1,4-butan)bis3-dodecylmethylimidazolium propionate (GC12P).

The nanoparticles obtained were characterized by transmission electron microscopy (TEM) and UV-Vis spectroscopy. For the silver nanoparticles solution obtained without the addition of gemini surfactant, we observed the plasmon resonance at the wavelength corresponding to the presence of silver nanoparticles of sizes ranging from 5 – 100 nm. TEM images show the presence of spherical, tetrahedral and rod-like nanoparticles (Fig. 1).

Acknowledgments: The present study was carried out with financial support from the Ministry of Science and Higher Education (grant nr N N202 127237).

References

- [1] Z.-J. Jiang, C.-Y. Liu, and L.-W. Sun, "Catalytic properties of silver nanoparticles supported on silica spheres," *Am. Chem. Soc.* **109**(5) (2004) 1730-5.
- [2] P. Jain, T. Pradeep, "Potential of silver nanoparticle-coated polyurethane foam as an antibacterial water filter," *Biotechnol. Bioen.* **90**(1) (2005) 59 – 63,
- [3] A.D. McFarland, R.P.V. Duyne, "Single silver nanoparticles as real-time optical sensors with zeptomole sensitivity," *Nano Lett.* **3**(8) (2003) 1057 – 1062.
- [4] J. Turkevich, P.C. Stevenson, J. Hillier, "A study of the nucleation and growth processes in the synthesis of colloidal gold," *Discuss Faraday Soc.* **11** (1951) 55 – 75.
- [5] X. Dong, X. Ji, H. Wu, L. Zhao, J. Li, W. Yang, "Shape control of silver nanoparticles by stepwise citrate reduction," *J. Phys. Chem. C* **113** (2009) 6573 – 6576.

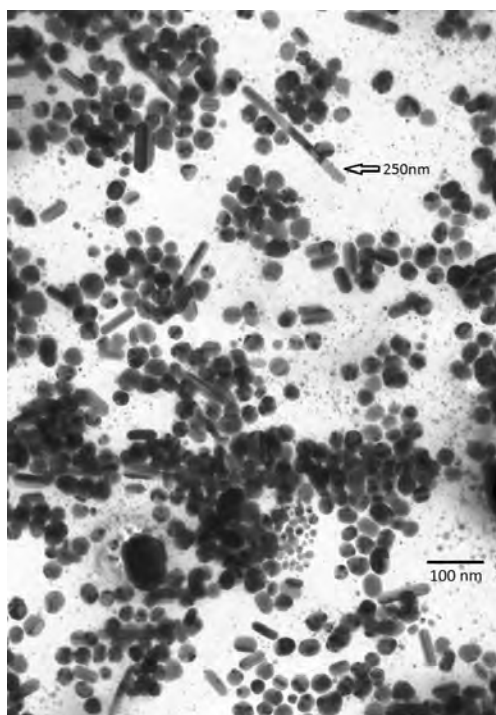


Figure 1: TEM images of silver nanoparticles obtained with the addition of surfactant GC12P.

THE STRUCTURE AND MORPHOLOGY OF GOLD NANOPARTICLES PRODUCED IN CATIONIC GEMINI SURFACTANTS SYSTEMS

M. Murawska¹, M. Wiatr¹, P. Nowakowski¹,
K. Szutkowski¹, A. Skrzypczak², and M. Kozak^{1*}

¹Department of Macromolecular Physics, A. Mickiewicz University,
Umultowska 85, 61-614 Poznań, Poland

²Faculty of Chemical Technology, Poznań University of Technology,
Piotrowo 3, 60-965 Poznań, Poland

Keywords: Au nanoparticles, gemini surfactants

*e-mail: mkozak@amu.edu.pl

Gold nanoparticles have a great number of applications, among others in material science, biology and medicine (for example as components of the specific drug delivery systems or accurate and less expensive nanosensors for diagnostic purposes) [1, 2].

A method for the synthesis of gold nanoparticles in solution with the use of gemini surfactant was proposed and the nanoparticles obtained were subjected to thorough characterization. The method proposed is a modification of that proposed by Turkevich [3], based on reduction of tetrachloroauric acid in the presence of trisodium citrate and a dicationic (gemini) surfactants - alkyloxymethylimidazolium derivatives.

Morphology and size distribution of gold nanoparticles obtained were examined using transmission electron microscopy (TEM), small angle scattering of synchrotron radiation (beam line BLI9-11-4 [4], MAXII storage ring of the MAX-Lab Lund, Sweden, $\lambda = 0.091$ nm) and NMR diffusion spectroscopy. For the nanoparticles solution obtained we observed the plasmon resonance at the wavelength corresponding to the presence of gold nanoparticles with sizes ranging from 5 – 100 nm. TEM images show the presence of gold nanoparticles with tetrahedral and spherical morphology

in solutions with surfactants GC12P, GC12N, and spherical morphology, but strongly aggregated in solution with cationic surfactant GOC12Cl (Fig. 1).

Acknowledgments: The present study was carried out with financial support from the Ministry of Science and Higher Education (grant nr N N202 127237).

References

- [1] M.S. Bakshi, P. Sharma, T.S. Banipal, "Au and Au-Ag bimetallic nanoparticles synthesized by using 12-3-12 cationic Gemini surfactant as template," *Mater. Lett.* **61** (2007) 5004 – 5009.
- [2] J. Polte, T.T. Ahner, F. Delissen, S. Sokolov, F. Emmerling, A.F. Thunemann, "Mechanism of gold nanoparticle formation in the classical citrate synthesis method derived from coupled in situ XANES and SAXS evaluation," *R. J. Am. Chem. Soc.* **132** (2010) 1296 – 3001.
- [3] J. Turkevich, P.C. Stevenson, J. Hillier, "A study of the nucleation and growth processes in the synthesis of colloidal gold" *Discuss. Faraday Soc.* **11** (1951) 55 – 75.
- [4] C.B. Mammen, T. Ursby, Y. Cerenius, M. Thunnissen, J. Als-Nielsen, S. Larsen, A. Liljas, "Design of a 5-station macromolecular crystallography beamline at MAX-lab," *Acta Phys. Pol. A* **101** (2002) 595 – 602.

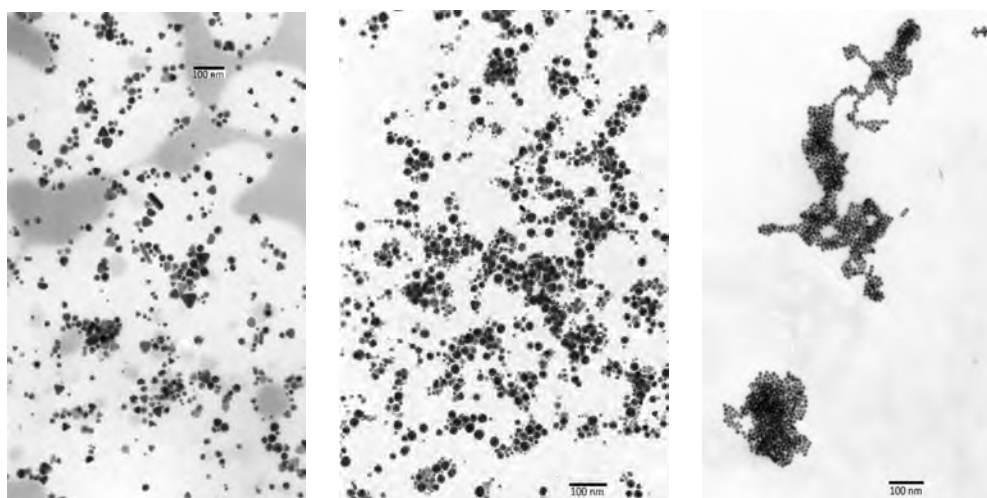


Figure 1: TEM images of gold nanoparticles obtained with the addition of surfactant (from left: GC12P, GC12N, GOC12Cl).

MULTI-CHANNEL IONIZATION CHAMBER DEVELOPMENT FOR SYNCHROTRON BEAM FLUCTUATION MONITORING AND TIME RESOLVE MEASUREMENT

A. Nasr*, U. Werthenbach, H.W. Schenk, and A.H. Walenta

Physics Department, Detectors physics group Prof. Walenta, University of Siegen,
Walter flix strasse 3, 57072 Siegen, Germany

Keywords: *synchrotron radiation*

*e-mail: amgad48@gmail.com

A new Multi-channel ionization chamber has been developed with segmented electrodes, for monitoring the relative intensity of two parallel monochromatic x-ray beams with energies ranging from 5 to 100 keV for the k-edge digital subtraction angiography (KDA).

Acknowledgments: Gratefully thank to the workshop of Physics Department of the University of Siegen for the mechanic development of the chamber, we would like to thank T. Nordan, k. Nurdan, D, Junge and D. Gebauer, for their grateful help and discussion

References

- [1] Waldemar H. Scharf, *Biomedical particle accelerators* (American Institute of Physics 1994).
- [2] Polyimide 35N, Arlon.
- [3] Inter connection NE, ShinEtsu.
- [4] Nova Press FLEXIBLE/815, Frenzelit-Werke GmbH, Germany.
- [5] V.K. Myalitsin, "A Multichanel position sensitive ionization chamber for x-ray intensity monitoring," *Nucl. Instr. and Meth.* **A323** (1992) 97 – 103.
- [6] M.M. Costin *Position sensitive beam monitor for medical imaging with synchrotron radiation* (M.Sc. Thesis University of Siegen, 2006).
- [7] S.N. Ahmed, "High precision ionization chamber for relative intensity monitoring synchrotron radiation," *Nucl. Instr. Meth.* **A449** (2000) 248 – 253.
- [8] Glenn F. Knoll *Radiation Detection and Measurement* (John Wiley & Sons Inc, 1999).

PHOTOEMISSION BINDING ENERGY LOCAL CHANGE CAUSED BY CRYSTALLINE LOCAL STRUCTURE

**B.A. Orlowski^{1*}, A. Szczerbakow¹, P. Dziawa¹, K. Gas¹,
A. Reszka¹, S. Thiess², and W. Drube²**

¹*Institute of Physics, Polish Academy of Sciences, Al. Lotnikow 32/46, 02-668 Warsaw, Poland*

²*Institut für Experimentalphysik, Universität Hamburg, Luruper Chaussee 149, 22761 Hamburg, Germany*

Keywords: crystalline structure, electronic structure, synchrotron radiation, photoemission spectroscopy

**e-mail: orbro@ifpan.edu.pl*

The paper is concern to the problem of crystalline local structure appearing in the ternary crystal and corresponding to it local electronic structure. In $\text{Pb}_{0.94}\text{Cd}_{0.06}\text{Te}$ [1, 2] crystal local crystalline structure is created due to introduction of Cd ion on a sit of Pb ion. In the case created ternary crystal still survive in the rock salt structure like it is for PbTe. As the ionic radius of Cd ion is smaller than Pb ion the lattice collapse appears around the introduced Cd ion. These crystalline local structure creates the electronic local structure.

The paper presents comparison of spectra of two kind of semiconductor samples. The one is the ternary crystal of $\text{Pb}_{0.94}\text{Cd}_{0.06}\text{Te}$ with the frozen rock salt structure. In these crystal the crystalline local structure is created due to differences of the radiuses size of cations Pb^{2+} and Cd^{2+} and due to frozen technology process of the crystal. The second one sample is the layer nanostructure $\text{CdTe}/\text{Pb}_{0.95}\text{Eu}_{0.05}\text{Te}/\text{CdTe}$ grown in thermal equilibrium by MBE method [3].

The bulk single crystals of $\text{Pb}_{1-x}\text{Cd}_x\text{Te}$ were grown by self-selecting vapor growth (SSVG) method which is marked by near equilibrium growth conditions [1, 2]. The metastable $\text{Pb}_{1-x}\text{Cd}_x\text{Te}$ crystals of about 1 ccm volume with (001) natural facets were obtained with FWHM rocking curve values of below 2 arcmin and almost absolutely uniform composition in respect to the CdTe molar fraction x . The study of X-ray diffraction of $\text{Pb}_{1-x}\text{Cd}_x\text{Te}$ ternary crystal performed in room temperature confirm a single-phase rock-salt solution. It means, that small ionic radius Cd^{2+} ion is taking a crystal region corresponding to the ion Pb^{2+} of big ionic radius.

The Tunable High Energy X-ray Photoemission Spectroscopy (THE-XPS) with the application of the synchrotron radiation was used to investigate electronic structure of the samples. The experiment was performed using the (THE-XPS) spectrometer at wiggler beam line station BW2 of the Doris III storage Ring, HASYLAB, DESY, Hamburg. Double crystal monochromator Si(111) covering an energy range from 2.4 to 10 keV with a monochromatic photon flux of about 5×10^{12} photons/s and with total energy resolution power of 0.5 eV for radiation energy around 3000 eV was used. The photoemission studies were performed at room temperature.

To simplify further consideration lets take one dimensional chains of the PbTe, PbCdTe and

CdTe presented in Fig. 1. First row of the figure presents PbTe clean crystal chain while the third row presents CdTe clean crystal chain. The distance between Pb–Te atoms are bigger than it is for distance between Cd–Te atoms. The middle row corresponds to the case when the Cd ion is introduced on the seat of Pb ion and the structure of PbTe chain changes locally and creates local structure around Cd ion. The Te ions nearest to introduced Cd ion will change their position to move closer to the Cd ion to approach the Cd–Te distance corresponding to CdTe chain (row 3). These movement of Te ions in direction to Cd ion will lead to the increase of the distance between these Te ions and their neighbors Pb ions. As a result we can obtain new local structure around the Cd ion. In the local structure region we can expect that the distance between Cd–Te and Pb–e ions will increase in comparison to these distances obtained for CdTe and PbTe chains.

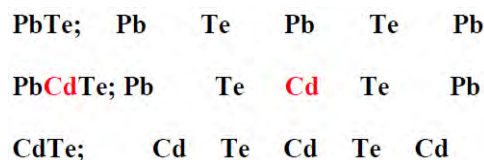


*Figure 1: One dimensional structure of PbTe, PbCdTe, and CdTe. The Cd ion is inserted on the place of Pb ion. Two Te ligands ions of Cd ion shift closer to the inserted Cd^{2+} ion. The distance between Cd–Te is now smaller than previous Pb–Te and bigger than in CdTe. The next Pb ion moves closer to Cd ion and its distance Pb–Te is bigger in comparison to the previous Pb–Te distance in PbTe crystal. Let's assume that the next distances of Pb–Te remains as previous in PbTe. Local change of binding energy E_B :
- for Cd^{2+} and Pb^{2+} electrons increases, conduction band is expected to shift down
- for Te^{2-} electrons E_B decreases, valence band is expected to shift up.*

Local crystalline structure leads to the creation of local electronic structure. Local increase of the distance between cation and anion leads to the increase of binding energy of electrons of cation and to the decrease of binding energy of electrons of anion.

The results of the measured binding energies are presented at Table I. In the local structure region the distance between Pb — Te increases and it leads to the increase of binding energies of Pb^{2+} ion

Table 1: Photoemission binding energies and their differences for frozen crystal $\text{Pb}_{0.94}\text{Cd}_{0.06}\text{Te}$ and layer $\text{CdTe}/\text{Pb}_{0.95}\text{Eu}_{0.05}\text{Te}/\text{CdTe}$ grown in thermal equilibrium.

| Samples | Core levels binding energy E_b (eV) | | | |
|---|---------------------------------------|--------------------------------|--------------------------------|--------------------------------|
| | Cation | | Anion | |
| | Pb $5d_{5/2}$ Pb $5d_{3/2}$ | Pb $4f_{7/2}$ Pb $4f_{5/2}$ | Te $4d_{5/2}$ Te $4d_{3/2}$ | Te $3d_{5/2}$ Te $3d_{3/2}$ |
| $\text{Pb}_{0.94}\text{Cd}_{0.06}\text{Te}$ | 18.67 | 137.18 | 39.86 | 572.02 |
| | 21.33 | 142.10 | 41.34 | 582.57 |
| $\text{CdTe}/\text{Pb}_{0.95} \dots$ $\dots \text{Eu}_{0.05}\text{Te}/\text{CdTe}$ | 18.45 | 137.32 | 39.87 | 571.94 |
| | 21.11 | 142.24 | 41.36 | 582.48 |
| $E_{b\text{FrCrystal}}, E_{b\text{Layer}}$ | +0.22 | +0.14 | -0.01 | -0.08 |
| | +0.22 | +0.14 | -0.02 | -0.09 |

electrons and to the decrease of ion Te^{2-} electrons binding energies (table I row 3).

The results consistently confirm the consideration of the presented abstract and leads to the conclusions: in crystal appears local structure, distance of Pb — Te increases in the region of local structure; binding energies (table I row 1 and 2) of electrons of Pb^{2+} ions are higher for frozen crystal than for layer grown in thermal equilibrium (Table 1, row 3), while for electrons of Te^{2-} ion the binding energies are smaller for frozen crystal (Table 1, row

1 and 2) than for layer grown in thermal equilibrium (Table 1, row 3).

Acknowledgments: The authors acknowledge support by MSHE of Poland research Projects DESY/68/2007 and by the European Community via the Research Infrastructure Action under the FP6 “Structuring the European Research Area” Programme (through the Integrated Infrastructure Initiative “Integrating Activity on Synchrotron and Free Electron Laser Science”) at DESY. Partially supported by European Union within the European Regional Development Fund, through an Innovative Economy grant (POIG.01.01.02-00-108/09) and (POIG.01.01.02-00-008/08).

References

- [1] A. Szczerbakow, K. Durose, *Prog. Cyst. Growth Charac. Mater.* **51** (2005) 81.
- [2] B.A. Orłowski, A. Szczerbakow, B.J. Kowalski, M.A. Pietrzyk, K. Gas, M. Szot, W. Szuszkiewicz, V. Domukhovski, S. Mickevicius, R.L. Johnson, S. Thiess, W. Drube, *J. Electron. Spectrosc. Relat. Phenom.* **184** (2011) 199 – 202.
- [3] B.A. Orłowski, S.P. Dziawa, K. Gas, A. Reszka, S. Mickievicius, S. Thiess, W. Drube, *Acta Phys. Pol. A* **120** (2011) 960 – 963.

CHARACTERIZATION OF POLYMER NANOCOMPOSITES BY MIKRO SR-FTIR SPECTROSCOPY

C. Paluszkiwicz^{1*}, W.M. Kwiatek², and E. Stodolak¹

¹AGH — University of Science and Technology, Faculty of Materials Science and Ceramics,
Al. Mickiewicza 30, 30-059 Kraków, Poland

²Institute of Nuclear Physics PAN, ul. Radzikowskiego 152, 31-342 Kraków, Poland

Keywords: bone defect, polymer-ceramic nanocomposites, SR-FTIR

*e-mail: cpalusz@agh.edu.pl

Bone defect is one of the most frequent problem in bone tissue reconstruction in which application of a biomaterial filling is necessary. It creates a still rising demand of biomaterials for the bone surgery. Polymer-ceramic nanocomposites is a group of novel materials which properties such as strength, Young's modulus, bioactivity and controlled degradation time make them suitable for filling a bone defects.

The aim of this work was chemical characterization of polymer nanocomposites. As a matrix for nanocomposite a natural polysaccharide — chitosan (CS) was used as well as a nanometric filler montmorillonite (MMT). The applied biopolymer (CS) is a biocompatible and biodegradable material which mechanical properties are similar to the bone ones. The ceramic nanofiller (MMT) was introduced in order to improve matching of mechanical properties of nanocomposite to a bone and to enable control of its degradation time.

The SR-FTIR (Synchrotron Radiation — Fourier Transform InfraRed) study was used to determine dispersion of MMT nanoparticles in the polymer matrix as well as chemical state of surface. A correlation between the concentration of nanoparticles and physico-chemical properties (roughness and wettability) of nanocomposite surfaces was observed.

SR-FTIR measurements of the samples were carried out in the transmission mode. Spectra were measured at 4 cm^{-1} resolution in the region from 4000 cm^{-1} to 900 cm^{-1} using synchrotron radiation at Frascati, Italy. The SR-FTIR spectra were collected with Bruker system OPUS-65. Bruker spectrometer was used with microscope (Hyperion-3000) equipped with MCT and FPA (64×64 pixel) detectors. The video camera enabled optical imaging of the investigated area. In case of FPA detector the analyzed area was $170\text{ m} \times 170\text{ m}$ and thus the spatial resolution was about $3\text{ }\mu\text{m}$.

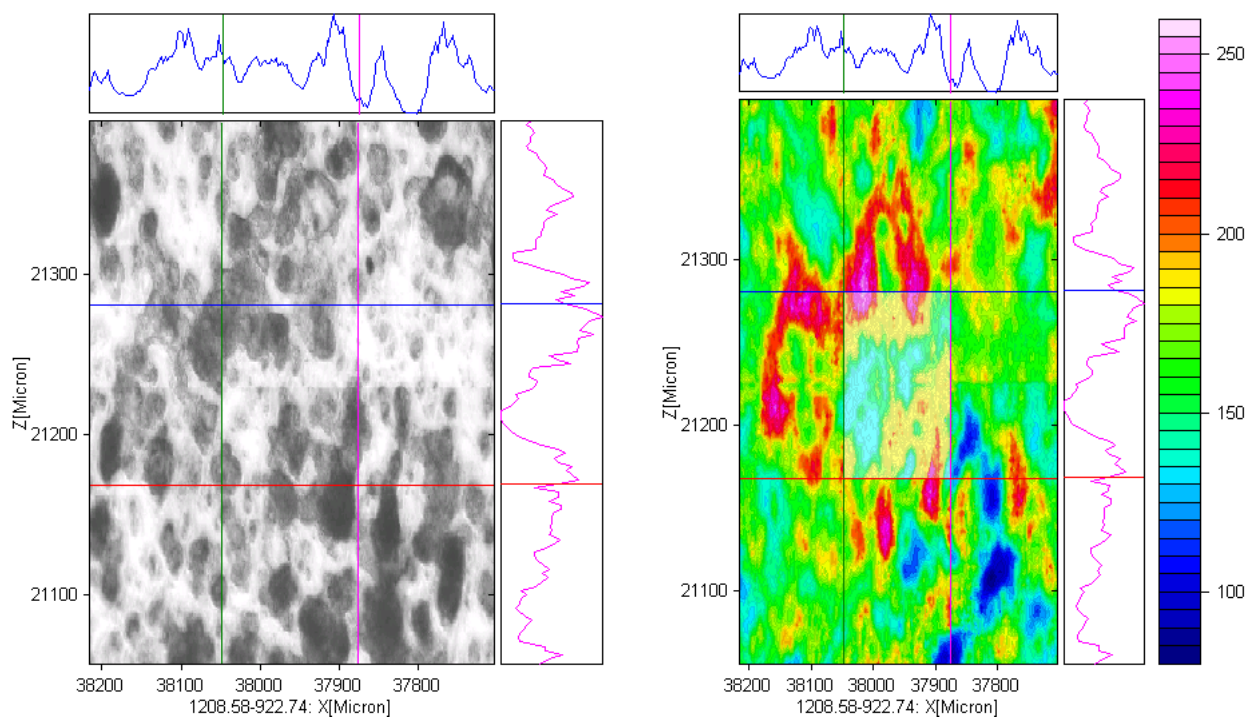


Figure 1: Optical and chemical images of CS/MMT foil analyzed in the region from 1208 cm^{-1} to 922 cm^{-1} .

The spectral data were baseline corrected. The band areas of the Si-O and COO- were calculated in the region from 1200 cm^{-1} to 900 cm^{-1} and from 1700 cm^{-1} to 1200 cm^{-1} respectively, which allow us to show chemical imaging of the samples.

As shown in Fig. 1 FTIR technique is a particularly efficient tool for the analysis of nanocomposite materials. This technique was used to determine dispersion of MMT nano-particles in polymer matrix (CS). We observed a correlation between the

concentration and distribution of nano-particles in nanocomposite samples. These results were confirmed by SEM/EDS studies and PIXE measurements which have been done at AGH University of Science and Technology and at Institute of Nuclear Physics PAN respectively, both in Kraków, Poland.

Acknowledgments: This work was supported by The Polish Ministry of Science and Higher Education, grant No. N N507 370735.

TOPOGRAPHIC AND HIGH-RESOLUTION DIFFRACTION STUDY OF DEFECT STRUCTURE OF RVO_4 SINGLE CRYSTALS

W. Paszkowicz^{1*}, O.N. Ermakova¹, W. Wierzchowski², K. Wieteska³, M. Berkowski¹,
M. Głowacki¹, H. Dąbkowska⁴, J. Domagała¹, J. Bąk-Misiuk¹, and C. Paulmann⁵

¹*Institute of Physics, Polish Academy of Sciences, al. Lotnikow 32/46, PL-02-668 Warsaw, Poland*

²*Institute of Electronic Materials Technology, ul. Wólczyńska 133, PL-01-919 Warsaw, Poland*

³*Institute of Atomic Energy, PL-05-400 Otwock-Swierk, Poland*

⁴*BIMR, Department of Physics, McMaster University, 1280 Main Street West, Hamilton L8S 4M1, Canada*

⁵*HASYLAB at DESY, Notkestr. 85, 22-603 Hamburg, Germany*

Keywords: orthovanadate, rare earth, defect structure, single crystal, X-ray topography

*e-mail: paszk@ifpan.edu.pl

Rare earth orthovanadates (RVO_4) have been reported to be applicable, in particular, as laser materials (see *e.g.* Ref. [1]), for remote thermometry, or as catalysts. The mostly studied orthovanadates are YVO_4 , LuVO_4 and GdVO_4 , due to their applicability in laser-diodes [2] and optical waveguides [3]. These materials typically crystallize in zirconite-type structure.

The defect structure of RVO_4 single crystals has not been extensively investigated. For crystals grown by various methods, the studies performed up to now indicate a variety of defects which can be formed in such crystals, for example cracks, inclusions, voids, glide bands, subgrain boundaries and dislocations. For a brief review of the knowledge in this field see Ref. [4]. For example, for a small $\text{LuVO}_4:\text{Yb}$ flux-grown crystal the FWHM of the 200 rocking curve has been reported to be 30 arcsec [4]. For $\text{LuVO}_4:\text{Nd}$ and GdVO_4 single crystals grown by Czochralski method [3, 5] the FWHM of the 200 rocking curve has been found to be as low as 67 arcsec. whereas in Czochralski grown YVO_4 and GdVO_4 crystals [6]-[8] the subgrains have been shown to exhibit misorientations of at least several arcsec.

The needle-shaped (up to $1 \times 2 \times 12 \text{ mm}^3$ size) crystals of RVO_4 ($\text{R} = \text{Gd}, \text{Pr}$ and Lu) were grown from PbO/PbF_2 flux by the slow cooling method. These crystals exhibit the natural 100 and 010 growth faces. Czochralski method was used for growth of RVO_4 crystals ($\text{R} = \text{Er}, \text{Ho}$ and Nd). The first of the two crystals have very distinct spiral habit. For transmission topographic studies these crystals were cleaved along $\{100\}$ faces.

The structure of the crystals was determined using a laboratory X-ray diffractometer. Defect properties of RVO_4 were studied using x-ray topography and high resolution (HR) diffraction. The HR diffraction study was performed using the PHILIPS XPERT/MRD diffractometer equipped with Cu tube ($\lambda = 1.54056 \text{ \AA}$), a four bounce $\text{Ge}(022)$ monochromator and a two bounce $\text{Ge}(022)$ analyzer. The topographic investigations included recording of the local rocking curves and the topographs in the monochromatic beam on the station

E2, and the investigation using back reflection white beam projection topography at the experimental station F1 (at the synchrotron DORIS III in HASYLAB). The HR diffraction curves were obtained for the 002 reflection. In the case of the monochromatic beam experiments, it was useful to take so called “zebra pattern” consisting in taking on a single film a series of topographs exposed at step-wise changed angular position. The monochromatic beam topographs and rocking curves were recorded in 400 reflection of the 0.115 nm radiation.

Example of topographic image for a flux-grown ErVO_4 crystal is shown in Fig. 1. The transmission section topographs confirmed low concentration of defects inside the needle flux-grown RVO_4 crystals. The linear contrasts visible in the reproduced topograph may be attributed to the growth sector boundaries and probably growth bands.

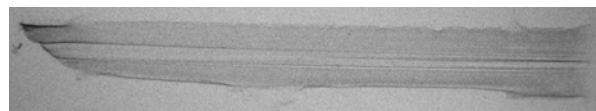


Figure 1: White beam reflection transmission section topograph of the needle-like ErVO_4 crystal grown by slow cooling method.

Examples of white-beam and monochromatic-beam topographs for Czochralski-grown crystals are presented in Fig. 2. With the use of white-beam topographic methods, these crystals are found, to be built from large single-crystal blocks, with misorientation of up to about one degree, the dominating defect within the blocks were subgrain boundaries characterized by relatively small disorientations. The rocking curves recorded with a $50 \mu\text{m}$ wide probe beam from a single large blocks were relatively narrow with FWHM in the range 3.8 – 6.3 arc seconds. The grain boundaries were of two types: many of them producing contrasts located along the $\langle 100 \rangle$ type directions, numerous other ones were of irregular shape. Tiny contrasts observed with both topographic methods inside the grains are attributed to uniformly distributed dislocations of density exceeding $5 \times 10^3 \text{ cm}^{-2}$. Densely distributed linear contrasts along $\langle 100 \rangle$ direction

may be interpreted as glide bands. The present topographs did not reveal any segregation fringes. We also observed, using the white- and monochromatic-beam topographs, round or less irregular clear contrasts with the diameter reaching tens of micrometers. As these contrasts are not connected with features of surface morphology, most likely they correspond to small amorphous inclusions, visible in white-beam images (Fig. 2).

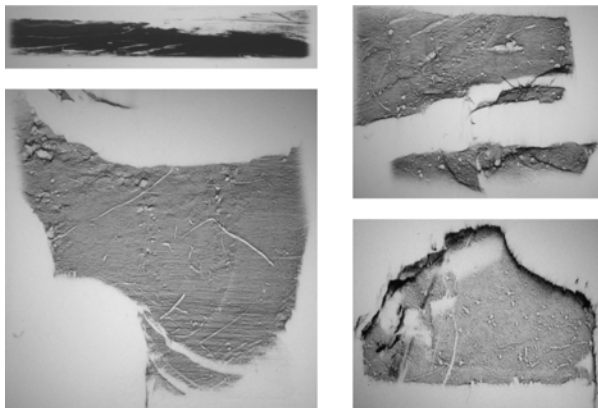


Figure 2: Monochromatic (upper left) beam topograph in 400 reflection ($\lambda = 0.115$ nm) radiation of Czochochalski grown sample of ErVO_4 crystal. White beam reflection projection topographs (lower left) of the cleaved surface of samples of ErVO_4 (lower left) HoVO_4 (upper right) and NdVO_4 (lower right) Czochochalski-grown crystals.

Acknowledgments: The measurements performed at HasyLab have received funding from the 7th Framework Programme (FP7/2007 – 2013) of European Community under ELISA grant agreement No. 226716.

References

[1] A.I. Zagumenny, T.V.G. Ostroumov, I.A. Shcherbakov, T. Jensen, J.P. Meyen, G. Huber, "The Nd:GdVO_4 crystal: A new material for

diode-pumped lasers," *Sov. J. Quantum Electron.* **22** (1992) 1071 – 1072.

- [2] L. Qin, X. Meng, J. Zhang, L. Zhu, H. Zhang, B. Xu, H. Jiang, "Growth and defects of Nd:GdVO_4 single crystal," *J. Cryst. Growth* **242** (2002) 183 – 188.
- [3] X.-L. Wang, K.-M. Wang, G. Fu, S.-L. Li, F. Chen, F. Lu, H.-J. Zhang, H.-K. Kong, J.-Y. Wang, X.-G. Xu, D.-Y. Shen, H.-J. Ma, R. Nie, "Optical planar waveguide fabricated in Nd:LuVO_4 crystal by MeV oxygen implantation," *Optics Express* **13** (2005) 675 – 680.
- [4] W. Paszkowicz, P. Romanowski, J. Bąk-Misiuk, W. Wierzchowski, K. Wieteska, W. Graeff, R.J. Iwanowski, M.H. Heinonen, O. Ermakova, H. Dąbkowska, "Characterization of an Yb:LuVO_4 single crystal using X-ray topography, high-resolution X-ray diffraction, and X-ray photoelectron spectroscopy," *Radiat. Phys. Chem.* **80** (2011) 1001 – 1007.
- [5] S. Zhao, H. Zhang, Y. Lu, "Spectroscopic characterization and laser performance of Nd:LuVO_4 single crystal," *Optical Mater.* **28** (2006) 950 – 955.
- [6] K. Wieteska, W. Wierzchowski, E. Wierzbicka, A. Malinowska, M. Lefeld-Sosnowska, T. Lukasiewicz, W. Graeff, "X-Ray topographic studies of defect structure in YVO_4 crystals," *Acta Phys. Pol. A* **114** (2008) 455 – 461.
- [7] A. Malinowska, E. Wierzbicka, M. Lefeld-Sosnowska, K. Wieteska, W. Wierzchowski, T. Lukasiewicz, M. Swirkowicz, W. Graeff, "Defect structure formed at different stages of growth process in erbium, calcium and holmium doped YVO_4 crystals," *Acta Phys. Pol. A* **117** (2010) 328 – 331.
- [8] E. Wierzbicka, A. Malinowska, K. Wieteska, W. Wierzchowski, M. Lefeld-Sosnowska, M. Świrkowicz, T. Łukasiewicz, and C. Paulmann, "Characterisation of the defect structure in gadolinium orthovanadate single crystals grown by the Czochochalski method," *Acta Phys. Pol. A* (2012), in print.

THERMAL EXPANSION OF CuInSe_2 W. Paszkowicz^{1*}, R. Minikayev¹, P. Piszora², M. Knapp³, D. Trots⁴, and R. Bacewicz⁵¹*Institute of Physics PAS, al. Lotnikow 32/46, 02-668 Warsaw, Poland*²*Faculty of Chemistry, A. Mickiewicz University, ul. Grunwaldzka 6, 60-780 Poznan, Poland*³*Karlsruhe Institute of Technology, KIT (Germany), IAM-ESS Institute for Applied Materials – Energy Storage Systems, Karlsruhe, Germany*⁴*Bayerisches Geoinstitut Universität Bayreuth Universitaetsstrasse 30, D-95447 Bayreuth, Germany*⁵*Institute of Physics, Warsaw Technical University, ul. Koszykowa 75, 00-662 Warsaw, Poland*Keywords: CuInSe_2 , thermal expansion, lattice parameter

*e-mail: paszk@ifpan.edu.pl

The CuSe_2 – In_2Se_3 phase diagram [1] includes several ternary compounds. The most known among them, copper indium diselenide, CuInSe_2 , (of chalcopyrite type, or, in a specially prepared nanocrystal form, of wurtzite type [2]) has been extensively studied because of opportunity of its application as an efficient absorber in polycrystalline-thin-film solar cells. In this case, good efficiency can be achieved using an absorbing layer of several micrometers thickness, only. The reported energy conversion efficiency approaches 20% [3, 4]. Recent studies show its possible use as a nanocrystal ink [5] in fabrication of dense absorber films.

Early studies on thermal expansion of CuInSe_2 were limited to temperatures above 30 and 60 K for a and c lattice parameters, respectively [6], and, for both parameters, to 80 K [7]. In the present study, the thermal expansion coefficient for CuInSe_2 are determined on the basis of the recently collected data [8] and compared with the existing literature data.

The crystals studied in this paper were grown at Warsaw University of Technology using the vertical Bridgman method without seed. The XRD measurements were carried out at a powder diffractometer at the B2 (Hasylab/DESY, Hamburg) beamline [9] using the Debye-Scherrer geometry. A diamond powder was used as internal wavelength calibrant.

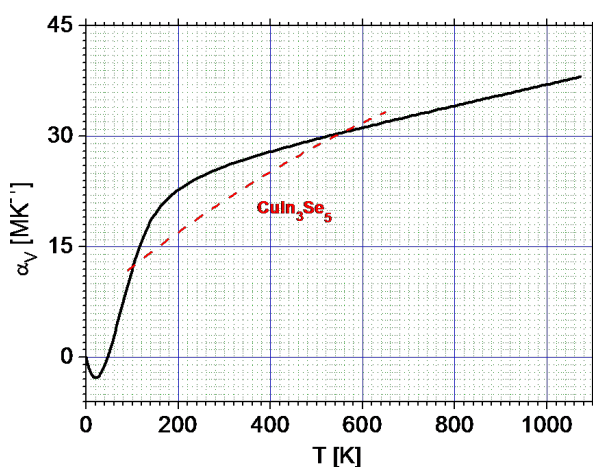


Figure 1: Volume thermal expansion coefficients of CuInSe_2 (solid line). Literature data for CuIn_3Se_5 [11] are shown for comparison (dotted line).

A preliminary study performed at the same synchrotron beamline without such standard has shown that the lattice parameters determined in this way suffer from non-smooth temperature behaviour [10], pointing out the necessity of elimination of the wavelength fluctuations. This problem was solved using the above-mentioned calibrant.

The obtained results of X-ray diffraction experiments show, in qualitative agreement with those reported in Ref. [6], that there is a vanishing tendency of the CuInSe_2 thermal expansion at the lowest temperatures; the values of the thermal expansion coefficients tend to be slightly negative below 50 K.

References

- [1] T. Gödecke, T. Haalboom, F. Ernst, “Phase equilibria of Cu-In-Se I. Stable states and nonequilibrium states of the In_2Se_3 - Cu_2Se subsystem,” *Z. Metallkd.* **91** (2000) 622 – 634.
- [2] M.E. Norako and R.L. Brutchey, “Synthesis of metastable wurtzite CuInSe_2 nanocrystals,” *Chem. Mater.* **22** (2010) 1613 – 1615.
- [3] J.R. Tuttle, J.S. Ward, A. Duda, T.A. Berens, M.A. Contreras, K.R. Ramanathan, A.L. Tennant, J. Keane, E.D. Cole, K. Emery, R. Noufi, “The performance of $\text{Cu}(\text{In}, \text{Ga})\text{Se}_2$ -based solar cells in conventional and concentrator applications,” *Mater. Res. Soc. Symp. Proc.* **426** (1996) 143 – 152.
- [4] M.A. Contreras, K. Ramanathan, J. AbuShama, F. Hasoon, D.L. Young, B. Egaas, R. Noufi, “Diode characteristics in state-of-the-art $\text{ZnO}/\text{CdS}/\text{Cu}(\text{In}_{1-x}\text{Ga}_x)\text{Se}_2$ solar cells,” *Prog. Photovolt.* **13** (2005) 209 – 216.
- [5] M.G. Panthani, V. Akhavan, B. Goodfellow, J.P. Schmidtke, L. Dunn, A. Dodabalapur, P.F. Barbara, B.A. Korgel, “Synthesis of CuInS_2 , CuInSe_2 , and $\text{Cu}(\text{In}_x\text{Ga}_{1-x})\text{Se}_2$ (CIGS) nanocrystal ‘inks’ for printable photovoltaics,” *J. Am. Chem. Soc.* **130** (2008) 16770 – 16777.
- [6] P. Deus, H. Neumann, G. Kuhn, B. Hinze, “Low-temperature thermal expansion in CuInSe_2 ,” *Phys. Stat. Sol. (a)* **80** (1983) 205 – 209.
- [7] I.V. Bodnar, N.S. Orlova, “Thermal expansion of CuAlSe_2 , CuGaSe_2 , and CuInSe_2 ,” *Izv. Akad. Nauk SSSR, Neorg. Mater.* **21** (1985) 1110; *Inorg. Mater.* **21** (1985) 967 – 970.

- [8] W. Paszkowicz, P. Piszora, R. Minikayev, M. Knapp, D. Trots, F. Firszt, R. Bacewicz, "Evolution of CuInSe₂ lattice parameters in a broad temperature range," *Z. Kristallogr. Proc.* **1** (2011) 373 – 378.
- [9] J. Ihringer, A. Köster, "Cryostat for synchrotron powder diffraction with sample rotation and controlled gas atmosphere in the sample chamber," *J. Appl. Crystallogr.* **26** (1993) 135 – 137.
- [10] W. Paszkowicz, P. Piszora, C. Bähitz, M. Knapp, F. Firszt, J. Bak-Misiuk, R. Bacewicz, "Lattice parameters of CuInSe₂ in the 10 – 295 K temperature range," *Hasylab Annual Report 2002*, pp. 217 – 218.
- [11] N.S. Orlova, I.V. Bodnar, T.L. Kushner, "Structural and physicalchemical properties of the CuGa₅Se₈, CuGa₃Se₅ and CuIn₃Se₅ compounds," *J. Phys. Chem. Solids* **64** (2003) 1895 – 1899.

THERMAL EXPANSION OF POLYCRYSTALLINE cBN IN THE LOW-TEMPERATURE RANGE

W. Paszkowicz^{1*}, P. Piszora², R. Minikayev¹, M. Brunelli³, and A. Fitch⁴

¹*Institute of Physics PAS, al. Lotników 32/46, 02-668 Warszawa, Poland*

²*Adam Mickiewicz University, Faculty of Chemistry, ul. Grunwaldzka 6, Poznań 60-780, Poland*

³*ILL Institut Laue-Langevin, BP 156, 38042 Grenoble cedex 9, France*

⁴*European Synchrotron Radiation Facility (ESRF), 6, rue Jules Horowitz,
BP 220, 38043 Grenoble Cedex, France*

Keywords: lattice parameter, thermal expansion, X-ray diffraction

**e-mail: paszk@ifpan.edu.pl*

Strong covalent bonding determines the elastic properties of hard materials such as diamond, cubic boron nitride (cBN) and a number of other binary or ternary carbides and nitrides. In particular, these crystals are characterized by high hardness, high bulk modulus and low thermal expansion (down to about 1 MK^{-1} at room temperature), accompanied by high melting point, and many of their applications are connected with these properties. Zincblende type boron nitride, a polymorph of boron nitride formed at high-pressure and considered as metastable one, has been discovered by Wentorf [1]. Its thermal expansion at low temperatures is expected, based on theoretical calculations, to be comparable to that of diamond, but experimental data are not available. To get a smooth experimental $a(T)$ curve and to derive a thermal expansion coefficient dependence on temperature, the conditions are challenging: the data must be collected at numerous temperature points and it is highly desirable that the lattice-parameter accuracy reaches the level of $10 - 4 \text{ \AA}$ or better.

The measurements were performed with a commercial sample (Sigma-Aldrich), purity 3N grain size $\sim 5 \text{ \mu m}$, using Debye-Scherrer geometry at beamline ID31 (ESRF). The cryostat (Janis)

ascertained a temperature stability and accuracy better than $\pm 0.1 \text{ K}$ over the studied temperature range. The applied detection system was based on a bank of nine point detectors, a Si(111) analyser crystals is located at each detector. Lattice parameters were calculated using the Rietveld refinement via the Fullprof program [3]. The obtained experimental $a(T)$ dependence shows a qualitative agreement with an earlier measured preliminary dataset. The resulting thermal expansion coefficient values are shown to be consistent with previously reported theoretical data.

References

- [1] R.H. Wentorf, Jr., "Cubic form of boron nitride," *J. Chem. Phys.* **26** (1957) 956 – 960.
- [2] V.V. Brazhkin, E.A. Ekimov, A.G. Lyapin, S.V. Popova, A.V. Rakhmanina, S.M. Stishov, V.M. Lebedev, Y. Katayama, K. Kato, "Lattice parameters and thermal expansion of superconducting boron-doped diamonds," *Phys. Rev. B* **74** (2006) 140502(R).
- [3] J. Rodriguez-Carvajal, *Physica B* **192** (1993) 55 – 69.

TERAHERTZ FEL SOURCE AT THE POLISH NATIONAL CENTER POLFEL. A CONCEPTUAL DESIGN

J.B. Pelka^{1*}, **O. Chołuj-Dziewiecka**², **J. Lorkiewicz**², **R. Nietubyć**^{2,3}, **J. Sekutowicz**⁴,
R. Sobierajski¹, **J. Szewiński**², **T. Wasiewicz**², and **G. Wrochna**²

¹*Institute of Physics, Polish Academy of Sciences, al. Lotników 32/46, PL-02668 Warsaw, Poland*

²*National Centre for Nuclear Studies, 05-400 Otwock-Świerk, Poland*

³*National Synchrotron Radiation Centre "Solaris," Jagiellonian University, Gronostajowa 7/p.1.6, PL-30387 Kraków, Poland*

⁴*Deutsches Elektronen Synchrotron, Notkestrasse 85, D-22607 Hamburg, Germany*

Keywords: Free Electron Laser, THz sources, 4th generation sources

**e-mail: pelkay@ifpan.edu.pl*

The present communication outlines the basic concept and design parameters of the THz-FEL 4th generation light source to be built in the planned National Center of Free Electron Laser POLFEL. The new terahertz source will be operating in the wavelength range of 6 – 1000 μm . The research capabilities of the powerful long-wavelength and fully tunable photon source, have been addressed to basic research in the wide range of disciplines, i.e., physical, biological, medical and material sciences, crucial to the key challenges facing development of science and technology. It is proposed to locate the facility at the National Centre for Nuclear Studies Świerk near Otwock.

The proposed concept includes innovative solutions in the photoinjector and RF Power systems. In order to concentrate efforts on those challenging subjects, the established technology will be adopted in other fields. This approach significantly reduces costs and helps in achieving high standards of the generated beam and operational performance.

In the THz-FEL facility construction it is planned, among others, to implement the continuous wave (CW) mode, unprecedented in other FELs. A high average power achieved in this way, significantly expands the application possibilities, also for technological tasks.

The construction will proceed in stages to accomplish eventually a full functionality of user

operation at the experimental beamlines. First, the emphasis will be put on the operation of low emittance, high repetition rate electron injector. It will ultimately produce 10^5 bunches per second, each carrying a charge of 1 nC. The bunches will be emitted by means of superconducting photocathode formed of lead film excited with 5th harmonic optical laser providing the light pulses of $\lambda = 204$ nm and energy of 5 μJ . Beam diagnostics and injector will be optimized to reach sufficient beam emittance, which allows to accelerate the electrons in resonant structure composed of two nine cell Tesla-type cavities housed by a cryogenic module. Continuous wave RF field will be generated by inductive output tubes. In CW mode of operation an electron beam energy of 30 MeV will be reached, however it will be possible to switch for pulse field operation in which electron energies up to 70 MeV will be available.

Initially a simple planar, fixed gap undulator will be installed which will emit a radiation in the wavelength range from 1000 μm down to 100 μm . The final step of THz-FEL radiation source construction at POLFEL will be completed with a linac extension by the second acceleration module and insertion of tunable planar undulator. In that way a light source will be capable to emit radiation with the wavelength range down to 6 μm .

SPECTROSCOPIC AND STRUCTURAL STUDIES OF INTERACTIONS BETWEEN GEMINI SURFACTANTS AND PHOSPHATIDYLOCHOLINE DERIVATIVES

Z. Pietralik, M. Kręcis, and M. Kozak*

Department of Macromolecular Physics, Faculty of Physics, Adam Mickiewicz
University, Umultowska 85, 61-614 Poznań, Poland

Keywords: gemini surfactants, phospholipids, SAXS, DSC, FTIR

*e-mail: mkozak@amu.edu.pl

Gemini surfactants are amphiphilic compounds which consist of two hydrophilic groups (“heads”) connected with a spacer group and two hydrophobic chains. The molecules of gemini surfactants above critical micellar concentration (CMC) can form aggregates or lamellar structures, which are packed in a certain way in the space [1]. Phosphatidylcholine derivatives are also amphiphilic molecules. They are built of a large polar head group and two hydrophobic chains. Phospholipids aggregate usually into a lamellar phase. The mixtures of phospholipids and surfactants are currently tested as delivery agents for gene therapy [2, 3].

The aim of this work was to investigate the influence of the spacer group length of cationic gemini surfactants: 1, 1’-(1, 4 hexane)bis3-dodecylloxymethyl-imidazolium chloride (C6) and 1, 1’-(1, 4 butane)bis3-dodecylloxymethylimidazolium chloride (C4) on the phase transitions of two derivatives of phosphatidylcholine - dimirystoyl- phosphatidylcholine (DMPC) and dipalmitoyl- phosphatidylcholine (DPPC) in the aquatic environment.

Infrared spectra were recorded by means of a BRUKER IFS 66 FTIR-RAMAN Spectrometer and DSC measurements were performed using a DSC-204 Phoenix Netzsch system equipped with high sensitivity μ -sensor.

A series of the SAXS data sets were collected in MaxLab, at Beam Line 7-11 and 9-11-4 (Lund, Sweden) [4]. The data were collected at temperatures from 6 to 30°C for DMPC and from 10 to 45°C for DPPC using the synchrotron radiation ($\lambda = 0.107$ nm and $\lambda = 0.091$ nm respectively) and a Mar 165 CCD detector. The scattering vector range was $0.05 < s < 3.42$ nm⁻¹. All data sets were processed (normalized to the incident beam intensity, corrected for detector response and the scattering of the buffer was subtracted) using the computer programs BLI7-11 [4] and PRIMUS [5].

The analysis of FTIR and DSC results showed that the addition of surfactant affects the phase

transition by shifting it towards lower temperatures. It is caused by formation of hydrogen bonds between the polar heads of lipids and surfactants as well as the interaction of surfactants with phospholipid acyl chains in the bilayer. It leads to changes in the trans-gauche conformation of phospholipids and the transition from rippled gel phase to lamellar liquid crystalline phase. The SAXS results implied a gradual disappearance of the lamellar phase typical of DMPC and DPPC and a probable formation of the mixed liposomes.

Acknowledgments: The research was supported by research grant (UMO-2011/01/B/ST5/00846) from National Science Centre (Poland).

References

- [1] R. Zana, “Dimeric and oligomeric surfactants. Behavior at interfaces and in aqueous solution: A review,” *Adv. Colloid Interface Sci.* **97** (2002) 205 – 253.
- [2] C.J.H. Porter, C.W. Pouton, J.F. Cuine, W.N. Charman, “Enhancing intestinal drug solubilisation using lipid-based delivery systems,” *Adv. Drug. Deliv. Rev.* **60** (2008) 673 – 691.
- [3] C. Bomelli, F. Faggioli, P. Luciani, G. Mancini, M.G. Sacco, “Efficient transfection of DNA by liposomes formulated with cationic gemini amphiphiles,” *J. Med. Chem.* **48** (2005) 5378
- [4] M. Knaapila, C. Svensson, J. Barauskas, M. Zackrisson, S.S. Nielsen, K.N. Toft, B. Vestergaard, L. Arleth, U. Olsson, J.S. Pedersen, Y. Cerenius, “A new small-angle X-ray scattering set-up on the crystallography beamline I711 at MAX-lab,” *J. Synchr. Radiat.* **16** (2009) 498 – 504.
- [5] P.V. Konarev, V.V. Volkov, A.V. Sokolova, M.H.J. Koch, D.I. Svergun, “PRIMUS: A Windows PC-based system for small-angle scattering data analysis,” *J. Appl. Crystallogr.* **36** (2003) 1277 – 1282.

STRUCTURAL ANALYSIS OF SELECTED GEMINI SURFACTANT (1-IMIDAZOLO-3-DECYLOXYMETHYL) PENTANE CHLORIDE LIPOPLEXES

Z. Pietralik, R. Krzysztoń, and M. Kozak *

¹Department of Macromolecular Physics, Faculty of Physics, Adam Mickiewicz University,
Umultowska 85, 61-614 Poznań, Poland

Keywords: gemini surfactants, phospholipids, DSC, FTIR

* e-mail: mkozak@amu.edu.pl

Cationic amphiphilic agents are one of the well established components for non-viral gene delivery vectors for gene therapy [1, 2]. Their natural ability to form self-assembled structures together with nucleic acids in water provides a protection of genetic material in vivo environment. Moreover, their positively charged hydrophilic parts demonstrate a great affinity to polyanionic nucleic acids, reducing strong repulsive interaction with cell membranes and causing significant condensation of attracted molecules. Those properties have a response in increased cell internalisation of nucleic acids and enhanced transfection [2].

A new class of amphiphilic cationic surfactants — gemini surfactants [3], is currently studied for gene delivery purposes [4, 5]. The gemini surfactant molecule is composed of two hydrophilic “head” groups attached to hydrophilic “tail” chains and connected via the molecular linker between them. The mixtures of cationic surfactants and lipids are recently under investigation [5, 6]. In our study mixtures of phosphatidylcholine derivatives (e.g. 1,2-dipalmitoyl-sn-glycero-3-phosphocholine [DPPC], 1,2-dimyristoyl-sn-glycero-3-phosphocholine [DMPC]) and gemini surfactants with cationic imidazole “head” groups are tested.

The influence of different concentrations of 1,5-bis (1-imidazolilo-3-decylooxymethyl) pentane chloride (cationic gemini surfactant) on the thermotropic phase behaviour of 1,2-dimyristoyl-sn-glycero-3-phosphocholine (DMPC) (PC derivative) bilayers was investigated using FTIR spectroscopy and differential scanning calorimetry DSC.

FTIR spectra were obtained by using BRUKER TENSOR 27 FT-IR spectrometer. DSC measurements were performed using DSC-204 Phoenix Netzsch system with a high sensitivity μ -sensor.

Thermotropic transitions between gel (L_β) \rightarrow rippled gel (P_β) and rippled gel (P_β) \rightarrow liquid

crystalline (L_α) phases were observed. FTIR analysis of CH_{2l} , CH_3 symmetric and antisymmetric stretching, as well as CH_2 scissoring bands showed discontinuous conformational changes in DMPC hydrophobic chains. Hydration of DMPC hydrophilic heads was investigated by analysis of $\text{C}=\text{O}$ stretching band. DSC analysis showed a decrease in enthalpy (ΔH) of the main transition ($P_\beta \rightarrow L_\alpha$) in correlation with the increase in (1-imidazolilo-3-decylooxymethyl) pentane chloride concentration.

Acknowledgments: The research was supported by research grant (UMO-2011/01/B/ST5/00846) from National Science Centre (Poland).

References

- [1] D. Deshpande, P. Blezinger, R. Pillai, J. Duguid, B. Freimark, A. Rolland, “Target specific optimization of cationic lipid-based systems for pulmonary gene therapy,” *Pharm. Res.* **15** (1998) 1340 – 1347.
- [2] W. Li, F.C. Szoka Jr., “Lipid-based nanoparticles for nucleic acid delivery,” *Pharm. Res.* **3** (2007) 438 – 449.
- [3] S.K. Hait, S.P. Moulik, “Gemini surfactants: A distinct class of self-assembling molecules,” *Curr. Sci.* **82** (2002) 1101 – 1111.
- [4] A.J Kirby *et al.*, “Gemini surfactants: New synthetic vectors for gene transfection,” *Angew. Chem. Int. Ed. Engl.* **42** (2003) 1448 – 1457.
- [5] C. Bomelli, F. Faggioli, P. Luciani, G. Mancini, M.G. Sacco, “Efficient transfection of DNA by liposomes formulated with cationic gemini amphiphiles,” *J. Med. Chem.* **48** (2005) 5378 – 5382.
- [6] J.A.S. Almeida *et al.*, “Structure and order of DODAB bilayers modulated by dicationic gemini surfactants,” *Phys. Chem. Chem. Phys.* **13** (2011) 13772 – 13782.

FTIR ANALYSIS OF PROTEIN SECONDARY STRUCTURE IN SOLID AND SOLUTION STATES

Z. Pietralik, I. Mucha-Kruczyńska, and M. Kozak*

Department of Macromolecular Physics, Faculty of Physics, Adam Mickiewicz University,
Umultowska 85, 61-614 Poznań, Poland

Keywords: ATR-FTIR, curve fitting, FSD, FTIR spectroscopy, protein structure

*e-mail: mkozak@amu.edu.pl

Currently there are a number of experimental methods for determination of secondary structure of polypeptides and proteins [1, 2]. Of all analytical tools, Fourier transform infrared spectroscopy (FTIR) is recognized as one of the most useful methods allowing characterization of proteins' secondary structure in aqueous solutions [2, 3], as well as lyophilized samples [4]. The determination of secondary structure of proteins using FTIR is based on the analysis of the amide absorption bands [1]-[6].

In this study, the percentage of the secondary structure elements of nine different proteins consisting of mainly α -helical structure (bovine serum albumin (BSA), hen egg white lysozyme (HEWL), xylose isomerase from *Streptomyces rubiginosus*), mixed α/β structure (albumin from chicken egg white, L-asparaginase from *Escherichia coli*, wheat germ agglutinin (WGA)), and β -sheet structure (human α -1-microglobulin (protein HC), β -lactoglobulin from bovine milk and human cystatin C) was estimated for lyophilized samples and in solution. FTIR data were collected in the transmission mode (proteins in KBr pellets) and using Attenuated Total Reflectance (ATR) for protein solutions in H₂O.

KBr pellets were made by grinding ca. 1 mg of protein with 200 mg of KBr and pressing the mixture using hydraulic press at 15 ton load. Protein solutions of at least 20 mg/ml were prepared by dissolving the appropriate amount of protein in H₂O. Infrared spectra were obtained from 500 co-added interferograms run on Bruker Tensor 27 FTIR spectrometer. All spectra were recorded from 400 cm⁻¹ to 4000 cm⁻¹ at both 2 cm⁻¹ and 4 cm⁻¹ spectral resolution.

Fourier self-deconvolution (FSD) was applied to amide I region (1705 – 1595 cm⁻¹) of protein spectra assuming an initial Lorentzian line-shape function with a FWHM of 13 cm⁻¹ [5]. Composite bands were assigned to helical segments, β -sheets, turns or unordered structures based on previous

experimental work [6] or calculated values [7]. The relative areas of the individual peaks were determined by an iterative curve-fitting procedure that assumed Gaussian (KBr samples) or Voigt (proteins in solution) band envelopes for the deconvolved components. Integrated peak areas were used to estimate secondary structure content for each of the nine proteins studied.

Acknowledgments: The present study was carried out with financial support from the Ministry of Science and Higher Education (grant nr N N202 127237).

References

- [1] J.T. Pelton, L.R. McLean, "Spectroscopic methods for analysis of protein secondary structure," *Anal. Biochem.* **277** (2006) 167 – 176.
- [2] P.I. Haris, F. Severcan, "FTIR spectroscopic characterization of protein structure in aqueous and non-aqueous media," *J. Mol. Catal. B-Enzym.* **7** (1999) 207 – 221.
- [3] A. Dong, P. Huang, W.S. Caughey, "Protein secondary structures in water from second-derivative amide I infrared spectra," *Biochemistry* **29** (1990) 3303 – 3308.
- [4] J.D. Meyer, M.C. Manning, J.F. Carpenter, "Effects of potassium bromide disk formation on the infrared spectra of dried model proteins," *J. Pharm. Sci.* **93** (2004) 496 – 506.
- [5] J.K. Kauppinen, D.J. Moffatt, H.H. Mantsch, and D.G. Cameron, "Fourier self-deconvolution — a method for resolving intrinsically overlapped bands," *Appl. Spectrosc.* **35** (1981) 271 – 276.
- [6] S. Matheus, W. Friess, H. Mahler, "FTIR and nDSC as analytical tools for high-concentration protein formulations, Pharmaceutical Research, 23 (2006), 1350 – 1363.
- [7] M. Levitt, J. Greer, "Automatic identification of secondary structure in globular proteins, *J. Mol. Biol.* **14** (1977) 181 – 293.

HYDROGEN REDUCTION OF LiMn_2O_4 : IDENTIFICATION OF PRODUCTS WITH SYNCHROTRON X-RAY POWDER DIFFRACTION

P. Piszora* and **J. Darul**

Department of Materials Chemistry, Faculty of Chemistry, Adam Mickiewicz University, Grunwaldzka 6, 60-780 Poznań, Poland

Keywords: lithium-manganese oxides, X-ray diffraction, Rietveld refinement

**e-mail: pawel@amu.edu.pl*

Lithium-manganese oxides are commonly used for cathodes in lithium-ion batteries because of their low cost and minimum toxicity, they are useful as catalysts [1] and as selective absorbents [2]. Removal of the Li cation from LiMn_2O_4 converts this spinel to a water oxidation catalyst [3]. The proton-exchanged LiMn_2O_4 showed high catalytic activity for the oxidation of methane and n-butane [4]. Heating of the LiMn_2O_4 sample under high pressure leads to oxides with the oxidation state of manganese lower than 3.5 [5]. This dynamic process of phase transformation and decomposition leads to reduction of Mn without a reducing atmosphere.

LiMn_2O_4 sample was obtained from mixture of Li_2CO_3 (Merck) and $\alpha\text{-Mn}_2\text{O}_3$ powders, by solid-state reaction in the air. The sintering temperatures was 1073 K (4h) and the sample was finally quenched in the solid CO_2 .

The temperature programmed reduction (TPR) were performed with a reducing gas mixture, 5% hydrogen in helium, flowed continuously over the sample. The reaction rate signal was recorded as a function of time and temperature. In this way it was possible to observe the intermediate reactions, depending from analytical conditions such as temperature rate, flow rate and concentration of reactive gas. Combined use of the synchrotron X-ray powder diffraction and the TPR methods enabled successfully qualitative and quantitative analysis of the hydrogen reduction of LiMn_2O_4 . Structure refinement with the Rietveld profile analysis, based on the synchrotron radiation X-ray diffraction data enabled phase analysis and extraction of the structural parameters for each identified crystal phases. The hydrogen consumption maxima in TPR spectra was correlated to the phase composition and chemical formula were proposed for each step of reduction.

The structural investigations of the reduction products samples with synchrotron radiation were performed at the Beamline B2 (HASYLAB), with the high-resolution X-ray diffractometer. The wavelength, determined by calibration using a NIST silicon standard, was 1.13961 Å. The X-ray data analysis was performed with GSAS software.

LiMn_2O_4 sample was examined in detail with XRD, after each TPR peak (Figure 1). The major

phase observed after the first TPR peak, at 724 K, is manganese(II) oxide. The tetragonally distorted spinel $\text{Li}_x\text{Mn}_{3-x}\text{O}_4$ was also detected after the hydrogen reduction at this temperature.

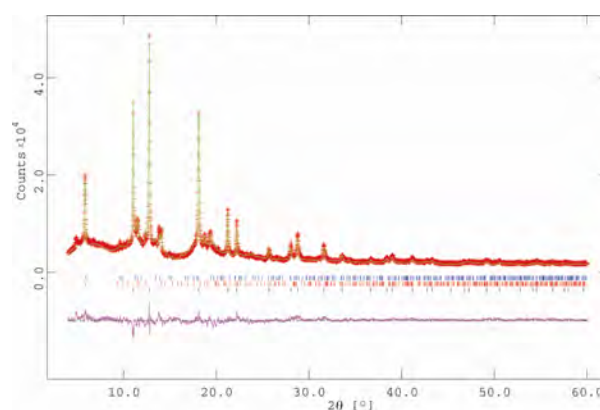


Figure 1: Results of Rietveld refinement after the hydrogen reduction of LiMn_2O_4 at 724 K.

Acknowledgments: The research leading to these results has received funding from the European Community's Seventh Framework Program (FP7/2007 – 2013) under Grant agreement no 226716.

References

- [1] X. Yang, H. Kanoh, W. Tang, K. Ooi, *J. Mat. Chem.* **10** (2000) 1903.
- [2] S.-Y. Sun, X. Song, Q.-H. Zhang, J. Wang, J.-G. Yu, *Adsorption* **17** (2011) 881.
- [3] D.M. Robinson, Y.B. Go, M. Greenblatt, G.C. Dismukes, "Water oxidation by $\lambda\text{-MnO}_2$: Catalysis by the cubical Mn_4O_4 subcluster obtained by delithiation of spinel LiMn_2O_4 ," *J. Am. Chem. Soc.* **132** (2010) 11467.
- [4] K. Sato, Y. Inoue, S. Yasukawa, H. Takahashi, "The surface structure formed by H_2 desorption from proton-exchanged $\text{H}_y\text{Li}_{1-(x+y)}\text{Mn}_2\text{O}_4$ and its catalytic activity for oxidation of methane and butane," *Appl. Surf. Sci.* **65 – 66** (1993) 308.
- [5] J. Darul, W. Nowicki, C. Lathe, P. Piszora, "Observation of phase transformations in LiMn_2O_4 under high pressure and at high temperature by in situ X-ray diffraction measurements," *Radiat. Phys. Chem.* **80** (2011) 1014.

X-RAY DIFFRACTION STUDY OF SOME LIQUID BINARY SOLUTIONS

A. Romaniuk*, H. Drozdowski, and Z. Błaszczak

Department of Optics, Faculty of Physics A. Mickiewicz University,
ul. Umultowska 85, 61-614 Poznań, Poland

Keywords: binary solution, X-ray diffraction patterns, angular intensity distributions

*e-mail: aniam@amu.edu.pl

This paper should be treated as an introduction in the attempts to apply radial distribution functions in the analysis of structure of a noncrystalline system which, for example, is selected binary solutions: *ortho*-nitrotoluene, *ortho*-chloroanisole, *ortho*-nitroanisole. Radial distribution function methods are applied [1]. The radial distributions are obtained by numerical analysis, applying computer methods to experimental angular functions of intensity distribution $I(S)$ (with all corrections included, and after normalization of the curves) with the help of the Fourier transform of the function $I(S)$ [2].

Measurements were performed by the Bragg-Brentano method [3] with an automatic goniometer

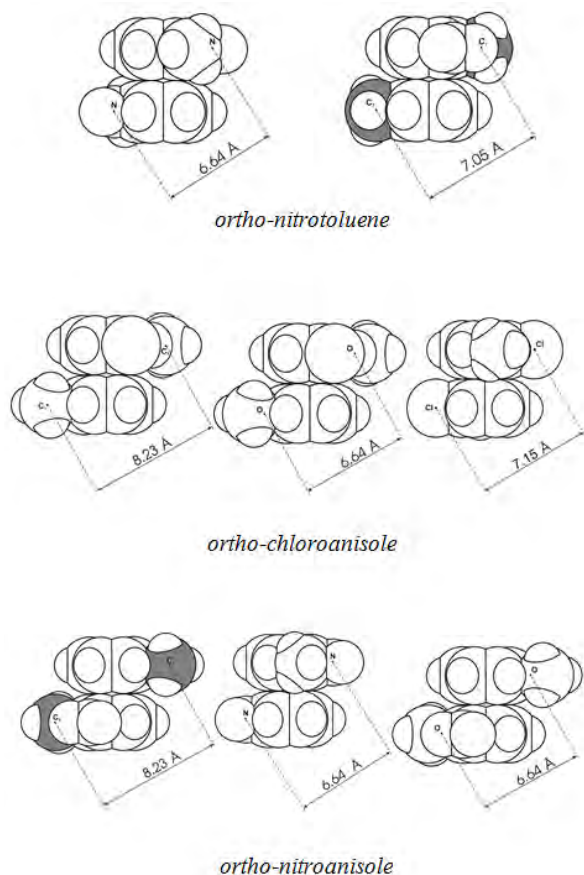


Figure 1: Models of the most highly probable mutual disposition of molecules in 10% solution of *ortho*-nitrotoluene, *ortho*-chloroanisole, *ortho*-nitroanisole in 1,4-dimethylbenzene.

working in cooperation with an X-ray generator characterized with high stability of supply current and high voltage.

The angular intensity distributions of X-ray radiation were normalized by bringing to electron units by the computer method applying a special programme. Each function $I(S)$ was normalized by the “oscillation method” or by the “area method,” i.e. the oscillation of the experimental function was compared with that of the theoretical function or the areas under the experimental function were compared to those under the theoretical one. In both cases the normalization was performed for high Bragg angles of scattering.

A simple model of short-range arrangement of the molecules in liquid binary solutions studied was proposed, Fig. 1. Local, most probable manners of packing and mutual orientations of molecules within the space of the first coordination sphere are discussed [4].

Because of the supposed role the ring in mutual configurations of molecules in liquid binary solutions, it seems very probable that the proposed models of local arrangement (Fig. 1) can also hold for other weakly polar derivatives of binary solutions in the liquid phase.

The approach proposed in this paper gives a good description of intermolecular interactions in liquid binary solutions and is a useful X-ray method for their analysis.

References

- [1] H. Drozdowski, “Local structure and molecular correlations in liquid 1-methylnaphthalene at 293 K,” *Chem. Phys. Lett.* **351** (2002) 53 – 60.
- [2] H. Drozdowski, A. Mansfeld, “X-ray analysis of intermolecular interactions in solution of *ortho*-nitroanisole $C_7H_7NO_3$ in 1,4-dimethylbenzene,” *Phys. Chem. Liq.* **46** (2008) 255 – 262.
- [3] A. Guinier, *Theorie et Technique de la Radiocristallographie* (Dunod, Paris 1986).
- [4] H. Drozdowski, A. Romaniuk, “X-Ray diffraction investigation of the crystalline and liquid *para*-chloroanisole,” *Polish Crystallogr. Meeting Wrocław* **51** (2009) 272 – 27.

Mn₄Si₇ NANOINCLUSIONS IN Mn-IMPLANTED Si

P. Romanowski¹, J. Bąk-Misiuk^{1*}, K. Sobczak¹, P. Dziawa¹, E. Dynowska¹,
A. Szczepańska¹, and A. Misiuk²

¹Institute of Physics, Polish Academy of Sciences, al. Lotników 32/46, PL-02668 Warsaw, Poland

²Institute of Electron Technology, al. Lotników 32/46, PL-02668 Warsaw, Poland

Keywords: Si:Mn, synchrotron radiation, annealing, Mn₄Si₇, nano-inclusions, ferromagnetism, X-ray diffraction, TEM

*e-mail: bakmi@ifpan.edu.pl

Among variety of materials silicon is very important from the viewpoint of the device integration. Recently it has been suggested that manganese silicide nanoparticles created in silicon implanted with manganese and next annealed at high temperatures show ferromagnetism [1]. In present work the influence of annealing conditions on creation of Mn₄Si₇ nano-inclusions and ferromagnetic behavior of Mn⁺-implanted silicon (Si:Mn) was studied.

Czochralski *p*-type 001-oriented Si (Cz-Si) as well as Floating zone *n*-type 001-oriented Si (Fz-Si) single crystals were implanted with 160 keV Mn⁺ ions to a dose 1×10^{16} cm⁻². To avoid amorphization, the temperature of the surface during the implantation was set to 610 K. Such a fluence of Mn ions results in the dopant concentration of 1.2 at. % at the maximum of Mn distribution profile. Next the samples were processed for 1 h up to 1070 K under ambient pressure.

To investigate phase composition of the near-surface implanted layer, glancing incidence diffraction and synchrotron radiation were applied. It was found that nanoparticles of Mn₄Si₇ phase were created by post-implantation high-temperature treatment.

The dimensions and concentration of the defects related with the silicides inclusions were calculated from the X-ray diffuse scattering observed in diffraction rocking curves, measured using synchrotron radiation [2, 3]. The double logarithmic plot of intensity versus the position of q indicate three different regions with slope -2 (Huang scattering), -3 (Stokes-Wilson scattering) and -2 (thermal scattering), respectively (see Fig. 1). The observed silicides are responsible for the Huang diffuse scattering very close to the Bragg peak. By study of slopes and transitions from the regions, the dimensions and concentration of the inclusions were assigned according to the method described in [3]. It was found that the sizes of the inclusions increase with the annealing temperature while their concentration decreases.

The dimensions of inclusions were also determined by transmission electron microscopy (TEM)

method and compared with X-ray diffraction methods.

Magnetic properties of the Si:Mn samples were studied using SQUID magnetometer device. The origin of ferromagnetism is discussed in conjunction of the nano-inclusions.

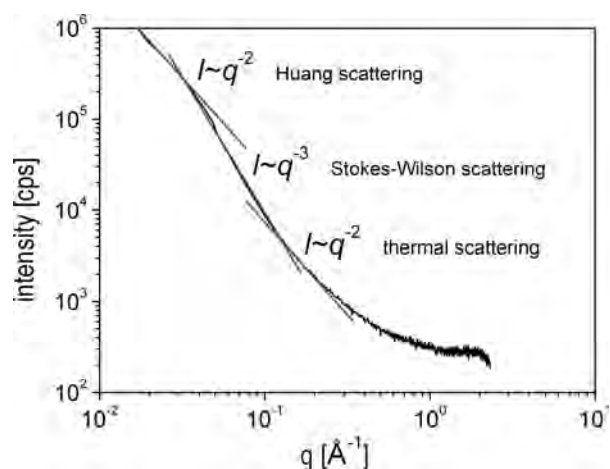


Figure 1: The double logarithmic plot of diffraction rocking curve measured for Cz-Si:Mn annealed at 870 K.

Acknowledgments: The authors thank Dr. Wolfgang Caliebe of HASYLAB at DESY in Hamburg for technical support during the diffraction measurements at W1/DORIS synchrotron beamline.

References

- [1] S. Yabuuchi, H. Kageshima, Y. Ono, M. Nagase, A. Fujiwara, E. Ohta, "Origin of ferromagnetism of MnSi_{1.7} nanoparticles in Si: First-principles calculations," *Phys. Rev. B* **78** (2008) 045307.
- [2] J.R. Patel, "X-ray diffuse scattering from silicon containing oxygen clusters," *J. Appl. Cryst.* **8** (1975) 186 – 191.
- [3] M. Moreno, B. Jenichen, V. Kaganer, W. Braun, A. Trampert, L. Däweritz, K.H. Ploog, "MnAs nano-clusters embedded in GaAs studied by X-ray diffuse and coherent scattering," *Phys. Rev. B* **67** (2003) 235206.

XAS STUDY OF Mo DOPED TiO₂ NANOPARTICLE MATERIALS

K. Schneider^{1,3*}, M. Sikora¹, J. Stępień¹, K. Biernacka¹, Cz. Kapusta¹, D. Zajac²,
K. Michalow-Mauke⁴, Th. Graule⁴, A. Vital⁴, K. Zakrzewska³, and M. Rekas⁵

¹Faculty of Physics and Applied Computer Science, AGH University of Science and Technology, Kraków, Poland

²Helmholtz-Zentrum Berlin für Materialien und Energie GmbH, Institute of Solar Fuels and Energy Storage Materials, Berlin

³Faculty of Electrical Engineering, Automatics, Computer Science and Electronics, AGH University of Science and Technology, Kraków, Poland

⁴EMPA, 129, Ueberlandstrasse, Duebendorf, Switzerland

⁵Faculty of Materials Science and Ceramics, AGH University of Science and Technology, Kraków, Poland

Keywords: titanium dioxide, nanomaterials, XAS spectroscopy

* e-mail: kryschna@agh.edu.pl

A XAS study of the Mo-doped TiO₂ (0.4 and 1 at % Mo) nanoparticle materials at the *K* edges of molybdenum are presented. The materials were prepared with Flame Spray Synthesis (FSS) process by oxidation of metal-organics precursors. The measurements at the molybdenum *K* edge were carried out at the E4 beamline with the total fluorescence detection at room temperature (HASYLAB, DESY, Hamburg, Germany).

The Mo:*K* EXAFS functions presented in the Fig. 1 show a considerable decrease of the second-neighbour-shell peak with increasing Mo content, which corresponds to increased number of cation vacancies. The Mo XANES spectra are very nearly the same, which indicates the same Mo oxidation state in both samples. A close similarity to the XANES spectrum of MoO₃ indicates a Mo⁶⁺ state with a similar distribution of oxygen distances in the nearest neighbour shell, confirmed by simulations.

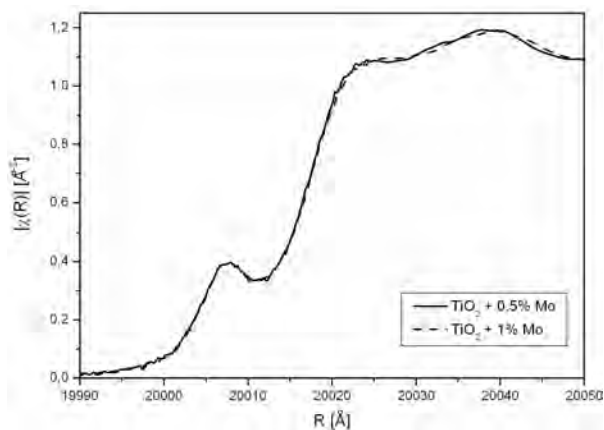


Figure 1: XANES spectra on Mo:*K* edge for Mo-doped TiO₂ (0.5 at % Mo — solid line and 1 at % Mo — dashed line).

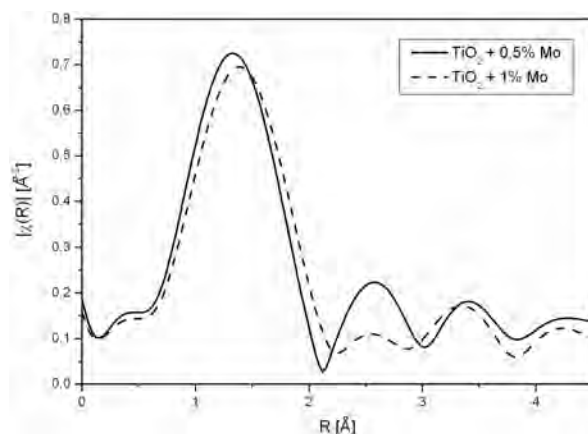


Figure 2: Fourier transforms of the Mo:*K* edge EXAFS functions for Mo-doped TiO₂ (0.5 at % Mo — solid line and 1 at % Mo — dashed line).

The EXAFS functions in the *R* space obtained from the Mo:*K* edge spectra are presented in the Fig. 2. The peak of the oxygen nearest neighbour shell is centered at 1.4 Å. The second peak, which is centered at 2.6 Å corresponding to the cations in the 2nd nearest neighbour shell is two times smaller in the sample with 1% Mo than for 0.5% Mo. This corresponds to a two times smaller number of cation nearest neighbours in the 1% Mo sample, i.e. to about 50% cation vacancies in the 2nd nearest neighbour shell of Mo ion. Having in mind that the number of cation neighbours in this shell corresponding to the anatase structure is 4 and in the rutile structure is 2 this would mean that the Mo ions in the 1% Mo sample have the local ionic environment characteristic for rutile. This is also confirmed by a slightly larger distance of the 1st oxygen neighbour shell in this sample.

HELICAL SCREW-TYPE MAGNETIC STRUCTURE OF THE MULTIFERROICS $\text{CaMn}_7\text{O}_{12}$

W. Sławiński^{1*}, R. Przeniosło¹, I. Sosnowska¹, and V. Petricek²

¹*Faculty of Physics, University of Warsaw, Hoża 69, 00-681 Warsaw, Poland*

²*Institute of Physics of the Academy of Sciences of the Czech Republic, v.v.i.,
Na Slovance 2, 182 21 Praha 8, Czech Republic*

*e-mail: wojciech@fuw.edu.pl

The modulated crystal structure and modulated magnetic ordering of the multiferroic $\text{CaCu}_x\text{Mn}_{7-x}\text{O}_{12}$ is studied by analysing neutron and SR powder diffraction data with a model based on the magnetic superspace group $\text{R}31'(00\gamma)\text{ts}$. Both atomic position modulations and magnetic modulations are described with the modulation vector $(0, 0, q)$. The magnetic ordering is a screw type circular helix where the magnetic moments are perpendicular to the \mathbf{c} direction. The temperature dependence of the modulation vector length and the ordered magnetic mo-

ments of Mn^{3+} and Mn^{4+} ions is given between $T = 50$ K and the Néel temperature $T_N = 90$ K. The atomic position modulation length L_p and the magnetic modulation length L_m fulfil the relation $L_m = 2L_p$ at all temperatures between 50 K and T_N .

References

- [1] W. Sławiński, R. Przeniosło, I. Sosnowska, and V. Petricek, *Acta Crystallographica B* 2012 (in press).

XFEL — EUROPEAN X-RAY FREE ELECTRON LASER**R. Sobierajski^{1*}, J.B. Pełka¹, R. Nietubyć^{2,3}, G. Wrochna², and J. Sekutowicz⁴**¹*Institute of Physics, Polish Academy of Sciences, al. Lotników 32/46, PL-02668 Warsaw, Poland*²*National Centre for Nuclear Studies, PL-05400 Otwock-Świerk, Poland*³*National Synchrotron Radiation Centre “Solaris,” Jagiellonian University, Gronostajowa 7/p.1.6, PL-30387 Kraków, Poland*⁴*Deutsches Elektronen Synchrotron, Notkestrasse 85, D-22607 Hamburg, Germany**Keywords: Free Electron Laser, THz sources, 4th generation sources***e-mail: sobieraj@ifpan.edu.pl*

Free Electron Lasers (FEL) are numbered among the most powerful sources of monochromatic pulsed radiation, tunable over a wide wavelength range.

Many properties of radiation generated by optical lasers and by FEL sources are similar to each other, though these devices are based on different principles. In fact, free electron lasers are more like a synchrotron radiation (SR) sources. The SASE (Self Amplified Spontaneous Emission) process forms the basis of high gain FELs (known as SASE-FELs), making it possible to generate extremely strong, femtosecond pulses of radiation in the short wavelength range, up to the hard X-rays. SASE-FELs create a new class of 4th generation SR sources, with their spectral brightness that exceeds the brightest known 3rd generation synchrotron radiation sources by more than eight orders of magnitude.

The European X-ray Free Electron Laser (XFEL), built in Hamburg, will be the largest and most advanced 4th generation source of short-wavelength synchrotron radiation, with an unprecedented combination of properties and a radically new research opportunities. After starting in 2015, it will generate very strong femtosecond pulses of

coherent monochromatic X-rays in a wavelength range down to 0.1 nm.

The peak power of radiation pulse will reach up to several GW, which corresponds to the peak spectral brightness of the order of 10^{33} photons/s/mm²/mrad²/0.1% BW. This value exceeds by more than 10^8 times the brightness of X-rays generated by the most powerful 3rd generation synchrotron sources currently operating. Like all free electron lasers, XFEL is fully tunable. Generated radiation is characterized by, among others, total polarization, high collimation and a high degree of spatial coherence.

The contribution is aimed at presenting the concept of the XFEL and its basic elements, such as a linear electron accelerator, undulators and experimental beamlines. The new revolutionary possibilities of excitation of exotic states of matter (warm dense plasma) and, above all, opportunity to study the structure and dynamics of condensed matter with atomic spatial and femtosecond temporal resolution has become important prerequisites for a decision on building a European X-ray free electron laser XFEL. In this project participates also Poland.

DAMAGE OF MULTILAYER OPTICS UNDER IRRADIATION WITH MULTIPLE FEMTOSECOND XUV PULSES

R. Sobierajski^{1*}, D. Klinger¹, P. Dłużewski¹, M. Klepka¹, J. Gaudin², C. Özkan²,
J. Chalupský³, S. Bajt⁴, T. Burian³, L. Vyšín³, N. Coppola², S.D. Farahani²,
H.N. Chapman⁴, G. Galasso², V. Hájková³, M. Harmand⁵, L. Juha³, M. Jurek¹, R. Loch⁶,
S. Mölle⁷, M. Nagasono⁸, H. Sinn², K. Saskl⁹, J. Schulz^{1,3}, P. Sovak¹⁰, S. Toleikis⁵,
K. Tiedtke⁵, T. Tschentscher², and J. Krzywinski⁷

¹*Institute of Physics, Polish Academy of Sciences, Al. Lotników 32/46, Warsaw, PL-02-668, Poland*

²*European XFEL GmbH, Albert-Einstein-Ring 19, Hamburg, D-22671, Germany*

³*Institute of Physics, Academy of Sciences of the Czech Republic, Na Slovance 2,
Prague 8, 182 21, Czech Republic*

⁴*Center for Free-Electron Laser Science, DESY, Notkestr. 85 Hamburg, D-22607, Germany*

⁵*HASYLAB/DESY, Notkestr. 85 Hamburg, D-22607, Germany*

⁶*FOM — Institute for Plasma Physics Rijnhuizen, NL-3430 BE Nieuwegein, The Netherlands*

⁷*SLAC National Accelerator Laboratory, 2575 Sand Hill Road, Menlo Park, California 94025, USA*

⁸*RIKEN/SPring-8 Kouto 1-1-1, Sayo, Hyogo, 679-5148 Japan*

⁹*Institute of Materials Research, Slovak Academy of Sciences, 040 01 Kosice, Slovak Republic*

¹⁰*Institut of Physics, P. J. Šafárik University, Park Angelinum, 04154 Kosice, Slovak Republic*

Keywords: synchrotron radiation, free electron laser

**e-mail: ryszard.sobierajski@ifpan.edu.pl*

Multilayer coated optics are used for control of XUV and soft X-ray radiation in many fields of science and technology, and has experienced a considerable boost of technology due to the application in advanced photolithography. A new field is the application in experiments at short wavelength Free Electron Lasers. This includes the x-ray sources — LCLS (USA), XFEL (Europe) & SACLA (Japan) and the XUV sources — FLASH (Germany), ELETTRA (Italy). Multilayer coated optics enables deflection angles much larger than those reasonably achieved with monolayer mirrors. In addition, due to its good wavelength selectivity, it can be used as a narrow band filter.

The photon flux from short wavelength Free Electron Lasers is extremely high. In the case of FLASH, operating in the XUV regime the 10 fs long pulses can have energy of up to 50 μJ , corresponding to 10^{11} W/cm² for a 4 mm beam spot on the optics. This is at least 10 orders of magnitude higher than in the case of lithography. Damage or even destruction of the optics can be expected, what could limit the performance of the multilayer optics.

We have carried out research on the flux resistivity of a MoSi multilayer for radiation of 4.7 nm wavelength by means of exposures at FLASH. Samples were irradiated at different intensity levels with single and multiple shots. Morphological and structural surface changes were measured with

phase-contrast microscopy, atomic force microscopy and scanning transmission electron microscopy.

The exposure to the single pulses of intensity higher than the damage threshold lead to surface modifications similar as in case of previous experiments at longer wavelength [1]. As expected the damage threshold in case of the multiple shot exposures was much smaller than in case of single pulses. The structural changes induced by radiations are much different than the previously observed for single shot exposures. The results of the experiments and the related physical processes will be discussed on presentation.

Acknowledgments: The authors wish to thank the staff of FLASH at DESY, Hamburg, Germany for supplying the beam time at FLASH. This work has been partially supported by the Foundation for Fundamental Research on Matter (Stichting voor Fundamenteel Onderzoek der Materie, FOM), the Nederlandse Organisatie voor Wetenschappelijk Onderzoek (NWO).

References

- [1] A.R. Khorsan *et al.*, “Single shot damage mechanism of Mo/Si multilayer optics under intense pulsed XUV exposure,” *Opt. Express* **18** (2010) 700.
- [2] R. Sobierajski *et al.*, “Damage mechanisms of MoN/SiN multilayer optics for next-generation pulsed XUV light sources,” *Opt. Express* **19** (2011) 193.

ON THE LOCAL STRUCTURE OF CATALYTIC Au/Pd NANOPARTICLES STABILIZED ON SPHERICAL POLYELECTROLYTE BRUSHES

W. Szczerba^{1*}, J. Kaiser², H. Riesemeier¹, U. Reinholz¹, M. Radtke¹,
L. Yu², M. Ballauff², and A.F. Thünemann¹

¹BAM Federal Institute for Materials Research and Testing, Unter den Eichen 97, 12205 Berlin, Germany

²Helmholtz-Centre Berlin, Hahn-Meitner-Platz 1, 14109 Berlin, Germany

Keywords: EXAFS, gold, palladium, nanoparticle, nanoalloy

*e-mail: wojciech.szczerba@bam.de

Nowadays, metal nanoalloys are attracting more interests than metal nanoparticles. Their physical and chemical properties can be variegated by the type of composition, size and structure. The main application of such alloys is in catalysis, because of their synergistic effect, which means that the alloy particles show much higher catalytic activity than that of the pure single metal particle.

Recently, we have demonstrated that spherical polyelectrolyte brushes (SPB) can work efficiently as carrier system for the immobilization of Au-Pd nanoalloys. HR-TEM demonstrates that well-defined alloy nanoparticles can be obtained with size in the range of 1 – 2 nm. Figure 1 shows the schematic structure of Spherical Polyelectrolyte Brushes and TEM images of Au/Pd alloys.

In order to get precise information about the structure and composition of alloy particles, ex-

tended X-ray absorption fine structure (EXAFS) was the method of choice for us. Noble metal alloys containing Au/Pd have been measured for various compositions at the Au L_3 -edge and Pd K -edge at BESSY II in Berlin.

In order to interpret the data models employing the FEFF code have been established. It has been found that the Au EXAFS is purely metallic, whereas the Pd EXAFS exhibits a strong non-metallic Pd signal, and a significantly smaller metallic contribution. The models suggest that the particles consist of a Au/Pd alloy with an increasing Au gradient toward the center. The particle surface is most probably covered by a monolayer of non-metallic palladium compounds, e.g. Pd-O, Pd-Cl, which does not give any contrast in TEM, but contributes significantly to the Pd XAFS signal.

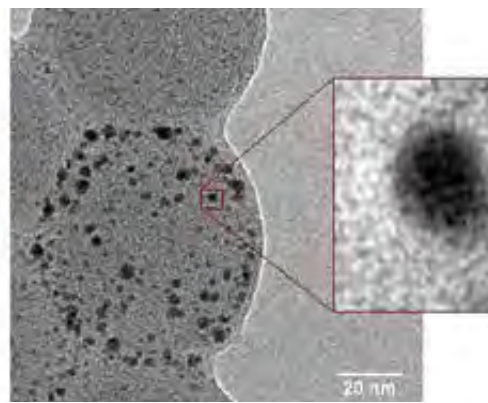
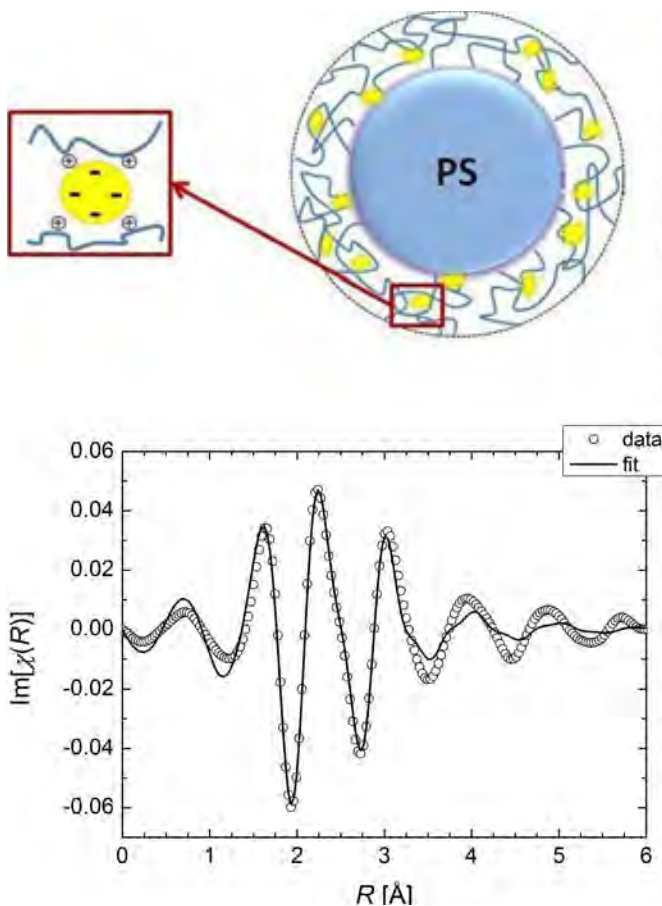


Figure 1: Au/Pd nanoalloys immobilised in spherical polyelectrolyte brush.

Figure 2: FT of the Au EXAFS of the Au₂₅Pd₇₅ nanoparticle and the first shell fit of a Au/Pd alloy model.

COMBINED SMALL ANGLE X-RAY SCATTERING AND X-RAY ABSORPTION SPECTROSCOPY STUDIES OF ELECTROCHROME METALLOPOLYELECTROLYTES

W. Szczerba*, H. Riesemeier, U. Reinholz, M. Radtke, and A.F. Thünemann

BAM Federal Institute for Materials Research and Testing, Unter den Eichen 87, 12205 Berlin, Germany

Keywords: SAXS, XAFS, metallopolymers

*e-mail: wojciech.szczerba@bam.de

We present the results of an ongoing study by means of synchrotron radiation based small angle x-ray scattering (SAXS) and x-ray absorption fine structure (XAFS) spectroscopy of the structure and oxidation state of self-assembled metallo-supramolecular coordination polyelectrolytes (MEPEs) [1]-[3] with Fe(II), Co(II), Ni(II) ions used as a functional material in electrochromic windows. The MEPEs change from opaque to transparent when placed between two electrodes to which a low DC voltage is applied. Moreover, these materials show remarkable self-healing abilities.

For the sake of the study a modification to the small angle scattering set-up, Saxsess by Anton Paar, has been done out by mounting an energy dispersive detector perpendicular to the beam path on top of the SAXS apparatus. This allows for simultaneous measurements of SAXS, XRF and XAFS.

Insofar it has been found that the MEPEs have a structure of solid rods of approx 0.5 nm radius and a length of > 50 nm when in water solution. When

solved in ethanol the rods are significantly shorter. The oxidation state of 2+ is being maintained in all samples regardless their history, i.e. thermal treatment, switching cycles etc. However, in NEXAFS and EXAFS, small changes occur between the tempered and non-tempered samples of the same series.

Acknowledgments: This work is supported by the German Federal Ministry of Education and Research (BMBF), grant No. 13N11285, Samples have been provided by the SmartWin Project partners ISC Fraunhofer and Uni Würzburg.

References

- [1] F.S. Ha *et al.*, *Thin Solid Films* **516** (2008) 2469 – 2473.
- [2] Y. Bodenthin *et al.*, *J. Am. Chem. Soc.* **131** (2009) 2934 – 2941.
- [3] F.S. Han, M. Higuchi, D.G. Kurth, *J. Am. Chem. Soc.* **130** (2008) 2073 – 2081.

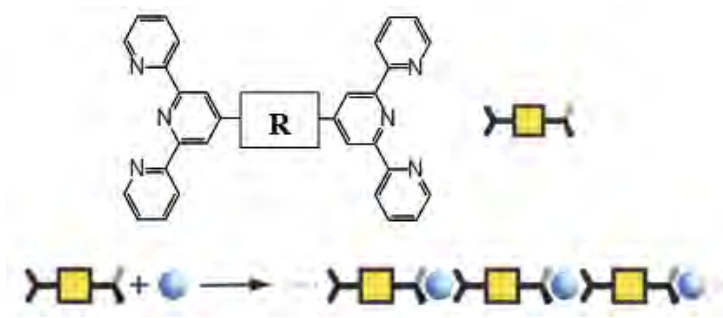
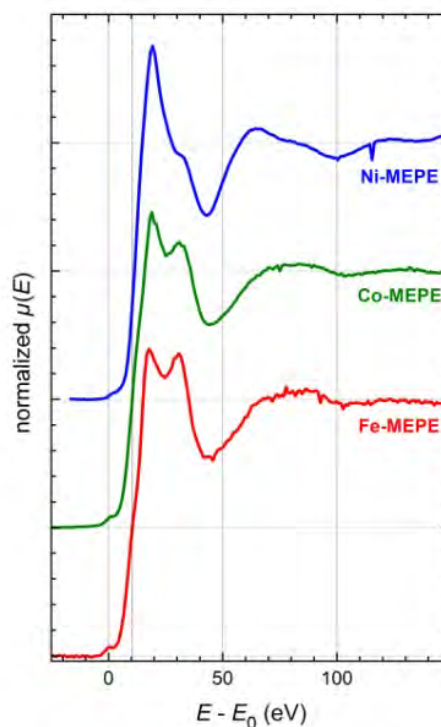


Figure 1: Schematic view of the MEPEs, blue balls represent the metallic divalent ions.

Figure 2: XANES *K*-edges of the MEPEs with Fe(II), Co(II) and Ni(II) ions.



LOCAL STRUCTURE OF IRON CARBIDE NANOPARTICLES

W. Szczerba^{1*}, H. Rieseemeier¹, U. Reinholz¹, M. Radtke¹, A.F. Thünemann¹,
A. Kaupner², and C. Giordano²

¹BAM Federal Institute for Materials Research and Testing, Unter den Eichen 87, 12205 Berlin, Germany

²Max-Planck-Institute of Colloids and Interfaces, Department of Colloids Am Mühlentberg 1,
14476 Potsdam-Golm, Germany

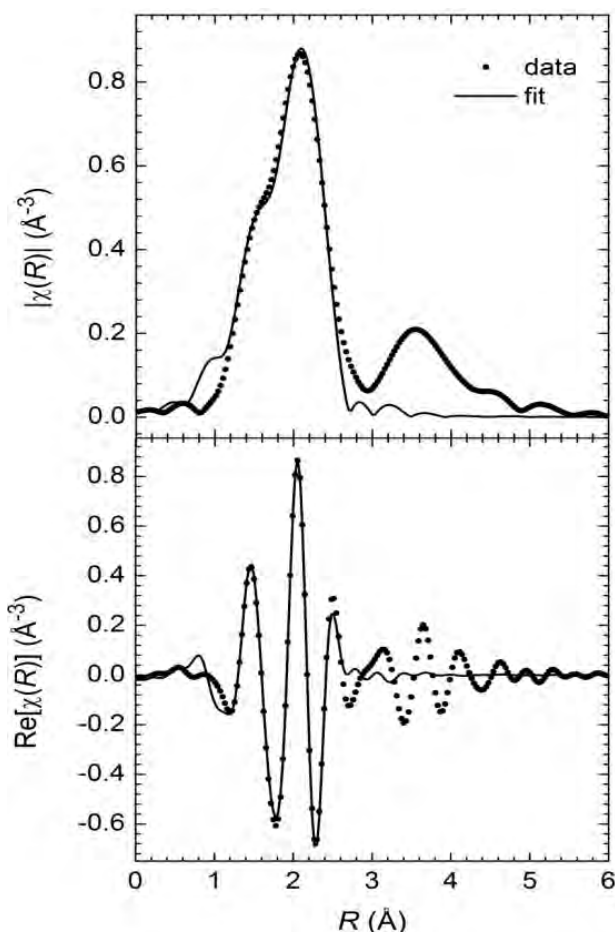
Keywords: EXAFS, iron carbide, nanoparticles

* e-mail: wojciech.szczerba@bam.de

Fe-C nanosystems are in focus of great interest because of their abundance, low cost, large stoichiometric range with improved magnetic properties leading to various applications such as sensors and catalyst. Interestingly, amidst all other iron carbides, Fe₃C is the oldest iron carbide which is metastable over long period of time and has tuneable properties depending upon the solute atom. Bulk iron carbide is most commonly found as a phase called cementite (Fe₃C) in steel products and cast iron.

Iron carbide (Fe₃C) nanoparticles have been investigated by means of x-ray absorption spectroscopy (XAFS). The experiment has been conducted at the iron *K*-edge at the BAMline at Bessy II in Berlin, Germany. Based on the analysis of the extended x-ray absorption fine structure (EXAFS) part of the spectra it was found that the nanoparticles have a local structure not resembling the possible bulk structures of iron carbide, neither the orthorhombic Pnma structure nor the hexagonal P6322. However, it could be determined that the iron absorber is surrounded by a close packed-like disordered iron shell at 2.54(3) Å being almost exactly the lattice constant of austenite (γ -Fe). Moreover, the absorbing iron atom has 3 to 4 carbon atoms at a distance of 1.97(4) Å in its vicinity.

Figure 1: Best fit achieved for a cluster model consisting of 12 Fe atoms and 4 C atoms around the iron absorber, magnitude FFT (top) and imaginary part (bottom). The agreement is in the fitting range (1.2 – 3.2 Å) excellent.



SYNCHROTRON RADIATION BASED STUDIES OF THE ELEMENTAL COMPOSITION AND CHEMICAL FORMS OF Fe AND Zn IN BRAIN GLIOMAS

M. Szczerbowska-Boruchowska^{1*}, M. Lankosz¹, M. Czyzycki¹, A. Wandzilak¹, P. Wrobel¹, E. Radwanska², and D. Adamek²

¹AGH University of Science and Technology, Faculty of Physics and Applied Computer Science, Al. Mickiewicza 30, 30-059 Krakow, Poland

²Department of Neuropathology, Chair of Pathomorphology, Faculty of Medicine, Jagiellonian University Medical College, ul. Botaniczna 3, 31-503 Krakow, Poland

Keywords: synchrotron radiation, X-ray fluorescence, X-ray absorption near edge structure spectroscopy, brain gliomas

*e-mail: Magdalena.Boruchowska@fis.agh.edu.pl

The literature published in recent years indicates an essential role played by minor and trace elements in a number of pathological processes including the carcinogenic process [1]. At present, there is a growing awareness of, and interest in, studies involving the determination of the elemental composition of normal and malignant tissues [2]. However, the exact role of chemical elements in carcinogenesis remains unknown. Synchrotron radiation XRF microprobe analysis (SRXRF) is a multi-elemental analytical technique which enables the simultaneous micro-imaging of chemical elements at trace concentrations. For this reason, X-ray fluorescence seems to be a promising tool for the investigation of cancerogenesis. Moreover, the identification of the chemical forms of trace elements in tissue microstructure may help us understand the carcinogenic processes. In this work, X-ray absorption near edge structure spectroscopy (XANES) is applied for the analysis of chemical forms of Fe and Zn.

The samples for biochemical micro-imaging were taken intraoperatively from brain tumors of different types and various grades of malignancy. The samples were diagnosed histopathologically at the Department of Neuropathology at the Jagiellonian University Medical College in Krakow. The samples were prepared in two ways. In the first case the specimens referred to as “frozen samples,” were cut to about 2 mm thick slices and placed in Plexiglas cups of 12 mm diameter. The containers were then covered with ultralene foil and frozen at -80°C . In addition, the so-called “dried samples” were studied. For this purpose the specimens were cryo-sectioned at $20\ \mu\text{m}$, mounted onto $4\ \mu\text{m}$ thickness ultralene foil suspended onto plexiglas holder, and freeze-dried at -80°C .

The SRXRF measurements were performed at the bending magnet beamline L at HASYLAB. The primary X-ray energy was set to 17 keV. The beam was focused to a size of $15\ \mu\text{m}$ in diameter. The sample areas were scanned to obtain two-dimensional images of elemental distributions. Depending on the sample kind the XANES

measurements were carried out at different synchrotron facilities / beamlines. The “frozen samples” were studied at the bending magnet beamline C at HASYLAB. The “dried samples” were analyzed at the wiggler line SUL-X at ANKA synchrotron as well as the bending magnet beamline L at HASYLAB. The Fe and Zn XANES profiles were measured. Moreover, two-dimensional imaging of chemical forms of both elements was performed.

The SRXRF technique allowed for the identification of a two-dimensional distribution of P, S, Cl, K, Ca, Fe, Cu, Zn, Br and Rb in neoplastic tissues on a micro-scale. The masses per unit area of elements were determined for various brain tumor types. The quantitative analysis shows that for all cases the content of the oxidized form of Fe is significantly higher in comparison with Fe^{2+} . The XANES analysis showed that the content of either Fe^{2+} or Fe^{3+} is increased in low grade gliomas in comparison to high-grade malignant tumors. It was found that Zn in all tissue structures (homogeneous neoplastic tissue, calcifications, blood vessel) occurs in oxidized form.

Acknowledgments: This work was supported by:

- the Polish Ministry of Science and Higher Education and its grants for Scientific Research (DESY/304/2006; N N518 377537),
- the European Community Seventh Framework Programme (FP7/2007-2013) under grant agreement n^o 226716.

References

- [1] M. Valko, C.J. Rhodes, J. Moncol, M. Izakovic, M. Mazur, “Free radicals, metals and antioxidants in oxidative stress-induced cancer,” *Chem. Biol. Interact.* **160** (2006) 1.
- [2] C. Theodorakou, M.J. Farquharson, “Classification of secondary colorectal liver cancer in human biopsy samples using angular dispersive x-ray diffraction and multivariate analysis,” *Med. Phys. Biol.* **54** (2009) 4945.

EVALUATION OF THE VARIABILITY IN ELEMENTAL COMPOSITION OF DOPAMINEGIC NEURONS IN SENILE BRAINS USING SYNCHROTRON RADIATION BASED X-RAY FLUORESCENCE

M. Szczerbowska-Boruchowska^{1*}, P. Wrobel¹, A. Sorowka¹, E. Radwanska², and D. Adamek²

¹AGH University of Science and Technology, Faculty of Physics and Applied Computer Science, Al. Mickiewicza 30, 30-059 Krakow, Poland

²Department of Neuropathology, Chair of Pathomorphology, Faculty of Medicine, Jagiellonian University Medical College, ul. Botaniczna 3, 31-503 Krakow, Poland

Keywords: synchrotron radiation, X-ray fluorescence, senile brains, substantia nigra, elemental microimaging

* e-mail: Magdalena.Boruchowska@fis.agh.edu.pl

A major risk factor for neurodegenerative diseases such as Parkinson's disease, Huntington's disease, amyotrophic lateral sclerosis, Alzheimer's disease and progressive supranuclear palsy is aging [1]. Multiple reports have documented an age-related loss of the pigmented neurons in the substantia nigra (SN) and other nigrostriatal structures of human brain. Two processes that have been implicated in aging are free radical-induced oxidative damage and mitochondrial dysfunction [1]. Trace elements especially metals play important role in the mentioned processes [2] and may induce significant cellular disturbances when present in excess concentrations. To address the questions related to chemical composition of dopaminergic neurons in senile brains and their age-related alterations, a combination of imaging and spectroscopic techniques is needed. For this purpose synchrotron radiation x-ray fluorescence (SRXRF) was used for two-dimensional imaging of elements in human substantia nigra.

The autopsy samples of SN of human senile brains were taken. The specimens were frozen and

cut into 20 μm -thick slices with the use of a cryomicrotome. The tissue slices were mounted immediately onto ultralene films and freeze-dried at -80°C .

The SRXRF measurements were carried out at the 7T-WLS/1 (mySpot) beamline of the Electron Storage Ring BESSY II (Berlin, Germany). The primary photon energy was set to 17 keV. Capillary optics was used to focus the X-ray beam on the sample surface to spot sizes of about 10 μm in diameter. The sample areas were scanned point by point with the step sizes equal to 10 μm both horizontally and vertically. The time of acquisition for tissue samples was equal to 10 s per one measurement point. The characteristic X-ray lines were measured by 7 element Si(Li) detector. The SRXRF analysis allowed for finding P, S, Cl, K, Ca, Fe, Cu, Zn, Se, Br, Rb and Sr in the samples investigated. The examples of the SRXRF maps of selected elements for SNc section are shown in Figure 1. The location of nerve cells is precisely visualized by the high levels of most elements in the scanned areas of the tissues.

In each case two areas were chosen for the quantitative analysis, i.e. nerve cell bodies and the extraneuronal spaces. It was found that the nerve cells from different samples reveal the biggest similarity in terms of phosphorus content. Whilst, the mass fractions of Cu differentiate neurons originating from various samples in the largest extent. The higher variation in elemental composition is observed between extraneuronal spaces of different samples than within nerve cells.

Acknowledgments: This work was supported by the Polish Ministry of Science and Higher Education and its grants for Scientific Research as well as European Community's Seventh Framework Programme (FP7/2007-2013) under grant agreement n^o 226716.

References

- [1] D.S. Albers, M.F. Beal, "Mitochondrial dysfunction and oxidative stress in aging and neurodegenerative disease," *J. Neural Transm. Suppl.* **59** (2000) 133.
- [2] K. Jomova, D. Vondrakova, M. Lawson, M Valko. "Metals, oxidative stress and neurodegenerative disorders," *Mol. Cell. Biochem.* **345** (2010) 91.

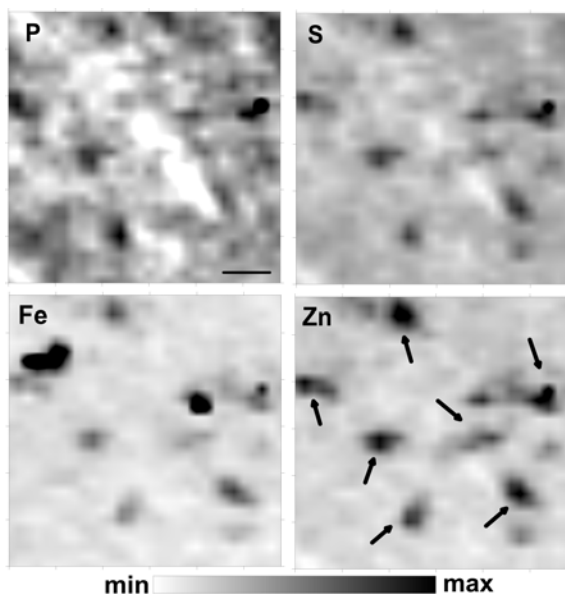


Figure 1: X-ray fluorescence maps of substantia nigra cryo-section taken from senile human brain. Arrows show neuron bodies. Scale bar: 60 μm .

DIRECT XES TO XAS RELATION FOR OFF-RESONANT EXCITATIONS AT L3 ABSORPTION EDGE: TOWARDS HIGH-RESOLUTION XAS AT SINGLE-SHOT

J. Szlachetko^{1,2*}, M. Nachtegaal¹, J.-Cl. Dousse³, J. Hoszowska³, E. Kleymenov^{1,4},
M. Janousch¹, J. Sa¹, O.V. Safonova¹, and J.A. van Bokhoven¹

¹Paul Scherrer Institut, 5232 Villigen PSI, Switzerland

²Institute of Physics, Jan Kochanowski University, 25-406 Kielce, Poland

³Department of Physics, University of Fribourg, 1700 Fribourg, Switzerland

⁴Institute for Chemical and Bioengineering, ETH Zurich, 8093 Zurich, Switzerland

Keywords: X-ray emission and X-ray absorption spectroscopy

*e-mail: jakub.szlachetko@psi.ch

A high energy resolved x-ray absorption spectrum can be reconstructed from an x-ray emission spectrum obtained at a single incident beam energy. We demonstrate a direct relationship between the x-ray emission and absorption process through the generalized Kramers-Heisenberg formalism. The experiment was performed using excitation energies tuned far below the resonant region of the *L3* x-ray absorption edge for *5d* elements.

Since x-ray emission spectra are collected at a single excitation energy using dispersive-type spectrometer for x-ray detection, a point-by-point normalization for the incoming beam fluctuation is not needed and the spectral shape is not affected by self-absorption process. Possibility of single-shot x-ray absorption experiment at the femto-time scale using x-ray free electron sources will be discussed.

STRUCTURE DEVELOPMENT DURING ISOTHERMAL CRYSTALLIZATION OF HIGH-DENSITY POLYETHYLENE: SYNCHROTRON SMALL-ANGLE X-RAY STUDY

Cz. Ślusarczyk*

*Institute of Textile Engineering and Polymer Materials, University of Bielsko-Biala,
2, Willowa Str, 43-309 Bielsko-Biala, Poland*

Keywords: SAXS, high-density polyethylene, crystallization

**e-mail: cslusarczyk@ath.bielsko.pl*

Crystalline polymers show ordering at different size scales, namely, the arrangement of molecules in the unit cell, lamellar crystals and the aggregation of these lamellae into superstructures such as spherulites [1]. The classical picture of polymer crystallization involves the creation of a stable nucleus from the supercooled polymer melt and then the growth of the crystalline region into the lamellar structures and beyond. For most polymers, two stages of crystallization are acknowledged. A fast primary stage during which spherulites grow linearly until they impinge on each other is denoted as primary crystallization. A slow secondary crystallization process is observed when the sample is completely composed of spherulites. The secondary crystallization involves the thickening of the crystals, growth of new lamellae within or between existing lamellae stacks, and growth of entire new lamellae stacks from remaining amorphous regions within the spherulites.

In the present paper isothermal melt crystallization in high density polyethylene (HDPE) was studied by time-resolved synchrotron small-angle X-ray scattering (SAXS) over a wide-range of supercoolings. The SAXS profile was analyzed both by correlation, $\gamma(r)$, and interface distribution, IDF, functions [2, 3]. Assuming an ideal two-phase system with sharp phase boundary the IDF is a superposition of three contributions associated with the size distributions of crystalline (lc), amorphous (la) layers and the distribution of the long period (LP). Curve fits may be performed to deconvolute these

contributions. In this study, curve fit was evaluated by assuming Gaussian distributions of lc , la , and LP . The relative standard deviation σ_C/lc is an additional parameter which is varied during crystallization and can be used for analysis of this process.

Results obtained indicate the following: (1) At large supercooling (40°C) the thickening of the crystalline layer does not occur. At lower supercooling all thicknesses increase with time. These results confirm the predictions that crystallization of HDPE involves the direct transformation of melt into orthorhombic phase. (2) At large supercooling lc presents a broad distribution which the relative standard deviation increases with time. At lower supercooling T_C shows much more sharper distribution. In this case the relative standard deviation decreases with time.

References

- [1] G. Reiter, G.R. Strobl, *Progress in Understanding of Polymer Crystallization* (Springer, Berlin Heidelberg 2007).
- [2] C. Ślusarczyk, "Time-resolved SAXS investigations of morphological changes in a blend of linear and branched polyethylenes during crystallization and subsequent melting," *J. Alloy. Comp.* **382** (2004) 68 – 74.
- [3] C. Ślusarczyk *Interface distribution function from SAXS data for heat treated polyethylene* in *Applied Crystallography* (H. Morawiec, D. Stróż, Editors, World Scientific 2004).

ELECTRONIC BAND STRUCTURE OF $\text{La}_{0.67}\text{Pb}_{0.33}\text{Mn}_{0.92}\text{Fe}_{0.08}\text{O}_3$ W. Tokarz^{1*}, M. Kowalik^{1,2}, R. Zalecki¹, and A. Kołodziejczyk¹¹AGH University of Science and Technology, Department of Solid State Physics,
30, Mickiewicza Str., 30-059 Cracow, Poland²Department of Physics, Rzeszów University of Technology,
6, Powstańców Warszawy Str., 35-959 Rzeszów, Poland

Keywords: density of states, density functional theory, perovskite, ultraviolet photoemission

*e-mail: tokarz@agh.edu.pl

We present theoretical study of some electric and magnetic properties in manganese perovskite $\text{La}_{0.67}\text{Pb}_{0.33}\text{Mn}_{0.92}\text{Fe}_{0.08}\text{O}_3$. The calculation was carried out based on first-principles density functional theory (DFT) with general gradient approximation GGA+U using Wien2K package. The P-3c1 crystal structure was taken from the detailed X-ray diffraction data for the perovskite [1]. The original unit cell was multiplied two times in all direction in order to place proper amount of Fe. Final crystal structure with 120 atoms was used for calculation.

According to our previous work [2], where it was shown that antiparallel magnetic moment configuration on Mn and Fe gives more reasonable results than parallel one, spins up and down for Mn and Fe were set up as initial parameters, respectively. For Mn and Fe *d* electrons the exact exchange energy was utilized. As a results half-metallic density of state (DOS) was obtained with top of valance band for spin down 1.5 eV below E_F and spin up filled up to Fermi level by Mn, Fe *d* and oxygen *p* electrons. In the valance band oxygen partial DOS follows sum of Mn and Fe ones. It is shown in Fig. 1 as an example. Comparison of total DOS with

ultraviolet photoemission spectroscopy (UPS) measurements shows similar features [2] up to -10 eV and especially the decrease in DOS from -2 eV to E_F . Computed total magnetic moment was overestimated as compared to measured one.

Acknowledgments: This work was supported by the Polish Ministry of Science and Higher Education and its grants for Scientific Research.

References

- [1] G. Gritzner, M. Koppe, K. Kellner, J. Przewoznik, J. Chmist, A. Kołodziejczyk, K. Krop, "Preparation and properties of $\text{La}_{0.67}\text{Pb}_{0.33}(\text{Mn}_{1-x}\text{Fe}_x)\text{O}_3$ compounds," *Appl. Phys. A* **81** (2005) 1491 – 1495.
- [2] M. Kowalik, R. Zalecki, A. Kołodziejczyk, "Electronic states of colossal magnetoresistive manganites $\text{La}_{0.67}\text{Pb}_{0.33}\text{Mn}_{1-x}\text{Fe}_x\text{O}_3$ from photoemission spectroscopy," *Acta Phys. Pol. A* **117** (2010) 257 – 260.

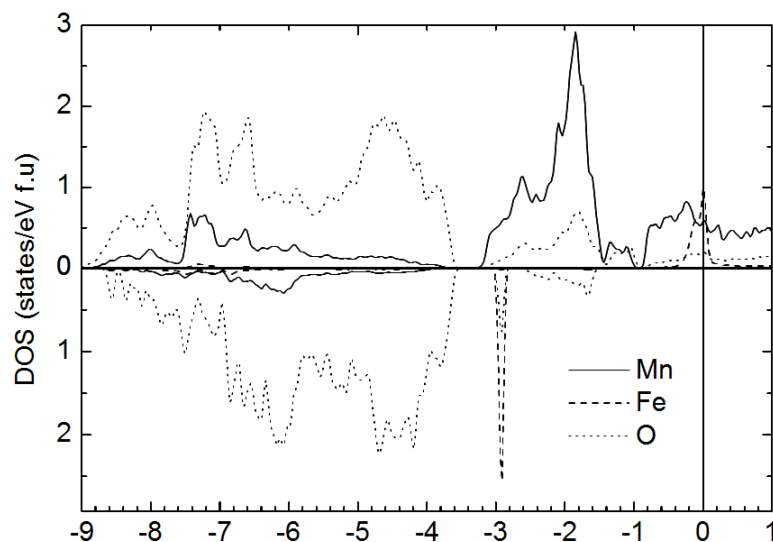


Figure 1: Partial DOS of manganese, iron and oxygen.

VACUUM SYSTEM OF THE POLISH LIGHT SOURCE — SOLARIS

L. Walczak^{1*}, J. Alhback², M. Berglund², E. Al-dmour³, J. Pasquaud³,
P. Fernandes Tavares², M. Eriksson², D. Einfeld³, C.J. Bocchetta¹, and M.J. Stankiewicz¹

¹National Synchrotron Radiation Centre Solaris at the Jagiellonian University,
Gronostajowa 7/P-1.6, Krakow, Poland

²Lund University MAX-lab, Ole Römers väg 1, Lund, Sweden

³CELLS-ALBA Synchrotron, Carretera BP 1413, de Cerdanyola del Vallès a Sant Cugat
del Vallès, Km. 3,3, Cerdanyola del Valles, Spain

Keywords: synchrotron radiation, vacuum system

*e-mail: lukasz.walczak@uj.edu.pl

The third generation synchrotron light facility Solaris will allow new research developments and innovation in disciplines like physics, chemistry, medicine and biology. The Polish National Synchrotron Radiation Centre — SOLARIS will be a unique facility in Poland [1]. The centre will be equipped with an electron storage ring and injection system based on the technology developed at MAX-lab, Sweden [2, 3, 4].

In order to guarantee an overall lifetime of 13 hours (taking into account Touschek events) the partial pressure in the Solaris storage ring will be lower than 10^{-9} mbar. Synchrotron radiation from both bending magnets and insertion devices will be used. Bending magnet radiation will be taken from the centre of the first 15° magnet of the double-bend achromat structure. The novel design of the small-bore achromat magnets from single iron blocks requires careful engineering of the vacuum chamber. Most vacuum chambers will be made of stainless steel with different cross sections to match the varying magnet gaps.

In this presentation a general description of vacuum system of both Solaris and the MAX IV 1.5 GeV storage rings, will be presented. The conceptual layout of the vacuum chambers in the

achromats and straight sections have been designed by the CELLS ALBA group (Figure 1). We will show the detailed design of vacuum chambers including the beam position monitors, discrete absorbers and vacuum pumps.

Acknowledgments: Support by the Polish Ministry of Science and Higher Education and European Union (grant: WND-POIG.02.01.00-12-213/09) is gratefully acknowledged.

References

- [1] C.J. Bocchetta *et al.*, *Project status of the Polish Synchrotron Radiation facility Solaris* (Proceedings of IPAC2011, San Sebastián, Spain).
- [2] S.C. Leemann *et al.*, “Beam dynamics and expected performance of Swedens new storage-ring light source: MAX IV,” *Phys. Rev. ST Accel. Beams* **12** (2009) 12071.
- [3] M. Eriksson *et al.*, *Challenge of MAX IV towards a multi purpose highly brilliant light source* (Proceedings of 2011 Particle Accelerator Conference, New York, NY, USA TUOBS4).
- [4] M. Eriksson, *The MAX IV synchrotron light source* (Proceedings of IPAC2011, San Sebastián, Spain).

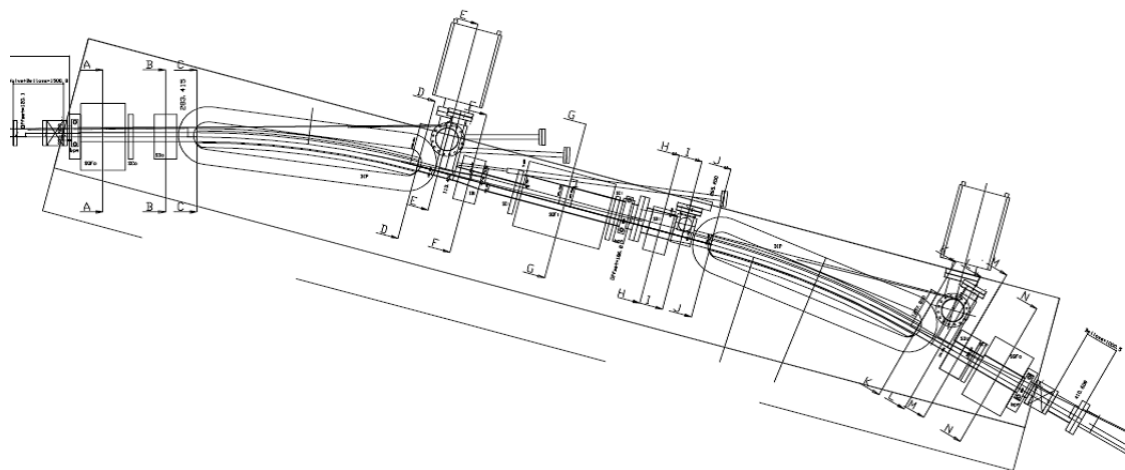


Figure 1: Design layout of the vacuum chamber with magnets in the storage ring.

SIZE DEPENDENCE OF MICROSTRAIN FLUCTUATIONS IN NANOCRYSTALLINE CHROMIUM

D. Wardecki^{1*}, R. Przeniosło¹, A. Fitch², M. Bukowski³, and R. Hempelmann³

¹Faculty of Physics, University of Warsaw, Hoża 69, 00-681 Warsaw, Poland

²European Synchrotron Radiation Facility, BP 220 F-38043, Grenoble Cedex, France

³Institute of Physical Chemistry, University of Saarbrücken, D-66123, Saarbrücken, Germany

Keywords: nanocrystalline chromium, synchrotron radiation, crystallite growth, microstrain fluctuations

*e-mail: dward@fuw.edu.pl

The microstructure of nanocrystalline chromium (n-Cr) has been studied by high resolution powder diffraction on beamline ID-31 at ESRF. During the diffraction measurements the samples of n-Cr, obtained by the electrodeposition method, were annealed in-situ at temperatures 400°C, 600°C and 800°C. In order to obtain the crystallite size D and the microstrain fluctuations $\Delta d/d$ as a function of the annealing time, the 'double-Voigt' [1] analysis was performed.

For all n-Cr samples the annealing process leads to relatively fast crystallite size growth in the first 6 min. At the same time there is a rapid decrease

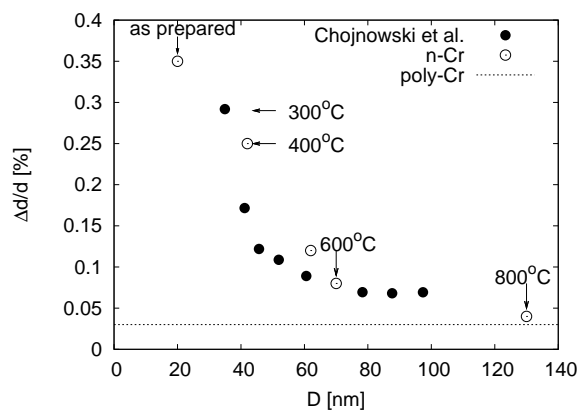


Figure 1: Microstrain fluctuations as a function of the crystallite size.

of the microstrain fluctuations. The final values of D and $\Delta d/d$ in n-Cr depend on the annealing temperature [2].

The results shows the clear relation between the crystallite size and the strains, which has been also noticed by other authors [3] for different nanocrystalline materials. Figure 1 shows the values of strains as a function of the crystallite size for n-Cr after 45 min. annealing at the three temperatures 400°C, 600°C and 800°C (open circles). The points are compared with the data from Chojnowski et al. [4] (black dots). One can see that for $D > 100$ nm the values of $\Delta d/d$ vary slightly as compared with the polycrystalline specimen.

References

- [1] D. Balzar, *Defect and Microstructure Analysis from Diffraction* (Oxford University Press, New York, 1999).
- [2] D. Wardecki, R. Przeniosło, A. Fitch, M. Bukowski, and R. Hempelmann, *J. Nanopart. Res.* **13** (2011) 1151.
- [3] E. Roduner, *Nanosopic Materials. Size-Dependent Phenomena* (RSC Publishing, 2006).
- [4] G. Chojnowski, R. Przeniosło, I. Sosnowska, M. Bukowski, H. Natter, R. Hempelmann, A. Fitch, and V. Urban, *J. Phys. Chem. C* **111** (2007) 5599.

SR-FTIR SPECTROSCOPY IN STUDY OF THE DOUBLE STRAND BREAKS IN SINGLE CELLS IRRADIATED BY PROTON MICROBEAM

A. Wiechec^{1*}, E. Lipiec¹, J. Lekki¹, M. Widel², and W.M. Kwiatek¹

¹The Henryk Niewodniczanski Institute of Nuclear Physics, Polish Academy of Sciences, Krakow, Poland

²Silesian University of Technology, Department of Automatics, Electronics and Informatics, Gliwice, Poland

Keywords: synchrotron radiation, double strand breaks, single cell irradiation, proton microbeam

*e-mail: Anna.Wiechec@ifj.edu.pl

The double strand breaks (DSBs) in DNA are the critical cell damage if unrepaired they may lead to cell death. Recently, many published data indicate that the formation of DSBs in DNA is followed by the rapid local phosphorylation of histone H2AX. The formation of discrete nuclear foci called γ H2AX foci is observed [1, 2]. The γ H2AX foci, a sensitive marker of DNA double strand breaks, might be visualized after conjugation with anti- γ H2AX monoclonal antibodies joint with fluorochrome.

From the possible physical methods, the SR-FTIR microspectroscopy is well known for its uniqueness as a noninvasive tool in identifying vibrational structure of biological materials. It has become a potential analytical method in single cells studies [3, 4].

The aim of this study was the evaluation of the DNA double strand breaks in proton irradiated single cells with application of SR-FTIR spectroscopy. The study tried to answer the question if and how the chemicals used in γ H2AX test affects the SR-FTIR cell spectra.

The DNA damage in single cells from prostate cancer PC3 cell line were induced with proton microbeam (2 MeV energy; 50 and 2000 protons per cell). The evaluation of DNA double strand breaks was done in γ H2AX test and by means of SR-FTIR spectroscopy. For the irradiation treatment the cells were seeded on the silicon nitride windows.

Detailed description of γ H2AX test is presented in [1, 2]. The 100 nucleus of irradiated and control cells were examined under fluorescent microscope Zeiss Axio Imager Z1.

SR-FTIR cell spectra were analyzed in transmission mode with a resolution of 4 cm^{-1} in spectral

range $400\text{ cm}^{-1} - 4000\text{ cm}^{-1}$.

The application of both biochemical and physical methods enabled detection of changes in irradiated cells at the chemical bonds level. The comparison of the results obtained from both methods is discussed.

Acknowledgments: This work was supported by the European Community's Seventh Framework Programme (FP7/2007 – 2013) under grant agreement n° 226716. The data were obtained during the realization of PSI Synchrotron project 20110190.

References

- [1] R. Ugenskiene, J. Lekki, W. Polak, K.M. Prise, M. Folkard, O. Veselov, Z. Stachura, W.M. Kwiatek, M. Zazula, J. Stachura, "Double strand break formation as a response to X-ray and targeted proton-irradiation," *Nucl. Instrum. Methods Phys. Res. B* **260** (2007) 159 – 163.
- [2] E.R. Foster, J.A. Downs, "Histone H2A phosphorylation in DNA double-strand break repair," *FEBS J.* **272**(13) (2005) 3231 – 40.
- [3] P. Dumas, G.D. Sockalingum, J. Sule-Suso, "Adding synchrotron radiation to infrared microspectroscopy: Whats new in biomedical applications?," *Trends Biotechnol.* **25** (2007) 40 – 44.
- [4] J. Pijanka, J.D. Sockalingum, A. Kohler, Y. Yang, F. Draux, G. Parkes, K.-P. Lam, P. Collins, P. Dumas, C. Sandt, D.G. Pittius, G. Douce, M. Manfait, V. Untereiner, and J. Sule-Suso, "Synchrotron-based FTIR spectra of stained single cells. Towards a clinical application in pathology," *Lab. Invest.* **90** (2010) 797 - 807.

SYNCHROTRON DIFFRACTION TOPOGRAPHY OF SBN ($\text{Sr}_x\text{Ba}_{1-x}\text{Nb}_2\text{O}_6$) AND CBN ($\text{Ca}_x\text{Ba}_{1-x}\text{Nb}_2\text{O}_6$) CRYSTALS

K. Wieteska¹, W. Wierzchowski^{2*}, A. Malinowska², M. Lefeld-Sosnowska³, M. Swirkowicz²,
T. Lukasiewicz², and C. Paulmann⁴

¹*Institute of Atomic Energy, PL 05-400 Otwock-Swierk, Poland*

²*Institute of Electronic Materials Technology, ul. Wólczynska 133, PL 01-919 Warsaw, Poland*

³*Institute of Experimental Physics University of Warsaw, Hoza 69, 00-681 Warsaw, Poland*

⁴*HASYLAB at DESY, Notkestr. 85, D-22603 Hamburg, Germany*

Keywords: strontium barium niobate, calcium barium niobate, defect structure, diffraction topography

**e-mail: Wojciech.Wierzchowski@itme.edu.pl*

The crystals of ferroelectric niobates with the structure of tungsten bronze such as $\text{Sr}_x\text{Ba}_{1-x}\text{Nb}_2\text{O}_6$ (SBN) and $\text{Ca}_x\text{Ba}_{1-x}\text{Nb}_2\text{O}_6$ (CBN) are the subject of intense investigations in view of their very interesting non linear electro-optical, dielectric, piezoelectric and pyroelectric properties. The doping with rare earth ions additionally increases the possibility of using these crystals in the laser technology [1]. Also growth of the crystals being the mixture of SBN and CBN is possible which enables controlling the Curie temperature.

The published results of crystallographic perfection studies of SBN and CBN crystals indicate the

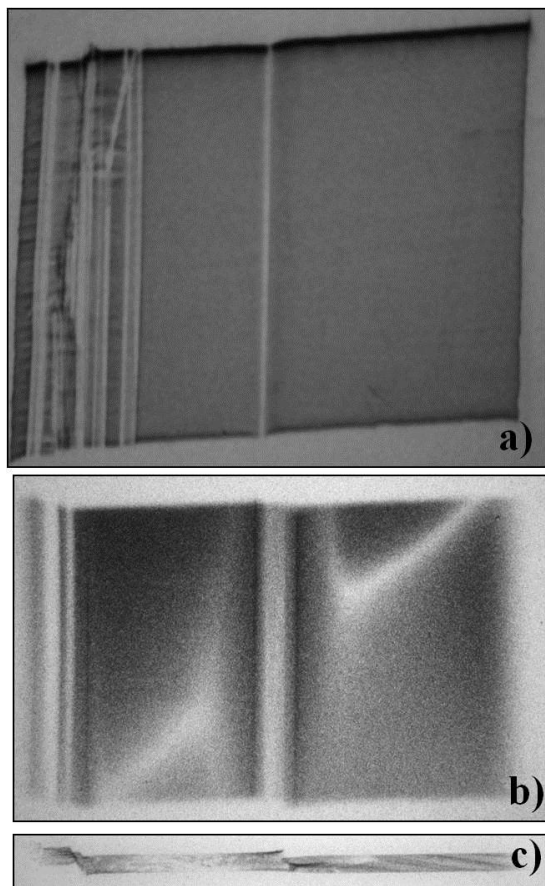


Figure 1: Representative synchrotron white beam topographs of $\text{Sr}_{0.35}\text{Ba}_{0.65}\text{Nb}_2\text{O}_6$ crystal: (a) back-reflection projection topograph, (b) transmission topograph, (c) transmission section topograph.

core, dislocations and glide bands. In some cases the dislocation loops were also observed [2].

In the present abstract we present some results of synchrotron diffraction topographic investigations of SBN and CBN crystals grown with the Czochralski method. The topographs were obtained both by means of white and monochromatic beam at DORIS III. The methods of characterization included the complementary use of different methods of conventional and synchrotron X-ray diffraction topography completed by polariscopic observations.

The typical elements of the defect structure revealed in SBN and CBN crystals were some faceted regions, particularly the core present in the middle region and some linear or — stripe-like contrasts, which are representatively shown in Figures 1 and 2 for the samples cut out respectively from $\text{Sr}_{0.35}\text{Ba}_{0.65}\text{Nb}_2\text{O}_6$ and $\text{Ca}_{0.26}\text{Ba}_{0.74}\text{Nb}_2\text{O}_6$ crystals.

The reported section and monochromatic beam topographs indicates a certain lattice disorientation between the regions separated by linear contrast. It confirm the suggestion that the linear or stripe contrasts observed in the topographs are caused by

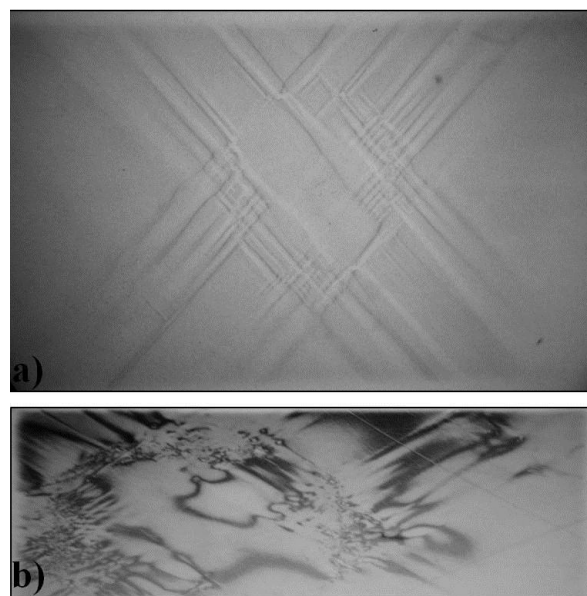


Figure 2: Representative synchrotron topographs of $\text{Ca}_{0.26}\text{Ba}_{0.74}\text{Nb}_2\text{O}_6$ crystal: (a) white beam back-reflection projection topograph, (b) monochromatic beam back-reflection projection topograph.

small-angle grain boundaries formed by glide bands. It was otherwise indicated with the use of selective etching method that the ferroelectric domains are of submicron dimension, and they cannot be directly resolved by the diffraction topography, but probably contribute to the enhanced intensity in some reflections.

Acknowledgments: The measurements performed at HasyLab have received funding from the 7th Framework

Programme (FP7/2007-2013) of European Community under ELISA grant agreement No. 226716.

References

- [1] J. Dec, W. Kleemann, S. Migay, V.V. Shvartsman, T. Lukasiewicz, and M. Świrkowicz, *Phase Trans.* **80** (2007) 131.
- [2] M. Muehlberg, M. Burianek, B. Joschko, D. Klimm, A. Danilewsky, M. Gelissen, L. Bayarjargal, G.P. Görlner, B.O. Hildmann, *J. Cryst. Growth* **310** (2008) 2288.

THE INVESTIGATIONS OF THE DAMAGES INDUCED BY FLASH PULSES IN SILICON CRYSTALS BY MEANS OF WHITE BEAM SYNCHROTRON SECTION TOPOGRAPHY

W. Wierzchowski^{1*}, K. Wieteska², D. Klinger³, R. Sobierajski³, J. Pelka³,
D. Zymierska³, T. Balcer¹, and C. Paulmann⁴

¹*Institute of Electronic Materials Technology, Wólczyńska 133, Warszawa 01-919, Poland*

²*Institute of Atomic Energy POLATOM, Otwock-Świerk 05-400, Poland*

³*Polish Academy of Sciences, Institute of Physics, al. Lotników 32/46, Warszawa 02-668, Poland*

⁴*Institute of Mineralogy and Petrography, University of Hamburg, Notkestr. 85, 22603 Hamburg, Germany*

Keywords: silicon, FLASH irradiation, X-ray topography, deformation fields

**e-mail: Wojciech.Wierzchowski@itme.edu.pl*

The development of new generation of short radiation sources exploring free electron lasers focused the interest in the problem of the interaction of the beam generated by these devices with solid matter. The strong excitation of electronic state induced by the beam can here reveal a number of new phenomena, which are important for practical development of optical elements and design of experiments, but also seems to be very interesting in cognitive aspects. The information about the phenomena requires a very careful structural characterization of the craters especially their geometrical features and the lattice deformation.

It is expected, that the irradiation with very intense femtosecond pulses can create states of very strong electronic excitation with a highly reduced influence of optical nonlinearities at the frequencies in the range between the plasma frequencies and the frequency in the inner shall absorption edge [1, 2]. The experiment included generation of the damages by the beam coming from the Free-electron Laser in Hamburg (FLASH) operating in the range 6 – 100 nm and focussed by an ellipsoidal mirror onto the surface of crystalline silicon. The analogous damages were previously studied with the micro-beam diffraction method together with AFM and Nomarski contrast microscopy [3, 4].

In our previous experiment the use of back reflection section and projection topography enabled us to reveal many important features of the strain fields connected with the craters [5]. It was in particular possible to demonstrate a significant similarity of the observed strain field to that of rod-like inclusion. The last results suggest unexpectedly large depth extension of the strain field connected with the craters.

In the present experiment we performed a successful attempt to confirm this observation by taking the synchrotron transmission section white beam topographs. Also a successful simulation of contrast in transmission section images were obtained using more adequate approximation of crater by droplet-like inclusion.

The observation of the deformation field of craters generated by FLASH pulses along the whole thickness of silicon wafers was performed by taking the synchrotron transmission section topographs using the beam perpendicular to the surface of the sample. Numerous relatively dense series of section topographs spaced by 10 μm provided a precise scan allowing the evaluation of geometrical shape and depth extension some various craters. In the obtained topographic images we observed the direct image connected with the boundary of the crater

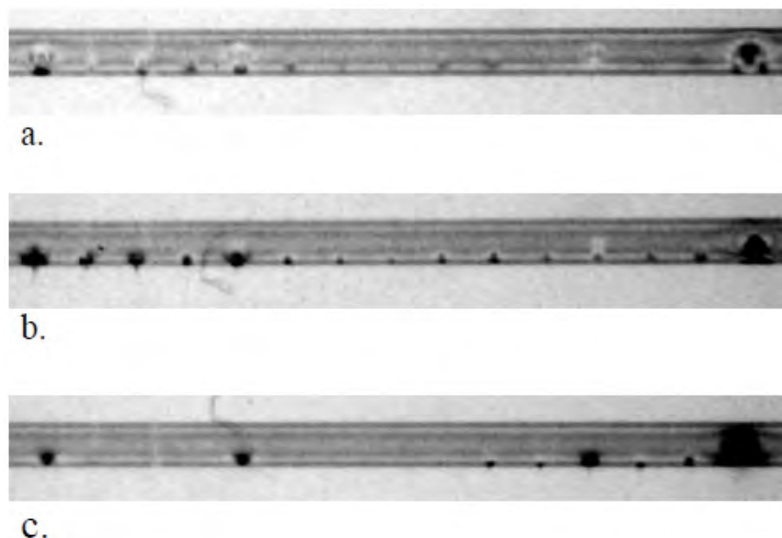


Figure 1: Three representative white beam transmission section topographs exposed using 5 μm beam perpendicular to the crystal surface corresponding to the sweeping of the row of craters with the maximal extension of the dark image from the lower edge of the section image corresponds to its depth extension.

accompanied by the some deformation of the Kato fringes.

The evaluated depth extension was different for individual craters and was in the range 30 – 100 μm and it may be expected that some of the craters were formed including the melting and recrystallization of the material. The evaluated depth values were confirmed also by evaluations basing on the vanishing the images of the series of spots in the Bragg case section topographs obtained when the beam entered the crystal at low 4° angle.

It was possible to reproduce the topographic contrast of the craters in transmission section topographs by numerical simulation based on integration of the Takagi-Taupin equations. The defects connected with craters were approximated as droplet-like inclusion.

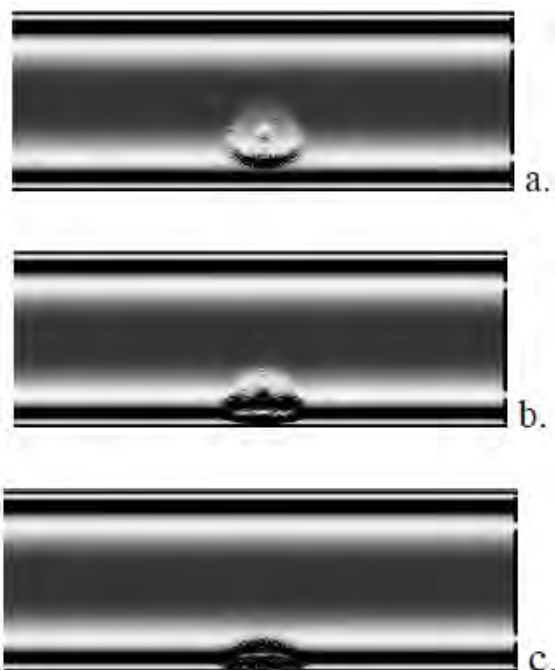


Figure 2: The series of three numerical simulations of transmission section images for the beam located at the position differing by 40 μm using the approximation of the craters by droplet-like inclusion — i.e. as the volume in the form of droplet uniformly filled with equally spaced point-like inclusion.

Acknowledgments: The synchrotron investigations were supported by the HASYLAB project I-20110423 EC.

References

- [1] S.P. Hau-Riege, R.A. Londo, R.M. Bionta, M.A. McKernan, S.L. Baker, J. Krzywinski, R. Sobierajski, R. Nietubyc, J.B. Pelka, M. Jurek, L. Juha, J. Chalupský, J.H. Cihelka, V. Hajkova, A. Velyhan, J. Krasa, J. Kuba, K. Tiedtke, S. Toleikis, H. Tschentscher, H. Wabnitz, M. Bergh, C. Caleman, K. Sokolowski-Tinten, N. Stojanovic, U. Zastra, "Damage threshold of inorganic solids under free-electron-laser irradiation at 32.5 nm wavelength," *Appl. Phys. Lett.* **90** (2007) 173128.
- [2] J. Krzywinski, R. Sobierajski, M. Jurek, R. Nietubyc, J.B. Pelka, L. Juha, M. Bittner, V. Letal, V. Vorlíček, A. Andrejczuk, J. Feldhaus, B. Keitel, E.L. Saldin, E.A. Schneidmiller, R. Treusch, M.V. Yurkov, "Conductors, semiconductors, and insulators irradiated with short-wavelength free-electron laser," *J. Appl. Phys.* **101** (2007) 043107.
- [3] J.B. Pelka, A. Andrejczuk, H. Reniewicz, N. Schell, J. Krzywinski, R. Sobierajski, A. Wawro, Z. Zytkeiwicz, D. Klinger, L. Juha, "Structure modifications in silicon irradiated by ultra-short pulses of XUV free electron laser," *J. Alloys Comp.* **382** (2004) 264.
- [4] J.B. Pelka, R. Sobierajski, D. Klinger, W. Paszkowicz, J. Krzywinski, M. Jurek, D. Zymierska, A. Wawro, A. Petroutchik, L. Juha, V. Hajkova, J. Cihelka, J. Chalupsky, T. Burian, L. Vysin, S. Toleikis, K. Sokolowski-Tinten, N. Stojanovic, U. Zastra, R. London, S. Hau-Riege, C. Riekel, R. Davies, M. Burghammer, E. Dynowska, W. Szuszkiewicz, W. Caliebe, R. Nietubyc, "Damage in solids irradiated by a single shot of XUV free-electron laser: Irreversible changes investigated using X-ray microdiffraction, atomic force microscopy and Nomarski optical microscopy," *Radiat. Phys. Chem.* **78** (2009) S46.
- [5] W. Wierzchowski, K. Wieteska, T. Balcer, D. Klinger, R. Sobierajski, D. Żymierska, J. Chalupský, V. Hájková, T. Burian, A.J. Gleeson, L. Juha, K. Tiedtke, S. Toleikis, L. Vyšín, H. Wabnitz, and J. Gaudin, *Radiat. Phys. Chem.* **80** (10) (2011) 1038.

XMCD STUDIES OF THE GaSb:MnSb LAYERS ON THE GaSb AND GaAs SUBSTRATES

A. Wolska¹, K. Lawniczak-Jablonska^{1*}, M.T. Klepka¹, and V. Sessi²

¹*Institute of Physics, Polish Academy of Sciences, Al. Lotnikow 32/46, PL-02668 Warsaw, Poland*

²*European Synchrotron Radiation Facility, 6 Rue Jules Horowitz, 38043 Grenoble, France*

Keywords: ferromagnetic precipitates, spintronics, XMCD

**e-mail: jablo@ifpan.edu.pl*

Despite of the intensive search for the proper semiconductor base materials for spintronics no appropriate material was proposed so far. In a single phase material, either ferromagnetism is observed below room temperature only [1] or there is no ferromagnetism at all (e.g. GaMnN) [2]. On the other hand, it was demonstrated that during growth of the magnetic III-V semiconductors, precipitates are fairly easily produced, yielding multi-phase ferromagnetic materials (often at room temperature) [2]. Recently the increase of interest in producing ferromagnetic precipitates can be observed. Among them there are materials consisting of the MnSb nanoinclusions in GaSb semiconductor matrix. It seems that magnetic properties of MnSb are more suitable for spintronic applications, than these of MnAs, since T_C of bulk MnSb is much higher — above 300°C and they are formed only in the hexagonal structure whereas MnAs inclusions usually form both cubic (GaMnAs) and hexagonal inclusions with different magnetic properties [3].

The GaSb:MnSb layers were grown on the GaSb(100) and GaAs(111)A substrates using the MBE technology. The layers on both substrates were grown in the same process in order to investigate how the type of a substrate influences the inclusions formation. First, the GaSb buffer of 40 – 45 nm was grown and then the GaMnSb layer. The MnSb hexagonal inclusions were formed directly during the epitaxial growth procedure without the post growth annealing. The detailed analysis of the structure of the inclusions by means of the extended X-ray absorption fine structure spectroscopy (EXAFS) and scanning electron microscopy (SEM) is provided in reference 4, while the magnetic properties are described in reference 5.

The X-ray magnetic circular dichroism (XMCD) experiment was performed at the beamline ID08 (ESRF, Grenoble). X-ray absorption spectra were collected in the total electron yield (TEY) and total fluorescence yield (TFY) modes simultaneously. The measurements were conducted at temperatures of 3 and 300 K, on the remanently magnetized samples as well as on the samples under the magnetic field of 5 T. The magnetic field used to magnetize samples was oriented along the X-ray path, the angle between the surface of the sample and the X-ray beam was being changed from grazing (70°) to normal (10°).

The TEY detection mode is sensitive to the near surface region, while the TFY mode is sensitive to the volume of the sample. For the measurements performed under the field, the TFY XMCD signal is considerably stronger than the TEY XMCD one. Moreover, the TEY XMCD signal shows structure which is not repeated in the TFY signal. In case of the measurements carried out in remanence the TEY XMCD signal cannot be detected.

The investigation on the TFY XMCD signal gathered on the remanently magnetized samples revealed that the GaSb:MnSb layers grown on the GaSb(100) and GaAs(111)A substrates exhibit the dichroic signal which shows the angular dependence. Moreover, this dependence is opposite for both substrates.

Acknowledgments: The measurements performed at the ESRF were supported from special project ESRF/73/2006 from the Ministry of Science and High Education. Authors thank Dr. J. Sadowski for providing the samples.

References

- [1] F. Matsukura, H. Ohno, A. Shen, Y. Sugawara, "Transport properties and origin of ferromagnetism in GaMnAs," *Phys. Rev. B* **57** (1998) R2037.
- [2] M. Zajac, J. Gosk, M. Kaminska, A. Twardowski, T. Szyszko, S. Podsiadlo, "Paramagnetism and antiferromagnetic dd coupling in GaMnN magnetic semiconductor," *Appl. Phys. Lett.* **79** (2001) 2432.
- [3] K. Lawniczak-Jablonska, J. Bak-Misiuk, E. Dynowska, P. Romanowski, J.Z. Domagala, J. Libera, A. Wolska, M.T. Klepka, P. Dluzewski, J. Sadowski, A. Barcz, D. Wasik, A. Twardowski, A. Kwiatkowski, "Structural and magnetic properties of nanoclusters in GaMnAs granular layers," *J. Solid State Chem.* **184** (2011) 1530.
- [4] A. Wolska M.T. Klepka, K. Lawniczak-Jablonska, J. Sadowski, A. Reszka, B.J. Kowalski, "MnSb inclusions in the GaSb matrix studied by X-ray absorption spectroscopy," *Radiat. Phys. Chem.* **80** (2011) 1026.
- [5] K. Lawniczak-Jablonska, A. Wolska, M.T. Klepka, S. Kret, J. Gosk, A. Twardowski, D. Wasik, A. Kwiatkowski, B. Kurowska, B.J. Kowalski, J. Sadowski, "Magnetic properties of MnSb nanoinclusions formed in GaSb matrix directly during MBE process," *J. Appl. Phys.* **109** (2011) 074308.

NEAR-ORDER STRUCTURE OF TRANSPARENT CONDUCTING OXIDES: X-RAY ABSORPTION STUDY OF Al-DOPED ZnO AND ZnMgO FILMS

D.A. Zajac^{1*}, A. Bikowski¹, M. Vinnichenko², and K. Ellmer¹

¹*Institut of Solar Fuels and Energy Storage Materials, Helmholtz-Zentrum Berlin für Materialien und Energie GmbH, Hahn-Meitner-Platz 1, 14109 Berlin, Germany*

²*Institut für Ionenstrahlphysik und Materialforschung, Helmholtz Zentrum Dresden-Rossendorf, Bautzner Landstraße 400, 01328 Dresden, Germany*

Keywords: X-ray absorption spectroscopy, transparent conductive oxides, solar cells, ZnO, ZnMgO, zinc oxide

** e-mail: dariusz.zajac@helmholtz-berlin.de*

ZnO belongs to the class of wide band gap semiconductors with $E_g = 3.37$ eV and exhibits very interesting optical and electrical properties. ZnO is also under development as a cost-efficient alternative to commonly used indium tin oxide (ITO) for applications in optoelectronic devices as a transparent conductive oxide (TCO) electrode [1]. Such applications require simultaneously high transparency in the solar spectral range and a low electrical resistivity, therefore ZnO has to be doped degenerately. While doping with Al leads to the required high carrier concentration [1], alloying with Mg increases the band gap up to 4.5 eV [2]. However, the increase of the conductivity by the increase of the carrier concentration (i.e. reaching the level of $N = 10^{21}$ cm⁻³) can lead to a significant increase of light absorption in the near-IR spectral range. Therefore, many researches focus on the increase of the electron mobility μ at fixed N , in accordance with formula $\rho = (eN\mu)^{-1}$.

The electron mobility is determined by the typical scattering processes in semiconductors, among other the extrinsic scattering on dopants and defects in the film. Since Al doped ZnO and ZnMgO layers, used for transparent electrodes are polycrystalline films, this process can be connected directly not only with dopant but also with local structure defects as Zn or/and O vacancies, stacking faults and grain boundaries. Small crystallographic domain size (< 100 nm), misorientation of domains with respect to the surface normal and incorporation the Al and Mg ions having ionic radius smaller than that of Zn³⁺ (respective crystal radii in tetrahedral coordination are: Al³⁺ 0.53 Å, Mg²⁺ 0.71 Å and Zn²⁺ 0.74 Å [3]), can cause the decrease of the local ordering of the samples.

In this paper we present XAS measurements on the Al doped ZnO and ZnMgO films. The XANES spectra were simulated with the program FEFF9 [4]. First results on the Al *K* edge (Figure 1), show that the Al substitutes preferably the Zn lattice site in the material. For both host materials (ZnO and ZnMgO), Al *K* edge spectra show a similar behaviour. The only clearly visible difference, the decrease of the intensity of the first peak for Al in ZnMgO compared to Al in ZnO, can be attributed to the higher substitution level (a similar effect is observed for higher Al doping of ZnO). The comparison of the

experimental data with the simulation shows that the measured samples (3 at.% Al doped ZnO and 3 at.% Al doped ZnMgO (6 at.% Mg)) are in the low doping regime, where only single Al doping ion can be considered. The effect of the expansion of the *c* axis and the compression of *a* axis for the growth on glass substrate is also observed.

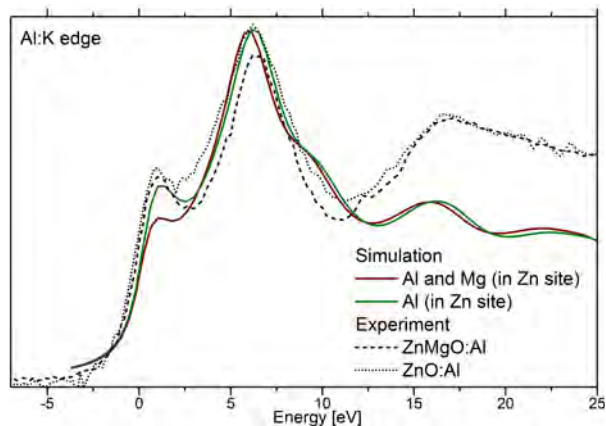


Figure 1: Comparison of Al:K edge XANES simulations for Al doped ZnO and ZnMgO and the experimental data for Al 3 at.% doping of ZnO and ZnMgO (Mg 6 at.%). For the simulation a 0.6 eV broadening has been added according to the energy resolution of the experiment.

Acknowledgments: The authors acknowledge financial support by the IGF Project No. 16595 BG (BMW/AiF, Germany).

References

- [1] K. Ellmer, A. Klein, B. Rechs, *Transparent Conductive Zinc Oxide: Basics and Applications in Thin Film Solar Cells* (Springer, Berlin 2008).
- [2] S. Choopun, R.D. Vispute, W. Yang, R.P. Sharma, T. Venkatesan, H. Shen, "Realization of band gap above 5.0 eV in metastable cubic-phase Mg_xZn_{1-x}O alloy films," *Appl. Phys. Lett.* **80** (2002) 1529.
- [3] R.D. Shannon, "Revised effective ionic radii and systematic studies of interatomic distances in halides and chalcogenides," *Acta Cryst.* **A 32** (1976) 751.
- [4] J.J. Rehr, J.J. Kas, M.P. Prange, A.P. Sorini, Y. Takimoto, F. Vila, "Ab initio theory and calculations of X-ray spectra," *Comptes Rendus Physique* **10** (2009) 548 – 559.

XANES AND EXAFS STUDY OF $(\text{Tl}_{0.5}\text{Pb}_{0.5})\text{Sr}_2(\text{Ca}_{1-x}\text{Gd}_x)\text{Cu}_2\text{O}_z$ SUPERCONDUCTORS**D.A. Zajac¹, W.M. Woch^{1*}, J. Stępień¹, Cz. Kapusta¹, A. Kołodziejczyk¹,
H. Sudra², and G. Gritzner²**¹*Department of Solid State Physics, Faculty of Physics and Applied Computer Science, AGH University of Science and Technology, Al. Mickiewicza 30, PL 30-059, Kraków, Poland*²*Institute for Chemical Technology of Inorganic Materials, Johannes Kepler University, 4040 Linz, Austria**Keywords: synchrotron radiation, thallium superconductors***e-mail: wmwoch@agh.edu.pl*

Results of X-ray absorption spectroscopy study on Gd doped $(\text{Tl}_{0.5}\text{Pb}_{0.5})\text{Sr}_2(\text{Ca}_{1-x}\text{Gd}_x)\text{Cu}_2\text{O}_z$ ($x = 0.1, 0.2$ and 0.3) superconductors are reported. The Gd L_3 absorption edges were studied in the XANES (near-edge) region and in the EXAFS (extended X-ray absorption) region. The XANES spectra are typical for Gd in oxide compounds with the absorption edge followed by a strong “white line” peak which slightly decreases its intensity with

increasing Gd content x . The Fourier transformed EXAFS spectra reveal two well resolved peaks corresponding to the oxygen nearest neighbours and the cation next neighbour shell, respectively. From simulations and fits of the EXAFS spectra to the structure of the host 1212 compound the location site of gadolinium is determined and its possible influence on the local structural environment of the site is analyzed.

LOCAL ELECTRONIC STRUCTURE AND PHYSICAL PROPERTIES OF $\text{Zn}_{1-x}\text{Ni}_x\text{Cr}_2\text{Se}_4$

P. Zajdel^{1*}, I. Jendrzewska², J. Goraus¹, T. Goryczka³, and T. Mydlarz⁴

¹*Institute of Physics, University of Silesia, ul. Uniwersytecka 4, 40-007 Katowice, Poland*

²*Institute of Chemistry, University of Silesia, ul. Szkolna 9, 40-006 Katowice, Poland*

³*Institute of Chemistry and Physics of Metals, University of Silesia, ul. Bankowa 12, 40-006 Katowice, Poland*

⁴*International Laboratory of High Magnetic Fields and Low Temperatures, ul. Gajowicka 95, 53-529 Wrocław, Poland*

Keywords: spinels, XAS

*e-mail: pawel.zajdel@us.edu.pl

We have performed X-Ray Absorption studies of nickel doped ZnCr_2Se_4 in order to elucidate the influence of Ni on the structural and electronic properties of the system.

Upon doping the structure is preserved up to $x = 0.3$, where traces of monoclinic phase start to appear. Lattice parameters of the spinel phase decrease with increased nickel content, which is in agreement with smaller crystal and ionic radii of Ni^{+2} (69 pm, 55 pm) vs Zn^{+2} (73 pm, 60 pm) (Figure 1).

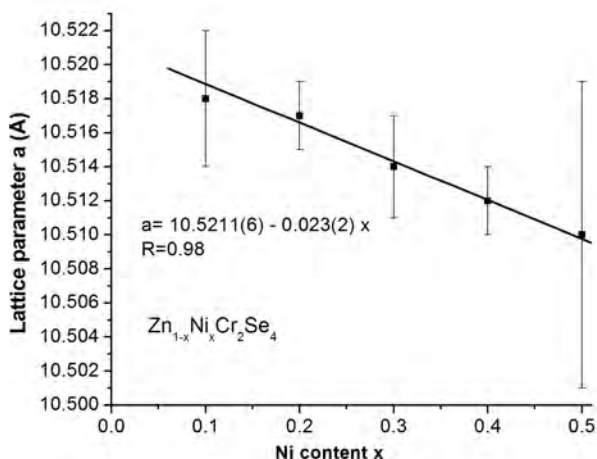


Figure 1: Lattice parameter of $\text{Zn}_{1-x}\text{Ni}_x\text{Cr}_2\text{Se}_4$.

For further study we have concentrated on single phase compounds with highest nominal nickel content $x = 0.2$. The chemical composition was verified with ICP-AES method to be $\text{Zn}_{0.79}\text{Ni}_{0.18}\text{Cr}_{2.18}\text{Se}_4$ and independently from the Rietveld refinement $\text{Zn}_{0.811(7)}\text{Ni}_{0.230(8)}\text{Cr}_{0.970(6)}\text{Se}_4$.

The principal question is the local structure and nominal oxidation state of nickel. In order to analyse it, we have performed room temperature X-Ray Absorption Spectroscopy (XAS) studies on Cr K,

Ni K and Se K edges of the compounds. The experiments were performed on stations 7.1 and 9.3 of the Daresbury SRS.

The analysis of the near edge (XANES) region of Ni K edge (Figure 2.) revealed that it slightly shifts to higher energies with increases Ni content. Its oxidation state is similar to nickel in NiCr_2Se_4 , nominally Ni^{+2} .

To corroborate this result we have performed Full Potential-Linear Orbital calculations of the band and electronic structure of $\text{Zn}_{0.8}\text{Ni}_{0.2}\text{Cr}_2\text{Se}_4$. The calculated densities of states (DOS) gave a good agreement with the experimental absorption edges similar as in the case of octahedrally coordinated Ni [1].

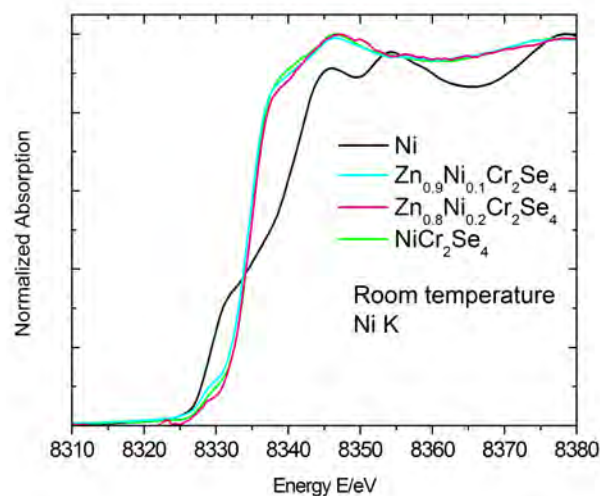


Figure 2: Room temperature XANES spectra of doped $\text{Zn}_{1-x}\text{Ni}_x\text{Cr}_2\text{Se}_4$.

References

- [1] I. Jendrzewska, P. Zajdel, T. Goryczka, J. Goraus, A. Kita, T. Mydlarz, *J. Alloy. Comp.* **520** (2012) 153 – 157.

SYNCHROTRON LIGHT NEWS

APPLICATIONS OF SYNCHROTRON RADIATION IN PHYSICS**Utility of quartz samples for optically stimulated luminescence dating (January 2011)**

— *Review Article*. The light emitted by proton-implanted quartz samples when they are was investigated by team from University of St. Andrews and University of Sussex (both in UK). The 3 MeV Van de Graaf particle accelerator at the University of Sussex was applied for the implantation. Evolution of the luminescence spectrum with increasing cumulative dose and the anisotropy of the light emitted was discussed in detail. The applicability of quartz for optically stimulated luminescence dating was demonstrated, limitations of this method were also pointed out. Numerous references to previous papers devoted to this dating method are provided, leading to creation of a valuable review.

G.E. King, A.A. Finch, R.A.J. Robinson, D.E. Hole, "The problem of dating quartz 1: Spectroscopic ionoluminescence of dose dependence," *Radiat. Meas.* **46** (2011) 1 – 9. (W.Sz.)

Raman spectroscopy as a useful tool to complete the X-ray diffraction data for biological systems (June 2011) — Review Article.

The complementarity of Raman spectroscopy and X-ray crystallography for the analysis of biological macromolecular systems is discussed in this review paper, prepared by team from Portsmouth (UK) and Grenoble (France) and published as a part of a special issue entitled: *Protein Structure and Function in the Crystalline State*. Raman spectroscopy offering an access to the structural information at sub-atomic level are opposed to X-ray diffraction method providing similar information at near-atomic resolution. The applicability of Raman microspectrophotometry for studies of X-ray radiation damage and crystalline DNA molecules are also emphasized. Several examples dealing with metallo-, photosensitive-, and redox -proteins are presented.

J.E. McGeehan, D. Bourgeois, A. Royant, P. Carpentier, "Raman-assisted crystallography of biomolecules at the synchrotron: Instrumentation, methods and applications," *Biochim. Biophys. Acta* **1814** (2011) 750-759. (W.Sz.)

Impact of non-muffin-tin effects on XANES (October 2010). Study of the local atomic structure is important from both fundamental point of view for understanding the physical properties and physico-chemical processes, and as well from ap-

plied research as a basis for designing materials with desired properties, or, for example, the catalysts of chemical reactions. One of such methods is based on analysis of the fine structure of x-ray absorption near-edge spectra (XANES). At present a complicating factor impeding the quantitative analysis of XANES is insufficient knowledge about how it is influenced by non-muffin-tin form of potential. Only a few papers are devoted to the study of such effects in crystalline systems. It is not known what features of the local structure may be important for the introduction of significant amendments and what changes the spectra will be affected by the introduced amendments. Consequently, the study of the effect of non-muffin-tin effects on the XANES of organometallic systems is important. This work is devoted to this subject.

G. Smolentsev, "Local structure refinement on the basis of XANES fitting: Application of FitIt software," *XAS Research Review* **4** (2010), <http://www.ixasportal.net/ixas/>. (I.N.D)

Ambient- and low-temperature synchrotron x-ray diffraction study of BaFe₂As₂ and CaFe₂As₂ at high pressures up to 56 GPa (February 2011).

The measurements have shown that at 300 K, the transition occurs at 27 GPa and 1.7 GPa (in Ba and Ca compounds, respectively). The transition in both compounds is observed when they are compressed to almost identical the unit-cell volume and attain similar axial ratios. It is also found that the FeAs₄ tetrahedra are much less compressible and more distorted in the collapsed tetragonal phase than those (of nearly regular shape) in the ambient-pressure phase.

R. Mittal, S.K. Mishra, S.L. Chaplot, S.V. Ovsyanikov, E. Greenberg, D.M. Trots, L. Dubrovinsky, Y. Su, Th. Brueckel, S. Matsuishi, H. Hosono, G. Garbarino, "Ambient- and low-temperature synchrotron x-ray diffraction study of BaFe₂As₂ and CaFe₂As₂ at high pressures up to 56 GPa," *Phys. Rev. B* **83** (2011) 054503. (R.P.)

Growth of HfO₂ studied *in situ* by XRF and GISAXS (June 2011).

HfO₂ is a high- κ dielectric with prospects for wide applications in microelectronics. The initial growth of this compound on Si and Ge surfaces was studied *in situ* at the National Synchrotron Light Source at Brookhaven National Laboratory. The atomic layer deposition (ALD) process was carried out in the reactor installed at the X21 beamline. The first stages of growth process were observed by x-ray fluorescence (XRF) and grazing incidence small angle x-ray scattering (GISAXS) techniques. During growth the

evolution of the amount of deposited material and surface roughness of the samples were recorded for oxidized and hydrogenated Si and Ge substrates.

K. Devloo-Casier, J. Dendooven, K.F. Ludwig, G. Lekens, J. D'Haen, C. Detavernier, "In situ synchrotron based x-ray fluorescence and scattering measurements during atomic layer deposition: Initial growth of HfO₂ on Si and Ge substrates," *Appl. Phys. Lett.* **98** (2011) 231905. (B.J.K.)

A theoretical treatment of RIXS using a real-space multiple-scattering Green's function formalism (June 2011). Resonant inelastic x-ray scattering (RIXS) spectroscopy is expected to become an important analytical tool, particularly in the field of materials science. However, this technique has not been widely applied, partly because of difficulties involved with interpretation of RIXS spectra. Many x-ray absorption fine-structure (XAFS) users are interested in the properties of their samples, which can be analyzed with the help of a suitable software based on RIXS methodology and physics. This has led to the need for simple RIXS analysis programs that are easy to use for beginners, yet powerful enough to tackle complex problems for advanced users. In this article, an *ab initio* theory of core and valence RIXS based on a real-space multiple-scattering Green's function formalism and a quasiboson model Hamiltonian implemented in a FEFF9 code, is presented. This formalism is meant to reproduce the direct RIXS and is currently limited to weakly correlated systems.

J.J. Kas, J.J. Rehr, J.A. Soinien, P. Glatzel, "Real Space Green's Function Approach to RIXS," *Phys. Rev.* **B 83** (2011) 235114. (I.N.D.)

Tunable soft x-rays for element-specific hysteresis loops and perpendicular exchange bias (July 2011). The exchange bias (EB) effect has become an integral part of spintronics with implications for basic research and for numerous device applications like random access magnetic storage units and spin valves. The origin of the EB effect is related to the magnetic coupling across the common interface shared by a ferromagnetic (FM) and an antiferromagnetic (AF) layer, when the system is cooled through the Néel temperature of the AF layer. For thin films an in-plane coupling is typically favored for most systems with a Néel temperature for the AF thin film layer often situated below room temperature.

For applications in spintronics, a robust and tunable exchange bias is required at room temperature. The tunable soft x-rays of the BESSY II storage ring at beam lines PM3 and UE46-PGM1 show experimental evidence for a perpendicular EB in a prototypical ferrimagnetic spin valve consisting of DyCo₅/Ta/Fe₇₆Gd₂₄, where the DyCo₅ alloy has the role of a hard ferrimagnet and Fe₇₆Gd₂₄ is a soft ferrimagnet. The authors use the elemental sensitivity obtained using the element specific excitation using soft x-rays with circular polarization to measure

element specific hysteresis loops and dichroic x-ray absorption spectra. The absolute value of the EB can be tuned through the thickness of the interlayer spacer and even reversed with relatively low magnetic fields of several hundred Oersteds. This flexibility in controlling a robust perpendicular EB at room temperature may be of outmost importance for applications in modern ultrafast storage media. F. Radu, R. Abrudan, I. Radu, D. Schmitz, H. Zabel, "Perpendicular exchange bias in ferrimagnetic spin valves," *Nature Commun.* **3** (2012) 715, www.nature.com/naturecommunications. (I.A.K.)

Synchrotron-based photoluminescence excitation spectroscopy as a tool to study the valence band structure (July 2011). A group of scientists from Magdeburg, Bonn, and Ulm (Germany) demonstrated, for selected wurtzite-type semiconductors, the efficiency of synchrotron-based photoluminescence excitation spectroscopy in studies of valence band structure. This method is particularly valuable in investigation of thin layers or materials with low absorption edge splitting. The determined values of the valence band splitting were of the order of 200 meV, whereas the experimental accuracy is better than 10 meV. The obtained results are supported by findings based on synchrotron ellipsometry data.

M. Feneberg, M. Röppischer, N. Esser, C. Cobet, B. Neuschi, T. Meisch, K. Thonke, R. Goldhahn, "Synchrotron-based photoluminescence excitation spectroscopy applied to investigate the valence band splittings in AlN and Al_{0.94}Ga_{0.06}N," *Appl. Phys. Lett.* **99** (2011) 021903. (W.Sz.)

Ferromagnetism of zincblende-type GaN:Mn studied by XANES (July 2011). Zincblende-type GaN:Mn was studied by XANES by collaborating groups from Russia, China and France. The local atomic structure around Mn impurity ions was determined in the nanoscale. The Jahn-Teller distortion around Mn ions was observed. The possible impact of local distortions on the magnetic properties is discussed.

N. Smolentsev, G. Smolentsev, S. Weid and A.V. Soldatov, "Local atomic structure around Mn ions in GaN:Mn thin films: Quantitative XANES analysis," *Physica B* **406** (2011) 2843 – 2846. (W.P.)

Imaging of solidification processes (October 2011). Solidification processes occurring on Earth can be visualized using the synchrotron radiation. For the purpose of studies in space, a compact x-ray microradiograph was designed and built to study the solidification and casting processes in metals. The aim of this work was to apply such a laboratory device for implementation in a sounding rocket or for a parabolic flight campaign imposing on x-ray imaging system both compact design requirements and high spatial and temporal resolutions needed for imaging of solidification processes. Investigation of solidification dynamics of alloys is based on a low-power microfocus x-ray tube being potentially

appropriate for x-ray diagnostics in space, where the synchrotron radiation cannot be applied. The whole setup was optimized to yield a high contrast x-ray images at short exposure times.

C. Rakete, C. Baumbach, A. Goldschmidt, D. Samberg, C.G. Schroer, F. Breede, C. Stenzel, G. Zimmermann, C. Pickmann, Y. Houtz, C. Lockowandt, O. Svenonius, P. Wiklund, R.H. Mathiesen, "Compact x-ray microradiograph for in situ imaging of solidification processes: Bringing in situ x-ray micro-imaging from the synchrotron to the laboratory," *Rev. Sci. Instrum.* **82** (2011) 105108. (I.N.D.)

A virtual reality helps in learning about the synchrotron light (September 2011). A team from Republic of China worked on the virtual reality technology and developed a virtual synchrotron light source model. The aim was to ascertain preparation of young students to use the synchrotron light sources. A success of teaching experiments using this model is presented.

W. Tarng, C.M. Lin, Y.T. Liu, Y.N. Tong, K.Y. Pan, "A virtual reality design for learning the basic concepts of synchrotron light source," *Int. J. Comput. Sci Eng.* **6** (2011) 175 – 184. (W.P.)

Pressure induced high spin-low spin transition in FeSe superconductor studied by x-ray emission spectroscopy and ab initio calculations (August 2011). The pressure effect on the spin state of Fe in FeSe superconductor has been studied with synchrotron x-ray emission spectroscopy by a team from the University of Nevada and Argonne National Laboratory. The pressure induced high spin to low spin transition was observed at both ambient and low temperatures with continuous suppression of Fe magnetic moments under increasing pressure. The observed spin transition is concluded to be related to the pressure induced structural transition from tetragonal to orthorhombic phase.

R.S. Kumar, Y. Zhang, Y. Xiao, J. Baker, A. Cornelius, S. Veeramalai, P. Chow, Ch. Chen, Y. Zhao, "Pressure induced high spin-low spin transition in FeSe superconductor studied by x-ray emission spectroscopy and ab initio calculations," *Appl. Phys. Lett.* **99** (2011) 061913. (R.P.)

Structural phase transitions of Ce-based metallic glass under pressure (December 2011). The $\text{Ce}_{70}\text{Al}_{10}\text{Ni}_{10}\text{Cu}_{10}$ metallic glass displays a strong hysteresis in volume per atom variation when applying and releasing of pressure. The hysteresis is attributed to pressure driven change in the localization of Ce 4f electronic states. An international team of scientists affiliated in Spain, Mexico, France, and China has correlated the observed structural changes of this alloy with the modification of elastic constants, acoustic mode frequencies, and sound speed. Three different amorphous phases (with a high, low, and intermediate density states) were found in the 0 – 25 GPa pressure range. An intermediate phase responsible for the hystere-

sis behavior is identified and the role of Ce 4f electrons in observed phenomena is pointed out and discussed.

M.J. Duarte, P. Bruna, E. Pineda, D. Crespo, G. Garbarino, R. Verbeni, K. Zhao, W.H. Wang, A.H. Romero, J. Serrano, "Polyamorphic transitions in Ce-based metallic glasses by synchrotron radiation," *Phys. Rev. B* **84** (2011) 224116. (W.Sz.)

Magnetism of cobalt clusters on graphene (October 2011). The structure and magnetic properties of cobalt clusters on the graphene/Ir(111) moiré, were studied, by scientists from France and Germany, combining the scanning tunneling microscopy with x-ray magnetic circular dichroism. Surprisingly, no magnetic anisotropy is observed for small clusters. The authors found indications for a magnetic coupling between the clusters.

C. Vo-Van, S. Schumacher, J. Coraux, V. Sessi, O. Fruchart, N.B. Brookes, P. Ohresser, T. Michely, "Magnetism of cobalt nanoclusters on graphene on iridium," *Appl. Phys. Lett.* **99** (2011) 142504. (R.P.)

Synchrotron radiation experiment on phase transition of FeO yields new insight into Earth's outer core (November 2011). Scientists from Japan demonstrate that sodium chloride (NaCl)-type FeO transforms to a cesium chloride (CsCl)-type phase above 240 GPa at 4000 K. They show that the phase-induced stratification is seismologically invisible but strongly affects the geodynamo. All the high P-T experiments were conducted at BL10XU of SPring-8.

H. Ozawa, F. Takahashi, K. Hirose, Y. Ohishi, N. Hirao, "Phase transition of FeO and stratification in Earth's outer core," *Science* **334** (2011) 792-794. (P.P.)

Observations of laser induced magnetization dynamics in Co/Pd multilayers with coherent x-ray scattering (December 2011). Collaborating groups from USA and Switzerland have studied the laser induced magnetization dynamics in Co/Pd multilayers, on the basis of results of time-resolved coherent x-ray scattering. Starting from a multidomain ground state, the magnetization is uniformly reduced after excitation by an intense 50 fs laser pulse. The authors conclude that the intensity of dynamic scattering is separated into (i) an elastic portion (at length scales > 65 nm) retaining the memory of the initial domain magnetization, and (ii) a fluctuating part (at smaller length scales) attributed to domain-boundary motion during recovery. B. Wu, D. Zhu, Y. Acremann, T.A. Miller, A.M. Lindenberg, O. Hellwig, J. Stöhr, A. Scherz, "Observations of laser induced magnetization dynamics in Co/Pd multilayers with coherent x-ray scattering," *Appl. Phys. Lett.* **99** (2011) 252505. (R.P.)

Monoclinic deformation of crystal lattice of bulk α -BiFeO₃ (March 2012). The BiFeO₃ lattice symmetry lowering from rhombohedral to monoclinic is studied by a team from Inst. Exp. Phys. of University of Warsaw (Poland) and ESRF

(Grenoble, France). This hypothesis is based on a careful lineshape analysis of diffraction patterns taken at ID-31 beamline (ESRF) for polycrystalline samples synthesized in different laboratories. The authors determine the lattice parameter values for the expected monoclinic phase.

I. Sosnowska, R. Przeniosło, A. Palewicz, D. Wardecki, A. Fitch, "Monoclinic deformation of crystal lattice of bulk — BiFeO₃: High resolution synchrotron radiation diffraction patterns," *J. Phys. Soc. Jap.* **81** (2012) 044604. (W.Sz.)

Other papers in this field.

H. Kondo, W. Takeuchi, M. Hori, S. Kimura, Y. Kato, T. Muro, T. Kinoshita, O. Sakata, H. Tajiri, M. Hiramatsu, "Synchrotron x-ray analyses of crystalline and electronic structures of carbon nanowalls," *Appl. Phys. Lett.* **99** (2011) 213110.

B. Kallinger, S. Polster, P. Berwian, J. Friedrich, G. Müller, A.N. Danilewsky, A. Wehrhahn, A.-D. Weber, "Threading dislocations in *n*- and *p*-type 4H-SiC material analyzed by etching and synchrotron X-ray topography," *J. Cryst. Growth* **314** (2011) 21 – 29.

P. Schroth, T. Slobodskyy, D. Grigoriev, A. Minkevich, M. Riotte, S. Lazarev, E. Foftung, D.Z. Hu, D.M. Schaadt, T. Baumbach, "Investigation of buried quantum dots using grazing incidence X-ray diffraction," *Mater. Sci. Eng B - Solids* (2012, in print).

APPLICATIONS OF SYNCHROTRON RADIATION IN CHEMISTRY (catalysis, environment, energy, structure solution, forensic studies, electrochemistry, astrochemistry)

Synchrotron studies clarify the properties of environmental nanoparticles (2012, in print)

— *Review Article*. Environmental nanoparticles are difficult to collect and analyze. As shows the review by researchers from National Taiwan University, Taipei, Taiwan, better understanding of such objects is possible when using synchrotron beams. For an example of red soils, the illite, kaolinite, goethite and hematite nanoparticles were found.

T.M. Tsao, Y.M. Chen, M.K. Wang, "Origin, separation and identification of environmental nanoparticles: A review," *J. Environ. Monitor.* **13** (2011) 1156 – 1163. (W.P.)

Merger of synchrotron *in situ* characterization techniques for catalysis reviewed with 83 references (May 2010) — *Review Article*.

The authors, both synchrotron beamline scientists, review current state and prospect for *in situ* 'bridging' XRD technique with vibrational spectroscopies like IR and Raman. Another 'bridge' considered is that between catalytic community and staff of central research facilities via construction of dedicated

beamlines and a closer integration to develop and maintain new experiments. Combinations of also other techniques including EXAFS, SAXS, XRF and Compton Scattering are reviewed for arriving at a holistic picture of a catalytic process.

M.A. Newton, W. van Beek, "Combining synchrotron-based X-ray techniques with vibrational spectroscopies for the *in situ* study of heterogeneous catalysts: A view from a bridge," *Chem. Soc. Rev.* **39** (2010) 4845 – 4863. (Z.K.)

Analytical techniques for minerals and contaminants in supergenic environment - a review (February 2011) — *Review Article*.

Environmental mineralogy and geochemistry describes the relationships and interactions occurring between the composition of lithosphere on one hand and hydrosphere/atmosphere/biosphere on the other hand. A particularly important field is the distribution of contaminants. Classical and synchrotron-based analytical techniques helpful in determination of such distributions are described by scientists affiliated at two Italian universities.

F. Frau, P. Marescotti, "Mineralogical and geochemical techniques to investigate the relationships between minerals and contaminants in supergenic environments: An update review," *Jb. Miner. Abh.* **188**, **1** (2011) 1 – 9. (W.P.)

Water oxidation on manganese catalyst-principal step of water splitting monitored by *in situ* XAS (June 2011).

The reaction of water-oxidation, the first step of water splitting enabling cheap production of hydrogen for fuel cells, has been monitored *in situ* via XAS technique in a constructed suitable photoelectrochemical device. The team of researchers based mostly around Australian Synchrotron used synthetic tetranuclear-manganese clusters embedded in Nafion as a catalyst mimicking the Mn₄CaO₄ cluster of Photosystem II used by oxygenic photosynthetic living organisms. A cyclic dissociation-reoxidation was demonstrated also by TEM.

R.K. Hocking, R. Brimblecombe, L-Y. Chang, A. Singh, M.H. Cheah, C. Glover, W.H. Casey, L. Spiccia, "Water-oxidation catalysis by manganese in a geochemical-like cycle," *Nature Chem.* **3** (2011) 461 – 466. (Z.K.)

Crystal structure of silver behenate (December 2011).

Silver behenate — low-angle standard and challenging material for structural XRPD, crystallizes as plates ~ 0.1 μm thick, too small for 'single crystal' study. Due to the size of crystallites, texture and 'dominant zone', only 00*l* lines were observed, even using synchrotron data. Although this compound was the subject of intensive research by: SEM, IR, EXAFS, a progress in structural studies was rather small. A team of researchers from the USA, performed optimized crystallization of this compound, and then collected synchrotron data at SUNY-X3B1 beamline, Brookhaven. Number of weak lines of *hkl* type was discerned. Having the cell parameters, the authors attempted to solve its

structure using the newest XRPD methods. The structure was solved by synergistic combination of a high-resolution synchrotron powder data, and density functional optimization (CASTEP). The structure, refined by Rietveld method, is basically consistent with the results obtained so far (IR, EXAFS). T.N. Blanton, M. Rajeswaran, P.W. Stephens, D.R. Whitcomb, S.T. Misture, J.A. Kaduk, "Crystal structure determination of the silver carboxylate dimer $[\text{Ag}(\text{O}_2\text{C}_{22}\text{H}_{43})]_2$, silver behenate, using powder X-ray diffraction methods," *Powder Diffr.* **26**, **4** (2011) 313 – 320. (W.L.)

Details of pyrite oxidation determined by synchrotron-based SPEM and micro-XPS (October 2011). Pyrite is an environmentally significant mineral being the major contributor to acid rock drainage. The authors from University of South Australia in Adelaide in order to understand the initial pyrite oxidation steps that take place during the natural weathering processes analyzed in detail the reactions of O_2 and H_2O gases with the fresh pyrite surface. They have demonstrated that the localized regions of the pyrite surface where Fe species of reduced coordination exist not only initiate the oxidation process but also facilitate the formation of highly reactive hydroxyl radical species, which then leads the sulfur oxidation process.

A.P. Chandra, A.R. Gerson, "Pyrite (FeS_2) oxidation: A sub-micron synchrotron investigation of the initial steps," *Geochim. Cosmochim. Acta* **75** (2011) 6239 – 6254. (W.Sz.)

Synchrotron studies show that the omnipresent glitter particles may serve as additional evidences in forensic investigations (2012, in print). Glitter particles are built of three or more distinct layers. Their presence at the crime scene may serve as an evidence during forensic investigations. This approach would work if a suitable database of glitter particles is created. The authors of the paper, from Caen (France), Berkeley, New York, and El Cajon (United States), present the results of the proposed approach, based on FT-IR microscope synchrotron measurements.

L. Vernoud, H.A. Bechtel, M.C. Martin, J.A. Reffner, R.D. Blackledge, "Characterization of multilayered glitter particles using synchrotron FT-IR microscopy," *Forensic Sci. Int.* (2012, in print). (W.P.)

Correlation of the formation of boronite with the oxidation of chalcopyrite in acidic media under atmospheric conditions (January 2012). A team from Brazil and US investigated the oxidation of chalcopyrite electrodes immersed in 0.1 mol/L H_2SO_4 solution, in great detail modifying several experimental conditions. The techniques appropriate for thin films analysis: micro-Raman spectroscopy and synchrotron small angle X-ray diffraction were applied. The formation of boronite (an iron-deficient sulphide), elemental sulphur, and covellite (CuS) were detected on the chalcopyrite surface. The results of work support the

hypothesis that the formation of intermediate iron-deficient sulfides contributes to the slow oxidation rate of chalcopyrite under atmospheric conditions. D. Majuste, V.S.T. Ciminelli, K. Osseo-Asare, M.S.S. Dantas, R. Magalhães-Paniago, "Electrochemical dissolution of chalcopyrite: Detection of bornite by synchrotron small angle X-ray diffraction and its correlation with the hindered dissolution process," *Hydrometallurgy* **111 - 112** (2012) 114 – 123. (W.Sz.)

Examination of battery materials by time-resolved X-ray diffraction (April 2012). Scientists from Korea and USA performed study of the effects of Li/Ti ratios on the particle and electrochemical properties of $\text{Li}_4\text{Ti}_5\text{O}_{12}$ synthesized by a solid-state reaction. To monitor the *in-situ* structural changes of $\text{Li}_4\text{Ti}_5\text{O}_{12}$ during electrochemical processes, the half-cell was mounted in the X7B beamline of the National Synchrotron Light Source at Brookhaven National Laboratory. The team showed with the time-resolved XRD technique the high structural stability of the studied material during the charge/discharge process.

J.-W. Shin, K.Y. Chung, J.H. Ryu, I.-W. Park, D.-H. Yoon, "Effects of Li/Ti ratios on the electrochemical properties of $\text{Li}_4\text{Ti}_5\text{O}_{12}$ examined by time-resolved X-ray diffraction," *Appl. Phys. A—Matter.* (2012, in print). (P.P.)

How synchrotrons can help in increasing the crime detectability? (2012, in print). The answer is: "through building a database of minerals and heavy elements in soil, with the data collected at 3024 geographical locations over the country." The composition of soil may be treated as a geographical fingerprint and may therefore be helpful in identification of the provenance of objects or people involved in a crime. A nationwide forensic soil sediment database for Japan is constructed by collaborating Japanese scientists on the basis of sediments phase composition, using the synchrotron radiation.

W.S.K. Bong, I. Nakaia, S. Furuya, H. Suzuki, Y. Abe, K. Osaka, T. Matsumoto, M. Itou, N. Imai, T. Ninomiya, "Development of heavy mineral and heavy element database of soil sediments in Japan using synchrotron radiation X-ray powder diffraction and high-energy (116 keV) X-ray fluorescence analysis: 1. Case study of Kofu and Chiba regio," *Forensic Sci. Int.* (2012, in print). (W.P.)

Other papers in this field.

N. Schleicher, U. Kramar, S. Norra, V. Dietze, U. Kaminski, K. Cen, Y. Yu, " μ -scale variations of elemental composition in individual atmospheric particles by means of synchrotron radiation based μ -XRF analysis," *AIP Conf. Proc.* **1221** (2010) 172 – 180.

P. Coppens, J. Benedict, M. Messerschmidt, I. Novozhilova, T. Graber, Y.-S. Chen, I. Vorontsov, S. Scheinsa, S. .-L. Zheng, "Time-resolved synchrotron diffraction and theoretical studies of very short-lived

photo-induced molecular species,” *Acta Crystallogr. A* **66** (2010) 179 – 188.

B.T. de Gregorio, R.M. Stroud, G.D. Cody, L.R. Nittler, A.L.D. Kilcoyne, S. Wirick, “Correlated microanalysis of cometary organic grains returned by Stardust,” *Meteorit. Planet. Sci.* **46** **9** (2011) 1376 – 1396.

APPLICATIONS OF SYNCHROTRON RADIATION IN BIOLOGY AND MEDICINE

Microbeam radiation therapy for tumor treatment (April 2010) — *Review Article*.

The microbeam radiation therapy (MRT) used in treatment of tumors is reviewed. It is presented from a historical perspective, but the issues connected with last achievements and future studies are also widely presented.

E. Bräuer-Krisch, R. Serduc, E.A. Siegbahn, G. Le Duc, Y. Prezado, A. Bravin, H. Blattmann, J.A. Laissue, “Effects of pulsed, spatially fractionated, microscopic synchrotron X-ray beams on normal and tumoral brain tissue,” *Mutat. Res.* **704** (2010) 160 – 166. (W.P.)

Importance of synchrotron radiation in crystallography (November 2011) — *Review Article*.

An extensive review begins with a presentation of Kathleen Lonsdale, a prominent woman in the history of crystallography and world science. Certainly, she may be counted among the greatest women of the XX century, such as Maria Skłodowska-Curie. Kathleen Lonsdale was an outstanding scientist, she was the first female President of the IUCr and of the BAAS, she was also a leading pacifist of her time. In the next part, the author discusses the development of research using synchrotron radiation, almost from its beginnings to the present time. The author, concentrating on the study of macromolecules, shows a lively description of the development of synchrotron radiation research techniques. Article is illustrated with photographs and drawings from the original publications (some are ~ 20 – 30 years old), which also shows the progress in science. In the review, the readers can also find information about the renaissance of the Laue method, with its application in studies of macromolecules, and also information about news in neutron diffraction.

J.R. Helliwell, “Evolution of synchrotron radiation and the growth of its importance in crystallography,” *Crystallogr. Rev.* **18**, **1** (2012) 33 – 93. (W.L.)

Damaging effects of synchrotron radiation on biological tissue: significance for medical applications (December 2011) — *Review Article*.

In this short review paper, Chinese scientists analyzed the fundamental mechanisms underlying the interaction between synchrotron X-ray beam with biological tissues. The damaging effects on

proteins, cells and tissues were briefly reminded. Differences between the damaging mechanisms of beams emitted by classical instruments and by synchrotrons are observed. The particularity of possible special safety standards for the synchrotron-based X-ray imaging are pointed out.

H. Chen, X. He, C. Sheng, Y. Ma, H. Nie, W. Xia, W. Ying, “Interactions between synchrotron radiation X-ray and biological tissues — theoretical and clinical significance,” *Int. J. Physiol. Pathophysiol. Pharmacol.* **3** (2011) 243 – 248. (W.Sz.)

The largest virus visualized with an X-ray free-electron laser (February 2011).

Mimivirus is the largest known virus with a size comparable to the size of the smallest living cells. A large international team composed of scientists from Sweden, Germany, France and US demonstrated the first virus image obtained with the use of an X-ray free-electron laser (LCLS), on the basis of a single shot diffraction pattern. The non-crystalline character of this biological sample should be emphasised. The reconstructed mimivirus images at 32 nm resolution are consistent with previous findings of cryo-electron microscopic studies.

M.M. Seibert, T. Ekeberg, F.R.N.C. Maia, M. Svenda, J. Andreasson, O. Jönsson, D. Odić, B. Iwan, A. Rocker, D. Westphal, M. Hantke, D.P. DePonte, A. Barty, J. Schulz, L. Gumprecht, N. Coppola, A. Aquilla, M. Liang, T.A. White, A. Martin, C. Calemen, S. Stern, C. Abergel, V. Seltzer, J.-M. Claverie, *et al.*, “Single mimivirus particles intercepted and imaged with an X-ray laser,” *Nature* **470** (2011) 78 – 81. (W.Sz.)

Aggregation of Mg and Fe atoms contributes to the asbestos toxicity mechanism in human lung tissue (February 2011).

Scientists from Italy have discovered a new phenomenon taking part in tissue response to the asbestos toxicity. By using synchrotron soft X-ray imaging and X-ray fluorescence microscopy (ELETTRA), they showed with submicrometric resolution that elemental lateral distribution in lung tissues containing asbestos fibres was significantly affected, i.e. Mg and Fe atoms were accumulated in the vicinity of the fibres.

L. Pascolo, A. Gianoncelli, B. Kaulich, C. Rizzardi, M. Schneider, C. Bottin, M. Polentarutti, M. Kiskinova, A. Longoni, M. Melato, “Synchrotron soft X-ray imaging and fluorescence microscopy reveal novel features of asbestos body morphology and composition in human lung tissues,” *Part. Fibre Toxicol.* **8** (2011) 7 – 11. (A.N.)

Structure determination of nanocrystals of macromolecules that cannot be grown as large crystals — a challenging experiment at LCLS (February 2011).

A team of 89 authors from Germany, US and Sweden presented a method for structure determination where single crystal X-ray diffraction ‘snapshots’ are collected from a stream of nanocrystals using femtosecond

pulses from a hard X-ray free-electron laser (LCLS). The nanocrystals of so-called photosystem I, one of the largest membrane protein complexes was chosen to prove an efficiency of proposed method. The detector module recorded high-angle diffraction to a resolution of 8.5 Å, more than three million diffraction patterns were collected in this study. The Monte Carlo integration over the reciprocal space volume of the Bragg reflection and the distribution of crystal shapes and orientations and variations of the X-ray pulse fluence enabled creation of the electron density map. This map showed the details expected at this resolution, including the transmembrane helices, membrane extrinsic features and some loop structures.

H.N. Chapman, P. Fromme, A. Barty, T.A. White, R.A. Kirian, A. Aquila, M.S. Hunter, J. Schulz, D.P. DePonte, U. Weierstall, R.B. Doak, F.R.N.C. Maia, A.V. Martin, I. Schlichting, L. Lomb, N. Coppola, R.L. Shoeman, S.W. Epp, R. Hartmann, D. Rolles, A. Rudenko, L. Foucar, N. Kimmel, G.G. Weidenspointer, P. Holl, *et al.*, "Femtosecond protein X-ray nanocrystallography," *Nature* **470** (2011) 73 – 77. (W.Sz.)

Supramolecular structures of biological nanoparticles for gene therapy studied by synchrotron SAXS (January 2012). A multinational group from Singapore has synthesized a series of novel nontoxic, cationic peptides with improved physicochemical properties leading to DNA condensation into nanoparticles. It was shown by synchrotron small-angle X-ray scattering (Beamline 23A SWAXS at the National Synchrotron Radiation Research Center, Hsinchu, Taiwan) that the ternary complexes, formed by DNA condensed by the peptides and lipids, self-assembled spontaneously to a supramolecular lamellar structures. Such structures provided enhanced cell membrane penetration. The results suggest possible application of these nanoparticles as gene delivery agents.

J. Yan, N. Korolev, K. Dong Eom, J.P. Tam, L. Nordenskiöld, "Biophysical properties and supramolecular structure of self-assembled liposome/ ϵ -peptide/DNA nanoparticles: Correlation with gene delivery," *Biomacromolecules* **13** (2012) 124 – 131. (A.N.)

Willow can absorb Cd and Zn from the soil (September 2011). Japanese researchers studied enrichment of a several metals concentration in various parts of the tree leaves with 2 μm^2 X-ray synchrotron beam (Spring-8, Hyogo, Japan) via XANES and XRF. The analysis revealed accumulation of the metal in the tip cells of the leaf serrations and no heavy metal (Cd, Fe, Cu, Zn) removal through secretions from the leaf hydathodes (water-excreting epidermal structure), although Mg, Si, P, Cl, S, K and Ca are removed this way. XANES data revealed binding of Cd with polysaccharides and lignins.

E. Harada, A. Hokura, I. Nakai, Y. Terada, K. Baba, K. Yazaki, M. Shiono, N. Mizuno, T. Mizuno, "Assessment of willow (*Salix sp.*) as a woody heavy metal

accumulator: Field survey and in vivo X-ray analyses," *Metallomics* **3** (2011) 1340. (Z.K.)

Synchrotron radiation shows how iron activates oxygen in living organisms (October 2011). Research teams from Korea and USA used X-ray absorption technique at the Stanford Synchrotron Radiation Lightsource (SSRL) on beam line 9-3 to capture the fine details of how iron-containing enzymes work. All three of these three most biologically relevant iron-oxygen intermediates have been spectroscopically characterized. One of these iron complexes exists for less than 2 milliseconds before converting into a different form.

J. Cho, S. Jeon, S.A. Wilson, L.V. Liu, E.A. Kang, J.J. Braymer, M.H. Lim, B. Hedman, K.O. Hodgson, J.S. Valentine, E.I. Solomon, W. Nam, "Structure and reactivity of a mononuclear non-haem iron(III)-peroxo complex," *Nature* **478** (2011) 502 – 505. (P.P.)

X-ray phase contrast imaging using table top synchrotron (September 2011). Scientists from UK and USA demonstrate that their table top synchrotron light source can be successfully applied to phase contrast X-ray imaging. They show results obtained for a tetra fish, damselfly and yellow jacket. They also discuss technical obstacles which after being solved may allow experiments like e.g. optical pump and probe, time resolved and advanced imaging commonly accessible for medical purposes.

S. Kneip, C. McGuffey, F. Dollar, M.S. Bloom, V. Chvykov, G. Kalintchenko, K. Krushelnick, A. Maksimchuk, S.P.D. Mangles, T. Matsuoka, Z. Najmudin, C.A.J. Palmer, J. Schreiber, W. Schumaker, A.G.R. Thomas, V. Yanovsky, "X-ray phase contrast imaging of biological specimens with femtosecond pulses of betatron radiation from a compact laser plasma wakefield accelerator," *Appl. Phys. Lett.* **99** (2011) 093701.

(M.T.K.)

Synchrotron helps in detection of trace elements in human bones (2012, in print). X-ray fluorescence data collected at VESPERs beamline at the Canadian Light Source led to determination of trace elements in historical human bones, for a population exposed to lead. The results show opportunity for finding evidences of antemortem biogenic uptake.

T. Swanston, T. Varney, I. Coulthard, R. Feng, B. Bewer, R. Murphy, C. Hennig, D. Cooper, "Element localization in archaeological bone using synchrotron radiation x-ray fluorescence: Identification of biogenic uptake," *J. Archaeol. Sci.* (2012), doi: 10.1016/j.jas.2012.01.041. (W.P.)

Structural insight into immunological response against viral infections by X-ray crystallography (October 2011). Synchrotron radiation is a powerful tool in determination of large biomolecular structures that are indispensable for gaining a deeper insight into biophysical bases of

human health and disease. A team of French scientists has determined (at ESRF in Grenoble) different variants of crystal structures of an important protein, called RIG-I, which is evolutionarily conserved within higher organisms. This is a crucial point in elucidating the molecular mechanism for an immunological response at the first step of defence against some viral infections.

E. Kowalinski, T. Lunardi, A.A. McCarthy, J. Louber, J. Brunel, B. Grigorov, D. Gerlier, S. Cusack, "Structural basis for the activation of innate immune pattern-recognition receptor RIG-I by viral RNA," *Cell* **147** (2011) 423 – 435. (A.N.)

Other papers in this field.

P. Liu, J. Sun, J. Zhao, X. Liu, X. Gu, J. Li, T. Xiao, L.X. Xu, "Microvascular imaging using synchrotron radiation," *J. Synchrotron Rad.* **17** (2010) 517 – 521.

S. Yue, P.D. Lee, G. Poologasundarampillai, Z. Yao, P. Rockett, A.H. Devlin, C.A. Mitchell, M.A. Konerding, J.R. Jones, "Synchrotron X-ray microtomography for assessment of bone tissue scaffolds," *J. Mater. Sci: Mater. Med.* **21** (2010) 847 – 853.

R. Serduc, E. Brauer-Krisch, E.A. Siegbahn, A. Bouchet, B. Pouyatos, R. Carron, N. Pannetier, L. Renaud, G. Berruyer, C. Nemoz, T. Brochard, C. Remy, E.L. Barbier, A. Bravin, G. Le Duc, A. Depaulis, F. Esteve, J.A. Laissue, "High-precision radiosurgical dose delivery by interlaced microbeam arrays of high-flux low-energy synchrotron x-rays," *PLoS ONE* **5**(2) (2010) e9028.

S. Gil, S. Sarun, A. Biete, Y. Prezado, M. Sabés, "Survival analysis of f98 glioma rat cells following minibeam or broad-beam synchrotron radiation therapy," *Radiat. Oncol.* **6:37** (2011) 1 – 9.

A. Momose, W. Yashiro, S. Harasse, H. Kuwabara, "Four-dimensional X-ray phase tomography with Talbot interferometry and white synchrotron radiation: Dynamic observation of a living worm," *Opt. Express* **19** (2011) 8423 – 8432.

W. Sun, Z.R. Li, Y.R. Yang, Z.C. Shi, B. Wang, B. Liu, S. Shi, "Experimental study on phase-contrast imaging with synchrotron hard X-ray for repairing osteonecrosis of the femoral head," *Orthopedics* **34**(9) (2011) e530-4.

THE USE OF SYNCHROTRON RADIATION IN MATERIALS SCIENCE (film growth, characterization of alloys, space and time resolved studies)

Techniques using lab-based and synchrotron radiation sources—a review of applications in nanoelectronics (August 2011) — Review Article. Advanced X-ray techniques are of high importance for characterization materials and devices used in nanoelectronics. A review on studies of nanoscale objects is presented by a team of

collaborating researchers from France and USA.

E. Zschech, C. Wyon, C.E. Murray, G. Schneider, "Devices, materials, and processes for nanoelectronics: Characterization with advanced x-ray techniques using lab-based and synchrotron radiation sources," *Adv. Eng. Mater.*, Special Issue: Application of Photons and Neutrons for the Innovation of Engineering Materials. (W.P.)

Usefulness of synchrotron radiation in studies of chalcopyrite and kesterite thin-film solar cell absorbers (2012, in print) — Review Article. Synchrotrons offer various analytical techniques useful in understanding the properties of solar cell absorbers. Collaborating groups from Helmholtz-Zentrum Berlin für Materialien und Energie (Germany) and from Yale University (USA) present an overview of application of these techniques for complete characterization of chalcopyrite and kesterite type absorbers.

S. Schorr, R. Mainz, H. Mönig, I. Laueremann, M. Bär, "The complex material properties of chalcopyrite and kesterite thin-film solar cell absorbers tackled by synchrotron-based analytics," *Prog. Photovoltaics: Research and Applications*, Special issue: Adventures in Cu-Chalcogenide Solar Cells (2012, in print). (W.P.)

Application of microdiffraction and microspectroscopy for nuclear material characterization (2012, in press). A team from Oak Ridge National Laboratory in US has discussed the opportunities of characterization of ultra-small nuclear-material samples (radioactive and irradiated materials) taking the advantage of high brilliance and pulsed nature of 3rd and 4th generation synchrotron radiation sources. In particular, the time-resolved measurements at these sources enable experimental studies of defect interaction and dynamics. Several examples of emerging new characterization opportunities are provided and discussed in detail.

G.E. Ice, E.D. Specht, "Microbeam, timing and signal-resolved studies of nuclear materials with synchrotron X-ray sources," *J. Nucl. Mater.* (2012, in print). (W.Sz.)

The breakdown of the direct correspondence between thermal expansion and anharmonicity in an Invar alloy (August 2011). Anomalous small thermal expansion over a wide temperature range in an iron-nickel Invar alloy with a nickel concentration of around 35% was discovered by Guillaume in 1897. The authors exploit the elemental sensitivity provided by tunable x-rays using synchrotron radiation in the Invar alloy Fe_{64.6}Ni_{35.4}. They have performed Fe and Ni K-edge extended x-ray-absorption fine-structure spectroscopic measurements and computational simulations based on the path-integral effective-classical-potential theory. The first nearest-neighbor (NN) shells around Fe show almost no thermal expansion, while those around Ni exhibit meaningful but smaller expansion than that of fcc Ni. At low temperatures, quantum

effects are found to play an essentially important role. The anharmonicity, linked with an asymmetric pair distribution function for the inter-atomic distances, clearly exists for all the first NN shells as in normal thermal expansion systems, implying the breakdown of the direct correspondence between thermal expansion and anharmonicity.

T. Yokoyama, K. Eguchi, "Anharmonicity and quantum effects in thermal expansion of an invar alloy," *Phys. Rev. Lett.* **107** (2011) 065901. (I.A.K.)

Synchrotron tomography helps improve reliability of many miniature devices (January 2012). Rapid x-ray synchrotron tomography measurements were used to resolve liquid-vapor interfacial dynamics during evaporation and condensation within submillimetric pores forming between sintered glass bead samples subjected to controlled ambient temperature and relative humidity. Spatially and temporally highly resolved observations of interfacial dynamics in grain contacts during prescribed evaporation or condensation conditions were obtained using synchrotron x-ray tomography measurements at TOMCAT beam line of the Swiss Light Source. The study provided high resolution, synchrotron-based observations of capillary evaporation-condensation dynamics at the pore scale as the confirmation of the pore scale analytical model for capillary condensation in a pore.

E. Shahraeni, D. Or, "Pore-scale evaporation-condensation dynamics resolved by synchrotron x-ray tomography," *Phys. Rev. E* **85** (2012) 016317. (P.P.)

Other papers in this field.

T. Rissom, , R. Mainz, C.A. Kaufmann, R. Caballero, V. Efimova, V. Hoffmann, H.-W. Schock, "Examination of growth kinetics of copper rich Cu(In,Ga)Se₂-films using synchrotron energy dispersive X-ray diffractometry," *Sol. Energ. Mat. Sol. C.* **95**, 1 (2011) 250 – 253 (Proc. 19th Int. Photovoltaic Science and Engineering Conference and Exhibition, PVSEC-19, Jeju, Korea, 9 – 13 November 2009).

D.R. Merrifield , V. Ramachandran, K.J. Roberts, W. Armour , D. Axford, M. Basham, T. Connolly, G. Evans, K.E. McAuley, R.L. Owen, J. Sandy, "A novel technique combining high-resolution synchrotron x-ray microtomography and x-ray diffraction for characterization of micro particulates," *Meas. Sci. Technol.* **22** (2011) 115703.

USE OF SYNCHROTRON RADIATION IN FOOD ANALYSIS

Presence of arsenic, germanium, selenium and other elements in rice grain—a review (April 2012) — Review Article. Elements such as arsenic, manganese, iron, phosphorus, germanium, and selenium are known to occur in low amounts in the rice grains. The presence of these elements may influence the human health. A team

of scientists affiliated in UK, Australia and USA presents a review of the status of knowledge on the presence and location of such elements in rice, and demonstrate the advantages of use of synchrotron radiation in such studies.

A.-M. Carey, E. Lombi, E. Donner, M.D. de Jonge, T. Punshon, B.P. Jackson, M.L. Guerinot, A.H. Price, A.A. Meharg, "A review of recent developments in the speciation and location of arsenic and selenium in rice grain," *Anal. Bioanal. Chem.* **402** (2012) 3275 – 3286. (W.P.)

Coffee beans in the synchrotron light (March 2011). Synchrotron radiation permitted to perform nondestructive 3D microtomography of green and roasted coffee beans. Effects of roasting were determined, in particular, the porosity was quantitatively determined.

P. Pittia, G. Sacchetti, L. Mancini, M. Voltolini, N. Sordini, G. Tromba, F. Zanini, "Evaluation of microstructural properties of coffee beans by synchrotron X-Ray microtomography: A methodological approach," *J. Food Sci.* **76**, 2 (2011) E222 – E231. (W.P.)

Other papers in this field.

P. Verboven, Q.T. Ho, E. Herremans, H.K. Mebatison, B. Nicolai, G. Kerckhofs, M. Wevers, P. Cloetens, "Fruit microstructure evaluation using synchrotron x-ray computed tomography," in: *Food Engineering Interfaces*, J.M. Aguilera, , R. Simpson, J. Welti-Chanes, D. Bermudez Aguirre, G. Barbosa-Canovas (Eds.), (Springer 2011) 589 – 598.

THE USE OF SYNCHROTRON RADIATION IN CULTURAL HERITAGE AND PALAEOLOGY

Synchrotron radiation used in studies of cultural heritage research (November 2011) — Review Article. The authors, experts in synchrotron radiation based studies of cultural heritage materials, review the broad field of research covering investigations of painting materials, stone, glass, ceramics, metals, cellulosic, and wooden materials as well as a clusters of organic-based materials. They present many experimental techniques, from X-ray spectroscopy and diffraction to infra-red microspectroscopy, which can be used in such studies. Fascinating examples of successful use of these methods in cultural heritage research are described in detail. L. Bertrand, L. Robinet, M. Thoury, K. Janssens, S.X. Cohen, S. Schöder, "Cultural heritage and archaeology materials studied by synchrotron spectroscopy and imaging," *Appl. Phys. A* **106** (2012) 377 – 396.

(B.J.K.)

Ancient metals under synchrotron light focuses on ancient metallic objects (February 2012) — Review Article. Archaeometallurgy joins two distant fields of science: archaeology and materials science. Marcus Young from Oregon State University presents a review of techniques and

achievements in this field, focused on the studies exploiting the synchrotron radiation via Fourier transform infrared spectroscopy and via four X-ray based techniques: imaging, diffraction, fluorescence and spectroscopy. Using more than one of these techniques to the same object is concluded to strongly increase the effectiveness of the analysis.

M.L. Young, "Archaeometallurgy using synchrotron radiation: A review," *Rep. Prog. Phys.* **75** (2012) 036504 – 1 – 15. (W.P.)

Unknown self-portrait of Rembrandt van Rijn revealed with use of synchrotron radiation (December 2011). The hidden unfinished self-portrait of Rembrandt was discovered during research into "Old Man with Beard" painted by Rembrandt around 1630. The team lead by Ernst van de Wetering (Emeritus Professor of Art History at the University of Amsterdam and head of the Rembrandt Research Project), Martin Bijl (restorer), Joris Dik (professor at the Delft University of Technology) and Koen Janssens (professor at the University of Antwerp) studied the painting at the European Synchrotron Radiation Facility (ESRF) in Grenoble (by a dual energy X-ray imaging), and at the Brookhaven National Laboratory (BNL) in New York (by Macro-scanning X-Ray Fluorescence spectrometry (MA-XRF)). The copper distribution in the lower layer of paint determined by XRF revealed a sketch of the figure with hair dress, white collar and black beret well known from many self-portraits of Rembrandt.

The Rembrandt House Museum is preparing a special exhibition devoted to XRF technique applied to research into paintings by Rembrandt (1 May – 1 July 2012). <http://www.rembrandt.ua.ac.be/>, BBC News (<http://www.bbc.co.uk/news/science-environment-15985943>). (B.J.K.)

Good-contrast visualization of fossilized embryos of extinct-species (February 2012). Structure of fossilized embryos is helpful in investigation of extinct species. Researchers from France (Grenoble, Lyon and Paris) and Bangkok (Thailand) have used the phase contrast synchrotron microtomography in order to reveal the nature of fossilized eggs discovered in Thailand. The technique is concluded to provide fine details of the fossilized objects.

V. Fernandez, E. Buffetaut, E. Maire, J. Adrien, V. Sueteethorn, P. Tafforeau, "Phase contrast synchrotron microtomography: Improving noninvasive investigations of fossil embryos *in ovo*," *Microsc. Microanal.* **18** (2012) 179 – 185. (W.P.)

MEASUREMENT METHODS

3D fluorescence-based tomography-the method and applications (a review) (June 2010) — Review Article. A team from ESRF, CEA and Joseph Fourier Univ. (all Grenoble,

France) presents the fluorescence-based tomography as a tool valuable in analysis of various 3D objects down to the micrometer scale and below. The method is described and compared to other methods of visualizing the chemical composition. Attractive examples nicely illustrate the applications of this non-destructive technique. A vision of future development is presented.

P. Bleuet, L. Lemelle, R. Tucoulou, P. Gergaud, G. Delette, P. Cloetens, J. Susini, A. Simionovici, "3D chemical imaging based on a third-generation synchrotron source," *Trends Anal. Chem.* **29** (2010) 518 – 527. (W.P.)

Focusing bright x-rays beams towards the diffraction limit (December 2011) — Review Article. This review paper describes how the field of hard x-ray spectroscopy develops to live up to the requirements of present-day science, which is extending to include samples close to applications from many areas of technology and life sciences. The new technical solutions allow for submicrometer hard x-ray beams penetrating from tens to hundreds of micrometers into samples buried in "hostile" environments. The penetrating power of the x-rays combined with their sensitivity to map trace elements and crystallographic structure permits to study materials from all scientific disciplines in a three dimensional manner.

G.E. Ice, J.D. Budai, J.W.L. Pang, "The race to X-ray microbeam and nanobeam science," *Science* **334** (2011) 1234 – 1239. (I.A.K.)

On application of single-pulse Laue technique in crystallography (September 2010). Researchers from University of Warsaw, University of New York, University of Chicago and from the SLAC National Accelerator Laboratory have studied the single-pulse pump-probe Laue technique and demonstrated its usefulness for determination of crystal structure. The accuracy and reproducibility of experiments are discussed.

R. Kamiński, T. Graber, J.B. Benedict, R. Henning, Y.-S. Chen, S. Scheins, M. Messerschmidt, P. Coppens, "Optimizing the accuracy and precision of the single-pulse Laue technique for synchrotron photocrystallography," *J. Synchrotron Rad.* **17** (2010) 479 – 485. (W.P.)

Other papers in this field.

L. Helfen, A. Myagotin, P. Mikulk, P. Pernot, A. Voropaev, M. Elyyan, M. Di Michiel, J. Baruchel, T. Baumbach, "On the implementation of computed laminography using synchrotron radiation," *Rev. Sci. Instrum.* **82** (2011) 063702.

B. Hahn and A.K. Louis, "Reconstruction in the three-dimensional parallel scanning geometry with application in synchrotron-based x-ray tomography," *Inverse Probl.* **28** (2012) 045013.

INSTRUMENTATION (detectors, monochromators, supports)

MEDIPIX3 synchrotron-radiation detector studied at a synchrotron beamline (January 2011). Scientists from UK and Switzerland have studied the problem of charge sharing in Medipix3 detector. They demonstrated, using a focused beam of linear size less than 3 micrometres, that charge-shared events are eliminated when detector operates in so called charge summing mode. This observation will lead to improvement in the resolution of this two-dimensional X-ray detector.

E.N. Gimenez, R. Ballabriga, M. Campbell, I. Horswell, X. Llopart, J. Marchal, K.J.S. Sawhney, N. Tartoni, D. Turecek, "Study of charge-sharing in MEDIPIX3 using a micro-focused synchrotron beam," *J. Instrum.* **6** (2011) C01031. (W.P.)

A universal monochromator for modern X-ray sources (February 2012). A high-resolution monochromator of good performance was constructed by collaborating researchers from Argonne National Laboratory, USA. It can be used in optics of advanced x-ray optics for synchrotrons and x-ray free-electron lasers.

S. Stoupin, Y. Shvyd'ko, D. Shu, R. Khachatryan, X. Xiao, F. DeCarlo, K. Goetze, T. Roberts, C. Roehrig, A. Deriy, "Hard x-ray monochromator with milli-electron volt bandwidth for high-resolution diffraction studies of diamond crystals," *Rev. Sci. Instrum.* **83** (2012) 023105. (W.P.)

New detectors for high-resolution soft X-ray spectroscopy at the synchrotron (June 2012). An American team developed a new type of X-ray detector array using tantalum-based superconducting tunnel junction (STJ). Tantalum has a smaller superconducting energy gap than (previously applied) niobium and thus a higher limiting energy resolution. Its high atomic number translates into increased detector quantum efficiency. The authors built also a compact, low-cost, remote-controllable preamplifier with a low electronic noise to be applied to large detector arrays.

S. Friedrich, M.H. Carpenter, O.B. Drury, W.K. Warburton, J. Harris, J. Hall, R. Cantor, "New developments in superconducting tunnel junction X-ray spectrometers for synchrotron science," *J. Low Temp. Phys.* **167** (2012) 741 – 747. (W.Sz.)

Other papers in this field.

P. Probst, A. Scheuring, M. Hofherr, D. Rall, S. Wünsch, K. Ilin, M. Siegel, A. Semenov, A. Pohl, H.-W. Hübers, V. Judin, A.-S. Müller, A. Hoehl, R. Müller, G. Ulm, "YBa₂Cu₃O₇ quasioptical detectors for fast time-domain analysis of terahertz synchrotron radiation," *Appl. Phys. Lett.* **98** (2011) 043504.

P.-A. Douissard, A. Cecilia, T. Martin, V. Chevalier, M. Couchaud, T. Baumbach, K. Dupré, M.

Kühbacher, A. Rack, "A novel epitaxially grown LSO-based thin film scintillator for micro-imaging using hard synchrotron radiation," *J. Synchrotron Radiat.* **17**(5) (2010) 571 – 583.

B. Kosciuk, V. Ravindranath, O. Singh, S. Sharma, "Development and testing of stable supports for the National Synchrotron Light Source II RF beam position monitors," *Diamond Light Source Proceedings* **1** (2011) e17.

E. Fonda, A. Rochet, M. Ribbens, L. Barthe, S. Belin, V. Briois, "The SAMBA quick-EXAFS monochromator: XAS with edge jumping," *J. Synchrotron Rad.* **19**, 3 (2012) 417 – 424.

K. Medjoubi, A. Thompson, J.-F. Béjar, J.-C. Clemens, P. Delpierre, P. Da Silva, B. Dinkespiler, R. Fourme, P. Gourhant, B. Guimaraes, S. Hustache, M. Idir, J.-P. Itié, P. Legrand, C. Meneglier, P. Mercere, F. Picca, J.-P. Samama, "Energy resolution of the CdTe-XPAD detector: Calibration and potential for Laue diffraction measurements on protein crystals," *J. Synchrotron Rad.* **19**, 3 (2012) 323 – 331.

BEAMLINES

Upgrade of the CHESS C1 beamline (August 2011). Upgrade of the CHESS C1 beamline serving for x-ray emission spectroscopy (XES) is described. The changes involve the optics, calibration, revamping analysis tools and adding a secondary X-ray source.

R. Cope, "Upgrades and developments for x-ray emission spectrography at CHESS," *CHESS report*, August 2011 (24 pages), <http://www.lepp.cornell.edu/ib38/reu/11/>. (W.P.)

Hard X-ray fluorescence/XANES microscopy at the Australian Synchrotron (September 2011). A beamline designed for hard x-ray fluorescence and XANES microscopy across an incident energy range from 4 to 25 keV is described in collaboration of scientists from the Australian Synchrotron and Brookhaven National Laboratory, Brookhaven, NY, USA. With the applied setting, ultrafast measurements are possible.

D. Paterson, M.D. de Jonge, D.L. Howard, W. Lewis, J. McKinlay, A. Starritt, M. Kusel, C.G. Ryan, R. Kirkham, G. Moorhead, D.P. Siddons, "The X-ray Fluorescence Microscopy Beamline at the Australian Synchrotron," *Proc. 10th International Conference on X-ray Microscopy, AIP Conference Proceedings* **1365** (2011) 219 – 222. (W.P.)

A research platform for cultural heritage research set up at SOLEIL (September 2011). A new research platform named IPANEMA has been set up at the French synchrotron facility SOLEIL. The platform is devoted to archaeology, cultural heritage, palaeontology and past environments research. The team of IPANEMA is going to support synchrotron projects on ancient and

historical materials and to carry out methodological research. The researchers involved in the project contributed to several related activities (like studies of pigment degradation in paintings, composition of musical instrument varnishes, and provenancing of medieval archaeological ferrous artefacts) at European synchrotrons since 2008. The methodological studies will cover advanced 2D/3D imaging, spectroscopy and statistical image analysis.

L. Bertrand, M.-A. Languille, S.X. Cohen, L. Robinet, C. Gervais, S. Leroy, D. Bernard, E. Le Pennec, W. Josse, J. Doucet, S. Schöder, “European research platform IPANEMA at the SOLEIL synchrotron for ancient and historical materials,” *J. Synchrotron Rad.* **18** (2011) 765 – 772. (B.J.K.)

New taste of spin- and angle-resolved photoelectron spectroscopy from ESPRESSO machine (October 2011). Highly efficient spin- and angle-resolved photoelectron spectrometer named ESPRESSO (Efficient SPin REsolved SpectroScopy Observation) machine has been developed at the beamline BL-9B in Hiroshima Synchrotron Radiation Center. It is one of the best experimental tools to investigate the spin structure of magnetic materials and many new materials with the spin degree of freedom for next generation electronic devices.

T. Okuda, K. Miyamaoto, H. Miyahara, K. Kuroda, A. Kimura, H. Namatame, M. Taniguchi, “Efficient spin resolved spectroscopy observation machine at Hiroshima Synchrotron Radiation Center,” *Rev. Sci. Instrum.* **82** (2011) 103302. (P.P.)

The first atomic inner-shell X-ray laser (January 2012). Scientists from USA and Germany describe the implementation of an X-ray laser in the kiloelectronvolt energy regime, based on atomic population inversion and driven by rapid *K*-shell photo-ionization using pulses from an X-ray free-electron laser. This resulted in femtosecond-duration, high-intensity X-ray pulses of much shorter wavelength and greater brilliance than achieved with previous atomic X-ray lasers. They achieved X-ray light which is a bit weaker than that of the free-electron laser, but it has a more stable wavelength, a smoother pulse profile and a shorter pulse length.

N. Rohringer, D. Ryan, R.A. London, M. Purvis, F. Albert, J. Dunn, J.D. Bozek, C. Bostedt, A. Graf, R. Hill, S.P. Hau-Riege, J.J. Rocca, “Atomic inner-shell X-ray laser at 1.46 nanometres pumped by an X-ray free-electron laser,” *Nature* **481** (2012) 488 – 491. (P.P.)

Beamline design for the National Synchrotron Light Source II, Brookhaven, USA (May 2012). A fast progress in the construction of the National Synchrotron Light Source II and in beamline design for (Brookhaven, USA). NSLS II will offer:

- at least 58 beamlines using 27 straight sections at insertion-device sources
- 31 beamlines at bending-magnet or three-pole-

wiggler sources,

- possible additional beamlines at canted insertion devices and multiple branches.

<http://www.bnl.gov/nsls2/beamlines/>. (W.P.)

Other papers in this field.

A. Somogyi, F. Polack, T. Moreno, “Nanoscopium: A scanning hard x-ray nanoprobe beamline at synchrotron SOLEIL,” *AIP Conf. Proc.* **1234** (2010) 395 – 398.

T. Graber, S. Anderson, H. Brewer, Y.-S. Chen, H.S. Cho, N. Dashdorj, R.W. Henning, I. Koshelova, G. Macha, M. Meron, R. Pahl, Z. Ren, S. Ruan, F. Schotte, V. Srajer, P.J. Viccaro, F. Westferro, P. Anfinrud, K. Moffat, “BioCARS: A synchrotron resource for time-resolved X-ray science,” *J. Synchrotron Rad.* **18** (2011) 658 – 670.

K. Martel, A. Astruc, R. Barrett, C. Henriquet, S. Huotari, G. Monaco, M. Sanchez del Rio, R. Verbeni, L. Zhang, “European synchrotron radiation facility upgrade beamline UPBL6 — inelastic scattering,” *Diamond Light Source Proceedings*, **1** (2010) e13.

Yu.A. Gaponov, Y. Cerenius, J. Nygaard, T. Ursby, K. Larsson, “Some aspects of SR beamline alignment,” *Nucl. Instrum. Methods Phys. Res. A* **649** (2011) 231 – 233.

M. Ortolani, C. Leonor A. Ricardo, A. Lausi, P. Scardi, “Thin film stress and texture analysis at the MCX synchrotron radiation beamline at ELETTRA,” *Mater. Sci. Forum* **681** (2011) 115 – 120.

C. Tarrío, S. Grantham, S.B. Hill, N.S. Faradzhev, L.J. Richter, C.S. Knurek, T.B. Lucatorto, “A synchrotron beamline for extreme-ultraviolet photolithography testing,” *Rev. Sci. Instrum.* **82** (2011) 073102.

R. Bingel-Erlenmeyer, V. Olieric, J.P. A. Grimshaw, J. Gabadinho, X. Wang, S.G. Ebner, A. Isenegger, R. Schneider, J. Schneider, W. Gletting, C. Praderwand, E.H. Panepucci, T. Tomizaki, M. Wang, C. Schulze-Briese, “SLS crystallization platform at beamline X06DA-A fully automated pipeline enabling in situ x-ray diffraction screening,” *Cryst. Growth Des.* **11**(4) (2011) 916 – 923.

F. Marone, R. Mokso, J.L. Fife, S. Irvine, P. Modregger, B.R. Pinzer, K. Mader, A. Isenegger, G. Mikuljan, M. Stampanoni, “Synchrotron-based X-ray tomographic microscopy at the Swiss Light Source for industrial applications,” *Synchrotron Radiation News* **24**, **6** (2011) 24 – 29.

R. Reininger, S.L. Hulbert, P.D. Johnson, J.T. Sadowski, D.E. Starr, O. Chubar, T. Valla, E. Vescovo, “The electron spectro-microscopy beamline at National Synchrotron Light Source II: A wide photon energy range, micro-focusing beamline for photoelectron spectro-microscopies,” *Rev. Sci. Instrum.* **83** (2012) 023102.

I. Yousef, S. Lefrancois, T. Moreno, H. Hoorani, F. Makahleh, A. Nadji, P. Dumas, "Simulation and design of an infrared beamline for SESAME (Synchrotron-Light for Experimental Science and Applications in the Middle East)," *Nucl. Instrum. Methods Phys. Res. A* **673** (2012) 73 – 81.

RADIATION SOURCES

Synchrotron ring affected by earthquake (September 2011). Photon Factory was affected by the earthquake of 11 March 2011. The resulting devastation is serious and the restoration period of about half a year appeared to be necessary.

S.S. Hasnain (ed.), "Current events," *J. Synchrotron Rad.* **18** (2011) 819 – 821. (W.P.)

On the construction of SESAME synchrotron in Jordan (March 2012). SESAME, the Middle East synchrotron situated near Amman, Jordan, is in construction. Efforts to complete the support for continuation of this international project are described by G. Brumfiel.

G. Brumfiel, "Clashing nations back SESAME," *Nature* **483** (2012) 21032012. (W.P.)

A high-brightness Compton radiation source (April 2012). In Compton scattering sources, collision of a relativistic electron bunch with an intense laser pulse leads to emission of intense radiation. A high-brightness Compton radiation source is reported by a group of researchers affiliated in France and USA. The described radiation generation method thought to lead to compact, tunable high-repetition-rate sources femtosecond, low-divergence beams.

K. Ta Phuoc, S. Corde, C. Thauray, V. Malka, A. Tafzi, J.P. Goddet, R.C. Shah, S. Sebban, A. Rousse, "All-optical Compton gamma-ray source," *Nature Photonics* **6** (2012) 308 - 311. (W.P.)

Other papers in this field.

R.P. Fliller, T. Shaftan, R. Heese, S. Kowalski, J. Rose, G. Wang, "Transverse beam stacking injection system for synchrotron light source booster synchrotrons," *Phys. Rev. ST Accel. Beams* **14** (2011) 020101.

J. Wang, K. Nasta, C.-C. Kao, "Industrial research enhancement program at the National Synchrotron Light Source," *Nucl. Instrum. Methods Phys. Res. A* **649** (2011) 19 – 21.

R. Dowd, M. Boland, G. LeBlanc, Y-R. E. Tan, "Achievement of ultralow emittance coupling in the Australian Synchrotron storage ring," *Phys. Rev. ST Accel. Beams* **14** (2011) 012804.

N. Hertel, S. Vrønning Hoffmann, "ASTRID2: A new Danish low-emittance SR source," *Synchrotron Radiation News* **24**, **1** (2011) 19 – 23.

K. Lilja, "MAX IV — New Light Source in Lund," *Synchrotron Radiation News* **24**, **4** (2011) 16 – 19.

ESRF upgrade is described in "ESRF Upgrade Programme Reaches Halfway Mark" by C. Habfast and G. Admans, this issue (page 10 of this issue).

J. Bisognano, M. Bissen, M. Green, K. Jacobs, C. Moore, E. Olson, M. Severson, R. Wehlitz, "Aladdin: Transforming science at SRC," *Nucl. Instrum. Methods Phys. Res. A* **649**, **1** (2011) 6 – 8.

C.-H. Chang, C.-S. Hwang, C.-H. Chang, H.-H. Chen, F.-Y. Lin, J.-C. Huang, C.-M. Wu, C.-Y. Wu, T.-C. Fan, K.-T. Hsu, "Construction and performance of an elliptically polarized undulator of type Apple-II," *J. Chin. Inst. Eng.* **35**, **1** (2012) 63 – 68.

NEWS AND EVENTS

Inge Lehmann Medal for Donald J. Weidner (December 2011). At the American Geophysical Union Fall Meeting (Dec. 7th 2011), professor Donald J. Weidner (Stony Brook University), working in the field of minerals under high pressure, has received the Inge Lehmann Medal. The medal is for "outstanding contributions to the understanding of the structure, composition, and dynamics of the Earth's mantle and core." In 2007, the medal recipient was Ho-Kwang Mao, working in the same field. It is worth noting that the recipient of 2009 Inge Lehmann Medal was Barbara A. Romanowicz, a Polish seismologist working in USA.

From fiction to the synchrotron ring and back (February 2012). Tania Hershman won the Light Reading flash fiction competition run by Diamond Light Source, the UK's national synchrotron. You can read her 300 word story on the Light Reading web site along with the other entries. There was also a short story contest, for stories up to 3000 words. An anthology of the winning stories will be published soon. <http://light-reading.org/LightReading/Flash-Fiction.html?return=true&id=9A8093DE-C80B-4BC2-9629-F9A7A98DA240#reading>.

Diamond Light Source Proceedings. *Diamond Light Source Proceedings* is a collection of proceedings of conferences held at the Diamond Light Source. A single volume has been published, with proceedings from the MEDSI-6 and SRMS-7 conferences (2010). The readers hope this series will be continued. <http://journals.cambridge.org/action/displayJournal?jid=DLS>.

On financing of access of Polish scientists to European synchrotrons and FELs. The European project CALIPSO resubmitted in frame of FP7 to European Commission by the European synchrotrons and free electron lasers has got financing. The details of contract are under negotiations. Maximum of funds which can be allocated for the project is 10 mln Euro for three years. The project is expected to officially start on June or July 2012. Most

of the funds will be for transnational open access to the European facilities.

At the beginning of May the Ministry of Science and High Education of Poland approved the funding of infrastructure projects. The Polish participation in ESRF is amongst the priority projects and is very likely to be financed in 2013 and onward. Nevertheless, not all formal problems are resolved up to now and the procedure for funding application will have to be obeyed. It assumes the payment of outstanding obligations of Poland for the last quarter of 2011 and for year 2012. It is possible, that on the ESRF council meeting in June 2012, the decision will be taken about invitation of Polish scientists for exper-

iments already in 2012, supposing the continuation of Polish membership in ESRF. (K.L.J.)

Prepared by:

W. Paszkowicz (W.P.)¹, W. Szuszkiewicz (W.Sz.)¹, P. Piszora (P.P.)², R. Przeniosło (R.P.)³, B.J. Kowalski (B.J.K.)¹, I.A. Kowalik (I.A.K.)¹, A. Niedźwiecka (A.N.)¹, I.N. Demchenko (I.N.D.)¹, Z. Kaszkur (Z.K.)⁴, W. Łasocha (W.Ł.)⁵, M.T. Klepka (M.T.K.)¹, Krystyna Ławniczak-Jabłońska (K.L.J.)¹.

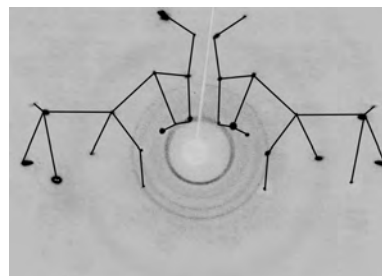
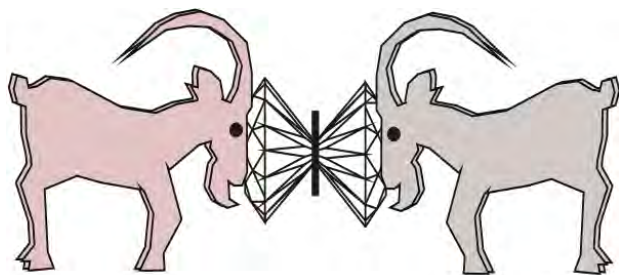
¹*Inst. Phys. PAS*, ²*Fac. Chem. A. Mickiewicz Univ.*, ³*Inst. Exp. Phys. Warsaw Univ.*, ⁴*Inst. of Physical Chemistry PAS*, ⁵*Fac. of Chemistry Jagellonian Univ.*

**ISSRNS climbs to the top:
Three proceedings papers on the *Radiation
Physics and Chemistry* Top25 list**

The Top 25 is a commonly known service providing lists of most read articles based on article downloads on SciVerse ScienceDirect: quarterly and yearly rankings (downloading statistics is not provided). The available lists include the rankings for specific journals (> 2000 journals) and for specific subjects (24 subjects). Three ISSRNS papers climbed, just after on-line publication, to the Top25 of *Radiation Physics and Chemistry* journal, all from the ISSRNS proceedings volume edited by M. Kozak, W. Paszkowicz and P. Piszora:

1. Observation of phase transformations in LiMn_2O_4 under high pressure and at high temperature by in situ X-ray diffraction measurements, by Darul J., Nowicki W., Lathe C., Piszora P., *Radiation Physics and Chemistry* **80**, 10, October 2011, 1014 – 1018, Top25 position 2 for the period July-September 2011, position 4 for the period October 2011-December 2011, position 5 for the whole year 2011.
2. Spontaneous exfoliation and self-assembly phenomena in polyvinylpyrrolidone/synthetic layered silicate nanocomposites, Zabska M., Jaskiewicz K., Kiersnowski A., Szustakiewicz K., Rathgeber S., Piglowski J., *Radiation Physics and Chemistry* **80**, 10, October 2011, 1125 – 1128, Top25 position 4 for the period July-September 2011.
3. Characterization of an Yb:LuVO₄ single crystal using X-ray topography, high-resolution X-ray diffraction, and X-ray photoelectron spectroscopy, Paszkowicz W., Romanowski P., Bak-Misiuk J., Wierzchowski W., Wieteska K., Graeff W., Iwanowski R.J., Heinonen M.H., Ermakova O., Dabkowska H., *Radiation Physics and Chemistry* **80**, 10, October 2011, 1001 – 1007, Top25 position 22 for the period July-September 2011.

This is the first time we noticed the presence of papers from any ISSRNS meeting at this list. Note that some among the authors of these papers have already been on the Top25 of other Elsevier journals. Congratulations to the authors of the cited papers, especially to those of the first one, Jolanta Darul, Waldemar Nowicki, Christian Lathe and Paweł Piszora, for keeping the high rank of their paper for a long period.



FROLIC GOATS WORKSHOPS ON HIGH PRESSURE DIFFRACTION

Frolic Goats High Pressure Diffraction Workshops (the name refers to the goats on the renaissance city hall, the symbol of Poznań) are held annually in spring at the Faculty of Chemistry, Adam Mickiewicz University. Already the 5th edition of this workshop has been organized this year. This anniversary is an opportunity to reflect on the past activities and to look ahead at future challenges.

The purpose of this conference was to encourage crystallographers to apply high pressure diffraction techniques. After the years of the workshops we noted that the main obstacle preventing scientists to start their own research into this fascinating area is the restraint from using new equipment. Therefore, we have tried to keep a balance between lectures and practical exercises in the lab. The workshop program covers the topics ranging from a comprehensive introduction into high pressure science, the principles of operation of diamond anvil cells, pressure calibration methods and data processing to the original contributions presenting the results of the high-pressure studies. The equipment and techniques related tutorials were delivered by our lab members and enriched by external speakers introducing the audience into loading diamond anvil cells with gases (Marek Tkacz, Institute of Physical Chemistry, Warsaw), solving and refining high pressure structures (Maciej Bujak, University of Opole) and high pressure powder diffraction (Armand Budzianowski, University of Warsaw). In the block of lectures on the results of high pressure investigations, our team reflected the research interests and explained how can the application of high pressure contribute to the understanding of interactions in molecular crystals. Noteworthy, the studies at the Faculty of Chemistry, Adam Mickiewicz University are currently supported by the Foundation for Polish Science TEAM Programme. The presentations by the other participants from Poland and abroad concentrated on the application of pressure to the specific subjects of chemistry and material science: electronic properties of materials (Ulrich Schwarz, Max Planck Institute, Dresden), protein crystallography (Krzysztof Lewiński and Katarzyna Kurpiewska, Jagiellonian University, Cracow), dielectric properties (Marek Szafranski and Marcin Jarek, Adam Mickiewicz University - Faculty of Physics, Poznań), super-

conductors (Armand Budzianowski, University of Warsaw), ionic conductors (Marek Daszkiewicz, Institute of Low Temperature and Structure Research, Wrocław) and photochemical reactions (Julia Bąkiewicz, Wrocław University of Technology). In order to emphasize the use of synchrotron radiation in high pressure studies the researchers from synchrotron facilities working in the beamlines dedicated to the high pressure structural investigations (David Allan from Diamond Light Source, beamline I19; Michał Dobrowolski from ESRF, beamline ID27) were invited. The lectures were followed by hands-on workshops, where the participants could adjust a diamond anvil cell, load a liquid sample and crystallize it. They were also trained in the diamond anvil cell centering procedure on a diffractometer and in running data collection. During the third part of workshops the trainees were taught to process the diffraction images, correct the reflection intensities for the specific absorption effects of diamond anvil cell, solve and refine the crystal structures. The meetings were always finished by roundtable discussions on the improvement of equipment as well as data collection and processing procedures. While during the scientific sessions the participants were kept constantly 'under pressure', they could relax during the excursions on draisines (rail vehicles) and kayaking down the Warta river.

This year, to further consolidate the community and encourage the participants of workshops to work together on a common goal a Frolic Goats Spring Project has been announced (website: <http://hpc.amu.edu.pl/fgsp>). Its aim is to carry out high-pressure experiments on a chosen sample in participants' home laboratories, write a joint paper on the results of experiments performed in different places and assess the reproducibility of high-pressure single-crystal measurements. Next year the Frolic Goats High Pressure Diffraction Workshop is tentatively planned on April 14 – 16, 2013.

CONTACT

Prof. Andrzej Katrusiak (chairman)
e-mail: katran@amu.edu.pl
website: <http://hpc.amu.edu.pl/hpd>
Faculty of Chemistry, Adam Mickiewicz University
ul. Grunwaldzka 6, 60-780 Poznań, Poland.
Tel: +48 618291443, fax: +48 618291505

JUBILEUSZOWE X KRAJOWE SYMPOZJUM UŻYTKOWNIKÓW PROMIENIOWANIA SYNCHROTRONOWEGO

W dniach 9–11.09.2013 roku w Filii Zamiejscowej KUL w Stalowej Woli odbędzie się jubileuszowe **X Krajowe Sympozjum Użytkowników Promieniowania Synchrotronowego**. W tym położonym na południowym wschodzie kraju mieście powstaje nowy kampus naukowo-dydaktyczny dla wydziałów zamiejscowych Katolickiego Uniwersytetu Lubelskiego. Powstają dwa nowe budynki — dla Instytutu Inżynierii Środowiska i dla Instytutu Inżynierii Materiałowej. Stalowa Wola to dynamiczny ośrodek ważnego regionu przemysłowego, gdzie większość zakładów przemysłowych istnieje i prosperuje, co jest zjawiskiem nieczęstym w Polsce. Rodzi się też tutaj ciekawa i ważna oś współpracy pomiędzy nauką, przemysłem i władzami samorządowymi. Warto przyjechać, zobaczyć i sprawdzić. Potencjalnie jest to też miejsce, z którego będą wywodzić się użytkownicy polskiego synchrotronu i będą przygotowywane projekty badawczo-wdrożeniowe realizowane we współpracy z przemysłem.

Tematyka:

1. Synchrotronowe źródła promieniowania
2. Spektroskopia emisyjna i absorpcyjna
3. Rozpraszanie i dyfrakcja promieniowania synchrotronowego
4. Topografia rentgenowska
5. Krystalografia białek
6. Inne techniki badawcze wykorzystujące promieniowanie synchrotronowe
7. Badania strukturalne polimerów
8. Badania materiałowe z wykorzystaniem promieniowania synchrotronowego
9. Zastosowania promieniowania synchrotronowego w badaniach medycznych i biologicznych

W trakcie Sympozjum przewidywane są sesje specjalistyczne dotyczące polskiego dorobku w zakresie optyki rentgenowskiej, wyników połączonych badań metodami dyfrakcji rentgenowskiej i absorpcji (EXAFS, XANES), oraz rezultatów badań tkanek twardych łączonymi metodami konwencjonalnymi i synchrotronowymi.

Zapraszamy

Andrzej Kuczumow
w imieniu Komitetu Organizacyjnego



Komitet Naukowy:

Dr hab. Edward Görlich (UJ)
Prof. dr hab. Krystyna Jabłońska (IF PAN)
Dr hab. Maciej Kozak, prof. nzw. (UAM)
Prof. dr hab. Andrzej Kuczumow (KUL),
przewodniczący
Prof. dr hab. Wojciech Kwiatek (IFJ PAN)
Prof. dr hab. Marek Majdan (UMCS)
Dr Jakub Nowak (KUL)
Dr hab. Wojciech Paszkowicz, prof. nzw. (IF PAN)
Dr Danuta Żymierska (IF PAN)

Komitet Organizacyjny:

Prof. dr hab. Andrzej Kuczumow (KUL),
przewodniczący
Prof. dr hab. Wojciech Kwiatek (IFJ PAN),
skarbnik
Dr hab. Wojciech Paszkowicz, prof. nzw. (IF PAN), edytor
Dr hab. Barbara Marczevska, prof. nzw. (KUL)
Dr Jakub Nowak (KUL)
Dr Sylwia Terpiłowska (KUL)
Dr Klaudia Giordano (KUL)
Mgr Dorota Nowak (KUL)

Kontakt:

Prof. Andrzej Kuczumow
Wydział Chemii
Katolicki Uniwersytet Lubelski
al. Kraśnicka 102
20-718 Lublin
kuczon@kul.lublin.pl

FUTURE CONFERENCES AND WORKSHOPS

Present and Future Methods for Biomolecular Crystallography: 45rd course of the International School of Crystallography (Erice, Italy, May 31 – June 10 2012)

<http://www.crystalalice.org/Erice2012/2012.htm>

23rd Conference on Crystal Growth and Epitaxy-CGEW12 (Fallen Leaf Lake, CA, USA, 3 – 6 June 2012)

http://www.crystalgrowth.us/accge_west23/index.php

X-FEL School 2012 (Lake Annecy, France, 4 – 8 June 2012).

<http://xfel2012.grenoble.cnrs.fr/index.php/en/>

Crystal Engineering (Waterville Valley, NH, USA, 10 – 15 June 2012)

<http://www.grc.org/programs.aspx?year=2012&program=crystaleng>

International Henry Moseley School and Workshop on X-ray Science (Turunç, Marmaris, Turkey, 14 – 23 June 2012)

http://itap-tthv.org/moseley_2012

4th European Conference on Crystal Growth — ECCG4 (Glasgow, Scotland, UK 17 – 20 June 2012)

<http://eccg4.org/>

Electron Backscattered Diffraction EBSD2012 (Pittsburgh, PA, USA 19 – 21 June 2012)

<http://www.microscopy-news.com/news/electron-backscatter-diffraction---ebsd-2012---june-19-21-2012---pittsburgh-pa.html>

2012 Gordon Conference on Research at High Pressure (Biddeford, ME, USA, June 24 – 29 2012)

<http://www.grc.org/programs.aspx?year=2012&program=highpress>

International Workshop on Radiation Imaging Detectors — iWoRID2012 (Figueira da Foz, Portugal, 1 – 5 July 2012)

<http://iworid2012.fis.uc.pt/venue.php>

54th Polish Crystallographic Meeting (Wrocław, Poland, 5 – 6 July 2012)

<http://komkryst.int.pan.wroc.pl/kk2012/kk2012.htm>

11th International Conference on Synchrotron Radiation Instrumentation — SRI2012 (Lyon, France, 9 – 13 July 2012)

<http://sri2012.org/>

Experimental and Computational Bio-Imaging and Visualization, a symposium within the 15th International Conference on Experimental Mechanics — ICEM15 (Porto, Portugal, July 22 – 27 2012)

www.fe.up.pt/clme/icem15/index.htm

Magnetic Symmetry and its Applications — MaThCryst, an ECM27 Satellite Conference (Bergen, Norway, 4 – 6 August 2012)

<http://www.crystallography.fr/mathcryst/bergen2012.php>

61st Denver X-ray Conference — DXC2012 (Denver, CO, USA, 6 – 10 August 2012)

<http://www.dxcicdd.com/>

European Crystallographic Meeting — ECM-27 (Bergen, Norway, 7 – 11 August 2012)

<http://ecm27.ecanews.org/>

2012 PSI Summer School on Condensed Matter Research (Zug, Switzerland, 11 – 17 August, 2012)

<http://www.psi.ch/summerschool>

34th International Free-Electron Laser Conference (Nara, Japan, 26 – 31 Aug 2012)

<http://fel2012.spring8.or.jp/>

American Crystallographic Association Meeting (Boston, MA, USA, 28 July – 1 August 2012)

<http://www.amercrystalassn.org/2012>

International Symposium on Zeolites and Microporous Crystals ZMPC2012 (Hiroshima, Japan , 28 July – 1 August 2012)

<http://www.zmpc.org/>

- 22nd Conference on Applied Crystallography** (Targanice/Andrychow, Poland, 2 – 6 September 2012)
<http://www.cac.us.edu.pl/>
- International Conference on Oxide Materials for Electronic Engineering — OMEE-2012** (Lviv, Ukraine, September 3 – 7 2012)
<http://www.omee.lp.edu.ua/announcements.html>
- Crystal Science: Crystal Engineering to Supramolecular Chemistry & BioCrystallography** (Waltham, USA, 5 – 6 September 2012)
<http://www.expressgenes.com>
- European Charge Density Meeting — ECDM5** (Štrbské Pleso, High Tatras, Slovakia, 15 – 20 September 2012)
<http://ecdm6.stuba.sk/>
- Neutrons and Synchrotron Radiation in Materials for Energy — HSC14 Hercules Specialised Course** (Grenoble, 17 – 21 September 2012)
<https://www.esrf.fr/misapps/workshops-web/index.jsp>
- Europaen Materials Research Society Fall Meeting — E-MRS 2012** (Warsaw, Poland, 17 – 21 September 2012)
http://www.emrs-strasbourg.com/index.php?option=com_content&task=view&id=500&Itemid=172
- IUCr Commission on High Pressure 2012 Meeting “Advances in Crystallography at High Pressures”** (Mito, Ibaraki, Japan, 23 – 27 September 2012)
<http://nsrc.jaea.go.jp/iucrhp2012/iucrhp2012.html>
- Thin film characterization with synchrotron radiation / X-rays and neutrons: Materials Science and Engineering Meeting** (Darmstadt, Germany, 25 – 27 September 2012)
<http://www.dgm.de/dgm/mse-congress/>
- European Powder Diffraction Conference — EPDIC13** (Grenoble, France, 28 – 31 October 2012)
<http://epdic13.grenoble.cnrs.fr/>
- International Small-Angle Scattering Conference — SAS2012** (Sydney Australia, November 18 – 23, 2012)
<http://www.sas2012.com/>
- MRS Symposium: Advanced Materials Exploration with Neutrons and Synchrotron X-Rays** (Boston, USA, 25 – 30 November 2012)
<http://mrs.org/f12-cfp-vv/>
- Nuclear Science Symposium and Medical Imaging 2012-IEEE NSS MIC 2012** (Anaheim, United States, 29 October – 3 November 2012)
<http://www.nss-mic.org/2012>
- Joint Meeting of the Asian Crystallographic Association, Society of Crystallographers in Australia and New Zealand and the BRAGG Symposium** (Adelaide, Australia, 2 – 6 December 2012)
<http://sapmea.asn.au/conventions/crystal2012/index.html>
- International School on Fundamental Crystallography** (Uberlândia, Brazil, 25 November – 3 December 2012)
<http://www.crystallography.fr/mathcryst/uberlandia2012.php>
- 6th Frolic Goats Workshop on High Pressure Diffraction** (Poznań, Poland, 14 – 16 April 2013)
<http://hpc.amu.edu.pl/hpd2013>
- 15th International Summer School on Crystal Growth** (Gdańsk, Poland, 6 – 10 August 2013)
<http://science24.com/event/isscg15/>
- 17th International Conference on Crystal Growth and (jointly) 15th International Conference on Vapor Growth and Epitaxy-ICCG-17 & ICVGE-15** (Warsaw, Poland, 11 – 16 August 2013)
<http://science24.com/event/iccge17/>
- 28th European Crystallographic Meeting — ECM28** (Warwick, UK, 25 – 29 August 2013)
<http://ecm28.org/>
- 10th Mational Synchrotron User Meeting (X Krajowe Jubileuszowe Sympozjum Użytkowników Promieniowania Synchrotronowego)** (Stalowa Wola, 9 – 11 September 2013).
- 23rd IUCr Congress and General Assembly** (Montreal, Canada, 5 – 12 August 2014)
<http://www.iucr2014.org/>

Conference proceedings of meetings organised by Polish Synchrotron Radiation Society (1992 – 2012)

Conference proceedings of twenty meetings organized / co-organized by Polish Synchrotron Radiation Society in the period 1992 – 2012 are listed. They include:

- | | |
|---|------------|
| • International Schools and Symposia of Synchrotron Radiation in Natural Science (ISSRNS) | 11 volumes |
| • Polish Meetings of Synchrotron Radiation Users (KSUPS) | 7 volumes |
| • other related meetings | 2 volumes |

- 1) 1st ISSRNS, Jaszowiec 13 – 21.05.1992. Eds.: K. Ławniczak-Jabłońska, G. Kowalski, **Acta Physica Polonica A**, Vol. 82, No 1 & No 2, 1992.
- 2) 2nd KSUPS, Mogilany, 1993. Ed. J. Konior, **Universitatis Jagellonicae Folia Physica**, Fasc. XXXVI, 1994.
- 3) 2nd ISSRNS, Jaszowiec 18 – 26.05.1994. Eds.: K. Ławniczak-Jabłońska, R. Iwanowski, **Acta Physica Polonica A**, Vol. 86, No 4 & 5, 1994.
- 4) **Zastosowanie promieniowania synchrotronowego**, 3rd KSUPS, Warszawa, 6 – 7.06.1995. Ed.: E. Sobczak (Fundacja im. Wojciecha Świątosławskiego, Gliwice, 1995).
- 5) 3rd ISSRNS, Jaszowiec 31.05 – 8.06.1996. Ed.: J. Konior, **Acta Physica Polonica A**, Vol. 91, No 4 & No 5, 1997.
- 6) **Application of Synchrotron Radiation to the Study of Inorganic and Biological Materials**, 4th KSUPS, Kraków-Przegorzaly, 18 – 19.06.1997. Ed.: J. Grochowski, **Universitatis Jagellonicae Folia Physica**, Fasc. XXXIX, 1998.
- 7) 4th ISSRNS, Ustroń-Jaszowiec, 15 – 20.06.1998. Eds.: W. Paszkowicz, E. Sobczak, **Journal of Alloys and Compounds**, Vol. 286, No 1–2, 1999.
- 8) **Synchrotron Radiation Studies of Materials**, 5th KSUPS, Warszawa, 31.05 – 1.06.1999. Eds.: M. Lefeld-Sosnowska, J. Gronkowski, (Institute of Experimental Physics, University of Warsaw, Warsaw 1999).
- 9) 5th ISSRNS, Ustroń-Jaszowiec, 12 – 17.06.2000. Eds.: Cz. Kapusta, W.M. Kwiatek, J. Konior, M. Stankiewicz, **Journal of Alloys and Compounds**, Vol. 328, No 1–2, 2001.
- 10) **Synchrotron Crystallography - from Source to Applications**, Synchrotron Crystallography (SYNCRYS) 2001, Krynica-Czarny Potok, 31.08 – 4.09.2001. Ed.: J. Grochowski in collaboration with W. Paszkowicz, **Acta Physica Polonica A**, Vol. 101, No 5, 2002.
- 11) 6th ISSRNS, Ustroń-Jaszowiec, 17 – 22.06.2002. Eds.: W. Paszkowicz, A. Burian, J. Gronkowski, B.J. Kowalski, **Journal of Alloys and Compounds**, Vol. 362, No 1–2 (2004).
- 12) **Development of Methods for Characterizing the Microstructure of Novel Materials**, European Materials Research Society Fall Meeting, Symposium B, 15 – 19.09.2003, Warsaw. Eds.: W. Paszkowicz, J. Pełka, **Journal of Alloys and Compounds**, Vol. 382, No 1–2, 2004.
- 13) 7th ISSRNS, Zakopane 8 – 13.06.2004. Eds.: W. Paszkowicz, B.J. Kowalski, E.A. Görlich, Z. Kaszukur, **Journal of Alloys and Compounds**, Vol. 401, No 1–2, 2005.
- 14) 8th ISSRNS, Zakopane 8 – 13.06.2006. Ed.: W. Paszkowicz, **Synchrotron Radiation in Natural Science**, Vol. 5 No 3, 2006.
- 15) 7th KSUPS, Poznań, 24 – 36.09.2007. Eds.: M. Kozak, W. Paszkowicz, **Acta Physica Polonica A**, Vol. 115 No. 2, 2008.
- 16) 9th ISSRNS, Ameliówka 15 – 20.06.2008. Eds.: W. Paszkowicz, B.J. Kowalski, E.A. Görlich, **Radiation Physics and Chemistry**, Vol. 78, Suppl. 10, 2009.
- 17) 8th KSUPS, Podlesice 24 – 26.09.2009. Eds.: W. Paszkowicz, M. Sikora, W. Szuszkiewicz, **Acta Physica Polonica A**, Vol. 117 No 1–2, 2010.
- 18) 10th ISSRNS, Szklarska Poręba 6 – 11.06.2010. Eds.: M. Kozak, P. Piszora, Z. Kaszukur, **Radiation Physics and Chemistry**, Vol. 80 No 10, 2011.
- 19) 9th KSUPS, Warszawa 25 – 27.09.2011. Eds.: Z. Kaszukur, W. Paszkowicz, **Acta Physica Polonica A**, Vol. 121 No 4, 2012.
- 20) 11th ISSRNS, Kraków, 20 – 25.05.2012. Proceedings to be published in **Radiation Physics and Chemistry**.

Authors Index

- Adachi S., 113
 Adamek D., 147, 148
 Ahlback J., 1
 Al-dmour E., 1, 152
 Aleshkevych P., 97
 Alhback J., 152
 Alonso Mori R., 42
 Andersson A., 1
 Andrejczuk A., 88
 Aoyama M., 46
 Appel K., 31, 76
 Arvanitis D., 108
- Bacewicz R., 130
 Baczewski L.T., 115
 Bajt S., 143
 Balcer T., 105, 157
 Balerna A., 65
 Balin K., 80
 Ballauff M., 144
 Banaś A.M. 65, 82
 Banaś D., 78, 81, 100, 110
 Banas K., 82
 Baranowska-Korczyk A., 53, 83
 Barnabas A., 116, 117
 Bartnik A., 51, 53, 107
 Bartosik M.R., 84
 Bähz C., 119
 Bąk-Misiuk J., 128, 139
 Beckers D., 45
 Bell A.M.T., 118
 Berglund M., 152
 Bergmann U., 42
 Berkowski M., 128
 Bialas M., 94
 Bielecki J., 86
 Biernacka K., 87, 140
 Bikowski A., 160
 Birarda G., 112
 Błaszczak Z., 74, 92, 93, 138
 Bocchetta C.J., 1, 48, 72, 84, 152
 Bokhoven Van J.A., 149
 Bordage A., 42
 Borysiewicz M.A., 111
 Brůža P., 53
 Brancewicz M., 88
 Braziewicz J., 81, 110
 Breese M.B.H., 82
 Bressler C., 42
 Briois V., 117
 Brudnik A., 87
 Brunelli M., 132
 Bukowski M., 153
 Burian T., 105, 143
- Caliebe W., 96, 97
 Cammarata M., 42
 Canton S., 42
 Celinski Z., 80
 Chalupský J., 105, 143
 Chapman H.N., 143
 Chernyshova M., 90
 Chołuj-Dziewiecka O., 133
 Chwiej J., 31, 36
 Cinque G., 65
 Connell S.H., 56
 Coppola N., 143
 Cramm S., 24
 Czapla J., 32
 Czech K., 81
 Czyżycki M., 147
- Dararutana P., 75
 Darul J., 137
- Dąbkowska H., 99, 128
 Dąbrowski K.M., 89
 Della Corte V., 54
 Della Ventura G., 54
 Demchenko I.N., 90, 163
 Denlinger J.D., 90
 Dietler G., 44
 Dittmann R., 71
 Dłużewski P., 83, 143
 Dobrzyński L., 88
 Domagała J.Z., 96, 128
 Doumy G., 42
 Dousse J.-Cl., 78, 100, 149
 Dowierciał A., 91, 101
 Driel van T., 42
 Drozdowski H., 74, 92, 93, 138
 Drube W., 124
 Dudala J., 94
 Dulińska J., 32
 Dul D.T., 89, 95
 Dumas P., 28, 36, 76, 116
 Dunford R., 42
 Dušek M., 47
 Dynowska E., 96, 97, 118, 139
 Dziawa P., 124, 139
 Dziedzic-Kocurek K., 98
- Echevarria G., 117
 Einfeld D., 1, 152
 Elbaum D., 53, 83
 Ellmer K., 160
 Eriksson M., 1, 152
 Ermakova O.N., 99, 128
- Fadley C.S., 61
 Farahani S.D., 143
 Fassbender J., 115
 Fedotova J., 68
 Fernández-Pacheco A., 67
 Fernandes Tavares P., 1, 152
 Ferrari M., 54
 Feyer V., 24
 Fiedorowicz H., 51, 53, 107
 Fitch A., 132, 153
 Frączyk T., 91
 Fransen M., 45
 Fritz D., 42
 Fronc K., 83
- Gaffney K., 42
 Gajda M., 76, 82
 Galasso G., 143
 Galler A., 42
 Gallo E., 42
 Garnuszek M., 81
 Gas K., 124
 Gateshki M., 45
 Gaudin J., 105, 143
 Gawelda W., 42
 George G.N., 29
 Gieraltowska S., 69
 Gilski M., 34
 Giordano C., 146
 Glatzel P., 42
 Gleeson A.J., 105
 Gładczuk W., 97
 Głowacki M., 128
 Godlewski M., 69, 108, 188
 Goraus J., 65, 162
 Goryczka T., 162
 Goryl P., 1, 72, 84
 Gottlob D., 24
 Göttlicher J., 32
 Graule Th., 140
 Grilli A., 65
 Gritzner G., 161
- Groeber S., 117
 Groot de J., 99
 Grubb A., 73, 120
 Guillon F., 116
 Guziejewicz E., 69, 108, 188
 Gzielo-Jurek K., 31
- Haldrup K., 42
 Hara T., 46
 Harmand M., 143
 Hałas T., 92
 Härtwig J., 56
 Hájková V., 105, 143
 Hempelmann R., 153
 Hofmann A., 57
 Hoshino M., 113
 Hoszowska J., 78, 100, 149
- Ibarra M.R., 67
 Ishikawa T., 46
 Itou M., 88
 Iwasaki A., 46
- Jagodziński P., 78, 100
 Jamme F., 116
 Janeczko K., 31, 36
 Janik E., 96
 Janousch M., 149
 Jarmuła A., 91, 101
 Jarocki R., 51, 53
 Jaskólski M., 5
 Jendrzewska I., 162
 Jeżabek M., 38
 Johansson M., 1, 102
 Johnson R.L., 69, 106
 Juha L., 105, 143
 Jurek M., 143
- Kaganer V.M., 50
 Kaiser J., 144
 Kajewski D., 71
 Kanter E., 42
 Kapusta Cz., 67, 68, 87, 140, 161
 Kasiuk J., 68
 Kaszukur Z., 103, 163
 Katrusiak A., 178
 Kaupner A., 146
 Kayser Y., 78, 100
 Kharchenko A., 45
 Kida W., 104
 Kierdaszuk B., 101
 Kiesel A., 65
 Kjaer K., 42
 Klepka M.T., 60, 111, 143, 159, 163
 Klymenov E., 149
 Klinger D., 105, 143, 157
 Knapp M., 119, 130
 Knoff W., 106
 Konior J., 65
 Kopalko K., 188
 Korbas M., 29
 Korczyk B., 107
 Korecki P., 89, 95
 Kostecki J., 51, 53, 107
 Kowalik I.A., 69, 108, 163
 Kowalik M., 151
 Kowalska J., 76
 Kowalski B.J., 69, 109, 163
 Kozak M., 5, 35, 73, 104, 114, 120–122,
 134–136
 Kołodziejczyk A., 151, 161
 Köhl A., 71
 Królas K., 1
 Kręcisz M., 134
 Krone P.H., 29
 Krug I.P., 24

- Krzysztoń R., 135
 Krzywinski J., 143
 Kubacki J., 71
 Kubala-Kukuś A., 78, 81, 100, 110
 Kuczumow A., 179
 Kumbaro D., 1
 Kurant Z., 115
 Kutorasinska J., 31, 36
 Kwiatek W.M., 32, 76, 82, 86, 112, 126, 154
- Lankosz M., 94, 147
 Lathe C., 99
 Lawniczak-Jablonska K., 60, 111, 159, 163
 Leeman S.C., 1
 Lefeld-Sosnowska M., 155
 Lekki J., 32, 112, 154
 Lemke H., 42
 Lenser Ch., 71
 Liedke M.O., 115
 Lindström V., 73
 Lipiec E., 86, 112, 154
 Loch R., 143
 Lorkiewicz J., 133
 Ludwikowska-Kędzia M., 110
 Lukaszewicz M.I., 108
 Lukaszewicz T., 155
 Luque F., 108
 Lusakowska E., 105
- Lasocha W., 163
 Lukaszewicz M.I., 188
- Mabied A.F., 113
 MacDonald T.C., 29
 Majewska U., 81, 110
 Malinowska A., 155
 Malmgren L., 1
 Małachowski M., 114
 Małecki P.H., 27
 Marcelli A., 54
 March A.M., 42
 Masiello F., 56
 Matsubara S., 46
 Mazalski P., 115
 Maziewski A., 115
 Mesjasz-Przybyłowicz J., 116, 117
 Michalow-Mauke K., 140
 Midorikawa K., 46
 Minikayev R., 90, 99, 118, 119, 130, 132
 Misiuk A., 139
 Młynarczyk M., 1
 Modeer J., 1
 Montargès-Pelletier E., 117
 Mölle S., 143
 Mucha-Kruczyńska I., 136
 Murawska M., 73, 120–122
 Müller S., 97
 Mydlarz T., 162
- Nachtegaal M., 149
 Nagasono M., 143
 Nasr A., 123
 Nickel F., 24
 Niedźwiecka A., 163
 Nielsen M.M., 42
 Nietubyc R., 40, 102, 109, 133, 142
 Nijenhuis te H., 45
 Nino M.A., 108
 Novikov D.V., 89
 Nowakowski P., 122
 Nowak S., 78, 100
 Nozawa S., 113
- Ohshima T., 46
- Olko P., 38
 Orłowski B.A., 69, 106, 124
 Otake Y., 46
 Owada S., 46
 Oyanagi H., 55
 Özkan C., 143
- Pace E., 54
 Pajek M., 78, 81, 100, 110
 Paluszkiewicz C., 126
 Pasquaud J., 152
 Paszkowicz W., I, 97, 99, 119, 128, 130, 132, 163
 Pattanasiriwisana W., 75
 Patt M., 24
 Paulmann C., 128, 157
 Paulmann T., 155
 Pawlicki B., 82
 Pánek D., 53
 Pełka J.B., 40, 83, 105, 133, 142, 157
 Petříček V., 47, 141
 Pettenkofer C., 57
 Pickering I.J., 29
 Pietralik Z., 35, 134–136
 Pietrzyk M.A., 106
 Piszora P., 119, 130, 132, 137, 163
 Podsiadlo S., 119
 Przeniosło R., 141, 153, 163
 Przewoźnik J., 68
 Przybyłowicz W., 116
- Radecka M., 87
 Radtke M., 144–146
 Radwanska E., 147, 148
 Ray D., 42
 Reinholz U., 144–146
 Rekas M., 140
 Reszka A., 69, 106, 124
 Riesemeier H., 144–146
 Rietmeijer F. J. M., 54
 Rode W., 91, 101
 Rogalev A., 64, 115
 Romaniuk A., 74, 93, 138
 Romanowski P., 96, 139
 Ronning C., 97
 Rotundi A., 54
 Rudolf P., 49
 Rypniewski W.R., 5, 27, 91, 101
- Sa J., 149
 Sadowski J., 109
 Safonova O.V., 149
 Sako T., 75
 Sakurai Y., 88
 Salomé M., 78
 Sandt Ch., 36, 116
 Saskl K., 143
 Sato T., 46, 113
 Sás N., 42
 Schenk H.W., 123
 Schneider C.M., 24
 Schneider K., 140
 Schulte K., 71
 Schulz J., 143
 Sechogela P., 116, 117
 Sekutowicz J., 40, 133, 142
 Serrano-Ramón L.E., 67
 Sessi V., 60, 159
 Setkowicz Z., 31, 36
 Sikora M., 63, 68, 87, 140
 Simon R., 31
 Sinn H., 143
 Skrzypczak A., 121, 122
 Sławiński W., 141
 Słomkiewicz P., 81
 Smolarek K., 121
- Smolentsev G., 42
 Sobczak K., 83, 139
 Sobierajski R., 40, 105, 133, 142, 143, 157
 Sosnowska I., 141
 Southworth S., 42
 Sova P., 143
 Speaks D., 90
 Spruce D., 72
 Stanek J., 98
 Stankiewicz M.J., I, 1, 37, 72, 84, 152
 Starowicz P., 65
 Steininger R., 32
 Stępień J., 140, 161
 Stodolak E., 126
 Story T., 106, 118
 Sudra H., 161
 Sundström V., 42
 Susini J., 78
 Swirkowicz M., 155
 Sylvain N.J., 29
 Szade J., 71, 80
 Szczepańska A., 139
 Szczepanik B., 81
 Szczërba W., 144–146
 Szczerbakowa A., 118, 124
 Szczerbowska-Boruchowska M., 94, 147, 148
 Szczurek M., 51, 53
 Szewiński J., 133
 Szukdlarek A., 67
 Szlachetko J., 78, 100, 149
 Szot K., 71
 Szuszkiewicz W., 97, 118, 163
 Szutkowski K., 122
 Szytuła A., 65
- Ślusarczyk Cz., 150
- Takahashi E.J., 46
 Tanaka H., 46
 Tanaka T., 46
 Tancharakorn S., 75
 Taniguchi M., 58
 Taube M., 73
 Teresa De J.M., 67
 Thiess S., 124
 Thorin J., 1
 Thünemann A.F., 144–146
 Tiedtke K., 105, 143
 Togashi T., 46
 Tokarz W., 151
 Toilekis S., 105, 143
 Tolkiehn M., 89
 Tomita A., 113
 Tomizawa H., 41, 46
 Tracz P., 1, 84
 Trots D., 118, 130
 Tschentscher T., 143
 Tyliczszak T., 67, 90
- Uhlig J., 42
 Uram L., 31
- Vaccari L., 112
 Vankó G., 42
 Vinnichenko M., 160
 Vital A., 140
 Vorgias C.V., 27
 Vyšín L., 105, 143
- Wabnitz H., 105
 Wachnicki L., 69, 188
 Wachulak P.W., 51, 53
 Walczak L., 1, 84, 152
 Walenta A.H., 123

Walukiewicz W., 90
 Wandzilak A., 147
 Wardecki D., 153
 Wasiewicz T., 133
 Watanabe T., 46
 Wawro A., 115
 Wawrzyniak A.I., 1, 72, 84, 102
 Wawrzyniak K., 72, 84
 Werthenbach U., 123
 Węgrzyński L., 53
 Wiatr M., 122
 Widel M., 154
 Wiecheć A., 112, 154
 Wiechecki J., 84
 Wiemann C., 24
 Wierzchowski W., 128, 155, 157
 Wieteska K., 105, 128, 155, 157
 Wilhelm F., 64, 115
 Wilk P., 91, 101
 Woch W.M., 161
 Wojnar P., 96
 Wolska A., 60, 111, 159
 Won-in K., 75
 Wrobel P., 147, 148
 Wrochna G., 40, 133, 142
 Wudarczyk-Moćko J., 81, 110
 Wu Z., 54

Yabashi M., 46
 Yamakawa K., 46
 Yamanouchi K., 46
 Young L., 42
 Yousef I., 116
 Yu K.M., 90
 Yu L., 144

Zając D.A., 140, 160, 161
 Zając M., 72, 84
 Zajdel P., 65, 162
 Zakharov A., 108
 Zakrzewska K., 87, 140
 Zalecki R., 151
 Zhang K., 54
 Ziaja-Motyka B., 33
 Zymirska D., 157

Żukowski E., 88
 Żukrowski J., 68
 Żymierska D., 105
 Żytniak Ł., 72, 84

Subject Index

- 1,3,5-trichlorobenzene, 92
 4th generation sources, 40, 133, 142
 II-VI compounds, 96
- ab-initio, 86
 amyloid, 73
 ancient Thai burnt rice, 75
 angular intensity distributions, 138
 annealing, 139
 asteraceae, 116, 117
 atherosclerosis, 76
 atomic force microscope, 44
 atomic resolution structures, 34
 atomic structure, 95
 atomic structure determination, 89
 ATR-FTIR, 136
 Au nanoparticles, 121, 122
- beam line, 5
Berkheya coddii, 117
 binary solution, 74, 138
 biochemical analysis, 94
 BioSAXS, 120
 bone defect, 126
 brain gliomas, 147
 bulk modulus, 99
- cadmium telluride, 69
 calcium, 76
 calcium barium niobate, 155
 calibration standards, 78
 cancer, 38
 censoring, 78
 chemotaxonomy, 116
 chitinase, 27
 chloroanisoles, 93
 circular polarization, 64
 cobalt, 97, 188
 Compton profile, 88
 Compton scattering, 88
 control, 72
 copper, 76
 creatine, 36
 crystalline structure, 124
 crystallite growth, 153
 crystallization, 150
 CuInSe₂, 130
 curve fitting, 136
 cystatin, 73
 cytology, 116
- defect structure, 128, 155
 deformation fields, 157
 density functional theory, 151
 density of states, 151
 DFT, 86
 diffraction topography, 155
 diluted magnetic semiconductors, 109
 dislocations, 50
 DNA, 44, 86
 DNA damage, 112
 double strand breaks, 154
 adrenal gland tumors, 94
 DSC, 134, 135
 DU-145, 112
- electronic structure, 63, 124
 electrospinning, 83
 elemental microimaging, 148
 emini surfactants, 35
 enzyme-ligand-cofactor complex, 101
 epilepsy, 36
 epitaxy, 50
 equation of state, 99
- europium valency, 80
 EXAFS, 111, 117, 144, 146
 external total reflection, 100
 extreme ultraviolet radiation, 46, 51, 53, 107
- ferromagnetic precipitates, 159
 ferromagnetism, 139
 films, 50
 FLASH irradiation, 157
 fluorescence spectroscopy, 82
 free electron laser, 40, 46, 133, 142, 143
 Fresnel zone plates, 53
 FSD, 136
 FTIR, 104, 134, 135
 FTIR microspectroscopy, 112
 FTIR spectroscopy, 136
- gallium nitride, 69, 119
 gemini surfactants, 104, 121, 122, 134, 135
 gene therapy, 35
 geochemical composition, 110
 GEXRF, 78
 gold, 144
 granular materials, 60
- halloysite samples, 81
 high electron mobility transistors, 111
 high temperature, 118
 high-density polyethylene, 150
 high-order harmonics, 46
 high-resolution ARPES, 58
 hot plasma, 51
 human cystatin C, 120
 hydrogen, 87
 hyperaccumulation, 117
- implantation, 97
 inelastic scattering, 88
 infrared microspectroscopy, 94, 116
 inhibitor, 101
 instrumentation, 72
 intermetallic alloys, 80
 intermolecular interactions, 74
 internal ordering degree, 92
 iron, 76
 iron carbide, 146
 irradiation, 115
- lattice parameter, 119, 130, 132
 linac, 102
 lithium-manganese oxides, 137
 low temperature, 118
- macromolecular crystallography, 27
 magnetic lattice, 102
 magnetic moments, 60
 magnetic nanoconstriction, 67
 magnetism, 64
 magnetooptics, 115
 magnetoresistive double perovskites, 63
 materials science, 5
 MAX phases, 111
 MBE, 96
 metallisations, 111
 metallopolymers, 145
 Mg, 88
 micro SRF-TIR, 76
 micro x-ray fluorescence analysis, 78
 micro-PIXE, 117
 micro-XRF, 76
 microfluidics, 55
 micromagnetic simulations, 67
 microscopy, 53
- microspectroscopy, 117
 microstrain fluctuations, 153
 Mn₄Si₇, 139
 modulated crystals, 47
 molecular function of structure, 93
 molecular structure, 92
 Monte-Carlo simulations, 100
 multilayered packing materials, 114
 multivariate analysis, 82
- nanoalloy, 144
 nanocrystal, 55
 nanocrystalline chromium, 153
 nanocrystalline materials, 45
 nanogranular composite films, 68
 nanoimaging, 53
 nanoinclusions, 139
 nanomaterials, 140
 nanoparticles, 144, 146
 nanowires, 96
 nickel hyperaccumulation, 116
- orthovanadate, 128
- pair distribution function, 45
 palladium, 144
 parasitic nematode, 91
 PEEM, 108
 perovskite, 151
 phase change material, 106
 phospholipids, 104, 134, 135
 phospholipids saturation level, 76
 phosphorus, 76
 photodimerization, 113
 photoelectrolysis, 87
 photoelectron spectroscopy, 71, 109
 photoemission microscopy, 24
 photoemission spectroscopy, 124, 188
 photoionization, 51
 pilocarpine model of epilepsy, 31
 polyamide, 114
 polycapillary optics, 89
 polyethylene, 114
 polymer crystallisation, 114
 polymer physics, 44
 polymer surface modification, 107
 polymer-ceramic nanocomposites, 126
 porphyrins, 98
 powder diffraction, 5, 113
 program Jana2006, 47
 prostate cancer, 32
 protein crystallography, 5
 protein secondary structure, 76
 protein structure, 136
 proton microbeam, 154
 proton radiotherapy, 38
 psychrophile, 27
- R platform, 82
 rare earth, 65, 128
 rare-earth orthovanadates, 99
 Rashba system, 58
 ray-tracing, 100
 relaxation, 50
 reversible valency transitions, 80
 rhenium compounds, 63
 Rietveld refinement, 137
 RIXS, 63
 root, 116
 RXES, 63
- samarium, 69
 SAXS, 5, 134, 145, 150
 scanning transmission X-ray microscopy (STXM), 67
 selective inhibitor, 91

- SEM-EDS, 75
 semiconductor, 106
 semimagnetic semiconductors, 69, 188
Senecio coronatus, 116, 117
 senile brains, 148
 Si:Mn, 139
 silicides, 65
 silicon, 157
 single cell irradiation, 112, 154
 single crystal, 128
 small cluster, 55
 small-angle X-ray scattering, 5
 soft x-rays, 108
 software, 72
 solar cells, 160
 Solaris project, 5, 72, 84
 speciation, nickel, 117
 spectromicroscopy, 24
 spin structure, 58
 spinels, 162
 spintronics, 60, 159
 SR FTIR microspectroscopy, 36
 SR-FTIR, 86, 126
 SRXRF, 75
 storage ring, 102
 strontium barium niobate, 155
 structural biology, 5
 structural dynamics, 42
 structure analysis, 47
 structure refinement, 118
 substantia nigra, 148
 sulphur, 32
 SVD, 113
 synchrotron, 5, 84
 synchrotron radiation, 5, 24, 27, 31,
 34, 36, 55, 57, 69, 71–73, 82,
 84, 86, 88, 90, 91, 96–101,
 106, 108, 109, 113, 115–118,
 123, 124, 139, 143, 147, 148,
 152–154, 161, 188
- TEM, 139
 thallium superconductors, 161
 thermal expansion, 118, 119, 130, 132
 thin films, 71, 80
 thymidylate synthase, 91, 101
 THz sources, 40, 133, 142
 till samples, 110
 time-resolved, 42, 113
 titanium dioxide, 87, 140
 topographic and quantitative elemen-
 tal analysis, 31
 topological insulator, 58
 transparent conductive oxides, 160
Trichinella spiralis, 91
 tuneable synchrotron radiation, 5
 tunnel magnetoresistance, 68
 TXRF, 78
- ultrafast, 42
 ultramafic soil, 116, 117
 ultraviolet photoemission, 151
 unconventional superconductor, 58
- vacuum system, 152
 van der Waals atomic radii, 93
- wavelet transform, 95
- X-ray absorption, 71, 89, 90
 X-ray absorption anisotropy, 95
 X-ray absorption near edge structure
 spectroscopy, 147
 X-ray absorption spectroscopy, 55, 68,
 149, 160
 X-ray crystallography, 34
 X-ray diffraction, 45, 96, 97, 132, 137,
 139
 X-ray diffraction in liquid solutions, 74
 X-ray diffraction patterns, 138
 X-ray emission, 90
 X-ray emission spectroscopy, 149
 X-ray fluorescence, 81, 110, 117, 147,
 148
 X-ray fluorescence microscopy, 31
 X-ray Free Electron Laser, 41
 X-ray microanalysis, 116
 X-ray polycapillary optics, 100
 X-ray powder diffraction, 81, 110
 X-ray spectroscopy, 64
 X-ray topography, 128, 157
 XAFS, 145
 XANES, 32, 87, 98, 117
 XAS, 65, 108, 162
 XAS spectroscopy, 140
 XES, 87
 XMCD, 60, 159, 108
 XRF, 82
- zinc, 76
 zinc oxide, 69, 160, 188
 ZnFeO, 83
 ZnMgO, 160
 ZnO, 97, 160
 ZnO nanofibers, 83

Co 3d STATES IN FERROMAGNETIC AND PARAMAGNETIC (Zn, Co)O FILMS – RESONANT PHOTOEMISSION STUDIES

E. Guzewicz*, M.I. Łukasiewicz, K. Kopalko, L. Wachnicki, M. Godlewski

Institute of Physics, Polish Academy of Sciences, Al. Lotnikow 32/46, 02-668 Warsaw, Poland

Keywords: synchrotron radiation, photoemission spectroscopy, zinc oxide, cobalt, semimagnetic semiconductors

*e-mail: guzel@ifpan.edu.pl

Zinc oxide with cobalt has been recently intensively studied for prospective spintronic applications. This is because high cobalt concentrations in ZnO matrix is expected due to the nearly identical Co^{2+} and Zn^{2+} ionic radii. Ferromagnetic ordering in ZnCoO films has been found and reported by several groups, but the origin of the ferromagnetism is still not fully clear. It has been related to formation of foreign phases, defects in the ZnO lattice, and Co metal precipitations inside the ZnCoO layer.

In this paper we present resonant photoemission results for a series of ferromagnetic and paramagnetic ZnCoO samples grown by the Atomic Layer Deposition (ALD) technique. The extensive structure characterization show that the films are polycrystalline and do not have any precipitations of cobalt oxides. In case of paramagnetic samples XANES and EXAFS studies indicate that most of Co^{2+} ions replace Zn^{2+} ions in the ZnO lattice, whereas in ferromagnetic layer about 20% of Co atoms are outside the substitutional positions and

form kind of metallic Co clusters [1]. It has been found that a ferromagnetic behavior is mostly related to the Co-rich layer at the ZnCoO/Si interface [1, 2]. In addition to the ferromagnetic signal, particularly well visible in thin FM samples, in all layers grown at high temperature (above 160°C) a superparamagnetic response has been observed. Based on the XPS profiling experiment this magnetization component has been assigned to metallic Co-rich nanoparticles that disperse over the film volume [1]. However, similar signal from Co-rich metallic inclusions has been observed for paramagnetic ZnCoO layers.

In the present study we investigated the Co3d contribution to the valence band electronic structure of a series of ZnCoO samples with various magnetic response. The Resonant Photoemission (RESPES) studies were directed to evaluate the Co3d contribution to the valence band of a series of ZnCoO films. The experiment was performed at the I3 beamline at the MAX III storage ring at MAXlab,

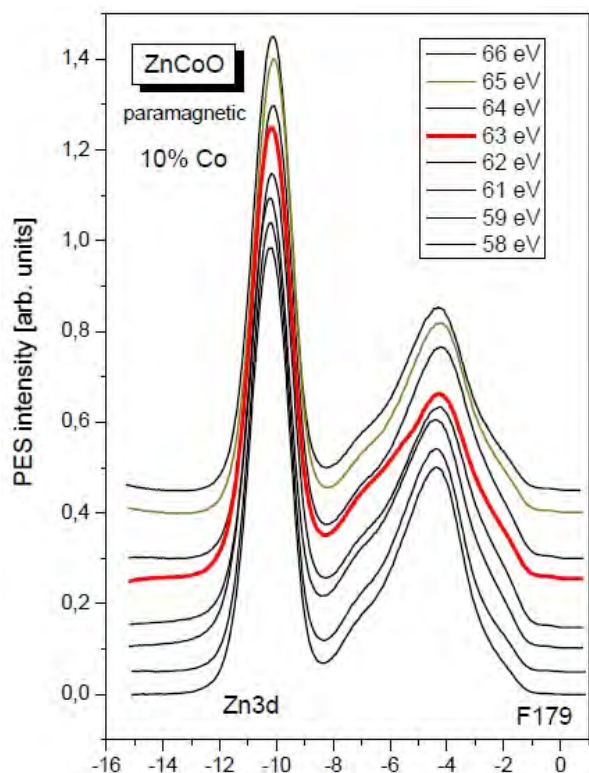


Figure 1: EDC spectra of the paramagnetic ZnCoO film with 10% of Co. The spectra were taken across the $\text{Co}3p\text{-Co}3d$ resonance.

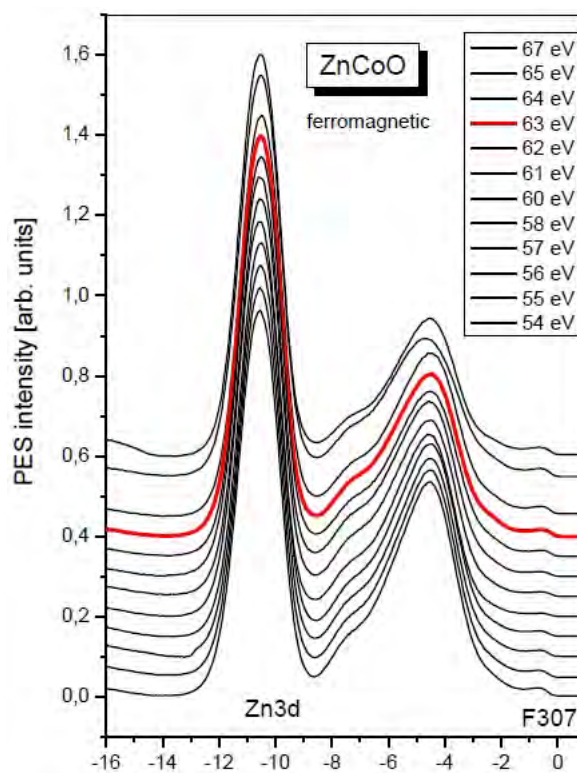
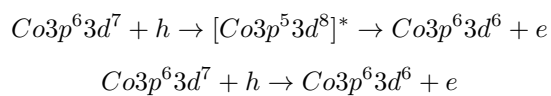


Figure 2: EDC spectra of the ferromagnetic ZnCoO film with 6% of Co. The spectra were taken across the $\text{Co}3p\text{-Co}3d$ resonance.

Sweden. Before the RESPES experiment each ZnCoO/Si film was cleaned in the same way under a ultra-high vacuum condition ($p \sim 4 * 10^{-10}$ Torr) using argon ions bombardment ($U = 600$ V, $p(\text{Ar}) = 5 * 10^{-6}$ Tr, 40 minutes) and annealing to 200°C (2h).

Photoemission spectra were recorded in the binding energy (BE) range between the Fermi level and 15 eV below. This BE region covers the ZnCoO valence band and the Zn3d core level. The overall resolution was evaluated as 200 meV at 50 eV photon energy.

RESPES experiment is an effective tool for identification of the Co3d contribution to the valence band electronic structure of the host ZnO material. The resonant photoemission process is a result of interference between two photoemission paths that can be expressed as follows:



As a result we observe an increase of photoemission intensity when photon energy is tuned to the Co3p \rightarrow Co3d photo-ionization threshold.

We investigated a series of paramagnetic and ferromagnetic ZnCoO samples. In Fig. 1 and Fig. 2 we present representative examples of photoemission spectra taken across the Co3p \rightarrow Co3d photoionization threshold. It was observed that Energy Distribution Curves (EDCs) of paramagnetic and ferromagnetic ZnCoO films differ considerably,

which indicate different Co3d states in ZnCoO layers showing different magnetic behavior. For paramagnetic sample we found clear contributions of the Co3d states at BE 2 eV and 7 eV below the Fermi level. Paramagnetic films show the RESPES enhancement in the region between 5 eV and 7 eV below the Fermi level. We observed that resonant enhancement of photoemission intensity does not scale with the cobalt content.

Acknowledgments: The research was partially supported by the European Union within the European Regional Development Fund, through grant Innovative Economy (POIG.01.01.02-00-008/08). Synchrotron studies was supported by the European Community's Seventh Framework Programme (FP7/2007-2013) under grant agreement n° 226716.

References

- [1] M. Sawicki, E. Guziewicz, M.I. Lukaszewicz, *et al.*, *Phys. Rev B* (under revision), arXiv: 1201.5268v1 [cond-mat.mtrl-sci] 25 January 2012
- [2] M.I. Lukaszewicz, B. Witkowski, M. Godlewski, E. Guziewicz, M. Sawicki, W. Paszkowicz, R. Jakiela, T.A. Krajewski, and G. Luka, *Phys. Stat. Sol. B* **247** (2010) 1666
- [3] E. Guziewicz, M.I. Lukaszewicz, L. Wachnicki, K. Kopalko, A. Kovács, R.E. Dunin-Borkowski, B.S. Witkowski, B.J. Kowalski, J. Sadowski, M. Sawicki, R. Jakiela, M. Godlewski, *Radiat. Phys. Chem.* **80** (2011) 1046

Polskie Towarzystwo Promieniowania Synchrotronowego (PTPS)

Siedziba:

ul. Radzikowskiego 152
31-342 Kraków
tel. (0) 12 662 82 35

Nr konta bankowego:

Bank PeKaO SA I Oddział w Krakowie
80 1240 1431 1111 0000 1045 5083

Adres do korespondencji:

Prof. UAM dr hab. Maciej Kozak
Zakład Fizyki Makromolekularnej
Uniwersytet im. A. Mickiewicza
ul. Umultowska 85
61-614 Poznań
Tel. +48-61-8295266
e-mail: mkozak@amu.edu.pl
<http://www.synchrotron.org.pl>

**Składki członkowskie dla członków
zwyčajnych:**

Wysokość składek członkowskich
(od 1 stycznia 2009 r.):
Samodzielni pracownicy naukowci – 50 zł
Doktorzy – 40 zł
Pozostali – 30 zł

Zarząd Polskiego Towarzystwa Promieniowania Synchrotronowego (kadencja: 2011 – 2014)

Prezes:

Dr hab. Maciej Kozak
Wydział Fizyki
Uniwersytet im. A. Mickiewicza
ul. Umultowska 85
61-614 Poznań
e-mail: mkozak@amu.edu.pl

Wiceprezes:

Prof. dr hab. Jacek Szade
Instytut Fizyki
im. A. Chełkowskiego
Uniwersytet Śląski
ul. Uniwersytecka 4
40-007 Katowice
e-mail: jacek.szade@us.edu.pl

Wiceprezes:

Prof. dr hab. Radosław Przeniosło
Instytut Fizyki Doświadczalnej
Uniwersytet Warszawski
ul. Hoża 69
00-681 Warszawa
e-mail: radek.przenioslo@fuw.edu.pl

Sekretarz:

Dr hab. Zbigniew Kaszukur
Instytut Chemii Fizycznej PAN
ul. Kasprzaka 44/52
01-224 Warsaw, Poland
e-mail: zkaszukur@ichf.edu.pl

Skarbnik:

Prof. dr hab. Wojciech Kwiatek
Instytut Fizyki Jądrowej PAN
ul. Radzikowskiego 152
31-142 Kraków
e-mail:
wojciech.kwiatek@ifj.edu.pl

Wydawca:

Dr hab. Wojciech Paszkowicz
Instytut Fizyki PAN
al. Lotników 32/46
02-668 Warszawa
e-mail: paszk@ifpan.edu.pl

Członek Zarządu d/s. Strony

Internetowej:
Dr hab. Paweł Piszora
Wydział Chemii
Uniwersytet im. A. Mickiewicza
ul. Grunwaldzka 6
60-780 Poznań
e-mail: pawel@amu.edu.pl

Członkowie:

Prof. dr hab. Krystyna Jabłońska
Instytut Fizyki PAN
al. Lotników 32/46
02-668 Warszawa
e-mail: jablo@ifpan.edu.pl

Prof. dr hab. Czesław Kapusta
Zakład Fizyki Ciała Stałego
Akademia Górniczo-Hutnicza
al. Mickiewicza 30
30-059 Kraków
e-mail: kapusta@agh.edu.pl

Prof. dr hab. Bogdan Kowalski
Instytut Fizyki PAN
al. Lotników 32/46
02-668 Warszawa
e-mail: kowab@ifpan.edu.pl

Prof. dr hab. Marek Stankiewicz
Instytut Fizyki
Uniwersytet Jagielloński
ul. Reymonta 4
30-059 Kraków
e-mail:
m.j.stankiewicz@uj.edu.pl

Zawiadomienie Walne Zebranie Polskiego Towarzystwa Promieniowania Synchrotronowego

Serdecznie zapraszamy Państwa na Walne Zebranie sprawozdawcze Towarzystwa, które odbędzie się w trakcie XI. International School and Symposium on Synchrotron Radiation in Natural Science w Krakowie-Tyńcu w hotelu „FERO EXPRESS” w czwartek, dnia 24. maja 2012 roku o godz. 20.00 w I terminie oraz o godz. 20.15 w II terminie.

Sekretarz PTPS
Z. Kaszukur

Prezes PTPS
M. Kozak

Porządek obrad:

1. Powitanie zebranych
2. Przyjęcie porządku obrad
3. Sprawy członkowskie
4. Sprawozdanie merytoryczne Zarządu PTPS
5. Sprawozdanie finansowe Zarządu PTPS
6. Sprawozdanie Komisji Rewizyjnej PTPS
7. Dyskusja nad sprawozdaniami

8. Informacja o planach działalności Towarzystwa
9. Problem dostępu do europejskich źródeł promieniowania synchrotronowego
10. Informacja o 10 Krajowym Sympozjum Użytkowników Promieniowania Synchrotronowego w 2013 roku
11. Sprawy bieżące
12. Wolne wnioski

| | Sunday, 20.05.2012 | Monday, 21.05.2012 | Tuesday, 22.05.2012 | Wednesday, 23.05.2012 | Thursday, 24.05.2012 | Friday, 25.05.2012 | | | | | |
|---------------|-----------------------|------------------------------|---|-----------------------------------|-------------------------|-----------------------|---------------|------------------|---------------------------|----------------------|-------------|
| 7.30-8.45 | | Breakfast | Breakfast | Breakfast | Breakfast | Breakfast | 7.30-8.45 | | | | |
| 9.00-9.40 | | L-3 P. Dumas | Conference Excursion | L-13 T. Tagashi | L-19 C. Pettenkofer | L-22 Cz. Kapusta | 9.00-9.40 | | | | |
| 9.40-10.20 | | L-4 M. Korbas | | L-14 V. Petricek | L-20 M. Taniguchi | L-23 E. Guzewicz | 9.40-10.20 | | | | |
| 10.20-10.40 | | O-1 J. Chwiej | | O-10 K. Ławniczak-Jabłońska | O-6 C. Bocchetta | O-15 J. Kubacki | O-16 P. Goryl | 10.20-10.40 | | | |
| 10.40-11.00 | | O-2 J. Czapla | | | | | | 10.40-11.00 | | | |
| 11.00-11.30 | | Coffee break | | | | | | Coffee break | Coffee break | 11.00-11.30 | |
| 11.30-11.50 | | L-5 B. Ziája-Motyka | | | | | | L-15 P. Rudolf | Visit to Tyniec Monastery | O-17 M. Kozak | 11.30-11.50 |
| 11.50-12.10 | | | | | | | | L-16 V. Kaganer | | O-18 H. Drozdowski | 11.50-12.10 |
| 12.10-12.30 | | L-6 M. Gilski | | | | | | | | O-19 P. Dararutana | 12.10-12.30 |
| 12.30-12.50 | | | | | | | | | | O-20 J. Kowalska | 12.30-12.50 |
| 12.50-13.10 | | O-3 Z. Pietralik | | | | | | | O-7 A. Bartnik | O-21 A. Kubala-Kukuś | 12.50-13.10 |
| 13.10-13.30 | | O-4 J. Kutorasińska | | | | | | | O-8 P. Wachulak | Closing Remarks | 13.10-13.30 |
| 13.30-15.00 | | Lunch | | | | | | | Lunch | Lunch | Lunch |
| 15.00-15.40 | | | Lunch | | | | | L-17 A. Marcelli | L-21 C. Fadley | | 15.00-15.40 |
| 15.40-16.00 | | | | | | | | L-18 H. Oyanagi | O-11 M. Sikora | | 15.40-16.00 |
| 15.40-16.20 | | | | | O-12 A. Rogalev | 15.40-16.20 | | | | | |
| 16.20-16.40 | | | | L-10 H. Tomizawa | O-9 J. Hartwig | O-13 P. Zajdel | 16.20-16.40 | | | | |
| 16.40-17.00 | | | | | O-14 A. Szkułlarek | 16.40-17.00 | | | | | |
| 17.00-17.20 | Opening | Special Session in City Hall | L-11 C. Bressler | Visit to Niepołomice Royal Castle | Coffee break | 17.00-17.20 | | | | | |
| 17.20-17.40 | L-1 C. Schneider | | Coffee break | | 17.20-17.40 | | | | | | |
| 17.40-18.00 | | | L-12 G. Dietler | | Poster Session | 17.40-18.00 | | | | | |
| 18.00 - 18.40 | L-2 W. Rypniewski | | L-7 M. Stankiewicz L-8 P. Olko L-9 G. Wrochna | | O-5 M. Gateshki | 18.00 - 18.40 | | | | | |
| 18.40-19.00 | | | | | | 18.40-19.00 | | | | | |
| 19.00-20.00 | Welcome Grill | Reception at City Hall | Dinner | | Dinner | 19.00-20.00 | | | | | |
| 20.00-21.00 | | | JANA WORK-SHOP | Poster Session | Conference Dinner | PTPS Meeting | 20.00-21.00 | | | | |
| 21.00-22.00 | | Kraków by night on your own | | | | 21.00-22.00 | | | | | |
| 22.00-22.30 | | | | | | 22.00-22.30 | | | | | |